# Thermo-mechanical energy storage applications for energy system decarbonisation

By

**Andrea Vecchi**
ORCiD: 0000-0002-4961-9643

Doctor of Philosophy
July 2022
University of Birmingham, College of Engineering and Physical Sciences
School of Chemical Engineering
&
University of Melbourne, Faculty of Engineering and Information Technology
Department of Electrical and Electronic Engineering

*Submitted in partial fulfilment for the jointly awarded degree of Priestley PhD*
*at the University of Birmingham and the University of Melbourne*

# UNIVERSITY OF BIRMINGHAM

# Abstract

Large penetration of renewable energy sources such as wind and sun underpins the transition towards future low-carbon energy systems worldwide. Yet, the intrinsic intermittency of these sources must be accommodated by a high degree of grid flexibility to guarantee continuous and safe power delivery and ensure constant supply-demand matching. By storing excess electricity to be delivered on demand when most needed, electrical energy storage can provide such required flexibility, thus playing a valuable role as enabling technology for the low-carbon transition. However, the future deployment of energy storage is tied to the techno-economic performance that can realistically be delivered, which ultimately identifies the most suitable investment across a range of storage technologies and alternative pathways to achieve grid flexibility.

This thesis work addresses thermo-mechanical energy storage, a class of grid-scale technologies intended for 100s MWh capacity, several hours storage duration and up to 100s MW power output, where electricity is stored in the form of thermal and/or mechanical potential. Focus is devoted to liquid air energy storage. First, plant design and off-design operation are studied, with the associated techno-economic performance. Then, the operation of liquid air energy storage within the grid is characterised when supplying energy and reserve services to the power system. Furthermore, the opportunities and limitations for combined electricity, heating and cooling provision from a single liquid air energy storage plant are assessed. To conclude, the potential of six between established and novel thermo-mechanical energy storage concepts is cross-compared and benchmarked with incumbent storage technologies for long-duration storage applications.

The methodological framework developed uses device and system-scale simulation, integrating the results in energy system assessments to enable a more accurate assessment of storage performance and, consequently, the associated value and contribution. Results prove the importance of modelling the effect of real-life performance variations, leading to 6-14% higher revenues for multi-service provision and the value of multi-energy operation for external delivery of electricity and heating. Also, the suitability of thermo-mechanical energy storage for long-duration storage is verified, with novel concepts potentially reaching below 14 $/kWh, i.e. comparable with the use of hydrogen. All in all, results point towards the financial value of a more diversified storage operation for energy balancing and reserve services, or local multi-energy provision, underscoring the necessity to gauge storage viability on a case-by-case basis. Further strategies are pointed out to progress thermo-mechanical energy storage application to long-duration storage and further support decarbonisation.

# Declaration

I hereby declare that:

- The work contained in this thesis comprises my own original work, to the extent indicated in the Preface. It has not been previously submitted to meet requirements for an award at the University of Birmingham, the University of Melbourne, or any other higher education institution

- To the best of my knowledge, this thesis contains no material previously published or written by another person except where due reference is made

- Due acknowledgement has been made in the text to all other material used

- This thesis is fewer than the 100,000 words limit in length, exclusive of tables, maps, bibliographies and appendices (and less than the 50,000 words limit in length, exclusive of abstract, acknowledgements, contents pages, appendices, tables, diagrams and figures with associated legends, the list of references, bibliography, footnotes and endnotes and any bound published material)

Signature: __*Andreas Vecil*_____

Date: ___01.07.2022_____

# Preface

Most of the results presented in this thesis have been published in peer-reviewed journal articles and conference proceedings, as listed hereafter. In all the listed contributions, the first author was responsible for over 50% of the work, as confirmed by co-authors in the declaration forms submitted alongside this document. No editorial assistance was received. Detailed contribution statements accompanying the journal articles are also provided in the following.

**Journal papers**

J1 **Vecchi A**, Li Y, Mancarella P, Sciacovelli A. Integrated techno-economic assessment of Liquid Air Energy Storage (LAES) under off-design conditions: Links between provision of market services and thermodynamic performance. *Applied Energy*. 2020; 262:114589.

Authorship contribution: **Andrea Vecchi:** Conceptualization, Methodology, Software, Formal Analysis, Writing – Original Darft, Writing- Review & Editing, Visualization **Yongliang Li:** Supervision, Writing-Review & Editing **Pierluigi Mancarella:** Supervision**,** Conceptualization, Writing- Review & Editing, Funding acquisition **Adriano Sciacovelli:** Conceptualization, Methodology, Supervision, Writing-Review & Editing, Funding acquisition.

J2 **Vecchi A**, Naughton J, Li Y, Mancarella P, Sciacovelli A. Multi-mode operation of a Liquid Air Energy Storage (LAES) plant providing energy arbitrage and reserve services e Analysis of optimal scheduling and sizing through MILP modelling with integrated thermodynamic performance. *Energy*. 2020.

Authorship contribution: **Andrea Vecchi:** Conceptualization, Methodology, Software, Formal Analysis, Writing – Original Draft, Writing – Review & Editing, Visualization **James Naughton:** Conceptualization, Methodology, Writing – Original Draft, Writing – Review & Editing, **Yongliang Li:** Supervision **Pierluigi Mancarella:** Supervision**,** Conceptualization, Writing – Review & Editing, Funding acquisition **Adriano Sciacovelli:** Conceptualization, Methodology, Supervision, Writing – Review & Editing, Funding acquisition.

J3 **Vecchi A**, Li Y, Mancarella P, Sciacovelli A. Multi-energy liquid air energy storage: A novel solution for flexible operation of districts with thermal networks. *Energy Conversion and Management*. 2021; 238:114161.

Authorship contribution: **Andrea Vecchi:** Conceptualization, Methodology, Software, Formal Analysis, Writing – Original Darft, Writing- Review & Editing, Visualization **Yongliang Li:** Supervision, Writing-Review & Editing **Pierluigi Mancarella:** Supervision**,** Conceptualization, Writing- Review & Editing, Funding acquisition **Adriano Sciacovelli:** Conceptualization, Methodology, Supervision, Writing-Review & Editing, Funding acquisition.

**J4**  **Vecchi A**, Li Y, Ding Y, Mancarella P, Sciacovelli A. Liquid air energy storage (LAES): A review on technology state-of-the-art, integration pathways and future perspectives. *Advances in Applied Energy*. 2021; 3:100047.

Authorship contribution: **Andrea Vecchi:** Conceptualization, Methodology, Software, Formal Analysis, Writing – Original Darft, Writing- Review & Editing, Visualization **Yongliang Li:** Supervision, Writing- Review & Editing **Yulong Ding:** Writing- Review & Editing, Funding acquisition **Pierluigi Mancarella:** Supervision**,** Conceptualization, Writing- Review & Editing, Funding acquisition **Adriano Sciacovelli:** Conceptualization, Methodology, Supervision, Writing- Review & Editing, Funding acquisition.

The following journal papers were also published within the period of doctoral studies but do not constitute part of this thesis.

**J5**  Zhang X, Ameli H, Dong Z, **Vecchi A**, Gallego-Schmid A, Strbac G, et al. Values of latent heat and thermochemical energy storage technologies in low-carbon energy systems: Whole system approach. *Journal of Energy Storage.* 2022; 50:104126.

**Xi Zhang**: Conceptualization, Methodology, Software, Formal analysis, Data curation, Writing – original draft, Visualization. **Hossein Ameli**: Conceptualization, Methodology, Writing – review & editing, Supervision, Project administration, Funding acquisition. Zihang Dong: Validation, Formal analysis, Visualization. **Andrea Vecchi**: Writing – original draft, Writing – review & editing. **Alejandro Gallego-Schmid**: Writing – review & editing, Project administration, Funding acquisition. **Goran Strbac**: Conceptualization, Writing – review & editing, Supervision. **Adriano Sciacovelli**: Conceptualization, Writing – review & editing, Supervision, Funding acquisition

**J6**  Liang T, **Vecchi A**, Knobloch K, Sciacovelli A, Engelbrecht K, Li Y, et al. Key components for Carnot Battery: Technology review, technical barriers and selection criteria. Renewable and Sustainable Energy Reviews. 2022; 163:112478.

**Ting Liang**: Conceptualization, Methodology, Data curation, Visualization, Writing – original draft, Writing - review & editing; **Andrea Vecchi**: Conceptualization, Methodology, Data curation, Writing - original draft, Writing - review & editing; **Kai Knobloch**: Conceptualization, Data curation, Writing - original draft, Writing - review & editing; **Adriano Sciacovelli**: Supervision, Writing - review & editing, Funding acquisition; **Kurt Engelbrecht**: Supervision, Writing - review & editing, Funding acquisition; **Yongliang Li**: Supervision, Writing - review & editing; **Yulong Ding**: Supervision, Writing - review & editing, Funding acquisition.

**J7**  **Vecchi A**, Knobloch K, Liang T, Kildahl H, Sciacovelli A, Engelbrecht K, et al. Carnot Battery development: A review on system performance, applications and commercial state-of-the-art. Journal of Energy Storage. 2022; 55: 105782.

**Andrea Vecchi:** Conceptualization, Methodology, Formal Analysis, Writing - Original Draft, Writing - Review & Editing, Visualization **Kai Knobloch:** Conceptualization, Methodology, Formal Analysis, Writing - Original Draft, Writing - Review & Editing, Visualization **Ting Liang:** Formal Analysis, Writing - Original Draft **Harriet Kildahl:** Writing - Review & Editing **Adriano Sciacovelli:** Supervision, Writing - Review & Editing, Funding acquisition **Kurt Engelbrecht:** Supervision, Writing - Review & Editing, Funding acquisition **Yongliang Li:** Writing - Review & Editing, **Yulong Ding:** Supervision, Writing - Review & Editing, Funding acquisition.

**Conference proceedings**

C1 **Vecchi A**, Li Y, Mancarella P, Sciacovelli A. Analysis of multi-mode operation of liquid air energy storage (LAES) plant – Link between provision of grid balancing services and thermodynamic performance. *ECOS 2019*.

C2 **Vecchi A**, Negoescu C, Li Y, Reip A, Sciacovelli A. Effect of cryogenic heat transfer at supercritical conditions on liquid air energy storage (LAES) performance – a combined experimental and numerical analysis. *HEFAT 2019*.

C3 **Vecchi A**, Li Y, Mancarella P, Sciacovelli A. Design of a liquid air energy storage - economic vs thermodynamic criteria. *ICAE 2019*.

C4 **Vecchi A**, Sciacovelli A. Thermo-mechanical energy storage options for long-duration storage – A techno-economic comparative assessment of established and novel concepts. *ECOS 2022*.

# Acknowledgements

Many people have directly and indirectly contributed towards this thesis work with their presence throughout the long and bumpy trail that doctoral studies truly are. First, I would like to thank my family: Carmelo, Valeria, Martino and Anna, for empowering me to take my own decisions in life and always giving me support, strength and the right motivation when necessary.

I am very grateful to my main supervisors, Adriano and Pierluigi, who helped me develop as a person and researcher during the last years, by sharing their passion, knowledge and drive for these topics in a contagious and inspiring manner. A sincere thank also to Prof Jihong Wang and Prof Christos Markides who took time to carefully assess the present thesis, providing valuable feedback and the chance to have a fantastic discussion during the viva.

Also, I wish to thank all my friends from Italy, Birmingham and Melbourne, who greatly enriched these years with their advice, insights and, simply, with their familiar presence. Thank you also to all past and present colleagues who provide daily learning opportunities, helpful contributions and feedback.

Finally, a big thank you to my special person, Silvia, who has been the most precious presence in these last four years and shared with me every piece along this journey: we walked together until the end, and I can't wait to do it many more times to come.

*Andrea*

# Table of Contents

# List of Figures

# List of Tables

# Nomenclature

## Symbols

| | |
|---|---|
| $\dot{C}$ | Heat capacity rate, W/K |
| $\dot{Ex}$ | Exergy rate, W |
| $\dot{Q}$ | Thermal power, W |
| $R^*$ | Specific gas constant, J/(kgK) |
| $\dot{W}$ | Power, W |
| $c_p$ | Specific heat capacity, J/(kgK) |
| $\dot{m}$ | Mass flow rate, kg/s |
| $h$ | Specific enthalpy, J/kg |
| $\Lambda$ | Storage thermal loss coefficient, 1/h |
| $\Pi$ | Compression/expansion ratio |
| $\Sigma$ | Entropy generation, W/K |
| $A$ | Heat transfer area, $m^2$ |
| $CAPEX$ | Capital expenditure, £ |
| $CF$ | Conversion factor |
| $CS$ | Cost saving |
| $D$ | Diameter, m |
| $E$ | Energy, J |
| $EC$ | Energy specific cost, £/(kWh) |
| $ED$ | Energy density, $kWh/m^3$ |
| $EER$ | Energy efficiency ratio |
| $EG$ | Excess gas |
| $Ex$ | Exergy, J |
| $H$ | Enthalpy, J |
| $K$ | Equipment cost, £ |
| $LAE$ | Liquid air expenditure, kg/s |
| $LAI$ | Liquid air inventory, kg |
| $MM$ | Molar mass kg/kmol |
| $N$ | Number of stages, breakpoints |
| $NTU$ | Number of transfer units |
| $PBT$ | Payback time, y |
| $PC$ | Power specific cost, £/W |
| $Q$ | Heat, J |
| $R$ | Universal gas constant, 8.314 J/(molK) |
| $RC$ | Reserve service commitment, W |
| $Rev$ | Revenue, £ |
| $S$ | Entropy, J/K |
| $T$ | Temperature, K |
| $U$ | Heat transfer coefficient, W/($m^2$K) |
| $V$ | Volume, $m^3$ |
| $W$ | Work, J |
| $Y$ | Liquid yield |
| $a$ | Generic coefficient |
| $b$ | Generic coefficient |
| $e$ | Specific energy, J/kg |
| $ex$ | Specific physical exergy, J/kg |
| $g$ | Gravitational acceleration, $m/s^2$ |
| $m$ | Mass, kg |
| $n$ | Rotational speed, rpm |
| $p$ | Pressure, bar |
| $q$ | Specific heat, J/kg |
| $s$ | Specific entropy, J/(kgK) |
| $t$ | Time, s |
| $u$ | Velocity, m/s |
| $v$ | Specific volume, $m^3$/kg |
| $w$ | Specific work, J/kg |
| $x$ | Generic variable |
| $y$ | Generic variable |
| $z$ | z-coordinate, m |
| $\alpha$ | Convective heat transfer coefficient, W/($m^2$K) |
| $\beta$ | Pressure loss coefficient |
| $\gamma$ | Isentropic exponent |
| $\delta$ | Thickness, m |
| $\varepsilon$ | Effectiveness |
| $\zeta$ | Thermal loss/gain coefficient |
| $\eta$ | Efficiency |
| $\kappa$ | Call probability |
| $\lambda$ | Thermal conductivity, W/mK |
| $\nu$ | Kinematic viscosity, $m^2$/s |
| $\xi$ | Part-load coefficient, split parameter |
| $\pi$ | Price |
| $\rho$ | Density, kg/$m^3$ |
| $\sigma$ | Void fraction |
| $\tau$ | Duration, s |
| $\chi$ | Share |
| $\psi$ | Specific chemical exergy, J/kg |
| $\omega$ | Auxiliary variable |
| $\phi$ | Specific irreversibility generation |

## Subscripts and superscripts

| | |
|---|---|
| 0 | Rated, ambient, standard |
| $h$ | Hot, heating |
| $B$ | Boiler |
| $C$ | Compressor |
| $CR$ | Cold recycle |
| $CV$ | Control volume |
| $DCN$ | District cooling network |
| $DHN$ | District heating network |
| $Ex$ | Exergy |
| $FR$ | Fast reserve |
| $HR$ | Hot recycle |
| $HX$ | Heat exchanger |
| $I$ | First-law |
| $MAX$ | Maximum |
| $P$ | Pump |
| $PW$ | Piecewise |
| $R$ | Ratio |

| | |
|---|---|
| *RC* | Reserve service commitment |
| *RT* | Roundtrip |
| *S* | Isentropic |
| *STOR* | Short term operating reserve |
| *T* | Turbine/expander |
| *TES* | Thermal energy storage |
| *ava* | Availability |
| *buy* | Buy |
| *c* | Cold, cooling |
| *chr* | Charge |
| *cap* | Capacity |
| *d* | Drag |
| *dsc* | Discharge |
| *el* | Electricity, electrical |
| *eq* | Equilibrium |
| *f* | Fluid, fuel |
| *feed* | Feeder |
| *g* | Gravitational |
| *gen* | Generation |
| *idl* | Idle |
| *in* | Inlet, input |
| *k* | Kinetic |
| *liq* | Liquid |
| *loss* | Loss |
| *min* | Minimum |
| *ml* | Logarithmic mean |
| *oil* | Thermal oil |
| *out* | Outlet, output |
| *pos* | Positional |
| *prod* | Product |
| *purch* | Purchase |
| *r* | Reactor |
| *s* | Solid |
| *sell* | Sell |
| *t* | Technical, Time |
| *th* | Thermal |
| *util* | Utilisation |
| *t* | Technical, Time |

| | |
|---|---|
| *th* | Thermal |
| *util* | Utilisation |

## Acronyms and abbreviations

| | |
|---|---|
| ACAES | Adiabatic CAES |
| ASU | Air separation unit |
| CAES | Mass flow rate |
| CAPEX | Capital expenditure |
| CES | Carbonates energy storage |
| DCN | District cooling network |
| DHN | District heating network |
| EES | Engineering equation solver |
| ES | Electricity storage |
| FR | Fast reserve |
| HES | Hydroxides energy storage |
| HGCS | High grade cold storage |
| HP | High-pressure |
| JT | Joule-Thompson |
| LAES | Liquid air energy storage |
| LDS | Long-duration storage |
| LNG | Liquefied natural gas |
| LP | Low-pressure |
| MDS | Medium-duration storage |
| MILP | Mixed integer linear programming |
| M-LAES | Multi-energy liquid air energy storage |
| MP | Medium-pressure |
| OES | Oxides energy storage |
| ORC | Organic Rankine cycle |
| PBT | Payback time |
| PHES | Pumped hydro energy storage |
| PRU | Power recovery unit |
| PTES | Pumped thermal energy storage |
| RES | Renewable energy source |
| SoC | State of charge |
| STOR | Short term operating reserve |
| TES | Thermal energy storage |
| TMES | Thermo-mechanical energy storage |
| TRL | Technology readiness level |

# CHAPTER 1

## Introduction

## 1.1  Energy landscape and the need for energy storage

Decarbonisation of the global economy represents arguably the most significant challenge humankind currently faces. Anthropogenic climate change [1] and the understanding of its disruptive effect on the social, environmental and geopolitical equilibria that underpin our system all call for rapid actions to cut greenhouse gas emissions. The Paris Agreement, signed by 196 countries in December 2015, represents the legally binding framework to shape decarbonisation efforts based on nationally determined contributions. The aim is to contain temperature rise by 2050 to *well below* 2 °C above pre-industrial levels [2]. At present, over 110 countries have submitted climate goals: among others, China pledged carbon neutrality by 2060[1], while the UK first committed to the net-zero target for 2050[2]. More than 130 nations have now set, or are considering, carbon neutrality goals by mid-century.

In 2018, 42% of the global $CO_2$ emissions came from the electricity and heating sector, 25% from transport, and 18% from industry[3]. Electricity generation represents today the single largest source of $CO_2$ emissions; at the same time, it is the sector where most changes are expected in the short term and, partially, already underway. Generation technologies based on renewable energy sources (RES) are now mature and cost-competitive: solar photovoltaics and off-shore wind currently represent the cheapest energy sources [3]. Under these premises, two key developments will jointly sustain the low-carbon transition: a doubling of electricity share in the final energy consumption – from approximately 20% in 2015 to 40% in 2050 – and a more than five-fold increase in RES installed capacity to cover between 70% [4] and 90% [5] of the final energy use in 2050. Other sectors too will vastly rely on electricity. However, large RES penetration – particularly in conjunction with the electrification of

---

[1] See: https://odi.org/en/insights/five-expert-views-on-chinas-pledge-to-become-carbon-neutral-by-2060/

[2] See: https://www.gov.uk/government/news/uk-becomes-first-major-economy-to-pass-net-zero-emissions-law

[3] See: https://www.iea.org/data-and-statistics/data-browser?country=WORLD&fuel=CO2%20emissions&indicator=CO2BySector

heating and transport sectors – requires coping with intrinsic resource unpredictability and volatility over space and time. Sources of flexibility like increased transmission and interconnection capacity, storage and demand-side management will be needed to achieve high shares of RES [6].

Energy storage involves the conversion of surplus energy into a form that can be stored and converted back when most needed [7]. Energy is stored at times of excess generation, low demand or low generation cost and produced at times of high demand, high generation cost or when other generation assets are unavailable. Figure 1 illustrates the benefits brought by energy storage to power system operation. Not only does storage help in continuously matching energy demand and supply. Studies found it also reduces backup capacity requirements from dispatchable power plants to 20% of the average demand, while transmission expansion only went as far as 30% [8]. Meeting rising energy demand with up to 90% RES penetration was estimated to be 40% cheaper with storage adoption instead of increasing transmission capacity only [6]. Additionally, storage enhances energy system resilience, provides black-start capacity, contributes to national energy security and can firm up the generation of large co-located RES plants. Therefore, while a simultaneous deployment of multiple flexibility sources is necessary for decarbonisation, energy storage has a prominent role to play among them. Future UK energy scenarios forecast a doubling of the installed storage capacity between 2025 and 2035 and a target of 24-63 GW in 2050 [9].
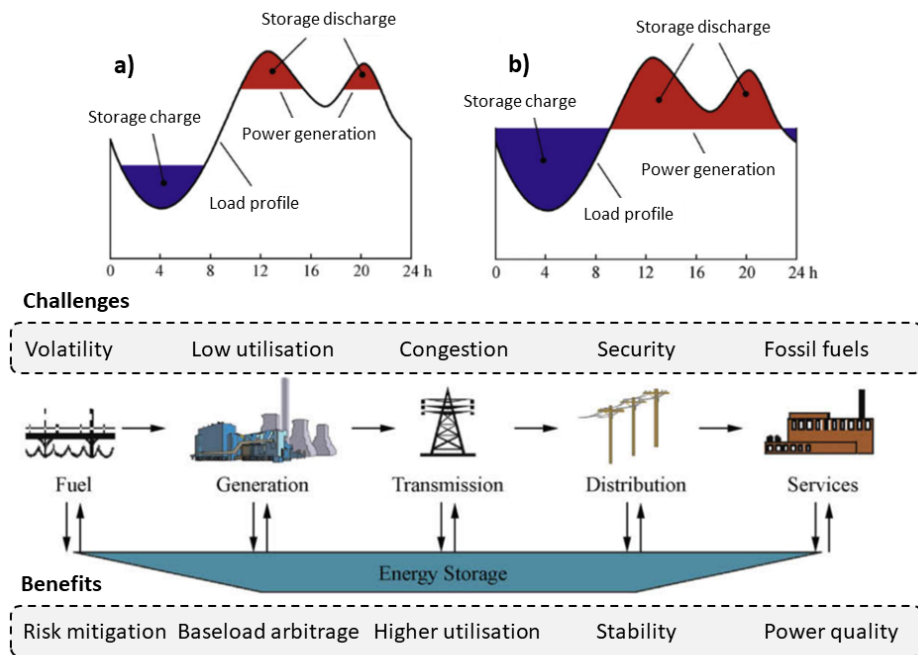


Figure 1: Operating principle of energy storage for a) peak shaving and b) load following; power system challenges and associated benefits from electrical energy storage (adapted from [7]).

## 1.2   Primer on electrical energy storage

Several technologies can be used for electricity storage applications, and many more are developing [10]. Electrical energy storage options are often classified based on the form in which energy is stored, into mechanical, chemical and electromagnetic. Mechanical technologies include flywheels, pumped

hydro energy storage (PHES) and gravitational storage. Flywheels store electricity as rotational kinetic energy; they guarantee high power densities, small losses and fast response but exhibit capacity limitations and low energy density. Improvements involve material science and drag minimisation by enhanced bearings/magnetic levitation [11]. On the other hand, PHES and gravitational storage are mature technologies with high efficiency, large capacity and low cost per unit of energy stored. Drawbacks are long construction times and environmental disruption [12]. Chemical storage accounts mainly for batteries. From residential to utility scale, installed batteries are growing worldwide and are further predicted to rise from 3 GW in 2019 to 120 GW in 2030 to over 240 GW in 2040 [5]. Batteries are responsive and geographically unconstrained. Drawbacks are restricted power and capacity rating, short lifetime and fast performance deterioration under deep-cycling conditions [13]. Supercapacitors and magnetic energy storage from the electrical/magnetic class feature high power density and quick response. Sill, they are costly, low-energy-density solutions and superconducting magnets require an additional cooling system [14].

Ragone plots such as the one in Figure 2 visualise and rank storage options by scale (from kW to GW output) and duration (seconds to days), giving useful technological information on the services each can provide to balance the power system. Short-duration storage (with sustained delivery up to 1 h) is suitable for fast response services and frequency regulation, medium-duration (2-10 h delivery) for peak shaving and load-following, while long-duration (above 10 h) can offset seasonal imbalances between energy supply and demand and provide black-start. Such technical division maps to storage economics so that batteries are cost-effective for short-term applications and increasingly adopted (with a record-high 5 GW addition in 2020[4]). On the contrary, other technologies are economically viable at large capacities. Nowadays, the long-duration segment is covered mainly by PHES (9000 GWh and over 95% of the installed electrical storage capacity [15]), but geographical constraints hinder further deployment. Storage solutions using hydrogen or other synthetic fuels are at the development stage [8]. Hence, rapid implementation of medium- and long-duration storage technologies is necessary.

---

[4] https://www.iea.org/reports/energy-storage
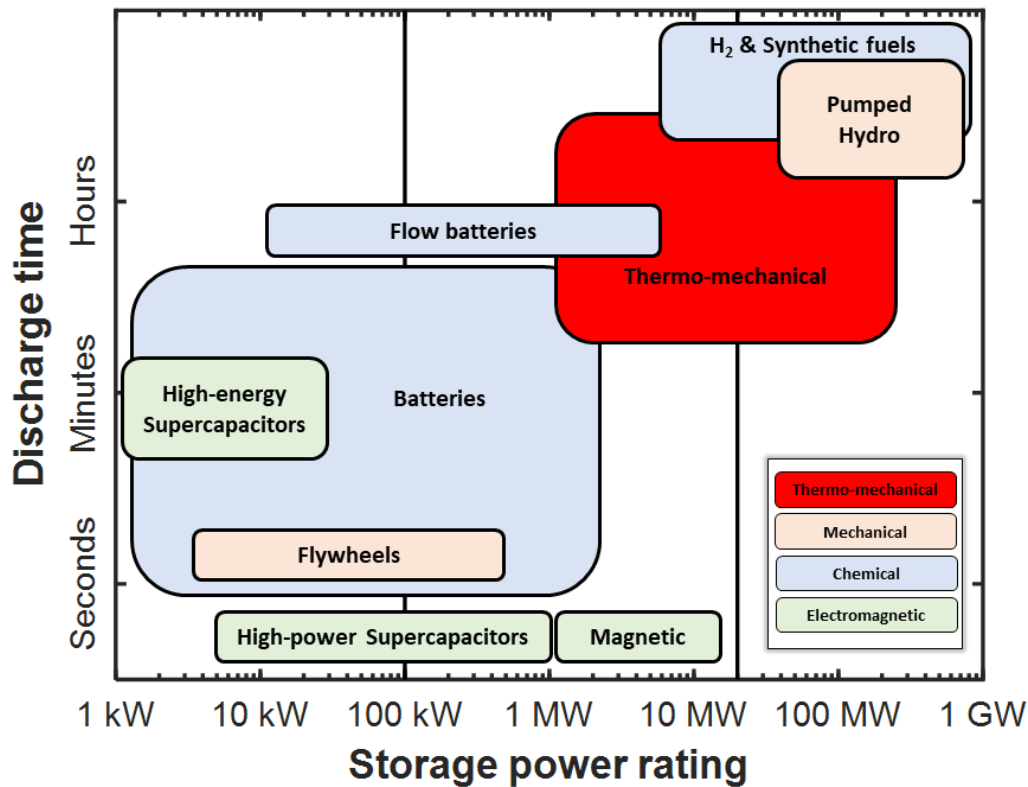
**Figure 2: Electricity storage technologies and intended size; adapted from** [16]**.**

Particularly suited for medium-duration storage (MDS) and 10s MW scales are thermo-mechanical energy storage (TMES) technologies. These are based on conversion processes between electricity, mechanical *and* thermal energy and rely on largely available components. TMES is composed of modular units and thus effective and adaptable for scale-up and deployment. However, only a few demonstration projects exist so far. Questions around the technical performance and the best applications for TMES are still largely unaddressed, with limited understanding of the associated value for the asset owner and the grid operator. This thesis investigates thermo-mechanical energy storage as a relevant contemporary research topic for the above reasons.

## 1.3    Liquid air energy storage and associated challenges

Among TMES technologies, liquid air energy storage (LAES) stores electricity in the form of liquid air at cryogenic temperatures. LAES operating principle is illustrated in Figure 3. During charge, excess electricity is used to compress ambient air. The high-pressure air stream is then cooled down to cryogenic temperatures, expanded – thus turning into the liquid state – and collected in an insulated vessel at ambient pressure. A direct power cycle using air as the working fluid is operated when electricity is required. Liquid air is retrieved from the vessel, pumped at high pressure, evaporated and expanded into a turbine train before being vented to the atmosphere.

4
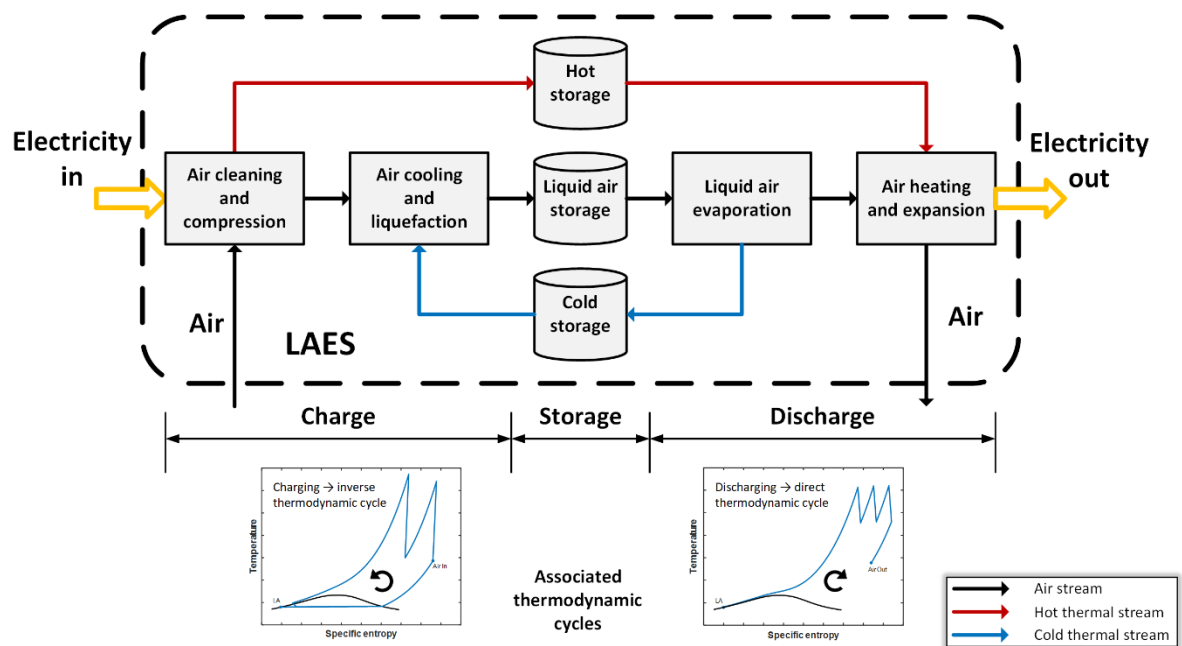
**Figure 3: Operating principle of a liquid air energy storage (LAES).**

LAES features have some key advantages in covering the medium/long-duration storage segment. First, the liquid nature of cryogenic air ensures 1-2 orders of magnitude more electricity can be extracted for a given storage vessel volume, as compared to other TMES [17]. Given the challenge of estimating storage system footprint, TMES comparison based on such energy storage density informs on technology compactness and ease of deployment. It also mirrors the relative power density of TMES technologies (i.e. the electric power generated from a unit volume of storage vessels), when the same storage duration is considered. Second, LAES is geographically unconstrained. Third, it offers multi-vector energy management opportunities, as will be described in this work. Additionally, LAES relies on well-established industrial processes and off-the-shelf equipment from the liquefied natural gas (LNG) and technical gas industries [18]; this enables quick deployment with minimal associated hazards [16]. For all these compelling features, LAES is the main TMES technology of interest here and the primary focus of the work in the present thesis.

Despite a widespread understanding of the working principles and a well-understood technical plant performance now proven at pilot scale, the current challenges for LAES mainly relate to its integration in the energy system. In particular, LAES performance should be addressed when operated as part of the grid, with external constraints and time variations of power input and output. LAES profitability, its value for the stability of the power system and its ideal scheduling and sizing should be determined under such realistic conditions, not limited to electrical energy storage applications. Chapter 2 provides more evidence supporting the relevance and need for research in these areas.

Additionally, as the share of renewables in the energy mix increases above 40-50% and supply-demand mismatch extends to several consecutive hours, long-duration storage (LDS) becomes increasingly important [19]. Therefore, the techno-economic performance of both developing TMES options such as LAES, and exploratory TMES concepts suitable for LDS should be assessed beyond typical daily cycling.

## 1.4    Thesis aims, objectives and methodology

Overall, this thesis aims at investigating the opportunities that TMES – particularly LAES – uptake offers to develop a future low-carbon energy system. Chapter 2 elucidates how research on LAES has so far mainly considered and compared the techno-economic performance of different system layouts in isolation. In the present thesis, the spotlight is shifted to the operation of LAES *within* the energy system, focusing on plant efficiency under realistic working conditions, on the flexibility that LAES can provide to the grid operator through different balancing services and the resulting techno-economic benefits. Additionally, the analysis presented in this thesis work goes beyond the traditional operation of LAES, by: i) considering opportunities for heating and cooling provision alongside electricity; and ii) cross-comparing LAES and other TMES technologies for LDS. The four specific objectives for this thesis are:

O1. **To characterise and techno-economically evaluate the off-design operation of LAES under real-life conditions**, including links between device and system performance, balancing services constraints and realistic duty cycles

O2. **To identify pathways for LAES value maximisation as part of the power system**, including plant thermodynamic limitations and considering optimal plant sizing and optimal allocation of a portfolio of balancing services

O3. **To techno-economically assess the opportunities and limitations for multi-energy provision from LAES**, compared to the traditional electricity-only operation

O4. **To assess selected TMES concepts for long-duration storage applications**, including techno-economic comparison and performance mapping to the target LDS design space.

The methodological framework developed in this thesis leverages device-, system- and energy system-scale modelling, together with linear and mixed-integer linear programming (MILP) optimisation techniques. In each of the studies presented, the level of detail for the storage models is carefully chosen to include the relevant technical features of TMES whilst preserving model tractability for optimisation purposes. Sometimes, this entailed a storage *model reduction* step. The resulting methodology is original and closely tied to the thesis aim. It captures real-life storage operation and performance and extends these findings to the system-scale assessment of TMES value.

### 1.4.1    Novelties

The work presented in this thesis differs significantly from the published studies and complements the existing body of literature. Table 1 summarises the research questions and thesis contributions to the literature. It also illustrates how each of the results chapters is designed to address specifically one of the four thesis objectives stated above. New understanding and evidence on the limitations, potential and value of TMES is the result of the following novelties:

- A validated off-design numerical model for LAES giving an accurate description of real-life plant operation
- A framework for the inclusion of LAES thermodynamic characteristics in dispatch and design optimisation problems
- An assessment of LAES operation beyond electrical storage only, as an asset for multi-energy provision
- A techno-economic assessment of the TMES potential for LDS applications

Novelties are further emphasised in the conclusion of each results chapter, with a point-by-point list of contributions from each presented study to the existing body of literature.

Table 1: Thesis objectives, contributions and associated research questions covered by the present work, with the respective link to the relevant results chapter.

| Thesis objective | Thesis contribution | Research questions | Chapter |
|---|---|---|---|
| O1.    To characterise and techno-economically evaluate the off-design operation of LAES under real-life conditions | Representative description of LAES real-life operation | - How may balancing services influence the operation of LAES?<br>- What is the techno-economic impact of off-design operation? | 4 |
| O2.    To identify pathways for LAES value maximisation as part of the power system | Framework for inclusion of LAES thermodynamic characteristics in dispatch problems | - What is the impact of including thermodynamic performance on LAES scheduling?<br>- How to optimise LAES size for different balancing services?<br>- How to identify the best portfolio of services to be provided? | 5 |
| O3.    To techno-economically assess the opportunities and limitations for multi-energy provision from LAES | Assessment of multi-energy provision from LAES | - How does multi-energy compare with electricity-only operation?<br>- How do temperature levels and user constraints affect provision? | 6 |
| O4.    To assess selected TMES concepts for long-duration storage applications | Techno-economic assessment of TMES potential for LDS | - Do TMES technologies match the requirements for LDS?<br>- What is the expected efficiency and cost of selected options?<br>- What are the promising TMES concepts to further develop? | 7 |

## 1.5    Thesis mind map and structure

Figure 4 illustrates the mind map and structure for this thesis. After the Introduction laying out the background, object and aim of the work, in Chapter 2 the state-of-the-art literature on TMES is reviewed. The research status, gaps and potential for further improvements are discussed, focussing on TMES performance and integration in the energy system. Chapter 3 outlines the relevant methodological background to the thesis, specifically on device and system modelling, MILP optimisation and model reduction techniques, with some examples. Results chapters link one-to-one to the thesis objectives from Table 1 and can be introduced based on higher levels of TMES model reduction or the integration setting representing an increasingly decarbonised energy system, as highlighted in Figure 4. More specifically, Chapter 4 presents LAES real-life operation under off-design conditions, Chapter 5 discusses the scheduling and sizing of LAES for multi-service applications in the power system. Chapter 6 characterises LAES potential for providing heating and cooling alongside electricity in district energy systems, and Chapter 7 assesses the capability and avenues for TMES to meet LDS requirements. Finally, the Conclusion highlights the key outcomes of this work, the applications and strategies for the uptake of LAES and other TMES technologies that can be derived, and provides recommendations for further research.

**1. Introduction**

**2. Literature review**

Techno-economic TMES performance

TMES integration within the energy system

Assessing TMES value through models

**3. Elements of modelling and optimisation**

Device and system modelling

MILP optimisation

Model reduction techniques

**Results**

Energy system decarbonisation

**4. Off-design LAES**

Temperature

Specific entropy

**5. Multi-service LAES**

Revenues

Arbitrage
STOR
FR

**6. Multi-energy LAES**

Energy out

Scenario 1  Scenario 2  Scenario 3

$\eta_l$=60.6%  $\eta_l$=49.3%  $\eta_l$=62.8%

Electricity
Heating
Cooling

**7. TMES concepts for LDS**

Capacity cost

Li-ion
VRFB
PHES
P-H₂-P

Baseline case
Best case

ACAES  LAES  PTES  QES  CES  HES

**TMES model reduction**

**8. Conclusion and future work**

Summary and contributions

Perspectives and recommendations

Figure 4: Mind map and structure for this thesis.

10

# CHAPTER 2

## Literature review

*Given the background outlined in the* Introduction*, this literature review chapter further expands on context, current understanding and open research questions concerning TMES and its integration in the energy system. It compiles the accepted knowledge in the above areas to point out existing research gaps and areas needing further investigation. To this end, the defining traits of TMES technologies are presented and individually reviewed first, with a focus on liquid air energy storage. Then, power system balancing services are discussed, followed by studies on the integration of TMES in the energy system. Discussion is also provided on the common modelling frameworks used to assess storage role and model TMES technologies in system-scale optimisations. It is demonstrated that work has been directed towards selective areas, rarely comprehensively considering all the necessary aspects for energy system integration. Unaddressed research questions involve: i) the real-life operation of liquid air energy storage; ii) the exploitation of flexibility arising from providing a portfolio of balancing services and/or multi-energy output; and iii) TMES characterisation for long durations. The specific thesis objectives are sharpened, clarified, and grounded on the critical assessment of the available scientific literature through the present chapter.*

## 2.1    Introduction

As presented in the Introduction, electrical energy storage is one of the enabling technologies for power system decarbonisation. With increasing RES penetration, further demand for grid balancing will require more installed storage capacity. However, new solutions are needed in the medium/long-duration storage segment, as commercially available options are geographically constrained or, in the case of batteries, not economically viable at the required capacity. TMES offers the appropriate technical and economic features to address such storage segment, with promising technologies like LAES currently under development.

In the present chapter, the relevant groundwork to this thesis is laid out concerning: i) TMES technical and economic performance; ii) TMES applications for power system balancing and LDS; and iii) optimisation of storage integration in the energy system through mathematical modelling. The understanding in the aforementioned areas is presented by reviewing the available scientific studies to date, especially those involving LAES. The reason for this focus is twofold: first, it is due to LAES compelling features among TMES, and second, driven by a fast-rising interest in such technology (see the surging number of publications in Figure 5). As a result of this literature review chapter, the reader is aligned with relevant findings from the body of literature so that the areas in need of further research can be clearly pointed out and appreciated in light of what is currently known. Therefore, the thesis objectives and their relevance to advancing the research field are justified.
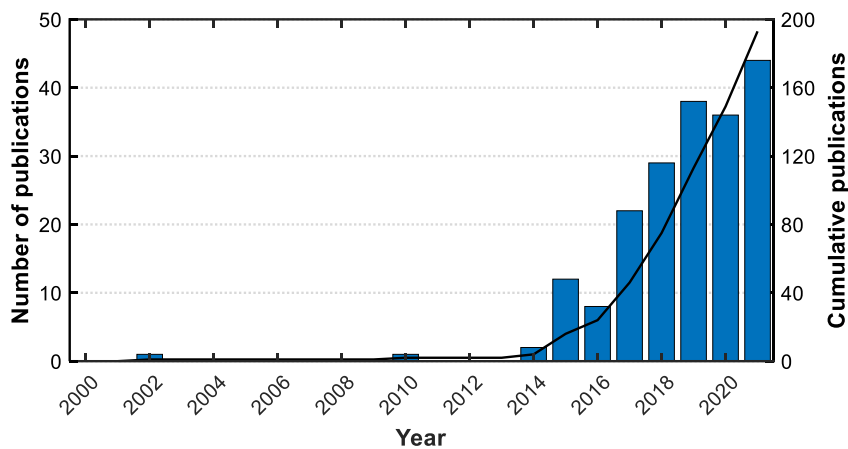


Figure 5: Scopus search results on the yearly number of publications with "liquid air energy storage" in the title, abstract or keywords.

The chapter is organised as follows: Section 2.2 presents a general definition and description of TMES, with a detailed discussion of the most prominent TMES technologies. In Section 2.3, the techno-economics of LAES are reviewed in depth. Then, relevant aspects for TMES commercialisation are presented in Section 2.4, together with the integration studies addressing storage operation within the energy system. Section 2.5 discusses the techniques used to model energy storage, to study and optimise its value; finally, Section 2.6 draws the conclusions.

## 2.2    Thermo-mechanical energy storage technologies

Steinmann first used thermo-mechanical energy storage to identify a class of technologies that store electricity via transformations between thermal and mechanical energy [20]. Figure 6 provides a

sketch of the TMES operating principle. During charge, excess electricity is converted through a suitable thermodynamic process into one or more of: hot energy, cold energy and mechanical potential energy. Such energy streams are stored and saved for later times: heating and cooling in thermal energy storage (TES) units; mechanical potential in a pressurised vessel. The stored energy is retrieved and used to operate a thermodynamic power cycle process during discharge. As Figure 6 suggests, a suitable combination of established chemical engineering process devices enables energy conversion during both charge and discharge. Due to the commercial size of components and favourable economics at scale, TMES is intended as MW-scale, large-capacity storage solution capable of sustaining the rated output across several hours [21].
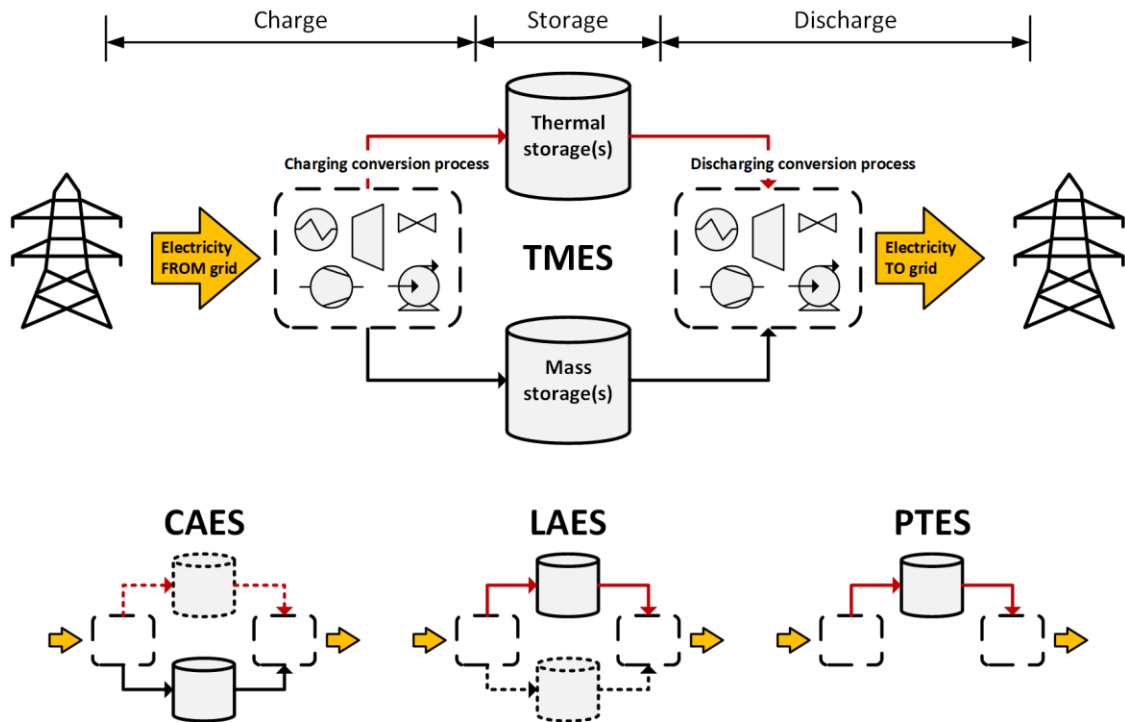


Figure 6: Generic representation of a thermo-mechanical energy storage (TMES) plant and visualisation of specific TMES technologies: CAES, LAES and PTES.

Three main technologies belong to TMES: i) compressed air energy storage (CAES); ii) liquid air energy storage (LAES); and iii) pumped thermal energy storage (PTES) [20]. These represent specific embodiments of the general TMES concept (see Figure 6) and are defined as follows:

- **Compressed air energy storage (CAES):** TMES where electricity is primarily stored in the form of mechanical potential, as pressurised air. The heat generated by the compression process may also be stored.
- **Liquid air energy storage (LAES):** TMES where electricity is primarily stored in the form of cold energy, as cryogenic air in liquid state; mechanical potential may also be stored if using pressurised air vessels. The heat generated by the compression process may also be stored.
- **Pumped thermal energy storage (PTES):** TMES where electricity is stored solely as hot and/or cold energy, in suitable thermal energy storage devices.

For all the above concepts, the one metric used in the literature to assess and compare TMES storage performance is *roundtrip efficiency* [22], i.e. the ratio between the electricity output and input, over a complete storage charge/discharge cycle:

$$\eta_{RT} = \frac{\int_0^{\tau_{dsc}} \dot{W}_{out} dt}{\int_0^{\tau_{chr}} \dot{W}_{in} dt}$$

2.1

In this thesis, roundtrip efficiency will often be used, with a thorough discussion of its merits and limitations as a performance metric uncovered by the research work undertaken. Additional indicators will also be adopted and defined in the individual results chapters to better characterise different aspects of storage operation.

A useful differentiation equally applying to all TMES technologies is between *standalone* and *hybrid* plants [23]:

- **Standalone TMES**: includes baseline TMES layout, where input and output energy streams are electricity only; no fluids other than the working fluid and the heat carriers are present in this configuration.
- **Hybrid TMES**: includes all the layouts where TMES interacts with external processes (i.e. it is not standalone) through hot or cold thermal streams or external fluids. Input and output energy streams can now be electricity, heating, cooling or chemical energy from a fuel; additional fluids may be present.

With the above definition, one can distinguish between cases where TMES operates as a self-sufficient entity and cases where integration with external processes is considered, so performance can be evaluated accordingly.

On top of standalone CAES, LAES and PTES schematically presented in Figure 6, and whose key specifications are gathered in Table 2, a number of hybrid concepts merging two of the above options have also been proposed [24,25], as well as TMES plants with extra inputs from neighbouring processes [26], external thermal streams [27] and power plant retrofits [28]. Emerging TMES layouts that exploit thermochemical reactions have also been reported; these concepts are in their infancy, with full-scale plants still far from commercial development [30]. They are briefly discussed hereafter.

Table 2: Main thermo-mechanical storage technologies and associated technical specifications.

|  | Compressed air energy storage (CAES) | Liquid air energy storage (LAES) | Pumped thermal energy storage (PTES) |
|---|---|---|---|
| Power output | 0.5 – 320 MW | 1 – 300 MW | 10 – 150 MW |
| Roundtrip efficiency | 42 – 70% | 45 – 70% | 48 – 75% |
| Capacity | Up to GWh | Up to 10s GWh | Up to GWh |
| Energy density* | 0.5 – 20 Wh/L | 50 – 200 Wh/L | 10 – 100 Wh/L |
| Response time** | mins | mins | s - mins |
| Lifetime | 20 – 40 y | 20 – 40 y | 25 – 30 y |

| | | | |
|---|---|---|---|
| CO$_2$ emissions | Yes (CAES)/No (ACAES)*** | No | No |
| Installed capacity | 431 MW | 5 MW | N.A. |
| Maturity | Early commercial | Developing/Demo | Developing |
| TRL level | 5 (ACAES) − 9 | 7 − 8 | 2 − 5 |
| Site constraints | Yes**** | No | No |

\* Energy density is here defined as the electricity generated per unit storage volume. The latter consists of the air cavern, for CAES, the liquid air vessel for LAES, the hot and/or cold thermal energy storage for PTES

\*\* For CAES and LAES, response time below 1 min has been demonstrated for operation in "Spin-Gen" mode: i.e. with turbine train synchronised to the generator and passively operated during idle periods.

\*\*\* Adiabatic CAES (ACAES) concepts reduce or avoid CO$_2$ emission from CAES, but they are not yet commercially mature.

\*\*\*\* Small systems ($\leq$ 5 MW) present no site constraints when using above-ground storage vessels.

### 2.2.1 Compressed air energy storage

A schematic of CAES system is reported in Figure 7. Excess electricity is used during the charging phase to compress air from the ambient through a multi-stage, intercooled compression train. The pressurised gas is then stored in a suitable reservoir and, for the discharging phase, it is expanded in a turbine. CAES is subdivided into diabatic, adiabatic and isothermal [29]. Diabatic CAES relies on a combustion chamber to further raise air temperature before turbine expansion. Two diabatic CAES facilities are currently in operation: a 290 MW plant in Huntorf, Germany and a 110 MW plant in McIntosh, USA. The former utilises a total of 310000 m$^3$ salt caverns between 4.8 and 6.6 MPa and sustains up to 4h discharge [30]. The latter uses a single salt dome up to 75 atm, a heat recuperator reducing fuel consumption by 22-25% and has 26 h discharge duration [31]. Over a complete charge/discharge cycle, diabatic CAES reaches energy efficiency of 54% [32]. However, the fuel input represents a major impediment to cutting CO$_2$ emissions. On the contrary, adiabatic CAES (ACAES) stores compression heat, alongside pressurised air, in a TES, which is later used to heat up gasses during discharge. This way, ACAES achieves higher efficiencies – up to 70% [32]. Demonstration projects are ongoing worldwide (e.g. the 200 MW/1 GWh ADELE project, a 50 MW project in Jiansu, China, or the plants from the company Hydrostor [33]). In isothermal CAES, an additional thermal fluid (oil) extracts heat during the compression stage and provides it during expansion. As a result, thermodynamic transformations resemble ideality, and efficiencies can be as high as 80% [32].
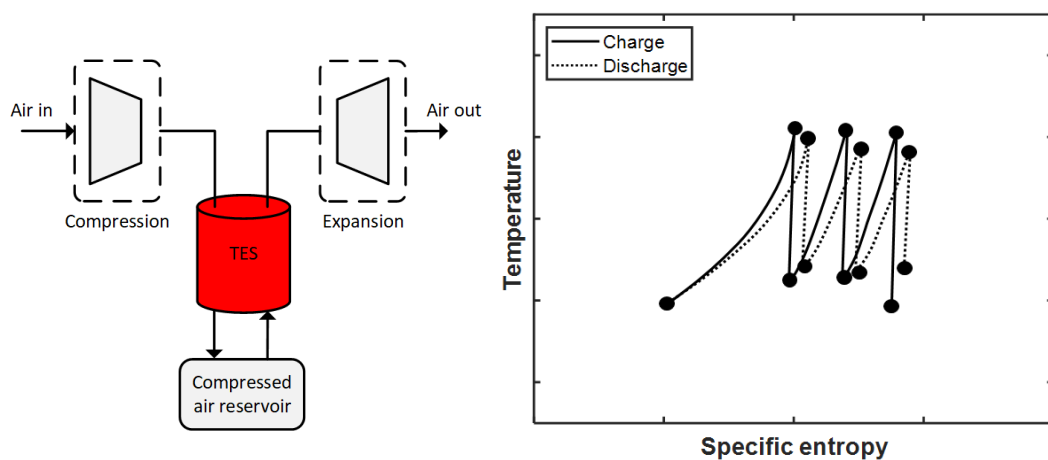


Figure 7: Process flow diagram (left) and qualitative T-s diagram (right) for ACAES. In diabatic CAES, a combustion chamber is added before the turbine, replacing the TES.

Despite achieving efficiency in the 50-70% range and having been already successfully operated in the grid, CAES shares with PHES the major limitation of geographical restrictions [13], as sites with porous rocks, depleted gas/oil fields or caverns in salt and rock formations are necessary for CAES deployment. Alternative concepts were proposed to overcome this issue, including pressurised vessels [34] and underwater solutions [35]; however, both are limited in size and by the associated capital costs.

## 2.2.2 Pumped thermal energy storage

In PTES, a reverse thermodynamic cycle establishes a temperature difference between two thermal reservoirs in the charging phase. Such temperature difference becomes the driver for a direct power cycle during system discharge [36]. In the limit of ideal Carnot cycles, storage roundtrip efficiency approaches 100% [37]. So, in order to achieve high system performance, both thermal losses during heat transfer and storage [38] and thermodynamic irreversibility in the power components (turbines and compressors) should be limited to a minimum [39]. Based on the selected thermodynamic cycle, Brayton PTES and Rankine PTES can be distinguished [40].

### *Brayton PTES*

As depicted in Figure 8, Brayton PTES run a reversible[5] Brayton cycle between a cold and a hot reservoir. During charge, a gaseous working fluid is compressed and heat is transferred to the hot reservoir; then, the gas is expanded to achieve low temperatures and cool down the cold reservoir. During discharge, the cycle is reversed. Heat is transferred from the hot TES to the pressurised working fluid to drive turbine expansion, while cold energy from the cold TES reduces compression work. Typical temperature and pressure ranges for Brayton PTES are -170 to 950 °C and 1-20 bar; efficiency is 52-70%.
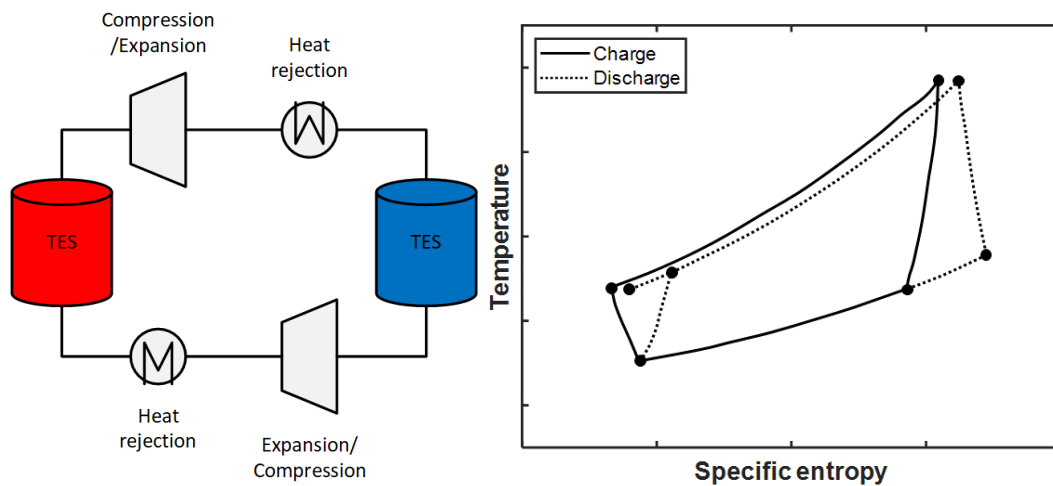


Figure 8: Process flow diagram (left) and T-s diagram (right) for a Brayton PTES.

Air [41], supercritical $CO_2$ [42], hydrogen [43] and nitrogen [44] have all been studied as working fluids for Brayton PTES. However, monoatomic gasses like argon or helium are usually selected. They both allow higher process temperatures and thus efficiency for any fixed compression ratio [45], while helium may result in lower pressure losses and better operational stability [46]. Operational

---

[5] Reversible here implies the same transformations are operated in reversed direction (counterclockwise and clockwise), during charge and discharge, but does not entail thermodynamic reversibility.

stability is also achieved through: i) one or two extra heat exchangers to reject heat generated from irreversibilities [47]; and ii) a buffer vessel to allow for gas thermal expansion [48], given Brayton PTES is a closed-loop cycle.

The typical system layout comprises two compressors and two expanders, each one dedicated to either charge or discharge [49]. Alternatively, two single devices can be used, which operate reversibly as a compressor or expander during charge and discharge [48]. Either way, high compression ratios in the machinery are key to Brayton PTES performance, which led to preferring reciprocating devices [50], with axial machines only proposed for scales above 100s MW [51]. Recent literature has been focusing on the unsteady and off-design behaviour of machinery [52], including dynamic effects and performance maps [53]. Concerning TES, most studies consider packed beds as thermal reservoirs due to low cost and temperature stability [54]. Gravel, magnetite and limestone are commonly selected among the 9 solid storage media compared by Benato and Stoppato for Brayton PTES applications [55]. TES can be either indirectly linked to the cycle via a coupling heat exchanger or directly crossed by the working fluid [38]. This latter option is more typical and results in better heat transfer; however, the storage vessel should withstand cycle pressures of up to 20-30 bar. Using an electric heater to decouple pressure and temperature values in the cycle, as Benato proposed [41], would allow containing pressure in the TES besides stabilizing turbine inlet temperature.

## *Rankine PTES*

As presented in Figure 9, Rankine PTES comprise a reverse charging cycle and a Rankine power cycle with the working fluid experiencing liquid-gas phase transition. During charge, the working fluid is evaporated, compressed, condensed – transferring heat to the hot reservoir – and finally expanded to low pressure. The working fluid in liquid state is pumped, evaporated, expanded in a turbine, and finally condensed during discharge. Like Brayton PTES, charge and discharge processes can be physically separated or share some of the components [56]. A regenerator is sometimes used to improve cycle performance, whilst also reducing performance sensitivity to turbine inlet temperatures [57]. Pressure and temperature for Rankine PTES typically vary between 1-140 bar and up to 200 °C, with cycle efficiency of 40-70%.
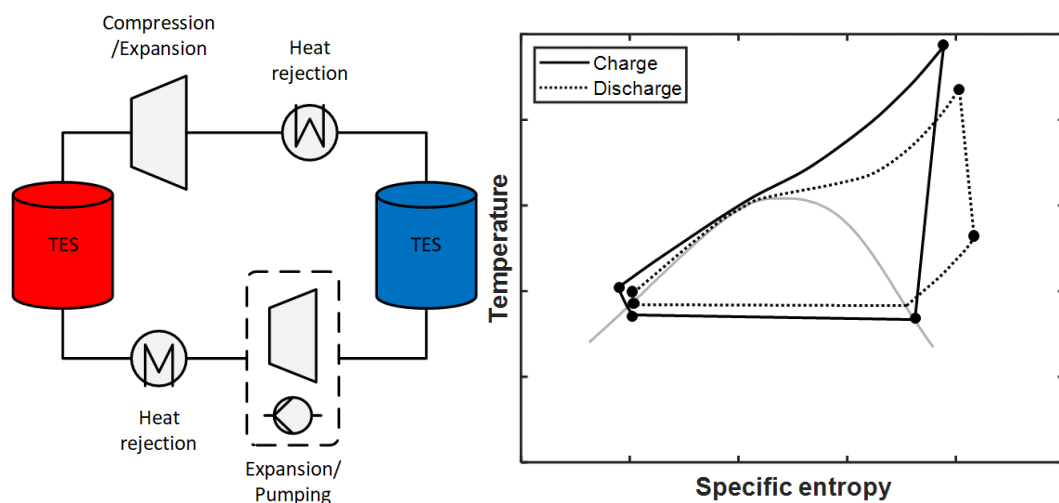


Figure 9: Process flow diagram (left) and T-s diagram (right) for a Rankine PTES.

17

Depending on the maximum temperature achieved, Rankine PTES solutions studied in the literature include stream, organic, supercritical or transcritical $CO_2$ cycles [58,59], as well as cascade cycles with ammonia and steam [60]. Phase transition of the working fluid allows saving compression work but poses challenges to effective heat transfer, which works in the literature addressed by using a latent TES to improve temperature glide matching [61], pinch analysis to optimise the heat transfer process [62], or supercritical conditions [63]. It is common in Rankine PTES layouts to only use a hot reservoir and the ambient as the cold sink/source, because of the suitable lowest temperatures values in the cycle [60,64]. However, choosing a lower temperature cold sink such as liquid natural gas was proven to increase system efficiency [65]. For the hot TES, water (pressurised, if necessary) and solar salt or other $NaNO_3/KNO_3$ mixtures are widely adopted [61,66], while an ice slurry is a popular choice for the cold TES, when present [63].

Device development to enable 2-phase or nearly-isothermal compression and expansion is an open research avenue, which Kim showed could lead to a 4-15% higher roundtrip efficiency than in the case of isentropic compression/expansion [67]. Another area of recent interest is hybrid Rankine PTES concepts featuring thermal integration with external sources of heat or cold, which is made possible by the limited operating temperature span when compared to Brayton PTES [68]. Roundtrip efficiency in these cases can surpass 100%.

### 2.2.3   Other thermo-mechanical storage technologies

Only recently, novel TMES concepts have been proposed which exploit reversible thermochemical reactions to store and release energy (see Figure 10 for a schematic of the working principle and some proposed layouts). The interest stems from the fact thermochemical reactions could, in principle, result in loss-free, 1-2 orders of magnitude higher energy density storage [69]. An example is the chemical looping energy storage by Saghafifar: an open Brayton PTES where heat is stored and released, respectively, by reduction and oxidation of a metal oxide, in a packed bed TES [70]. Energy density increase from 50-100 to 250-350 $kWh/m^3$, and, through the inclusion of thermal regeneration and an electric heater in the layout, roundtrip efficiency of 40-55% is achievable [71]. Another concept is the thermochemical battery, where a couple of metal hydrides mutually exchange heat and $H_2$ [72]. Compression work establishes the pressure difference to trigger hydrogen release/adsorption reaction during charge, while the induced $\Delta p$ between hydrides drives an expander during discharge. Conceptual analysis for the system demonstrated 31-47% efficiency and 28.2-62.6 $kWh/m^3$ energy density. Another option is the Lamm-Honigmann storage, where the steam pressure difference between a water reservoir and a water solution (e.g. $LiBr/H_2O$ or $NH_3/H_2O$) is used to generate work [73] and can be reversed by compression [74]. As with most systems involving thermochemical energy storage, studies cover material selection, but challenges for these novel TMES are related to system scale-up.
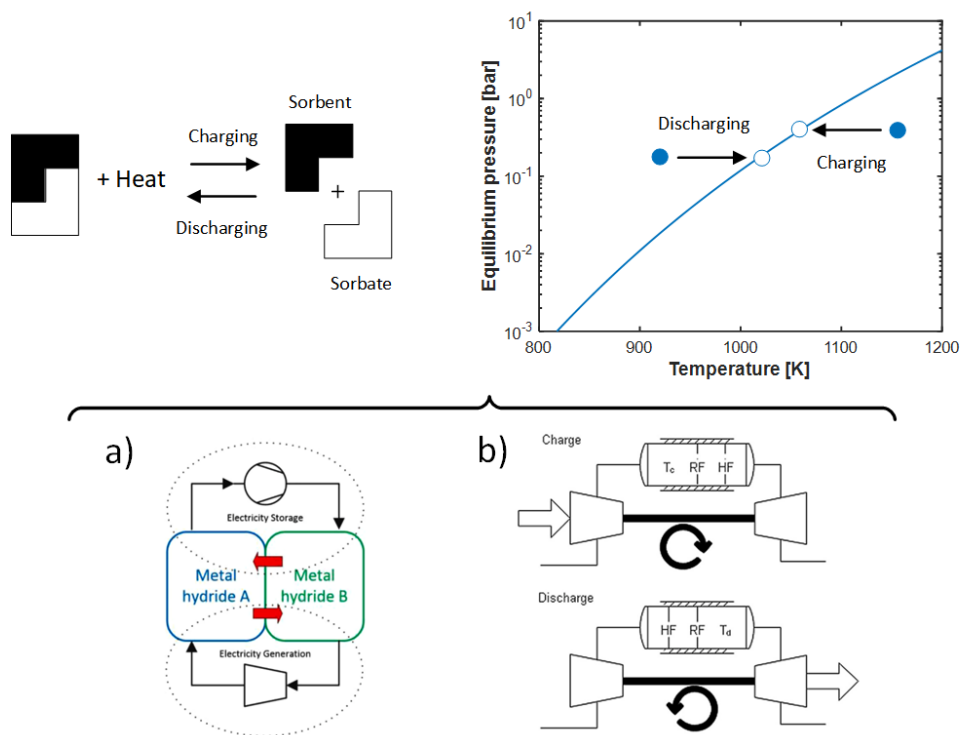
Figure 10: Summary of the operating principle and proposed application layouts of thermochemical energy storage to thermo-mechanical concepts: a) the thermochemical battery [72], and b) the chemical looping energy storage [70].

Alternatively, thermochemical storage has been widely investigated for applications involving the conversion from heat to power – such as concentrated solar power (CSP) – and thus lacking a charging phase to be considered TMES. High-temperature reactions result in large energy density [75] for the investigated oxidation [76], hydration [77] and carbonation reactions [78]. Transferring such technical solutions to TMES can leverage the acquired knowledge from literature, so far focussing mainly on material cyclability and stability [79], reactor design and optimisation [80]. Should these challenges be solved, temperature range and technical features like negligible standing losses [81] are potentially relevant for LDS. Still, the addition of a power-to-heat charging process and the extension of these thermochemical technologies to the field of TMES have not been tackled.

## 2.3 Liquid air energy storage

The use of supercritical liquid air as a storage medium was first proposed by Smith, in 1977 [82]. However, the principle started being actively investigated only several years later and, as shown in Figure 11, has quickly hit significant milestones since then. In the year 2000, Mitsubishi Heavy Industries successfully operated a 2.6 MW air-driven Rankine cycle, which showed excellent output stability [83], while researchers from Hitachi were considering a layout with a gas combustor and a concrete regenerator to enhance gas liquefaction [84]. Efficiencies as high as 70% were predicted for the system [85]. The idea started receiving attention from the wider research community and a joint venture between Highview Power and the University of Leeds, UK, led to the liquid air energy storage process being patented [86], the system being designed and finally constructed [87]. The resulting 350 kW, 2.5 MWh pilot-scale plant was the first fully integrated LAES plant in the world, which was run in 2010, setting a cornerstone for LAES development and stimulating great research interest in

the technology. After several field tests, the plant has now been relocated to the University of Birmingham for further investigations. A further 5 MW, 15 MWh pre-commercial plant by Highview Power was built and operated in June 2018 in the Greater Manchester county [88], anticipating the deployment of two LAES 50 MW plants (named CRYOBattery) in the UK and US, recently unveiled by the same company [89]. These will represent the first grid-connected LAES projects worldwide.
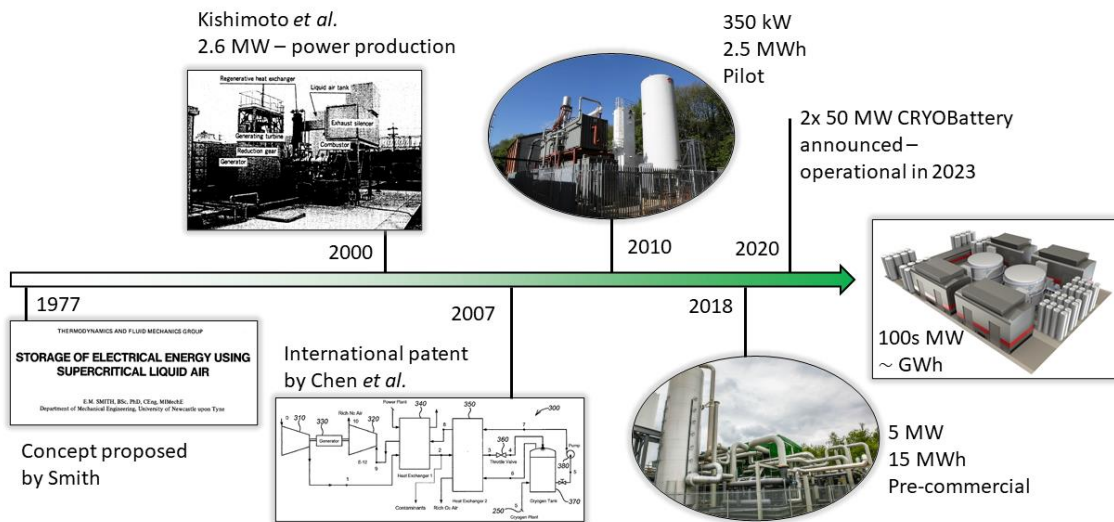


**Figure 11: Cornerstones in LAES development history – timeline.**

Figure 12 presents a model standalone and hybrid LAES plant, according to the definition from Section 2.2, to which the working principle presented in the Introduction and comprising a charging, storage and discharging process equally applies. The next sections discuss these processes, and then outline the indicated techno-economic performance for standalone and hybrid LAES plants.
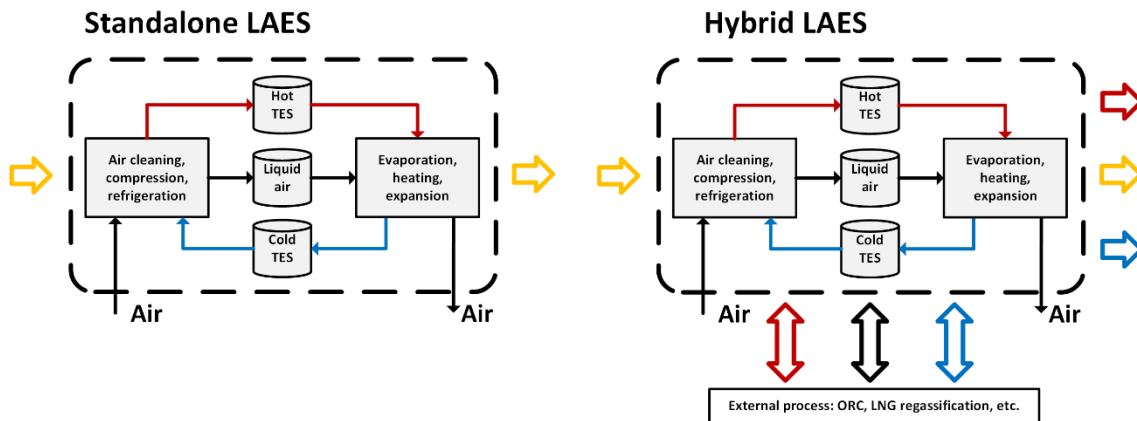


**Figure 12: Schematic representation of a standalone (left) and hybrid (right) LAES plant.**

## 2.3.1  Charging and discharging process

State-of-the-art, recuperative air liquefaction processes are used for LAES charge [90]. These cycles include the initial filtering and dehumidification of feed air by molecular sieves and a multi-stage, intercooled, compression. High-pressure, supercritical air is then brought to cryogenic temperatures in a multi-stream heat exchanger (the cold box) [91] and liquefied via expansion through a Joule-Thompson (JT) valve or a cryoturbine. The uncondensed gas portion leaving the cryoturbine is

20

recirculated through the cycle. Many alternative liquefaction layouts have been suggested for LAES application [22], but a comparative assessment by Hamdy et al. [92] demonstrated Claude, Heylandt and Kapitza outperform the alternatives techno-economically, and, indeed, are typically selected also at micro-gird scales below 1 ton/h [93].

The three most common air liquefaction layouts for LAES are reported in Figure 13. Interestingly, most of the pathways examined in the literature to improve air liquefaction performance apply to all of them. For example, the use of a cryoturbine instead of the JT valve was shown to improve system performance by up to 6.9% [94], regardless of the layout. Pressurised liquid air vessels are also beneficial: Borri et al. [93] claimed 21% lower specific energy consumption for the liquefier when storing air at 4 bar rather than ambient conditions. Values as high as 210 bar were even explored [95], although the same authors chose 18 bar in recent publications [96] for technical feasibility. Additionally, an external air expansion and recirculation circuit can be designed to match the temperature glide in the cold box [97] and minimise entropy generation. The operating pressure in the cycle can also be adjusted for the same purpose [98], but the optimal value differs based on the liquefier layout, between 70 bar [99] and up to 180 bar [100]. With the above arrangements, typical values of specific liquefaction work for LAES are around 200-300 kWh for the production of 1 ton of liquid air [97,101], which corresponds to a ~30% reduction in comparison with state-of-the-art cryogenic cycles [18].
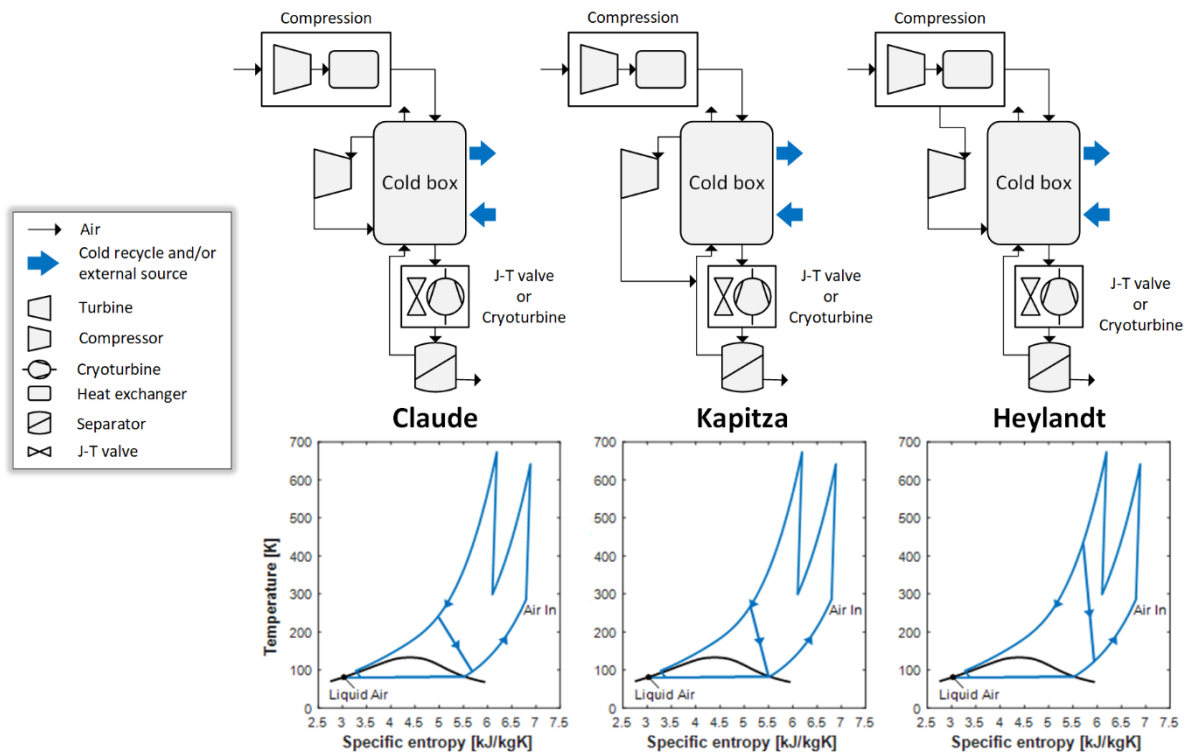


Figure 13: Most common layouts for the air liquefaction process of a LAES.

Concerning plant discharge process or power recovery unit (PRU), both Brayton and Rankine cycles (direct or indirect) have been tested to extract power from a cryogen: the best solution depends on the availability temperature of the heat source [102]. However, for LAES discharge, a direct Rankine is by far the most used solution, being it with [98] or without [94] a recuperator (see Figure 14). The number of turbine stages either matches [103] or overcomes the number of compression stages

[104] to benefit from higher temperatures, and, when increased, it allows to better approximate isothermal expansion at the expense of additional investment costs [105].

As far as the operating parameters are concerned, higher discharge pressures were found beneficial for higher specific work output and more effective heat transfer in the evaporator [106], although reducing the cold that can be recovered [107]. Values above 50 bar and up to 200 bar are typically selected [108]. Effects of supercritical heat transfer during LAES evaporation were investigated by Yu et al. [109], who suggested an optimal heat exchanger configuration with two consecutive stages where the mass flow rate of the secondary fluid can be adjusted to overcome pinch point limitations. Depending on the chosen layout and operating parameters for the PRU, specific work output can be between 330 and 550 kJ/kg.
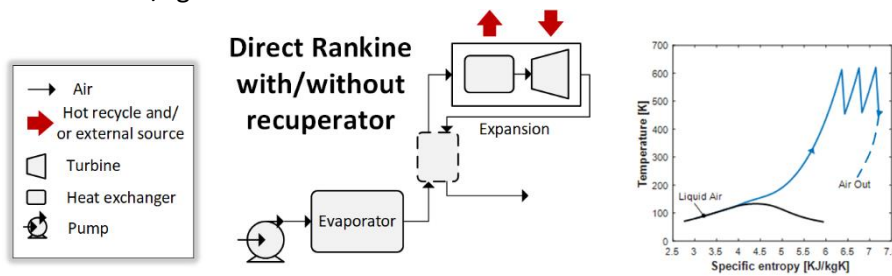


Figure 14: Typical system layout for the power recovery unit of a liquid air energy storage.

### 2.3.2 Hot and cold thermal recycle

Along the LAES process, compression heat is generated during air liquefaction, while high-grade cold from evaporation is released by the power cycle. A suitable heat transfer fluid and TES arrangement can be employed to recover such thermal streams, reusing the heat for power generation and the cold to support air liquefaction. This way, the charge and discharge subprocesses are coupled through a so-called hot and cold recycle; this is illustrated in Figure 15.
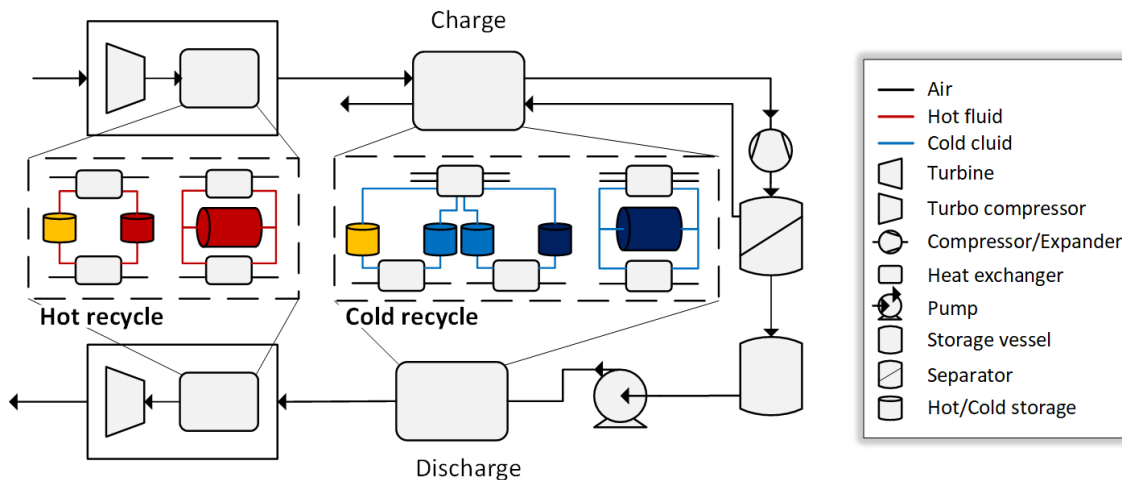


Figure 15: Hot and cold recycle coupling LAES charge and discharge subprocesses.

The traditional storage material and layouts investigated for hot and cold recycles are presented in Table 3. Early literature focussed on cold recycle to boost LAES efficiency [110]. Consensus is now on its use to provide extra cooling in the cold box, although air precooling upstream compression was also proposed [111] Cold temperatures ~90 K mean material stability is required, hence solid

regenerators and packed beds of rock have been considered [112] and experimentally investigated [113]. The alternative is a two-fluids arrangement using liquid TES, with no clear view on which one is best [114]. Thermal efficiency as high as 95% has been reported for packed beds [115], but thermocline effects mean larger volumes are necessary [116]; special designs such as partitioned TES [117] or radial flow [118] were proposed to alleviate this. Conversely, liquid TES solutions are more compact [98], but different fluids are needed to cover different temperature ranges, such as propane and methanol [99], R218 and methanol [119], or propane and R213, which led to 91% thermal efficiency for a small-scale test facility [120], thus showing slightly higher losses than packed beds. Similar technical solutions with packed beds [121] or two-tank layouts [122] have been considered for hot recycle, with the aim of using the compression heat released during liquefaction to increase turbine inlet temperature [123].

Table 3: Most commonly used TES media and technological solutions for LAES hot and cold recycle.

| Medium | Technical solution | Specific heat [kJ/kgK] | Density [kg/m³] | T range [K] | Notes |
|---|---|---|---|---|---|
| Quartzite | C, PB | 0.5-0.6 | 2560-2650 | 80-293 | Variable properties; cost ~0 |
| Propane | C, 2-T | 1.9-2.3 | 732-581 | 93-210 | High-grade cold only |
| R218 | C, 2-T | 0.8-0.9 | 1711-2137 | 93-210 | High-grade cold only |
| Methanol | C, 2-T | 2.2-2.4 | 904-810 | 210-293 | Low-grade cold only; cost ~0.4 $/kg |
| R123 | C, 2-T | 0.9-1.0 | 1477-1727 | 185-293 | Low-grade cold only |
| Water | H, 2-T | 4.2-4.4 | 890-998 | 300-450 | Pressurisation needed, cost ~0 |
| Solar salt | H, 2-T | 1.6 | 1900 | 493-873 | Solidifies for lower T, cost ~0.5 $/kg |
| Diathermic oil | H, 2-T | 2.2-2.4 | 750-850 | 293-630 | Cost ~1 $/kg |
| CaLiNaK | H, 2-T | 1.7 | 1917 | 373-673 | Solidifies for lower T |
| Steatite | H, PB | 0.8-0.9 | 2680 | 250-573 | Variable properties; cost ~0 |

Abbreviations: H: hot recycle, C: cold recycle, PB: packed bed regenerator, 2-T: two-tanks liquid TES

At system scale, cold recycle significantly affects LAES performance. A comparison from Peng et al. [101] showed that the same 5% thermal loss results in a 1 percentage point reduction in roundtrip efficiency when applied to the hot recycle, but a 9 percentage point reduction when affecting the cold recycle. Phase change materials have recently been shown to improve LAES performance through enhanced operation of the high-grade cold storage (HGCS) [124], with less than 3 years return on investment [125]. Although no conclusive techno-economic comparison of different cold recycle layouts and materials is available, these results prove high technical efficiency of HGCS should be privileged. Concerning compression heat, thermodynamic losses and the asymmetric number of stages result in 20-40 % excess availability [126], thus justifying the low sensitivity of plant performance on effective hot recycle. Yet, rejection of such extra heat is unavoidable in a standalone LAES, and, together with component irreversibility, it represents the biggest thermodynamic loss [98]. Hence the rationale for the external use of such thermal stream in hybrid LAES configurations.

### 2.3.3 Standalone and hybrid LAES plant performance

Summaries of the most relevant studies dealing with standalone LAES and hybrid LAES, as reported in Appendix A, show that interest has shifted from standalone to hybrid LAES solutions, which now represent the majority of investigated plants. In hybrid LAES, external fuels and/or heat/cold thermal streams enhance plant techno-economic performance [127,128]. Alternatively, LAES can be coupled

with nearby processes such as power plants, LNG terminals and organic Rankine cycles (ORC), creating opportunities for system co-design, symbiosis and mutual performance enhancement [129,130]. Finally, a recent research thread for hybrid LAES involves the provision of additional functions (thermal energy, industrial gasses, etc.) to nearby processes [131,132].

## *Technical performance*

Figure 16 compares standalone and hybrid LAES based on their predicted efficiency; boxes span from 25th to 75th percentile and whiskers include 99.3% of the plants analysed from the literature. For standalone LAES, roundtrip efficiencies vary between 40% (18%, if ambient air is the heat source for reheating [128]) and 67% for very efficient cryogenic pumps [94] and pressurised storage vessels [133]. Hybrid plants display the largest variability and achieve higher values of roundtrip efficiency, especially when including combustion [127] (reaching over 900 kJ/kg specific work output), integrating LNG regasification terminals [134] (with liquefaction work as low as 580 kJ/kg [88] and possible full air liquefaction [130]), or nuclear plants [135]. Efficiency values can surpass 100%, in these cases. On the contrary, exergy efficiency is rather stable for both standalone and hybrid LAES, sitting between 55 and 65%. LAES plants with bottoming ORC or Kalina cycles achieve the best values [136]. Conversely, hybrid LAES implementing trigeneration [137] reach the highest energy efficiency values (up to 88%) but, because of the quality of different energy vectors, exergy efficiency is lower compared to other concepts. Nonetheless, a trigenerative concept was proven to bring primary energy savings and lower carbon emission [138].
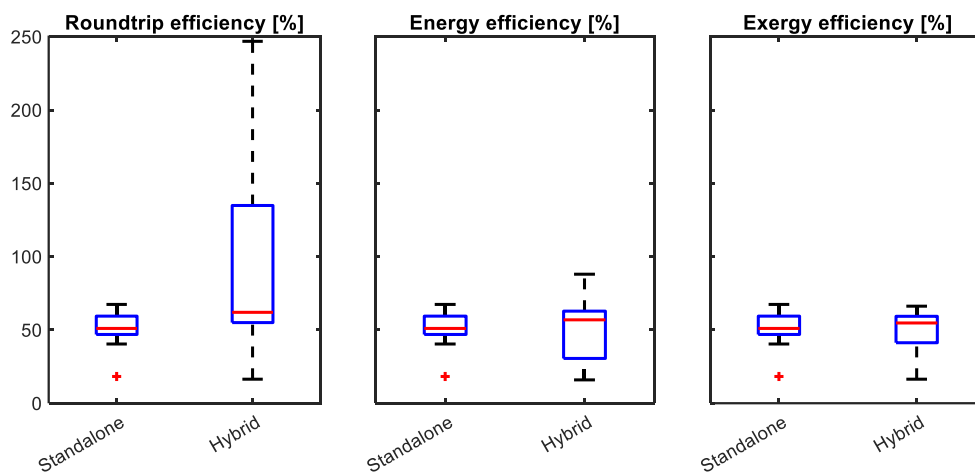


Figure 16: Boxplot with typical values of roundtrip, energy and exergy efficiency for standalone and hybrid LAES concepts.

Reported efficiency values from the literature are all obtained under steady operation. They show that, apart from the full use of compression heat with LAES-ORC, the main reason to prefer hybrid to standalone LAES concepts relates to the use of external waste streams or the external provision of additional functionalities. Both conditions are location-dependent. There is no significant difference in terms of exergy efficiency, i.e. thermodynamic efficiency of the conversion processes. LAES scale is similar across studies and plant layouts, involving 10 to 100 MW power output, 10-50 MW input (corresponding to 8-10 h overnight charge) and 2-8 h discharge capacity.

*Economic performance*

Results from the studies addressing LAES investment costs are reported in Figure 17 for standalone plants, and Figure 18 for hybrid concepts; figures range significantly due to different adopted methodologies. These include using cost functions for individual [139] or groups of components [140], manufacturers' quotations [97] and specific costing software [141], as well as combinations of all the above [142]. Morgan et al. [97] also included a learning rate of 17,5% – despite the off-the-shelf nature of LAES components – and derived the power-specific costs for a 10th-of-a-kind standalone LAES at 995 £/kW. Three costing approaches were compared in [139] to add a confidence interval to investment cost predictions. Results are in line with other studies (see Figure 17) and projections for TMES [143], although obtained for a rather small, i.e. 12 MW, LAES plant. Larger scales would further decrease specific capital expenditure (CAPEX), stressing the importance of considering appropriate system sizes for CAPEX estimation and comparison purposes. Indeed, specific investment more than halved, from 5 to 2.1 k$/kW, for a 12 MW/50 MWh LAES, compared to a 2 MW/11.5 MWh plant [139]. Similar considerations apply to a 100 MW and a 300 MW plant, whose specific costs were estimated as 2100 and 1400 €/kW [92].

Concerning investment costs breakdown, references agree on the large impact of power equipment (turbines and compressors) and the major contribution by the liquefaction subsystem (45-70% of the CAPEX); the share of liquid air and TES tanks is limited below 10% [139,140]. By boosting technical performance and reducing liquefaction power rating, efficient cold recycle would also enhance LAES economy. Hamdy et al. [142] described the techno-economic trade-off between roundtrip efficiency and investment cost, showing how compression pressure, reheater outlet temperature and heat carrier fluid can be adjusted at design stage to prioritise either of the two. Specific costs for a 100 MW/400 MWh standalone LAES plant could drop from 2087 €/kW to 1270 €/kW, under a moderate efficiency reduction from 47% to 40%.
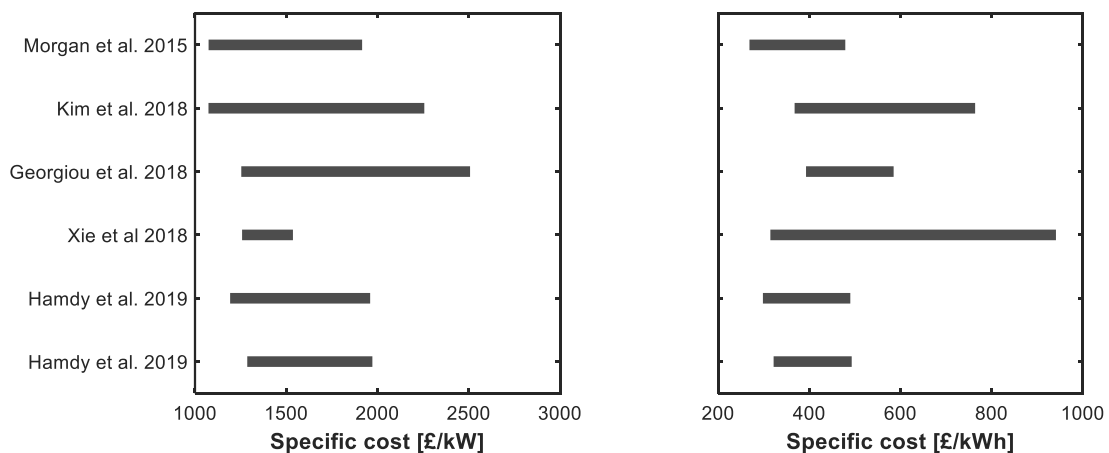


Figure 17: Predicted investment cost (CAPEX) in studies on liquid air energy storage from the literature.

Waste heat utilisation or fuel combustion in hybrid LAES leads to specific cost values consistently on the lower hand of the predictions for standalone plants. Waste heat recovery boosts LAES power output and financial viability at a limited marginal cost, depending on the associated temperature level [144]. Fuel combustion has higher associated costs but is well compensated by the increase in power output, so that the cost per peak energy generation for a hybrid LAES peaker is comparable

with natural gas plants [145]. Cost projections for other hybrid plants such as LAES-PTES [24] or CAES-LAES [146] are also lower than the separate costs of the two technologies. The only hybrid LAES concept with significantly higher specific investment cost is in the case of LNG integration, mostly due to the contribution of heat exchangers with large associated duties. Results report 2164 $/kW for the optimised LNG-LAES plant [147] and 2800 $/kW for the non-optimised system including an ORC [148].
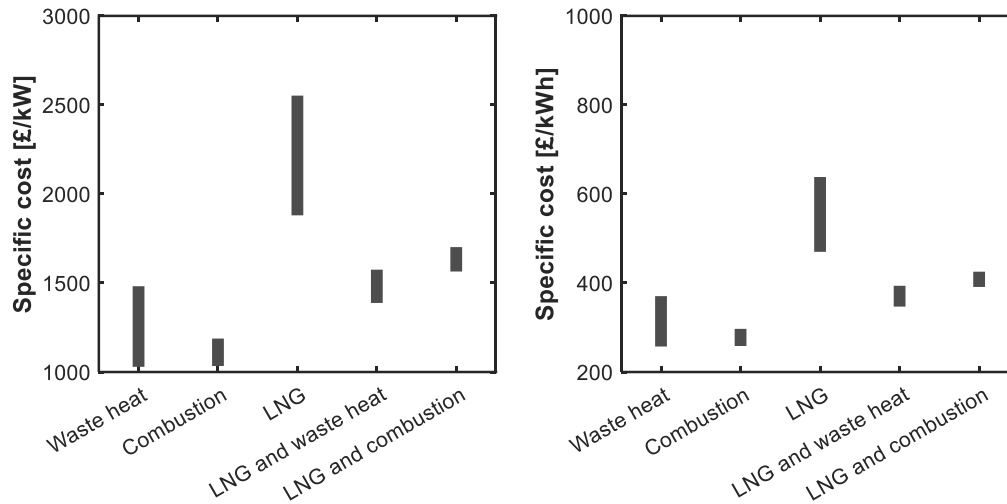


Figure 18: Predicted investment cost (CAPEX) in studies on hybrid liquid air energy storage from the literature.

## 2.4 Path to commercialisation of thermo-mechanical energy storage

Besides the few CAES plants in operation, Novotny et al. [149] reviewed 30 announced, pilot and in-construction projects, showing TMES is currently entering the commercialisation stage. However, future uptake hinges on identifying favourable business cases where the storage functions are valued to pay back investment costs over the project lifetime. Since compensation schemes are decided within the context of local regulatory frameworks and market structures [150], it becomes essential to contextualise TMES techno-economic performance with the energy market landscape in which it is required to operate. This section defines, first, the balancing services of interest for TMES and the potential storage requirements in energy systems with large RES penetration. Then, it discusses works where the broader energy system features are included in the analysis of LAES and LAES operation, hence realising its value *within* the energy system. Two keywords to define in this context are *integration* and *application*:

- **Integration**: identifies the TMES plant-energy system pair, whereby TMES operates by providing selected services, through the exchange of electricity and/or thermal streams with the energy system.
- **Application**: identifies the specific service or the set of services provided by TMES to the energy system in each integration case.

### 2.4.1 Primer on balancing services

Power systems rely on the principle that supply must exactly match demand at any point in time [151]. By storing surplus and injecting power upon request, energy storage helps balance supply and demand and can contribute to power system orchestration [152]. Such contribution may be monetised in structured electricity markets. However, because of relatively recent storage adoption, evolving power systems facing new and diverse challenges and fundamental differences between storage and traditional generation assets, existing energy markets are seldom designed to reward the full value of energy storage to the system [153]. In some cases, benefits to different grid players may be compensated through contractual agreements between parties, such as contracts for energy price caps with retailers [154] or firm capacity guarantees with RES generators [155].

Figure 19 presents a general landscape of balancing services storage can provide – minor market-specific variations are possible. In there, balancing services included in the present thesis have been highlighted. Additional storage benefits such as RES generation firming, reduction of overcapacity requirements, transmission and distribution upgrade deferral pertain to the area of power system planning rather than balancing and have therefore been disregarded.
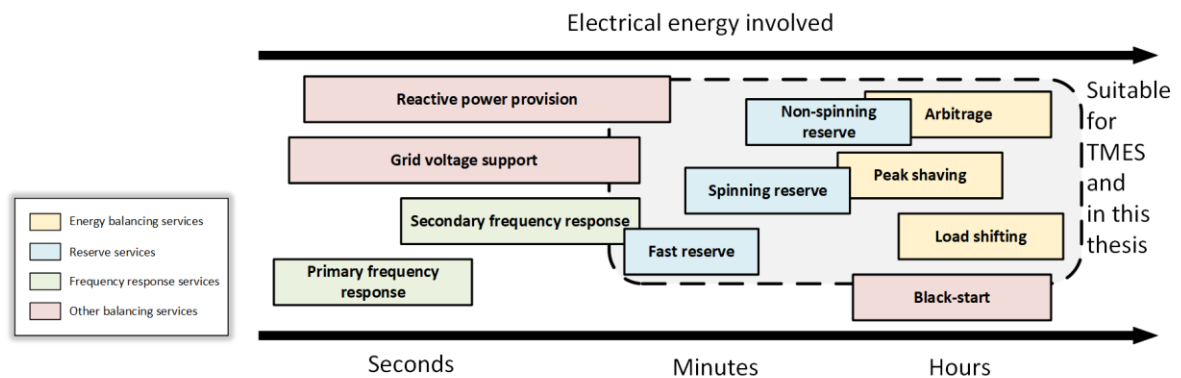


Figure 19: Power and energy balancing services supporting power system orchestration that energy storage can provide.

*Energy balancing services*

Energy balancing services, in this thesis, denote peak shaving, load shifting and arbitrage. They all involve the time shift of large electricity portions, a timeframe of 30 min or more, and are scheduled in the day-ahead market [156]. Their difference lies in the driver for operation. Arbitrage involves charging the storage when the electricity price is low (or even negative, as registered for the European energy exchange, due to wind penetration [157]) and discharging it when high. Price differentials generate a revenue stream for the storage owner [158]. Conversely, the driver for peak shaving and load shifting is the time-varying electricity demand; more specifically, excess generation (when storage is charged) or excess load signals (when storage is discharged). Associated benefits are a steadier and more efficient operation of generating assets and the limited use of expensive peakers, resulting in cost cuts that favour both the end customer and the system operator [159]. It is worth noting that arbitrage results in similar advantages since supply-demand imbalance is often aligned with electricity price fluctuations; however, especially for large RES penetration, the shape and extent of these latter ones are likely to change in the future [160].

### Reserve services

Reserve services are designed to help the grid cope with unforeseen mismatches between generation and demand. They are sometimes included in a capacity market [161] and involve the delivery of active power to the gird in response to a dispatch call from the system operator [162]. Specifications to be met by a supplier to provide each of these services require a fast-enough response time, a minimum sustained period of power output and capacity volume committed; exemplary values for the UK electricity market are reported in Table 4. In addition, reserve service providers must be available within tendered availability windows – typically a morning and an evening window – which may vary throughout the year [163]. The contractual revenue streams include an availability fee (£/MW/h), paid for the periods the unit is made available, a positional fee (£/h), paid upon call by the operator, and a utilisation fee (£/MWh), for the energy injected following a delivery instruction [164].

Table 4: Typical specifications for accessing different reserve services in the UK electricity market [165,166].

|  | STOR | FR |
|---|---|---|
| Response time* | ≤ 240 min | ≤ 2 min |
| Minimum sustained period | 120 min | 15 min |
| Minimum power commitment | 3 MW | 50 MW |
| Minimum delivery rate | - | 25 MW/min |

* National Grid also adds that "*response times within 20 minutes are preferable*", and indeed technical requirements have been modified so STOR providers must now be able to respond to an instruction within a maximum of 20 min.

### Frequency response services and other balancing services

In the event of a mismatch between supply and demand, the grid frequency deviates accordingly. Frequency response services are needed to ensure the frequency is restored at its rated value, as this is a requirement for stable power system operation [152]. Primary frequency response represents the quickest reaction to the imbalance to be provided within 10 s from the event, for up to 20 s. Secondary response kicks in within 30 s after the event, for up to 30 minutes [167]. Service providers must operate either a reduction or increase in their power output when instructed, but, other then reaction time, there is typically no minimum capacity obligation for participating in frequency response services. Payment schemes may include a holding fee (£/h) for the provider availability and a response fee (£/MWh) remunerating the positive or negative energy delivered [164]. Figure 20 illustrates how different balancing services concur in stabilising grid frequency over different timescales.
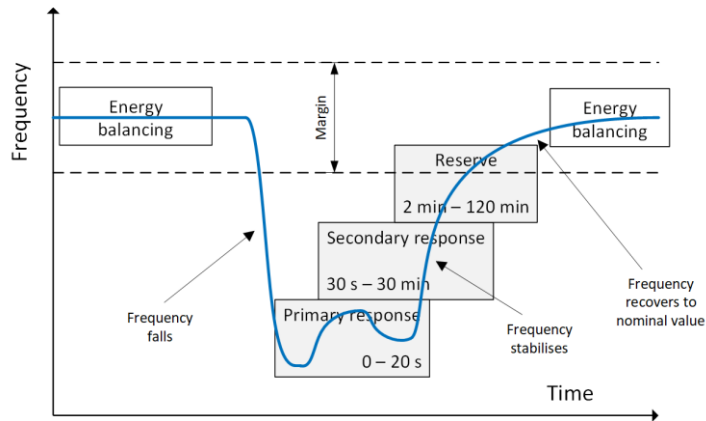
**Figure 20: Reserve services supporting the grid in the event of a frequency drop.**

Other balancing services include reactive power provision for grid voltage support and black start to restore energy systems or to activate and bring online large generators [152]. Market schemes are typically in place to compensate for the delivery of such services. However, reactive power provision is paid only a utilisation fee, and black start is rewarded only when required; so these additional balancing services were not considered in this thesis.

### 2.4.2   Long-duration storage requirements for a highly decarbonised energy system

Similarly to Zhang et al. [168], long-duration storage (LDS) identifies in this thesis technologies with above 10 h capacity, capable of energy balancing over multi-day periods and up to seasons, to cover, for example, wind droughts [169]. Although 80-95% storage benefits are for energy shifts of 8 h or less [168], studies for Alberta under an 80% RES penetration found the events contributing the most to storage charging are significantly longer and up to more than 60-80 h or 5 consecutive days [19]. For the UK supplying the aggregated demand for power, heating and transportation in 2050, with a 100% RES mix, overproduction can be stored 82% of the times [170]. Similar studies for the US predict equivalent storage of up to 5 days of average demand for 80% RES penetration in California [171] and 72 h storage to cover 99.9% load over four years, with only 80% RES overcapacity [172]. Therefore, LDS relevance is tied to RES-dominated scenarios, where systemic overgeneration will occur in some seasons and energy deficit in others and be exacerbated by heat electrification [153].

LDS can also ensure decarbonisation goals are met cost-effectively. Storage and other flexibility options all have projected costs well below those of generation overcapacity to balance supply and demand [15]; however, storage can reduce backup capacity needs to 20% of the average demand, while transmission only goes as far as 30% [8]. Also, for above 90% RES penetration, storage adoption made meeting demand 40% cheaper than transmission expansion [6]. In Europe, LDS covering 5% of the annual energy demand was necessary to contain the costs of the last 5-10% emission reduction [173], yielding a levelised cost of electricity for a fully renewable power system of 9-12 € cent/kWh. Interestingly, LDS penetration was deemed the most sensitive parameter for electricity cost reduction [174], and scenarios with batteries alone are always the most expensive [172].

Driven by its future relevance, few studies focussed explicitly on determining the LDS techno-economic requirements and design space. As long as storage uptake is small compared to the installed RES capacity, storage efficiency does not influence significantly LDS value [175], so design

29

space criteria are mostly economic. Sepulveda et al. [176] found LDS capacity-specific costs below 20 USD/kWh can reduce electricity costs by over 10% and estimated at 1 USD/kWh the target to displace all low-carbon generation. Elsewhere, the combination of power and capacity costs of 1000 USD/kW and 20 USD/kWh and a duration of 100 h was found sufficient to enable steady power output 100% of the time [177]. Albertus et al. [178] argue that for above 90% RES penetration, LDES systems with greater duration than 100h will be needed, with capacity-specific costs below 40 USD/kWh and power costs in the range of 500-1000 USD/kW. These studies concur with the identified requirements which suitable LDS technologies should meet to sustain decarbonisation. Interestingly, power and capacity costs are not dissimilar from the ranges described for LAES and other TMES solutions, in Section 2.2 and Section 2.3. Yet, different power/capacity requirements from values generally addressed in the literature make the bottom-up assessment of TMES solution for LDS a not-fully-covered area worthy of further investigation.

### 2.4.3 LAES integration with the energy system

Literature studies on LAES integration with the energy system, as summarised in Table 5, are significantly less than techno/economic system assessments reviewed in Section 2.3. Applications currently investigated for LAES span from arbitrage provision in the day-ahead market [187] to arbitrage and reserve services provision in the intra-day market [188] to supply of electricity, heating and cooling in a trigenerative configuration [142]; they are summarised in Figure 21. As a developing storage technology, no single application has yet been designated for LAES. However, the independent sizing of charge, discharge and storage sections allows tailoring the plant to the specific integration settings and operation strategies, thus fostering business cases across applications [179]. For example, a 3 h charge and long-discharge plant was preferred to the common 8 h charge setup to accommodate large photovoltaic generation in the central part of the day [100], while storage capacities above 4-5 h can be cost-effective when LAES is used for load-shifting (with daily or weekly scheduling [180]). To this end, plant sizing can be obtained directly, e.g. through a genetic algorithm [140], or indirectly, through sensitivity analysis.
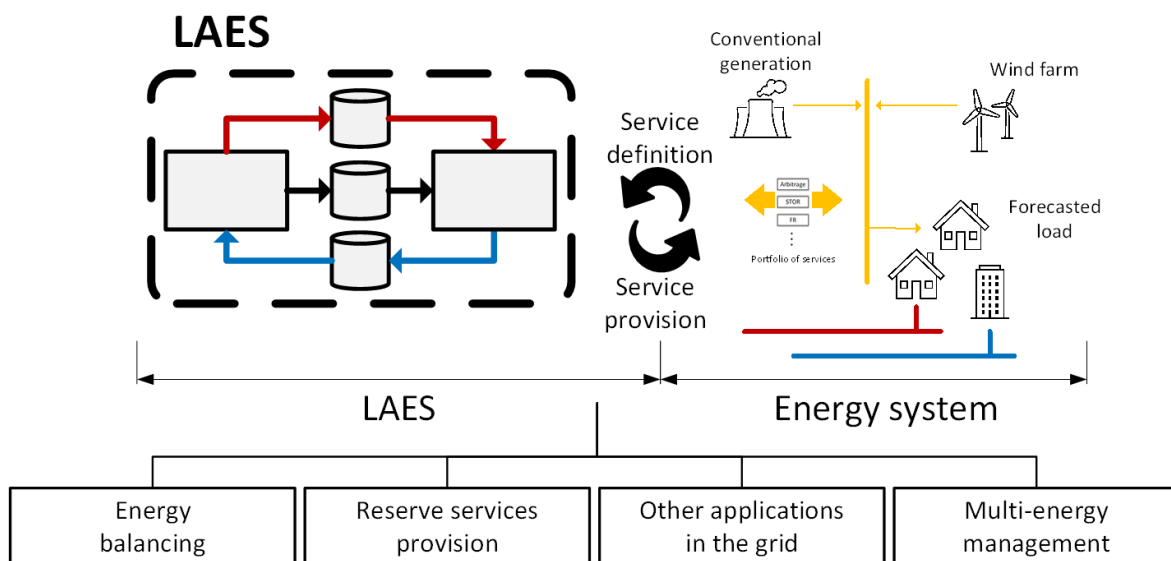


Figure 21: Typical applications considered in LAES integration studies with the energy system.

### Energy balancing applications

Most studies from Table 5 consider arbitrage as the chief operation strategy for LAES, notably concluding that this is not sufficient for financial viability in the absence of subsidies [181] or waste heat integration [179]. Similar results were already described for other grid-scale storage technologies [182] or even batteries [183]. A peak-to-valley price ratio between 3.2 and 4.4, as indicated by Khani et al. for LAES profitability, is currently too high for the day-ahead market [181]. In the absence of significant price modification from large RES uptake [184] and long scheduling horizons with high associated uncertainty in electricity price predictions [180], other applications should be explored to make the financial case for LAES.

### Applications for reserve service provision

As discussed, storage participation in reserve service markets necessitates sufficiently large scales and capacity, fast power delivery and rapid output adjustment when requested. Field tests for LAES showed the PRU can deliver power output within 2-3 min from instruction [112] and follow 5 min duration load ramps with 99% compliancy [185]. At 100s MW scale, the ramp rates from gas turbine manufacturers spanning from 20 to 50 MW/min [186,187] can be used as a reference for LAES, thus showing reserve service markets are suitable for LAES and can be accessed for further revenues. Xie at al. [140] showed 10% to 30% higher revenue, depending on plant size, from providing short term operating reserve (STOR) in the UK market. Energy and reserve services participation yields cost reductions between 20 and 40% for a 10 MW air separation unit with power production [188]. Based on these few studies, reserve provision seems a clear avenue to boost LAES profitability.

### Other applications within the grid

Other studies aim at quantifying LAES benefits beyond power system stability through selected flexibility indicators. These include a reserve margin increase from 17.7 to 21.4%, showing steadier electricity supply thanks to the operation of a LAES-LNG plant [189], resilience improvement with only 0.4 hours/year loss of load expectation and a loss of load probability of 39.3 events per year [190]. Alternatively, the level of energy import or level of RES penetration in a microgrid can be used as a proxy for lower dependence on the grid [191]. Although quantifying benefits and values from LAES, limitations of these studies lie in the local nature of the assessment and the fact no remuneration to the storage owner is considered to assess the LAES integration business case.

### Application as a multi-energy management asset

Several works look at hybrid LAES as a means for multi-energy management, absorbing or generating thermal streams alongside electricity. For microgrid applications, the operation of LAES over electricity and cooling provision can make it more economically attractive than a battery [192], and some studies even found LAES could be an economically viable option for cold storage only at scales above 500 MWh [193]. LAES integration with refrigerated warehouses is also currently under investigation by the CryoHub consortium [194,195]. Similarly for heating, compression heat utilisation in a co-generative LAES was shown by Wang et al. [131] to bring about 10% extra revenues to the electricity sales, whereas a trigenerative LAES supplying heating, electricity and cooling could reach a payback period within 5 and 7 years [137]. As the study of multi-energy LAES operation is currently in its infancy, with the majority of works exploring the vector-coupling potential for other

TMES such as CAES [196–198] or PTES [199], more work is required to characterise the potential and limitations for this kind of LAES integration.

**Table 5: Summary of the reviewed studies dealing with energy system integration of LAES.**

| Reference | Type of integration | Methodology | Research questions | LAES plant | $\eta_{RT}$ | Findings | Notes |
|---|---|---|---|---|---|---|---|
| Khani *et al.* 2015 [181] | ES – Ontario open retail electricity market | MILP optimal scheduling | Profitability, subsidy scheme, planning horizon | Standalone 57-100 MW | 60%* | Not profitable unless subsidised, wrong price prediction hinders revenues | Arbitrage only LAES centric model |
| Zhang *et al.* 2015 [188] | ES + industrial gas production – ASU-PRU integration | MILP optimal scheduling | Integration benefits | Decoupled ASU-PRU 10 MW | 70%* | 10% relative savings, suitable for underutilised ASU | Arbitrage and reserve Robust optimisation No recycle PRU-ASU |
| Ahmad *et al.* 2016 [200] | ES + air conditioning from liquid N₂ - residential | Techno-economic assessment | Techno-economic viability of 5 system layouts | Only discharge 10 kW | N.A. | Profitable vs conventional HVAC | Not a LAES, small scale External use of high-grade cold |
| Tafone *et al.* 2017 [201] | ES for chiller operation – cooling load provision | Techno-economic assessment | Profitability | Standalone | 45%* | Profitability only for high price differentials and LAES efficiency | Parametric analysis Introductory assessment |
| Comodi *et al.* 2017 [193] | Cold TES | Multicriteria assessment | Comparison with other cold TES solutions | Standalone 1-21 MW | 25-60% | Competitiveness at large scale | Based on ideal conversion parameter |
| Zamani-Gargari *et al.* 2018 [190] | ES – LAES and wind farm | Monte Carlo simulation | LAES contribution to system reliability | Standalone 5-10 MW | 70% | LOLE and LOLP decrease linearly with more LAES | Technical aspects of grid support only |
| Xie *et al.* 2018 [140] | ES – UK energy market | Optimal dispatch algorithm + GA for independent sizing | Profitability of decoupled LAES | Standalone 50-250 MW | 60%** | Extra revenues, large scales needed, waste heat boosts PBT from 25 to 5 years | Arbitrage + STOR |
| Wang *et al.* 2018 [202] | ES – multi-energy hub | MILP optimal scheduling | ES operation in realistic multi-energy setting | Standalone 350 kW | 60% | LAES smoothens load peaks | Simple LAES black box model Small scale |
| Kalavani *et al.* 2019 [191] | ES – ASU + PRU with wind farm | MINLP optimal scheduling | Local storage value in presence of DR schemes | Standalone 50 MW | 70% | Revenues: +33%, cost of generation: -8% | No recycle PRU-ASU One day horizon |
| Mazzoni *et al.* 2019 [192] | ES + cold TES – LAES in microgrid | MIQP optimal scheduling | LAES comparison with a battery | Standalone 300-2000 kWh | N.A. | Contribution to cooling supply, LAES convenient for large sizes | Functional dependence cooling-power output |
| Lin *et al.* 2019 [179] | ES – UK energy market | Optimal dispatch algorithm + GA for independent sizing | Expected NPV for different LAES sizes | Standalone 50-200 MW | 60%** | Large scales needed, waste heat crucial, PBT from 40 to 10 years | Arbitrage only |
| Kalavani *et al.* 2019 [203] | ES – ASU + PRU with wind farm and microgrid | 2-stage, stochastic optimal sizing and operation | Profitability and best independent sizing | Standalone Up to 10 MW | 70% | 15% overall cost reduction for 7 MW, 35 MWh best design | LAES enables RES uptake in local settings |

33

| Legrand et al. 2019 [100] | ES - Spanish power grid | Residual load analysis | LCOE in future scenarios with high PV penetration | Standalone | 51.2% | LCOE is 150 €/MWh, energy is charged during the day, adaptability to generation mix | Ideal LAES efficiency Aggregated LAES capacity nationally |
|---|---|---|---|---|---|---|---|
| Georgiou et al. 2020 [204] | ES – European power grid | System-level unit commitment | LAES value for different penetrations, comparison with PTES | Standalone 12 MW, 50 MWh | 55% | Storage value 2000 £/kW, decreasing for higher penetrations 5-15 GW required | Role of power/capacity ratio Contrast with other flexibility measures |
| Gao et al. 2020 [137] | Trigenerative LAES – Regional scale | Techno-economic assessment | Technical-economic potential | Hybrid 2 MW | N.A. | Electrical efficiency 40-48%, LCOE 0.11$/kWh, dynamic payback period 4-6 years | Parametric analysis on plant layout Conversion efficiency varies with seasons |

\* Sensitivity analysis on the value

\*\* With waste heat recovery the value increases

\*\*\* Rated value – it changes with operation

## 2.5 Assessing energy storage value through models

Optimisation techniques are often employed to assess storage integration with the energy system, typically by optimising storage operation, sizing, or both [205–207]. In these studies, TMES is considered along with several interlinked users, other generation and energy conversion assets, networks, etc. Such inherent complexity in the interactions to be captured implies a trade-off between model accuracy and mathematical tractability. Hence, there is no single established energy storage or energy system model, but rather model features should be case by case tailored to the specific aim of the analysis [208].

A broad spectrum of modelling and optimisation techniques has currently been applied to study storage value in the energy system. Energy system components are typically treated as black-box models and described by constant conversion parameters [209], piecewise linearisations [210], convex operating regions [211] or fully non-linear characteristics [212]. Networks (electrical, thermal etc.) are often 0-dimensional entities with a constrained capacity [213]; more refined models include network topology – through a 2-D description of the district or the associated incidence matrix – power losses and dynamic behaviour [214,215]. Also, since distributed resources are of great interest, aggregation techniques are widespread [216], including energy hubs, independent microgrids, and virtual power plants.

### 2.5.1 Optimal operation and optimal design problems

The problem paradigms for optimising storage integration with the energy system are presented in Figure 22. Optimal operation problems deal with how to best schedule a given set of generation, conversion and storage assets to fulfil the services required by the users. MILP optimisation is typically adopted, with integers representing plant on-off status or storage charge/discharge. High time granularity is possible for operational problems, which enables tackling specific aspects of service provision: examples are reserve services and demand response constraints [154], transients in building envelope [217], highly nonlinear off-design component behaviour [218], or the flexibility from leveraging district heating networks capacity and heat-electricity cross-coupling [219]. Model time resolution can vary from hours to 5 minutes, depending on technical and energy market constraints considered [154]; rolling horizon optimisations are also used to adjust dispatch based on the unfolding scenario [220,221].

Optimal design problems involve the best choice and sizing of generation, conversion and storage units and transmission networks to supply users' needs. Because design problems are often discrete in nature [222], modelling frameworks adopted include mixed-integer linear and nonlinear programming, Monte Carlo techniques, particle swarm optimisation [223] and genetic algorithms [224]. Hourly timesteps are typical, but downsampling and clustering techniques are used for design purposes to select representative design days [225] and limit the number of cases [226]. Since environmental and financial performance are the main criteria driving energy system design and both are intertwined with operation, design optimisation is often jointly addressed with operation (see Figure 22) [227]. Fully coupled approaches have been followed where system design and operation are determined simultaneously and treated as a unique coupled problem [228]. However,

this approach may pose limits on problem complexity; alternatively, system design and operation can be decoupled and treated as two nested optimisations through multi-layer algorithms with a master-slave structure [229].
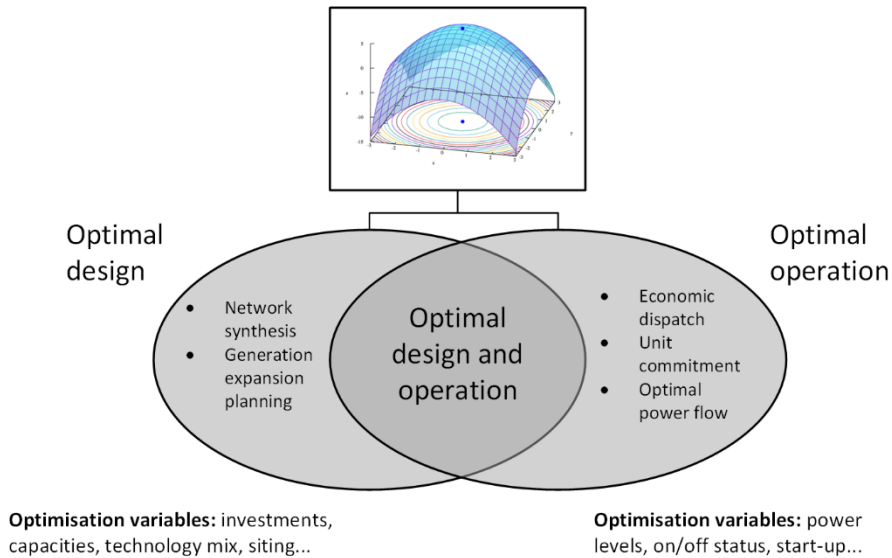


**Figure 22: Optimisation frameworks for storage integration studies and some exemplary applications to the power system.**

## 2.5.2 Thermo-mechanical energy storage modelling approaches

The simplest and most widespread approach to model storage integration with the energy system is through a battery-like formulation. This consists of characterising storage with its capacity and constant conversion efficiency parameters for charge and discharge; a standing loss may also be included. Then, a transient energy balance, minimum and maximum capacity and power constraints fully describe storage. This model is linear and extensively used given its simplicity, mostly when energy storage is a part and not the main focus of the optimisation [230,231]. However, no in-depth analysis of storage operation is possible with a battery-like model, which, especially for TMES where charge and discharge involve complex conversion processes (see Sections 2.2 and 2.3), may be restrictive. A first step towards improving TMES model accuracy is to derive parameters for battery-like representation directly from detailed system models [204]. However, even first-principle thermodynamic analysis for a CAES plant showed inherent nonlinearities in the compression and expansion processes [232], meaning constant parameters can only represent specific operating conditions.

More accurate TMES models proposed in the literature are described in Table 6. Ibrahim et al. [233] proposed a PTES model with separate conversion efficiency for charging and discharging, individually fitted through a polynomial regression to capture nonlinear variations with the state of charge, power exchanged and temperature distributions within the storage. In [234] and [235], CAES thermodynamics was captured by a stepwise function relying on published data from system assessment. Different conversion efficiency and feasible gas mix for an air separation unit were implemented by convex subregions, to characterise plant start-up [188]. Only this approach could underscore the potential of underutilised air separation units for integration with cryogenic power

generation, compared to plants that mostly run at full load. Advanced analysis with the inclusion of off-design conditions was presented for CAES in [236].

Table 6: Detail of studies where the modelling of TMES overcomes the simple battery-like model.

| Study | Year | TMES | Type of study | TMES model | Phenomena captured | Limitations | Notes |
|-------|------|------|---------------|------------|--------------------|-------------|-------|
| [233] | 2017 | PTES | Day-ahead scheduling | Efficiency curves f(SoC) Charge and discharge separated | Reservoir temperature variation | Nonlinear | Cyclic operation of PTES reservoir assumed Fitted to thermodynamic model |
| [234] | 2018 | CAES | Energy and reserve provision | Stepwise conversion efficiency | Generation level Reservoir SoC | Stepwise | Can be linearised From literature results |
| [188] | 2015 | ASU retrofit | Reserve and gas provision | Convex subregions | Plant start-up | Stepwise changes | Linear 2 operating regions |
| [192] | 2019 | LAES | Electricity and cold provision in microgrid | Empirical function | Variation of cold recycle | Nonlinear | From thermodynamic model |
| [237] | 2017 | ACAES | Multi-energy provision | Energy hub formulation Charge and discharge separated | Multi-vector output | Constant efficiency | Linear From thermodynamic model |
| [238] | 2016 | ACAES | Multi-energy provision | Charge and discharge separated | Multi-vector output | Constant efficiency | Linear From thermodynamic model |
| [236] | 2020 | ACAES | Day-ahead scheduling | Analytical | Off-design included Wide power output | Only electricity | Linearised Explicit thermodynamic model |
| [235] | 2018 | CAES | Real-time dispatch with uncertainty | From other model regression | Off-design included Wide power output | Only electricity | Linearised From thermodynamic model |

Accurate TMES models are relevant also in the case of multi-energy operation, which, as Section 2.4.3 demonstrates, is attracting growing interest. Multi-energy flexibility has been formally defined through a general framework using Minkovsky vector summation in [239]; for the proposed representation, a model linking the feasible levels of storage output over different energy vectors is needed. To this end, convex operating maps have been used for combined heat and power plants [240], but never for TMES. Few attempts toward multi-energy TMES investigation – for instance, running CAES as an electricity and heating provider [237] – involve using an energy hub representation with fixed conversion efficiencies [236]. Constant multi-energy conversion efficiencies and separated charge/discharge CAES subprocesses were used by Li et al. [238].

## 2.6   Conclusion

Chapter 2 exposes the shared knowledge of TMES and their integration with the energy system through a synthesis of the available scientific literature to date. It demonstrates how LAES and TMES performance are mostly investigated and understood for rated operating conditions. On the other hand, the optimal integration of LAES – and TMES in general – in low-carbon power systems is a crucial yet marginally-addressed research area. Such evidence supports the research objectives formulated in the Introduction and their relevance for advancing the ongoing research. Consideration of the constraints and requirements arising from the participation of LAES in balancing services and their impact on storage performance is hardly discussed. However, addressing the interlink between storage application and performance in the energy system is essential to determine TMES financial viability compared to alternatives and to identify favourable business cases.

Key research gaps identified are the *assessment of storage operation outside rated conditions* and the *evaluation of power system integration pathways beyond arbitrage alone.* These are significant given storage operation should accommodate variable power input and output setpoints enforced by system-level constraints, while the simultaneous provision of different market services may result in favourable business cases. Other research gaps involve the only partial characterisation of TMES potential to support decarbonisation. More specifically, the literature does not fully address *the multi-energy operation of LAES,* which may provide a unique means to reduce fossil fuel dependence across power, heating and cooling sectors. Similarly, there is a lack of *assessment and cross-comparison of TMES concepts for long-duration storage*, hence missing awareness of the techno-economic suitability of TMES to provide the LDS services needed in a highly decarbonised power system.

Across the above gaps, research should also overcome the lack of a suitable modelling framework that accurately predicts TMES performance in integration assessments. Advancements in the simplistic battery-like model for TMES, whose limitations were pointed out by several authors, would lead to a more accurate representation of storage performance and value. Only this way could a representative techno-economic assessment of versatile storage operation be achieved, with combined energy balancing and reserve services provision or multi-energy output. This area is unaddressed for LAES, but it would benefit the whole TMES field, whose ultimate uptake will be

determined by the technical and economic comparison with incumbent storage technologies and other flexibility enablers.

### 2.6.1  Chapter relevance within this thesis

This chapter lays the groundwork for the present thesis, making the reader understand and appreciate both its relevance and novel contributions to the existing body of literature. In the following, Chapter 3 outlines the methodological elements used to overcome current modelling bottlenecks. Then, each results chapter presents the results and discusses the new understanding around each of the highlighted research gaps.

# CHAPTER 3

## Elements of modelling and optimisation methodologies used in this research work

*Following the presentation of scientific understanding around TMES and its integration with the energy system in Chapter 2, the present chapter outlines the research methods used in this thesis. Integration studies require simultaneously accounting for technical storage characteristics, energy system and market constraints. Therefore, a methodology is developed to merge the above aspects into a unified framework for the assessment of TMES and its integration. This chapter covers three main areas: i) device and system modelling, for the simulation of TMES; ii) mixed-integer linear programming optimisation to assess storage operation as part of the energy system; and iii) model reduction techniques to capture relevant physics of the investigated storage process within computationally efficient models. Foundations for each area are laid out with exemplary applications. By combining the above areas, the proposed methodology contributes to the energy storage modelling field with a more accurate simulation of storage operation. Outcomes from the application of the proposed methodology to the study of TMES and the associated merits compared to existing approaches are thoroughly discussed in the results chapters.*

## 3.1 Introduction

Two areas of significant research interest emerging from the literature presented in Chapter 2 are: i) LAES – and, in general, TMES – techno-economic assessment at system scale; and ii) storage simulation as part of the broader energy system. However, while system-level assessments under steady-state conditions are abundant, LAES integration studies are limited in number and scope, thus requiring further research. Additionally, each area relies on methodologies tied to the individual research questions to be answered, at very different levels. System- and device-scale numerical modelling, in conjunction with energy, exergy and economic analysis, is commonly used in system assessments; mathematical optimisation techniques such as linear and non-linear programming are relevant to studying storage operation and scheduling within the energy system.

To complement the available literature and merge the merits of detailed process modelling with system-level optimisation, this thesis develops a novel methodology described in the present chapter, which uses model reduction to preserve technical characteristics from storage operation into system-level assessments. The aim is to bridge the traditionally exclusive areas of system modelling and system-scale optimisation. In so doing, results include a more accurate description of storage performance. This allows to rectify the assessment of LAES and TMES integration in the energy system and advance the field by evaluating potential applications for power and energy balancing. The present chapter outlines the basis for the proposed methodological framework.

The chapter is subdivided into three main parts: following foundations on device and system modelling in Section 3.2 and linear programming optimisation in Section 3.3, Section 3.4 discusses the model reduction techniques relevant to this thesis. Some applications for the described methods are also presented. Finally, Section 3.5 concludes the chapter.

## 3.2 Device and system modelling

Modelling a device or a system entails creating a simplified numerical representation of its real-life behaviour, which meets a desired level of accuracy. The first step in any numerical model is to identify the thermodynamic system to be studied; a generic system is illustrated in Figure 23. Then, mass and energy and conservation equations can be specified:

$$0 = \frac{dm_{CV}}{dt} \pm \sum_{i=1}^{I} \dot{m}_i \qquad \qquad 3.1$$

$$\sum_{j=1}^{J} \dot{Q}_j - \dot{W} = \frac{dE_{CV}}{dt} \pm \sum_{i=1}^{I} \dot{m}_i \big( h + e_k + e_g \big)_i \qquad \qquad 3.2$$

where the *i*-th mass stream is positive if leaving the system and negative otherwise, a positive power $\dot{W}$ means work is performed *by* the system and the *j*-th heat flux – exchanged with a thermal reservoir at temperature $T_j$ – is positive (heat gain) when entering and negative (heat loss) when leaving the system. In addition, momentum conservation along system ducts allows accounting for distributed and localised losses $w_d$:

$$\dot{m}w_d = \pm \sum_{i=1}^{I} \dot{m}_i \left( vp_i + \frac{u_i^2}{2} + gz \right) \qquad \text{3.3}$$

In principle, one momentum conservation equation such as Equation 3.3 should be specified for each velocity component in the considered reference frame; however, ductwork is often treated as 1-D so that only the velocity along the duct axis is of interest [241].
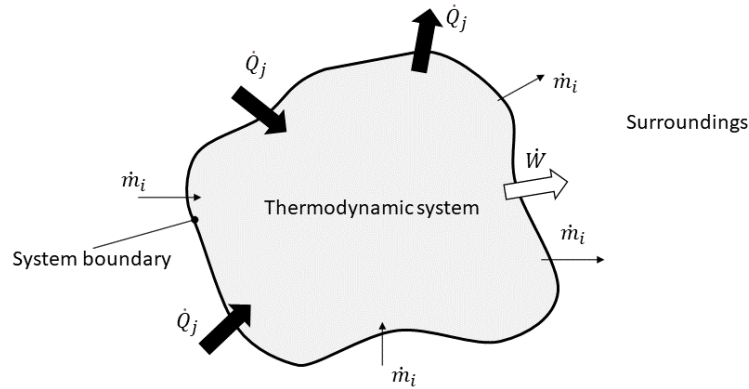


**Figure 23: A generic thermodynamic system interacting with its surroundings through mass, heat and work exchange.**

The second law of thermodynamics can also be specified. When combined with Equation 3.2 and solved for the heat flux exchanged with the environment, it results in the exergy conservation equation used for exergy analysis [242]:

$$\begin{aligned}
\sum_{j=1}^{J} \dot{Q}_j &\left( 1 - \frac{T_0}{T_j} \right) - \dot{W}_t \\
&= \frac{d(E_{CV} + p_0 V + T_0 s)}{dt} \pm \sum_{i=1}^{I} \dot{m}_i ex_i \pm \sum_{i=1}^{I} \dot{m}_i \psi_i \\
&\quad + T_0 \Sigma
\end{aligned} \qquad \text{3.4}$$

Fundamental conservation equations provide relationships between the state variable in the system. In a model, they are complemented by characteristic equations – which link inputs and outputs to technical features specific to each component – and constitutive equations between state variables. For instance, Equation 3.5 links input and output temperatures of a generic heat exchanger to the characteristic heat transfer effectiveness for the device, while a simple constitutive equation for ideal gasses is given in Equation 3.6, where $R^*$ is the specific gas constant:

$$\varepsilon = \frac{\dot{C}_h \left( T_{h,in} - T_{h,out} \right)}{\dot{C}_{min} \left( T_{h,in} - T_{c,in} \right)} = \frac{\dot{C}_c \left( T_{c,out} - T_{c,in} \right)}{\dot{C}_{min} \left( T_{h,in} - T_{c,in} \right)} \qquad \text{3.5}$$

$$pv = R^* T \qquad \text{3.6}$$

Combining conservation, characteristic and constitutive equations for any given device results in its component model.

As a system consists of the sequential operation of multiple devices, a system model is obtained by specifying individual device models and solving the resulting large set of equations simultaneously. Such framework notably offers a significant degree of flexibility, with, for instance, state variables varying over time in dynamic models or depending on any number of spatial coordinates to introduce dimensional effects. However, 0-D, steady-state conditions are typically assumed for system modelling [243].

### 3.2.1 Device and system modelling under rated conditions

Design or rated conditions correspond to the best case for system operation. Devices operate at the design point, maximising efficiency and running steadily in the absence of external disturbances. Hence, most studies on TMES consider rated conditions for system operation [63,107,244]. At rated conditions, characteristic parameters for each device remain constant at their rated value, which can be substituted in the energy conservation and the characteristic equations presented in Table 7, to model the most common TMES components in this work.

Table 7: Model equations for the main devices used in TMES.

| Component | Energy conservation | Characteristic equation | Notes |
|---|---|---|---|
| Turbine | $\dot{W} = \eta_{S,T}\dot{m}(h_{in} - h_{S,out})$ | $\eta_{S,T} = \dfrac{(h_{in} - h_{out})}{(h_{in} - h_{S,out})}$ | Expansion ratio needed |
| Compressor | $\dot{W} = \dfrac{1}{\eta_{S,C}}\dot{m}(h_{S,out} - h_{in})$ | $\eta_{S,C} = \dfrac{(h_{S,out} - h_{in})}{(h_{out} - h_{in})}$ | Compression ratio needed |
| Heat exchanger (two streams) | $\dot{Q} = \dot{m}_h(h_{h,in} - h_{h,out})$ $\dot{Q} = \dot{m}_c(h_{c,out} - h_{c,in})$ | $\varepsilon = \dfrac{\dot{Q}}{\dot{C}_{min}(T_{h,in} - T_{c,in})}$ | |
| Cold box (multi-stream heat exchanger) | $0 = \sum_{i=1}^{I} \dot{m}_i h_i$ | | Partitioned approach required |
| Pump | $\dot{W} = \dfrac{1}{\eta_P}\dot{m}(h_{out} - h_{in})$ | $\eta_P = \dfrac{\dot{V}(p_{out} - p_{in})}{\dot{W}}$ | |
| Valve | $h_{in} = h_{out}$ | | |
| Thermal energy storage | $\dot{Q}_{in} - \dot{Q}_{out} - \dot{Q}_{loss} = V\dfrac{d(\rho c_p T)}{dt}$ | | $\rho c_p$ often constant |

However, equations in Table 7 are by no means unique, as this modelling framework can accommodate arbitrarily accurate component models, allowing a higher level of detail to be used only for selected key devices. For instance, dynamic models of packed bed TES or air purification units have been coupled to TMES system models to study dynamic oxygen production from LAES [245], effects of temperature dynamics on cycle efficiency [246] or working fluid volume flow rates [44]. In all these works, remaining components are modelled under rated conditions. Fully dynamic models of all the main components were used to study the control of a supercritical CAES [247].

### 3.2.2 Off-design device modelling

Although TMES assessment at rated conditions is useful for comparison purposes, off-design device operation often happens in real-life applications, where input variables are likely to differ because of external constraints on storage inputs and outputs. Examples are power system constraints [181] or abrupt changes in RES input [190]. Air pressure buildup in the cavern during charge and pressure decrease during discharge result in intrinsic boundary condition changes to CAES operation [248],

often overlooked or addressed with suitable control strategies [249]. So, off-design component models are necessary to fully describe these phenomena, where the characteristic parameters change over time with the operating conditions. The following sections detail the off-design modelling of devices used in TMES.

### *Turbines and compressors*

Off-design models of turbines and compressors are in general component-specific and depend for instance on the investigated size, geometry and flow pattern. Semiempirical off-design maps are typically adopted, which relate corrected flow rate and speed parameters through some component-specific coefficients. Corrected flow rate and speed parameters are defined as [250]:

$$m' = \frac{\dot{m} \, p_{in,0} \, \sqrt{T_{in}}}{\dot{m}_0 \, p_{in} \, \sqrt{T_{in,0}}} \tag{3.7}$$

$$n' = \frac{n \, \sqrt{T_{in,0}}}{n_0 \, \sqrt{T_{in}}} \tag{3.8}$$

Isentropic efficiency is defined as:

$$\frac{\eta_C}{\eta_{C,0}} = \left(1 - a_1(1 - n_C')\right) \frac{n_C'}{m_C'} \left(2 - \frac{n_C'}{m_C'}\right) \tag{3.9}$$

$$\frac{\eta_T}{\eta_{T,0}} = (1 - a_2(1 - n_T')^2) \frac{n_T'}{m_T'} \left(2 - \frac{n_T'}{m_T'}\right) \tag{3.10}$$

The $C$ subscript refers to compressors and $T$ to turbines. Empirical parameters $a_1$ and $a_2$ are to be obtained experimentally. In this work, values reported in the literature have been used: $a_1 = 0.3$ and $a_2 = 0.3$ [251]. Compression ratio is computed as:

$$\frac{\Pi_C}{\Pi_{C,0}} = b_1 m_T'^2 + b_2 m_T' + b_3 \tag{3.11}$$

$$b_1 = n_C' \Big/ \left[a_3 \left(1 - \frac{a_4}{n_C'}\right) + n_C'(n_C' - a_4)^2\right] \tag{3.12}$$

$$b_2 = \left(a_3 - 2a_4 n_C'^2\right) \Big/ \left[a_3 \left(1 - \frac{a_4}{n_C'}\right) + n_C'(n_C' - a_4)^2\right] \tag{3.13}$$

$$b_3 = -\left(a_3 a_4 n_C' - a_4^2 n_C'^3\right) \Big/ \left[a_3 \left(1 - \frac{a_4}{n_C'}\right) + n_C'(n_C' - a_4)^2\right] \tag{3.14}$$

Similarly, empirical parameters sourced from reported studies on axial devices have been used in this work: $a_3 = 1.8$, $a_4 = 1.8$. For turbines, the relationship between mass flow rate and expansion ratio is described by the Flügel formula:

$$\frac{m_T'}{m_{T,0}'} = \sqrt{1.4 - 0.4 \frac{n}{n_0} \sqrt{\frac{T_{T,in,0}}{T_{T,in}}} \sqrt{\frac{\Pi_T^2 - 1}{\Pi_{T,0}^2 - 1}}} \tag{3.15}$$

Off-design maps for compression and expansion are reported in Figure 24.
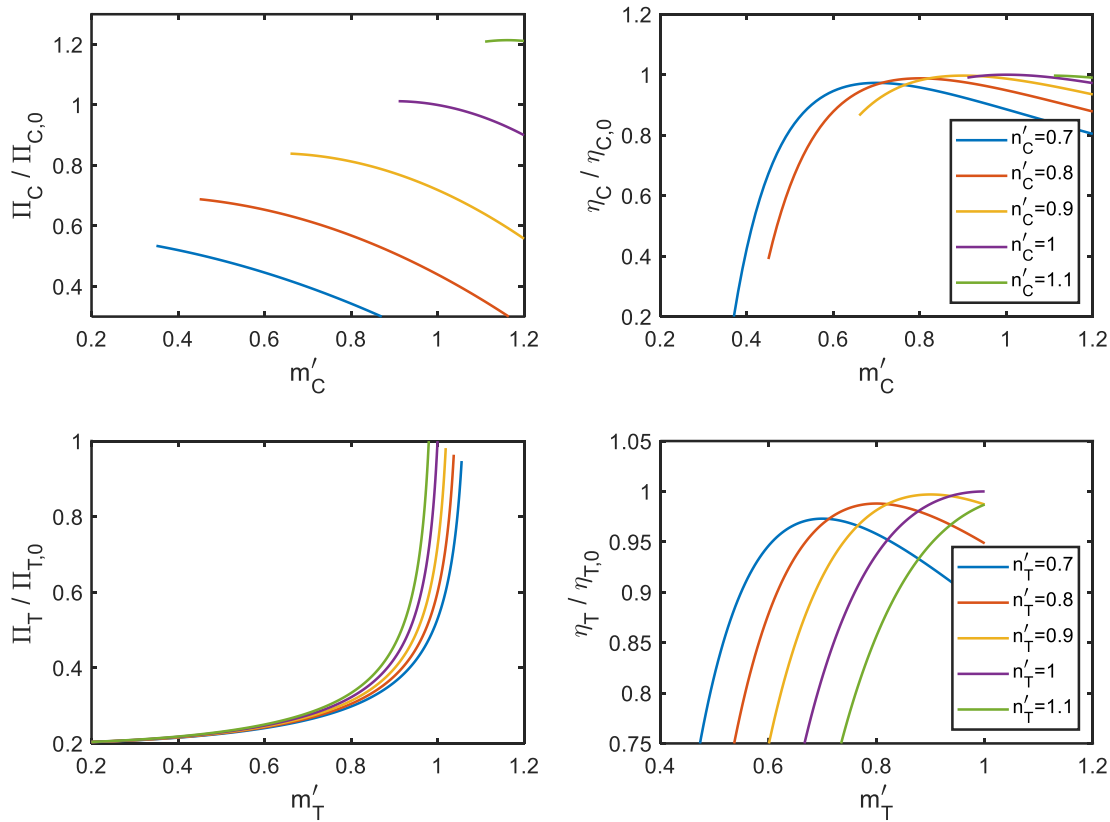
**Figure 24: Off-design maps for compressors (top row) and turbines (bottom row).**

## Pumps

The affinity law can be used to relate the off-design pressure head and mass flow rate across a pump [252]:

$$\frac{\Delta p}{\Delta p_0} = \left(\frac{\dot{m}}{\dot{m}_0}\right)^2 \qquad 3.16$$

Pump efficiency can be obtained as a function of the elaborated mass flow rate from the manufacturer datasheet and fitted to a second-order polynomial:

$$\frac{\eta_P}{\eta_{P,0}} = a_1 \left(\frac{\dot{m}_P}{\dot{m}_{P,0}}\right)^2 + a_2 \frac{\dot{m}_P}{\dot{m}_{P,0}} + a_3 \qquad 3.17$$

The efficiency curve for a centrifugal pump is represented in Figure 25.
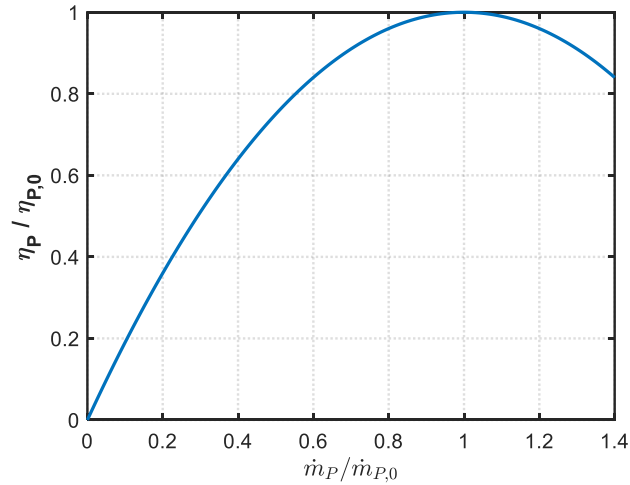
Figure 25: Off-design efficiency map for a centrifugal pump.

### *Heat exchangers*

An effective way to model heat exchanger performance is through the $\varepsilon - NTU$ model [253]; for a specific geometry, heat exchanger effectiveness can be determined from two dimensionless numbers: $NTU = UA/\dot{m}c_p$ and $\dot{C}_R = \dot{C}_{min}/\dot{C}_{MAX}$. In the case of a generic, counter-flow heat exchanger:

$$\varepsilon = \frac{1 - exp[-NTU(1 - \dot{C}_R)]}{1 - \dot{C}_R exp[-NTU(1 - \dot{C}_R)]} \qquad 3.18$$

Under off-design conditions, $NTU$ and $\dot{C}_R$ are computed under a fixed surface $A$ and using an appropriate correlation to estimate the variation of the overall heat transfer coefficient $U$. Figure 26 compares the $\varepsilon$ variations for a counterflow and a co-flow heat exchanger.
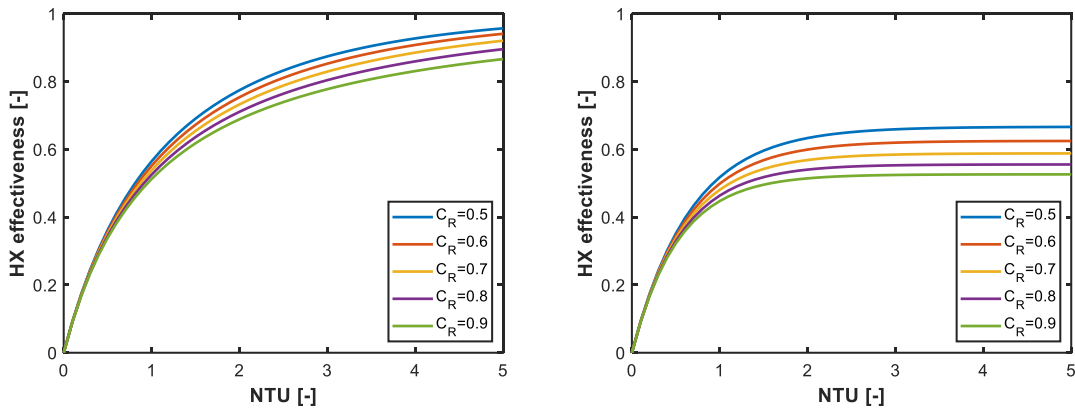


Figure 26: $\varepsilon$-NTU relation for two geometries of heat exchangers: counterflow (left) and co-flow (right).

### *Thermal energy storage*

It is uncommon to refer to off-design conditions for TES devices, whose charging and discharging are intrinsically dynamic processes. However, model accuracy depends to a large extent on the capability of correctly accounting for such dynamics and predicting the TES outlet temperature. The simplest

approach to do so is a lumped parameter model, where TES thermal mass is pointwise, and a time dependency of TES temperature is preserved [254].

$$\frac{dQ_{TES}}{dt} = \dot{Q} + \dot{Q}_{loss}$$ 3.19

The mean logarithmic temperature difference [255] or the $\varepsilon - NTU$ model [256] can be used to estimate the heat transfer between the heat carrier and the TES, based on the TES state:

$$\dot{Q} = UA\Delta T_{ml}$$ 3.20

$$\dot{Q} = \varepsilon \dot{Q}_{MAX}$$ 3.21

$\dot{Q}_{loss}$ can also be computed as a function of TES temperature through semi-empirical heat transfer correlations [257].

Alongside dynamics, spatial effects could also be accounted for when modelling a TES. Coupling 3-D or 2-D models to system-level simulations involves a high computational burden, so 1-D or layered approaches are often pursued [258]. These TES models are obtained by specifying energy conservation equations for a unit volume of the heat transfer fluid and storage medium and result in a set of partial differential equations coupled by the heat transfer term. A constitutive equation expressing the heat transfer based on TES and fluid temperatures is needed, together with boundary and initial conditions. For a packed bed of rocks, which is a common yet not the only TES solution for TMES (see Section 2.3.2), a 1-D, transient model reads:

$$\rho_f c_{p,f} \frac{\partial T_f}{\partial t} + \rho_f c_{p,f} u \frac{\partial T_f}{\partial z} = \frac{\partial}{\partial z}\left(\lambda_f \frac{\partial T_f}{\partial z}\right) - U\frac{1-\sigma}{\sigma}(T_f - T_s)$$ 3.22

$$\rho_s c_{p,s} \frac{\partial T_s}{\partial t} = \frac{\partial}{\partial z}\left(\lambda_s \frac{\partial T_s}{\partial z}\right) + U(T_f - T_s) - U_{loss}(T_s - T_0)$$ 3.23

The model is completed by a heat transfer correlation such as [259]:

$$U = 700\left(\frac{4\dot{m}_f}{d\pi D^2}\right)^{0.76}$$ 3.24

where $D$ represents the packed bed diameter and $d$ is the average diameter in the packing.

Differential models reproduce the operation of TES devices with high levels of detail. Thermal stratification, inlet and exit losses, charging and discharging transients can all be captured. The inclusion of differential TES models within a system-scale simulation allows to properly simulate system operation and link performance to TES dynamics. Typical examples include CSP plants, CAES and LAES [260].

## 3.3    Linear programming optimisation

A recurring problem in engineering applications is assigning the value to a specific set of variables so that a certain function of the variables themselves is minimised (or maximised). This paradigm represents an optimisation problem. The function to be minimised or maximised is called *objective function,* and the set of values leading to the best result represents the *optimal solution*. Additionally, optimisation problems may be subject to a number of *constraints*, meaning specific relations between variables, or a combination of variables, that any feasible solution must satisfy.

If the problem objective function and constraints only involve either continuous or integer variables and linear relationships between them, the generic optimisation problem can be formulated as:

$$
\begin{aligned}
&\min_{x,y}(c^T x + d^T y) \\
&\text{s.t.} \\
&Ax + By = b \\
&x \geq 0 \ \in \mathbb{R}^{N_x}, y \in \{1,0\}^{N_y}
\end{aligned}
\qquad\qquad 3.25
$$

where $x$ and $y$ are, respectively, continuous and binary decision variables, $c$ and $d$ represent the cost vectors, $A$ and $B$ the coefficient matrices and $b$ the vector of known terms that are used to express the constraints; $N_x$ and $N_y$ represent the dimension, respectively, of the continuous and the integer variable vectors. Here and in the rest of this thesis, problem decision variables are denoted by bold-face characters to be distinguished from model parameters.

The model problem of Equation 3.25 is an MILP optimisation. MILP is not the only paradigm of optimisation – a number of alternative approaches have been studied, including nonlinear programming, stochastic programming, evolutionary algorithms, heuristics and hybrid solutions [261]. Yet, MILP provides a convenient idealisation of many real-life problems and is often used for engineering applications. Examples include the optimal design of heat exchanger networks [262], optimal planning of industrial clusters [263] and optimal design of multi-energy districts [206]. A particularly relevant application of MILP for this thesis work is the optimal scheduling of energy generation assets for operational problems [264,265].

### 3.3.1    Solution techniques

Commercial solvers such as CPLEX [266] or Gurobi [267] efficiently solve linear programming problems through the Simplex method [268]. However, the discrete nature of integer variables introduces an additional layer of complexity to MILP solution. This is typically tackled by sequentially *relaxing* integer constraints into continuous ones and using the Simplex to obtain a lower bound (for minimisation problems) to the objective function of the original problem. A solution algorithm for MILP problems will consecutively select the most suitable relaxations to progressively reduce the gap between the best objective value evaluated and the bound from the relaxed problem. Common MILP solution techniques are branch-and-bound or branch-and-cut [269], where tree size and solution time decrease with decreasing numbers of integer variables. For this reason, MILP models often rely on formulations that reduce the number of integers in the problem [207] or on solutions obtained only for typical days, through clustering or other statistical methods [270].

The computational speed and robustness of the solution procedure and its independence from an initial guess are the main pros of MILP optimisation [223]. Cons involve the impossibility of including nonlinear relations between variables, which enforces simplifications and relaxation of the real problem constraints [271]. Yet, approximation of nonlinear relations and constraints can be included in a MILP problem through a prior manipulation or suitable model formulation with, for instance, linearisation techniques [218]. The linearisation methods used in this thesis to model nonlinear TMES thermodynamic characteristics are presented in Section 3.4.3.

## 3.4 Model reduction techniques

In optimisation problems, retaining simplicity is key to model tractability and efficient solution. Device and system models presented in Section 3.2 include nonlinear dependencies and an arbitrary level of complexity tied to the characteristic and constitutive equations considered, to the inclusion of dimensional effects and dynamic behaviour. On the contrary, the MILP optimisation framework presented in Section 3.3 can handle only linear relations between model variables.

In order to improve the state-of-the-art modelling of TMES in system integration studies discussed in Section 2.5.2, the present research work relies on a number of techniques aimed at reducing device and system model complexity and including higher-order models into a MILP framework. The discussion of such techniques in the following sections is accompanied by specific applications to TMES assessment.

### 3.4.1 Empirical characteristic parameters

Characteristic device parameters such as polytropic efficiency of compressors and turbines [272] or heat exchanger effectiveness [273] are linked to the process variables by given equations. However, devices may experience operating conditions for which general equations or constant characteristic parameters are inaccurate. On the other hand, modelling system physics can be computationally demanding. In these cases, empirical coefficients may be used. Ad-hoc experimental rigs allow extracting the characteristic parameters to be integrated with device models for the investigated operating conditions. Alternatively, characteristic parameters may be obtained by refined simulation (e.g. CFD) [274] and applied to low-order models at a later stage.

An example is heat transfer in LAES evaporator. In this device, transcritical conditions are associated with high variations of air thermodynamic properties, which result in large inaccuracies for traditional heat transfer correlations. On the other hand, studies pinpoint this device [109] as a major source of irreversibility [106] within the LAES process. For these reasons, the test rig illustrated in Figure 27 was set up and used to directly measure the heat transfer coefficient of supercritical nitrogen.
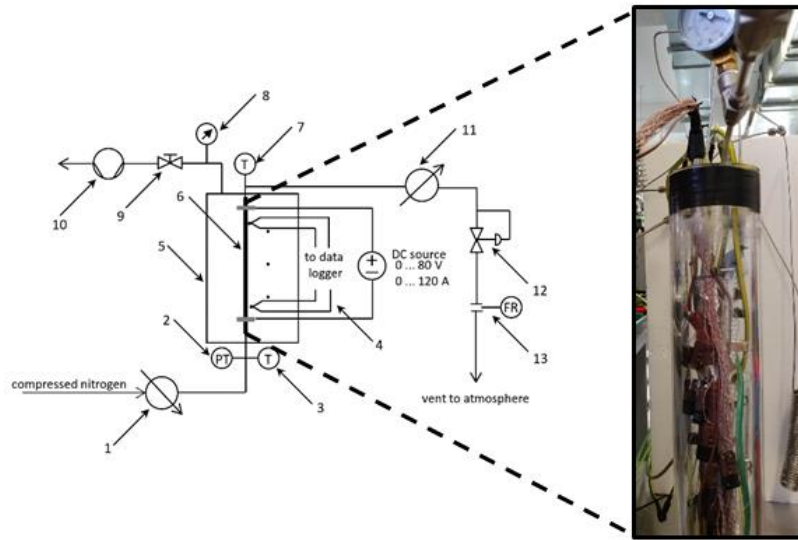
**Figure 27: Schematic of the test rig used to measure nitrogen heat transfer coefficient in supercritical conditions and detail of the evacuated tube with thermocouples where Nitrogen heat transfer takes place.**

The heat transfer coefficient was predicted from the local measurements of 30 T-type thermocouples and then averaged over the test pipe. It was treated as a dimensionless Nusselt number to adapt experimental measurements to different geometries:

$$\alpha = \frac{\alpha_0 D_0}{D} \left( \frac{uD}{u_0 D_0} \right)^{4/5} \qquad\qquad 3.26$$

An overall heat transfer coefficient for supercritical conditions was evaluated from the series of heat transfer resistances across the test pipe:

$$U = \left( \frac{1}{\alpha_{in}} + \frac{\delta_{HX}}{\lambda} + \frac{1}{\alpha_{out}} \right)^{-1} \qquad\qquad 3.27$$

Finally, the effectiveness of a balanced heat exchanger was computed based on the experimental measurements:

$$\varepsilon = \frac{NTU}{1 + NTU} \qquad\qquad 3.28$$

In the results from Figure 28, a supercritical convective heat transfer coefficient of 6000 W/m$^2$K was computed with Equation 3.26 for the operating conditions of LAES (70 bar), overall heat transfer coefficient $U$ of 420 W/m$^2$K and 91% heat exchange effectiveness.
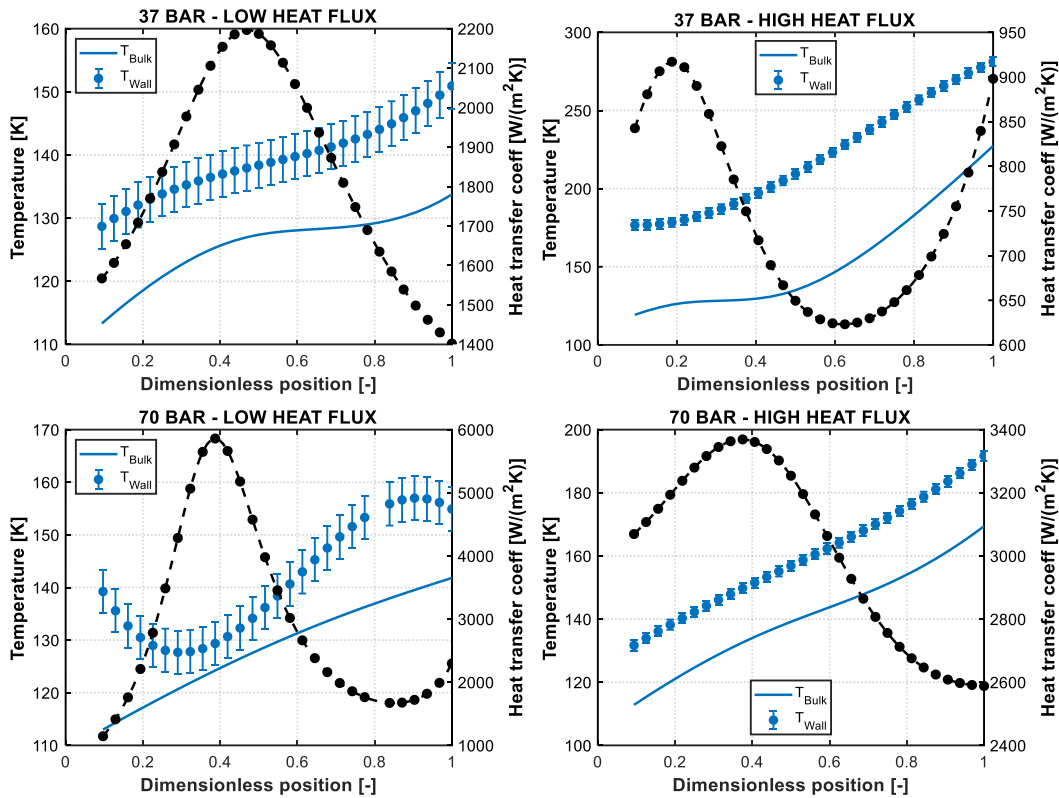
**Figure 28: Experimental results used to derive the convective heat transfer coefficient in supercritical conditions and the value of heat exchanger effectiveness.**

The experiment thus returned the characteristic effectiveness parameter without the need to model the heat exchanger. Benefits from heat transfer enhancement were also empirically measured and reflected by variations of the effectiveness parameter, as shown above. Substituting such enhanced effectiveness into system models translates into techno-economic benefits at system scale.

### 3.4.2 Approximation of device operation through analytical functions

Another option to simplify system modelling is approximating the input-output relations of a process or a selected part of it through analytical functions. The first step consists in individuating a suitable mathematical function and a fitness metric. Then, a dataset describing system operation is fitted to the reduced model to obtain specific model parameters for the situation investigated. The training dataset can be obtained experimentally, from on-site measurements, or can be the outcome of a higher-order model which needs to be reduced. One application is linear or polynomial regression – univariate or multivariate – extensively used within machine learning [275], for example, to predict battery life and degradation based on the early cycles discharge data [276]. Other exemplary applications include model fitting to analytical functions to work out kinetic parameters during the sorption and desorption processes of thermochemical energy storage materials [277].

In the present thesis, analytical functions were used to simplify the numerical model of a packed bed TES presented in Equation 3.22 to 3.24. Studies have shown good agreement of thermocline profiles with the logistic cumulative distribution function [278]. This approach was validated for a thermocline TES [279] and applied in the case of CSP [260], proving capable of capturing variations in the operating conditions. The functional relationship reads:

$$T(x,t) = T_{min} + \frac{T_{MAX} - T_{min}}{1 + e^{-\frac{(x-a(t))}{b}}}$$

<div align="right">3.29</div>

where $T_{MAX}$ and $T_{min}$ represent the maximum and minimum temperatures within the storage. The parameters $a$ and $b$ individuate, respectively, the central point and the slope of the logistic curve as a function of time.

In this thesis, a set of numerical runs of the 1-D dynamic model discussed in Section 3.2.2 was carried out under different operating conditions. A least-square fitting problem [280] was solved using the sum of square errors as the fitness metric to estimate the parameters $a$ and $b$, and their dependence on the air flow rate circulating through the packed bed. Results of the curve fitting are shown in Figure 29 for rated flow rate conditions, but the analytical model fitness to numerical results was satisfactory in all the tested cases, with coefficients of determination between 0.992 and 0.995. Only minor discrepancies between the logistic curves and the full numerical model results demonstrate the analytical function suitability as a simplified description of packed bed TES devices.
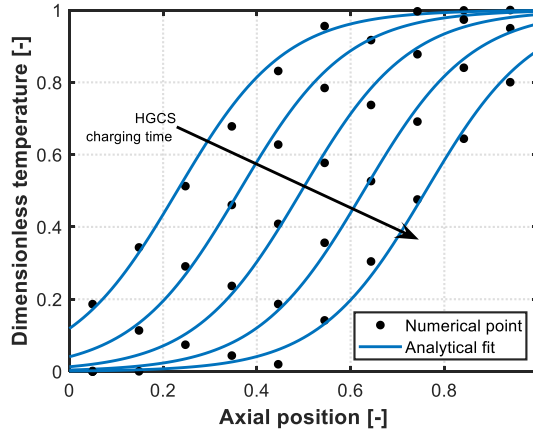


Figure 29: Packed bed fitting results during high-grade cold storage (HGCS) charging.

### 3.4.3 Linearisation techniques and treatment of nonlinear constraints

Linearisation techniques simplify nonlinear dependencies in a way that can be handled by MILP optimisation. Application examples include equipment costs and their variation with component capacity, which follows power laws [281], heat pumps coefficient of performance variations with temperature [282], off-design conversion efficiency of generating assets [283]. Given a function $y = f(x)$ of a single variable $x$, its value can be sampled at $I$ +1 points, $y_i$, which coincide with coordinates $x_i$. Then a continuous variable $\omega_i$ can be introduced for each interval $i$ between two breakpoints, which assumes values between 0 and 1. A further binary variable is introduced $\Phi_i$ for each interval, with dummy value 0 at the extremes ($\Phi_0 = \Phi_I = 0$). Now, the value of $y = f(x)$ can be approximated to a linear combination of the values at the two closest breakpoints, through the following set of constraints:

$$\sum_{i=1}^{I-1} \Phi_i = 1$$

<div align="right">3.30</div>

$$\omega_i \leq \Phi_{i-1} + \Phi_i \qquad\qquad \forall\, i \in \{1, \dots, I\} \qquad\qquad 3.31$$

$$\qquad\qquad 3.32$$

$$\sum_{i=1}^{I} \omega_i = 1$$

$$\qquad\qquad 3.33$$

$$x = \sum_{i=1}^{I} \omega_i\, x_i$$

$$\qquad\qquad 3.34$$

$$\tilde{y} = \sum_{i=1}^{I} \omega_i f(x_i)$$

Above, Equation 3.30 impose at most one single active interval $i$ at a time, Equation 3.31 ensure only the linear combination parameters $\omega_i$ and $\omega_{i+1}$ associated to the active interval are nonzero. Finally, equations 3.32, 3.33 and 3.34 estimate the value $\tilde{y}$ of the approximated function at coordinate $x$. This procedure is exemplified in Figure 30.
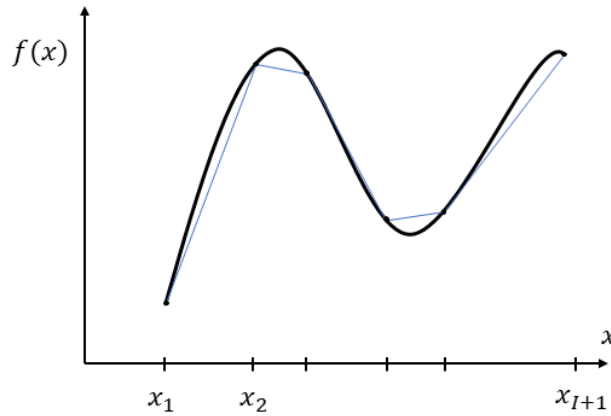


**Figure 30: Piecewise linear approximation of a univariate function.**

Similarly, piecewise linearisation techniques can be applied to bivariate functions, either by extending the 1-D method presented above or with the triangle or the rectangle methods explained in [284]. The multidimensional 1-D method extension is computationally faster but less accurate. The triangle and rectangle methods exhibit comparable computational time, with the former being typically more accurate. Vielma and Nemhauser proposed a new formulation for the triangle method, whose computational burden escalates favourably with the number of binary variables and constraints [285].

In problem constraints, bilinear terms can be approximated by McCormick envelopes, where variable products are substituted by a new variable bounded between the maximum and the minimum value of the product itself, and equality constraints are substituted by inequalities [286]. The big-M formulation proposed in [234] can be used to linearise the product between binary and continuous variables.

### 3.4.4 Characteristic envelopes/maps of a device or system

Characteristic envelopes are another convenient approach to represent device or system performance during operation. Through them, complex system behaviour is synthesised as a function of selected influential parameters. Envelopes can be obtained by experiments or simulation

procedures; in both cases, relevant parameters are varied, observing the evolution of one or more target variables. For a single relevant parameter, envelopes are visualised as line graphs, for instance, capturing the active power limit for aggregation of prosumers in low-voltage distribution networks as a function of time [287]. For two, characteristic maps can be visualised in a 3-D space. One example is the power output from an ORC as a function of temperature and humidity, with a given amount of thermal input [288].

Operating envelopes for three TMES technologies (CAES, LAES and a Rankine PTES) were computed in this research, starting from a detailed system model for each technology and allowing selected plant parameters to vary over their operating range. Results reported in Figure 31 show the envelopes obtained for the discharge process, i.e. the conversion between heat and power. They report the mass flow rate of working fluid as a function of the thermal input to the power cycle and TMES power output.
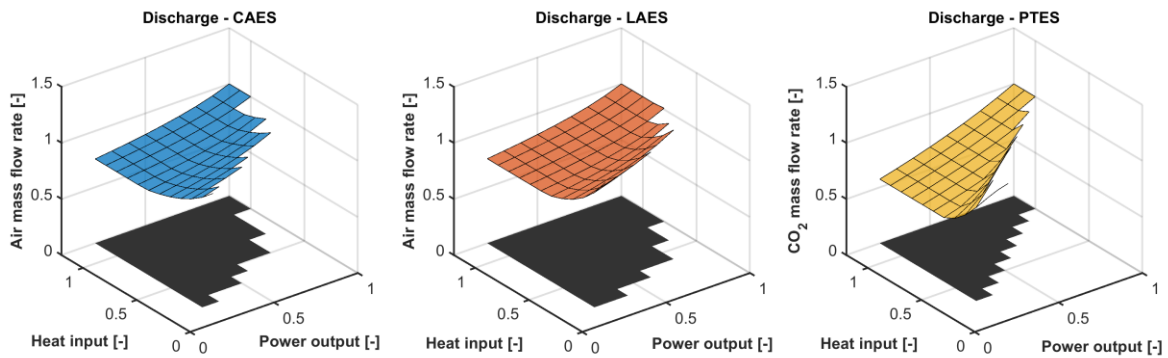


Figure 31: Example of characteristic maps for CAES, LAES and Rankine PTES discharge process.

Although not used to generate other results presented in this thesis work, the above characteristic envelopes illustrate the approach and encapsulate instructive aspects of TMES operation, which will be further discussed in the results chapters. For instance, they show a feasible operating region for each technology, linked to minimum temperature levels at the turbine outlet. They capture the nonlinear change in the working fluid mass flow rate for lower heat input, due to lower temperatures and off-design conditions in the turbines (PTES is the most affected). They show different working fluid consumption for variations in the power output and the compounding effect of off-design in the multi-stage turbines of CAES and LAES. Similar envelopes for the TMES charging process can be derived and normalised to be size-independent. Variables in the characteristic envelopes can then be selected as the variables for any relevant optimisation problem, using the linearisation techniques discussed in Section 3.4.3 to include them within MILP problem formulation.

## 3.5    Conclusion

In this chapter, the relevant methods to this thesis are introduced and discussed alongside application examples. The proposed methodological framework leverages system- and device-scale thermodynamic modelling and MILP optimisation techniques with the aim of achieving a more representative description of TMES. As discussed in Chapter 2, this should include storage technical characteristics and limitations, with the associated nonlinearities, to advance integration studies and result in a more accurate assessment of storage value.

In summary, *system and device modelling* enable a representative and arbitrarily complex description of TMES physics, but outcomes are not directly compatible with system-scale optimisation. *MILP optimisation* is convenient for studying storage operation within the energy system but requires suitable simplification and assumptions on technical storage performance. *Model reduction techniques* are used in this thesis to merge the above areas whilst preserving a sufficiently accurate storage description for MILP optimisation.

### 3.5.1 Chapter relevance within this thesis

The extension and application of the methods described in this chapter to the study of LAES operation and integration with the energy system is the object of the following results chapters. More specifically, off-design process modelling is exploited in Chapter 4 to obtain characteristic maps for LAES operations in the power system. Map linearisation and integration in an MILP optimisation are used in Chapter 5 and Chapter 6. Chapter 7 develops simplified device and system-scale models for different TMES concepts. All in all, the material presented in Chapter 3 lays the foundations for the methodological framework developed in the rest of this work to address the highlighted research questions and fulfil the thesis research objectives.

# CHAPTER 4

## Off-design operation of liquid air energy storage under real-life conditions

*Following the presentation of this thesis' background in the* Introduction *and Chapter 2 and the methodology in Chapter 3, this is the first of four results chapters, each addressing one of the identified thesis objectives. Existing LAES performance predictions refer to steady operation at rated conditions and arbitrage applications. However, in this results chapter, the real-life thermodynamic performance of LAES is explored outside those restrictive conditions, extending the analysis to the provision of energy balancing and reserve services in the electricity market. A validated off-design model of LAES is presented and used to understand the links between the market services considered and the performance of each component in the LAES process. Results demonstrate that: i) a strong link between market service and LAES operation exists and cannot be neglected; ii) roundtrip efficiency and liquid air consumption can vary by up to 30% during off-design operation, causing some 10 k£/MW of missed yearly revenues; iii) the effect of off-design conditions mainly affects low-pressure turbines among LAES components. A suitable regulation strategy is shown to alleviate the insurgence of off-design conditions yet not prevent it. In this chapter, the thesis objective to characterise and techno-economically evaluate the off-design operation of LAES under real-life conditions is fulfilled by showing the associated impact both on performance and revenue prediction. These outcomes enable studying the energy system integration of LAES with a realistic estimation of its thermodynamic performance, as presented in Chapter 5.*

## 4.1 Introduction

One of the major research questions resulting from the literature survey of Chapter 2 concerns the accurate representation of LAES during real-life operation when plant and device experience performance variation outside rated conditions. Simple models for design-point operation have been proposed so far; yet, the integration of LAES within the energy system involves external constraints on the power levels to be satisfied, which result in variable setpoints. Indeed, even in the simplest energy balancing case according to arbitrage alone, studies have shown time variations of the optimal power input and output profiles of LAES [140,181]. The methodological foundations for predicting device and plant performance under off-design conditions have been presented in Chapter 3. Their application to study LAES operation with a variable output setpoint is detailed hereafter.

This results chapter tackles the lack of thermodynamic assessment of LAES operation under variable power output conditions. In particular, the fact that LAES can provide a portfolio of storage services for both energy balancing and reserve provision – which introduce new charging/discharging requirements alongside part-load operation – is addressed. Thorough discussion focuses on: i) the understanding of why and how LAES technical performance is affected by the requirements of different market services to be provided; and ii) what is the technical and economic impact of LAES off-design operations when providing different market services. Finally, alternative operating strategies are compared based on their impact on the LAES techno-economic performance. The results in this chapter are particularly relevant from the perspective of a more diversified operation of LAES, which increases its contribution to grid balancing and may foster business cases. They progress the current understanding of standalone LAES off-design operation and provide a more accurate picture of both the capability of LAES to provide market services and the financial value to be extracted.

The chapter is organised as follows: the background and assumptions relevant to the current study are outlined in Section 4.2; specific elements of the mathematical model developed and its validation are reported in Section 4.3. Then, Section 4.4 presents the results from off-design LAES operation, and Section 4.5 further elaborates on their techno-economic implications, also presenting and assessing a regulation strategy to improve variable LAES performance. Finally, Section 4.6 presents this chapter's conclusions and outlook.

## 4.2 Background and assumptions

### 4.2.1 LAES standalone plant

The analysed plant is based on previous work [106] and is represented in Figure 32. It consists of a 100 MW LAES system with 3 hours of rated sustained discharge (300 MWh capacity) and 70 MW power input to air liquefaction during charge. It is a standalone plant, which was chosen to avoid case-specific considerations linked with process co-location, yet reaching comparable exergy efficiency with hybrid plants, as explained in Section 2.3.3. The plant features internal recycle of evaporation cold through high-grade cold storage (HGCS). Due to thermal stability and low cost, a

packed bed layout using quartzite-based gravel and direct heat transfer with an air loop was chosen [97]. Conversely, compression heat is recycled via a two-tanks sensible TES using diathermal oil. This way, the internally produced thermal streams are recirculated to boost system performance and enhance overall efficiency.

The main figures for the proposed plant design are gathered in Table 8, which includes the thermodynamic properties of the thermal storage materials considered for the study. The operational parameters of the plant were defined in order to optimise its roundtrip efficiency at design conditions (interested readers can refer to [106] for further information). According to the literature, conservative values of efficiency for power-related equipment were used [98].

Table 8: Main parameters for the proposed standalone plant.

| Quantity | Value |
|---|---|
| Rated power output | 100 MW |
| Rated discharging pressure | 75 bar |
| Energy capacity | 300 MWh |
| Nominal discharge time | 3 h |
| Liquefaction power input | 70 MW |
| Rated charging pressure | 185 bar |
| Liquid air storage tanks | 3000 ton |
| Specific heat capacity of rocks | 541 J/kgK |
| Cold storage volume | 9200 m$^3$ |
| Specific heat capacity of diathermic oil | 2200 J/kgK |
| Hot storage volume | 4000 m$^3$ |
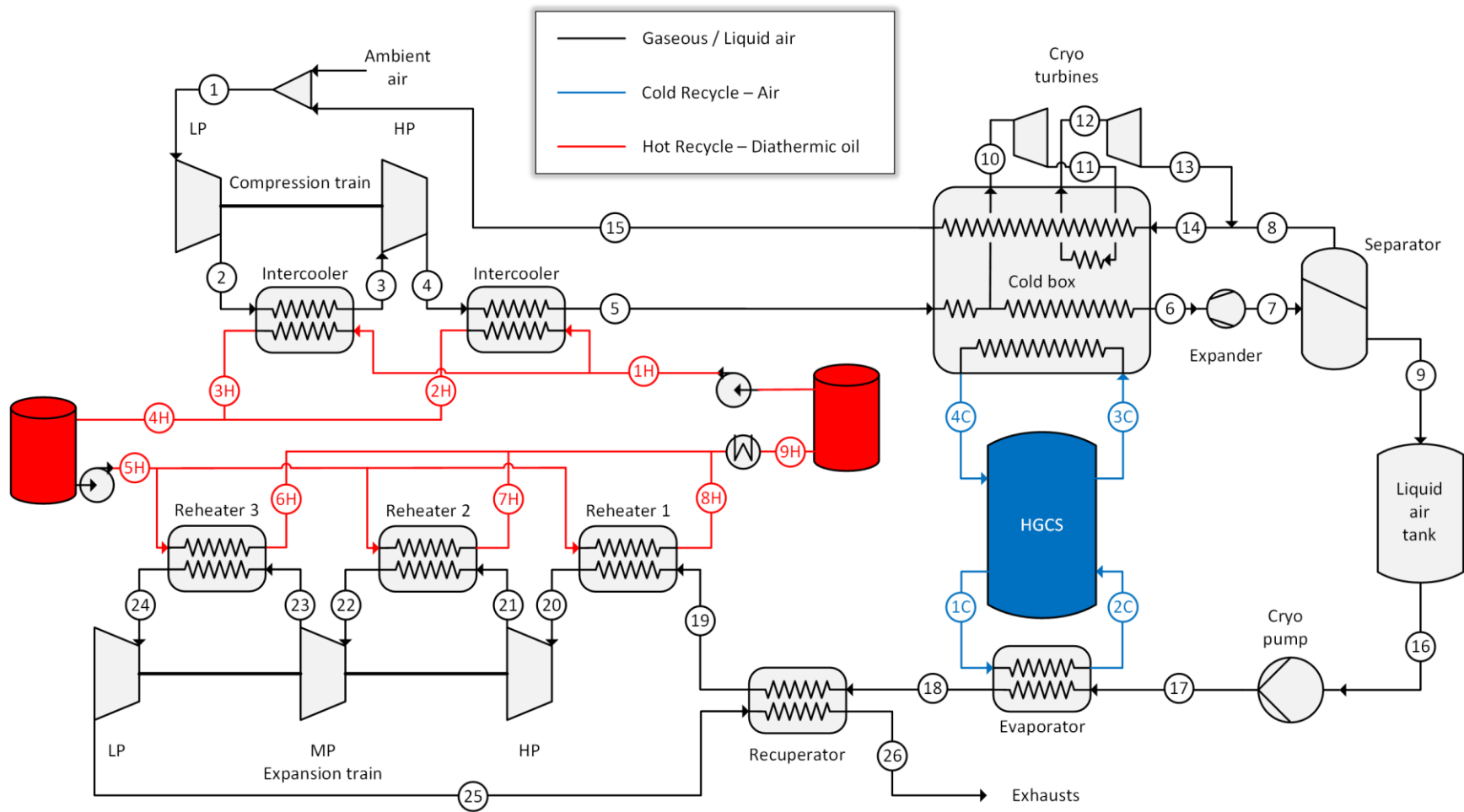
**Figure 32: Process flow diagram of the investigated 100 MW/300 MWh LAES standalone plant.**

### 4.2.2 Balancing services and LAES duty cycle

As discussed in Section 2.4, LAES participation in multiple balancing services is advisable in future energy systems. In the UK electricity market, short term operating reserve (STOR) and fast reserve (FR) appear suitable for LAES technical features and were considered in the present analysis, alongside arbitrage. Specifically, STOR providers must be ready in the availability windows to supply a minimum capacity of 3 MW within 4 h from instruction, while, for FR, at least 50 MW and less than 2 min response time is required [164]. Three operational modes were defined, as illustrated in Figure 33 to account, respectively, for LAES participation in arbitrage alone, arbitrage and STOR, or arbitrage and FR and thus portray different contributions of LAES to grid balancing. Within each mode, the power committed to the reserve services was assumed based on the reports from the UK energy system operator. In Mode 2, 10 MW were reserved for STOR (in the season 2016-2017, 67.1% of the UK providers offered to STOR between 3 and 10 MW [163]), while 50 MW were assigned to FR, in Mode 3 (see Table 9), in compliance with the specification on minimum power commitment presented above.
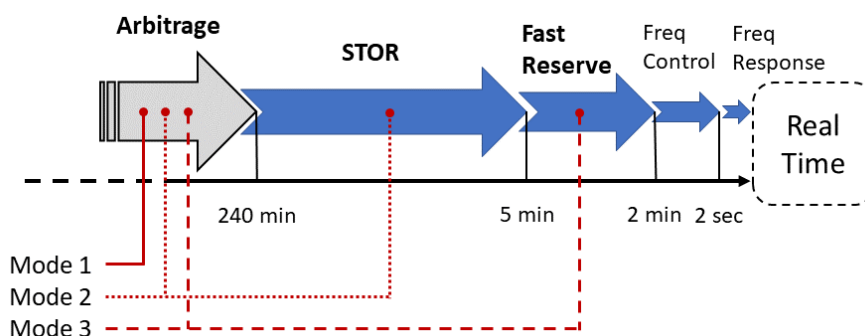


**Figure 33: Schematic of the considered services, among the ones available in the UK market.**

For each mode of operation, a representative LAES duty cycle was designed in such a way that fulfils the requirements of the balancing services considered for the specific mode of operation. Hence, charging and discharging times are consistent with the electricity price evolution, while power setpoints during the reserve availability windows ensure the committed capacity can be delivered. The duty cycles are illustrated in Figure 34. Such archetype cycles served as input to the numerical model of LAES developed, which allows simulating LAES operation once following the cycles. Ultimately, a representative LAES thermodynamic performance is achieved by the combination of the two above elements: a realistic operational cycle for each combination of balancing services considered and a thermodynamic system model capable of evaluating LAES performance when operating according to such cycle.

**Table 9: Selected operating modes for LAES.**

| Operating mode | Arbitrage | | STOR | | Fast reserve | |
|---|---|---|---|---|---|---|
| Mode 1 | ✓ | 100 MW | | | | |
| Mode 2 | ✓ | 90 MW | ✓ | 10 MW | | |
| Mode 3 | ✓ | 50 MW | | | ✓ | 50 MW |

Across all the modes, LAES charging process was considered to take place during night-time, which commonly coincides with low electricity price period. Best charging and discharging periods were determined with 1-h resolution, based on the inspection of UK electricity spot prices referring to winter 2017[6]. Then, the power allocated to STOR (Mode 2) and to FR (Mode 3) was deducted from the total discharge power of the LAES plant. This is because the ideal discharging period for arbitrage was found to coincide with the reserve availability window. On the other hand, no delivery of reserve services was considered at this stage, since available market reports showed less than 3% call probability for STOR [163] and about 5% for FR [289] over a typical year. Even if real-time reserve market participation could, in the event of a service call, result in a different duty profile for Mode 2 and 3, in most cases daily operation will involve service commitment only. On the other hand, it is unlikely variations in the electricity price profile would displace discharging period outside the availability windows. Hence cycles for Mode 2 and 3 can be considered sufficiently accurate and thus appropriate to assess their impact on the thermodynamic performance of LAES.
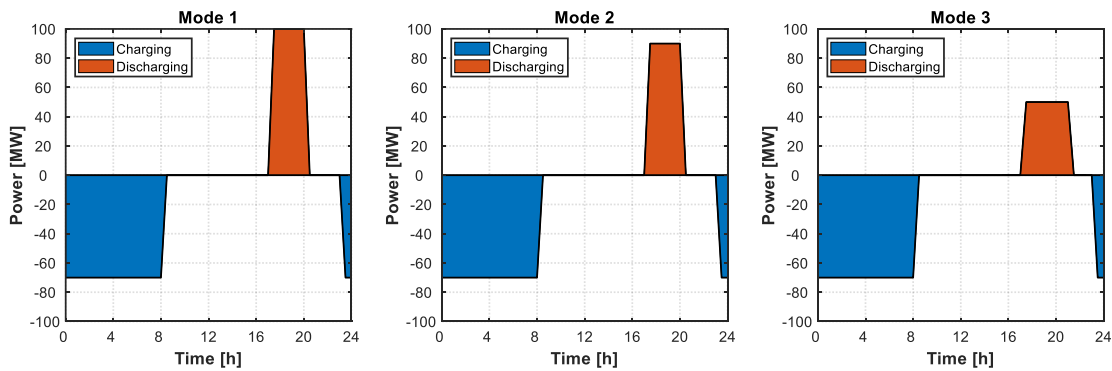


Figure 34: Selected duty cycles for LAES in the different operating modes.

## 4.3    Numerical modelling of LAES and performance assessment

Figure 35 schematically describes the framework used for setting up the numerical model of LAES, which was then implemented in EES (Engineering Equation Solver), in conjunction with MATLAB. The LAES model thoroughly described in [106] was used as the backbone; it comprises energy, mass and momentum conservation equations for each LAES component (following the approach presented in Section 3.2). On top of it, characteristic equations capturing off-design operation of turbines, heat exchangers and cryogenic pumps were systematically implemented for the PRU.
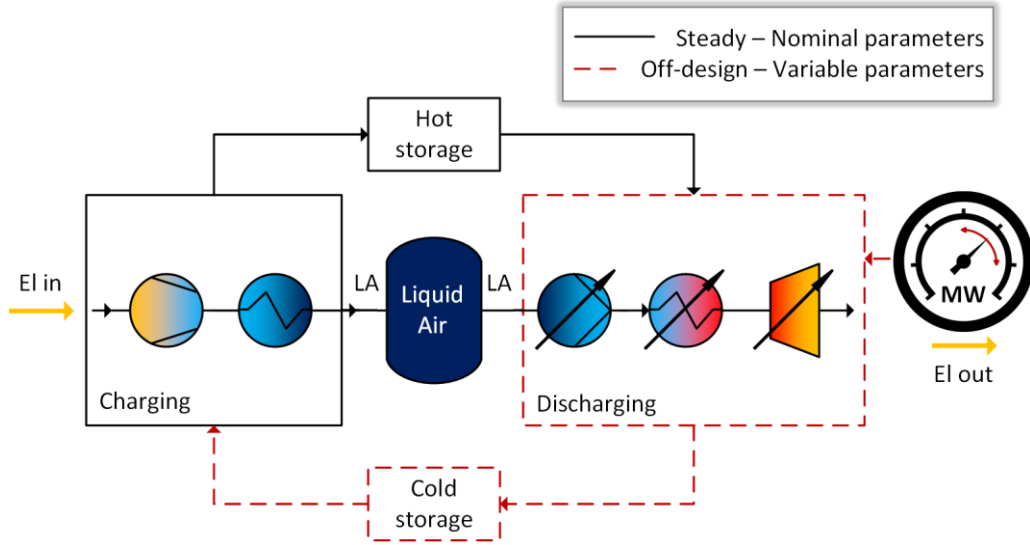
**Figure 35: Conceptual drawing of the modelling framework for the present analysis.**

More specifically, turbine maps were used to describe the variation of device efficiency and expansion ratio as a function of the corrected rotational speed and mass flow rate parameters:

$$\frac{\eta_T}{\eta_{T,0}} = f_1(n'_T, m'_T) \qquad 4.1$$

$$\frac{\Pi_T}{\Pi_{T,0}} = f_2(n'_T, m'_T) \qquad 4.2$$

The effect of flow and fluid properties on heat transfer in the heat exchangers was accounted through the $\varepsilon - NTU$ method [253]:

$$\varepsilon = f\left(NTU, \dot{C}_R, HX\ geometry\right) \qquad 4.3$$

The specific function from Equation 4.3 was chosen considering a counterflow heat exchanger configuration. Also, the Dittus-Boelter correlation was used to link the rated and off-design overall heat transfer coefficient for the calculation of $NTU$ [273], in the case of turbulent flow regime, so that:

$$U = U_0 \left(\frac{\dot{m}_{HX}}{\dot{m}_{HX,0}}\right)^{0.8} \qquad 4.4$$

The affinity law was used to model the cryogenic pumps, with device efficiency curve as a function of the mass flow rate retrieved from [290] and fitted to a second-order polynomial (coefficients are $a_1 = -1$, $a_2 = 2$ and $a_3 = 0$; the coefficient of determination 0.991). An analytical model for the HGCS was used, as described in Section 3.4.2, which uses a logistic cumulative distribution function to approximate the thermocline behaviour. This allowed close approximation of the results from a validated 1-D, transient storage model developed in COMSOL [106] at a minimal computational expense. Model parameters for LAES discharging process are gathered in Table 10.

**Table 10: Model parameters for LAES discharging process.**

| Parameter | Value |
| --- | --- |
| Rated mass flow rate | 212 kg/s |
| Turbine rated efficiency | 0.85 |
| Turbine rated rotational speed | 1500 rpm |
| Turbine rated inlet temperature | 613 K |
| High-pressure (HP) turbine rated inlet pressure | 74 bar |
| Medium-pressure (MP) turbine rated inlet pressure | 19 bar |
| Low-pressure (LP) turbine rated inlet pressure | 5 bar |
| Cryopump rated efficiency | 0.75 |
| Heat exchanger rated effectiveness | 0.95 |
| Evaporator effectiveness | 0.95 |
| Mechanical efficiency | 0.97 |
| Components pressure drop | 1% |

Concerning LAES discharging process, i.e. air liquefaction, costant power input and no off-design for power devices were considered because: i) the selected reserve services imply extra power generation rather than reduction of the plant load; ii) LAES charging conventionally takes place outside reserve windows; and iii) air liquefaction is a highly energy-intensive process thus run at rated conditions. However, as charge and discharge subprocesses are linked by the cold and hot recycle streams (see Figure 35), off-design temperatures along the charging cycle can be driven by deviations of the PRU and the developed LAES model captures such behaviour. Model parameters for LAES discharging process are gathered in Table 11.

**Table 11: Model parameters for the LAES charging process.**

| Parameter | Value |
| --- | --- |
| Ambient temperature | 288.15 K |
| Ambient pressure | 1.01 bar |
| Compressor efficiency | 0.85 |
| Cryoturbine efficiency | 0.7 |
| Heat exchanger effectiveness | 0.97 |
| Mechanical efficiency | 0.97 |
| Components pressure drop | 1% |
| Pinch point ΔT in the cold box | 5 K |

### 4.3.1 Model validation

The capability of the model to replicate nominal LAES operation was first validated by comparing the obtained predictions with those from [106], where steady-state, rated conditions are considered. Furthermore, the reference model in [106] was already proven to be consistent for simulation at design conditions, as successfully validated in previous works. Table 12 compares the predictions of the model presented here with the reference values. In Table 12, discrepancies always remained well within 2%, which clearly shows the robustness and accuracy of the LAES plant model proposed here. Furthermore, in absence of experimental data of LAES operation ultimately needed for the validation of the full off-

design LAES model, its suitability for investigating the thermodynamic performance of LAES when operated according to the modes presented in Section 4.2.2, is inferred by: i) model validation at rated conditions and ii) use of validated off-design models for individual components (pump and turbine maps, packed bed cold storage).

Table 12: Validation of LAES off-design model. Selected thermodynamic and characteristic values.

| Property | Reference value | Model prediction | Deviation |
|---|---|---|---|
| HP turbine efficiency [-] | 0.85 | 0.85 | **0.0%** |
| MP turbine efficiency [-] | 0.85 | 0.85 | **-0.1%** |
| LP turbine efficiency [-] | 0.85 | 0.85 | **-0.2%** |
| HP turbine expansion ratio [-] | 3.7 | 3.69 | **-0.3%** |
| MP turbine expansion ratio [-] | 3.7 | 3.70 | **0.1%** |
| LP turbine expansion ratio [-] | 3.7 | 3.71 | **0.2%** |
| Cryopump efficiency [-] | 0.75 | 0.75 | **0.0%** |
| Recuperator effectiveness [-] | 0.95 | 0.95 | **-0.2%** |
| Discharging mass flow rate [kg/s] | 211.8 | 211.5 | **-0.1%** |
| Specific work output [kJ/kg$_{liq}$] | 472.2 | 472.8 | **0.1%** |
| Specific cold recycle [kJ/kg$_{liq}$] | 362.4 | 361.0 | **-0.4%** |
| Cryopump duty [kW] | 2389 | 2389 | **0.0%** |
| PRU outlet pressure [bar] | 1.41 | 1.40 | **-1.0%** |
| Maximum air temperature [K] | 621.1 | 620.7 | **-0.1%** |

## 4.3.2 Performance indicators

On top of the typical performance indicators, namely specific work $w$, hot and cold recycle $q_{HR}$ and $q_{CR}$ and roundtrip efficiency $\eta_{RT}$, liquid yield was quantified for the liquefaction cycle as the ratio of the produced liquid mass flow rate to the total air mass flow rate through the Claude cycle: $Y = \dot{m}_{liq}/\dot{m}_{chr}$. To achieve further thermodynamic insights, exergy analysis was carried out. Exergy streams were clustered as feeders, losses, exergy destruction and useful products for each individual component so that:

$$\dot{Ex}_{feed} = \dot{Ex}_{prod} + \dot{Ex}_{loss} + T_0\Sigma \qquad 4.5$$

Table 13 reports the definition of feeders, losses and products for the individual devices making up the LAES plant. Finally, exergy (second law) efficiency and specific irreversibility generation were calculated, respectively, by equations 4.6 and 4.7:

$$\eta_{Ex} = \frac{\dot{Ex}_{prod}}{\dot{Ex}_{feed}} \qquad 4.6$$

$$\phi = \frac{T_0\Sigma}{\dot{Ex}_{feed}} \qquad 4.7$$

Table 13: Equations used for computing the exergy parameters of every component.

| Component | Feeder ($\dot{Ex}_{feed}$) | Entropy generation ($T_0\Sigma$) | Product ($\dot{Ex}_{prod}$) |
|---|---|---|---|
| Mixing device | $\sum_{in} \dot{m}_i\,ex_i$ | $\sum_i \dot{m}_i\,ex_i$ | $\sum_{out} \dot{m}_i\,ex_i$ |
| Compressor | $-\dot{W}$ | $-\dot{W} + \dot{m}(ex_{in} - ex_{out})$ | $\dot{m}(ex_{out} - ex_{in})$ |
| Heat exchanger | $\sum_{feed} \dot{m}_i\,(ex_{in} - ex_{out})_i^{*}$ | $\sum_i \dot{m}_i\,(ex_{in} - ex_{out})_i$ | $\sum_{prod} \dot{m}_i\,(ex_{in} - ex_{out})_i^{*}$ |
| Turbine | $\dot{m}(ex_{in} - ex_{out})$ | $-\dot{W} + \dot{m}(ex_{in} - ex_{out})$ | $\dot{W}$ |
| Cryo expander | $\dot{W} + \dot{m}_{liq}ex_{liq}$ | $-\dot{W} + \sum_i \dot{m}_i\,ex_i$ | $\dot{m}_{in}ex_{in} + \dot{m}_{vap}ex_{vap}$ |
| Pump | $-\dot{W}$ | $-\dot{W} + \dot{m}(ex_{in} - ex_{out})$ | $\dot{m}(ex_{out} - ex_{in})$ |
| J-T valve | $\dot{m}(ex_{in} - ex_{out})$ | $\dot{m}(ex_{in} - ex_{out})$ | 0 |

$^{*}$ In the case of heat exchangers, feeders are all the streams whose specific exergy $ex$ reduces, while products are all the streams whose specific exergy increases through the component.

### 4.3.3   Economic analysis

To study the economic impact of considering accurate system performance on the LAES revenues for operation in Mode 1, Mode 2 and Mode 3 (see Table 9), plant operation based on design-point and off-design models were compared for each of those three case studies. Average sell and buy prices for arbitrage were used. On the other hand, reserve service remuneration consists of an availability fee, a utilisation fee and, for FR only, a positional fee (see Section 2.4.1). Numerical figures were retrieved from the UK energy system operator [163,289] and are listed in Table 14, alongside other inputs to the economic analysis.

Table 14: Key input parameter to the economic assessment

| Parameter | Value | Units | Source |
|---|---|---|---|
| Average buy price, $\pi_{buy}^{el}$ | 27 | [£/MWh] | [140,291] |
| Average sell price, $\pi_{sell}^{el}$ | 80 | [£/MWh] | Calculations* |
| STOR availability fee, $\pi_{STOR}^{ava}$ | 42.5 | [£/h] | [163] |
| STOR utilisation fee, $\pi_{STOR}^{util}$ | 150 | [£/MWh] | [163] |
| FR availability fee, $\pi_{FR}^{ava}$ | 210 | [£/h] | [289] |
| FR positional fee, $\pi_{FR}^{pos}$ | 90 | [£/h] | [289] |
| FR utilisation fee, $\pi_{FR}^{util}$ | 100 | [£/MWh] | [289] |
| Arbitrage cycles | 300 | [1/year] | Assumption |
| STOR calls, $\tau_{STOR}$ | 112 | [h/year] | [163] |
| STOR availability, $\tau_{STOR}^{ava}$ | 3884 | [h/year] | [163] |
| FR calls, $\tau_{FR}$ | 304 | [h/year] | [289] |
| FR availability, $\tau_{FR}^{ava}$ | 6107 | [h/year] | [289] |

*Given electricity price time series, computed average value for 3 hours daily discharge.

LAES was assumed to be charged for 300 yearly cycles of 9 h each, according to its nominal design. The energy output devoted to the $i$-th reserve service, $\dot{W}_{dsc,i}\,\tau_i$ was computed once knowing the yearly

duration of calls to STOR and FR (see Table 14). The remaining capacity used for arbitrage and the *actual* plant roundtrip efficiency, $\eta'_{RT}$, were computed by ensuring energy conservation:

$$\begin{cases} \dot{W}_{chr}\tau_{chr}\eta'_{RT} = \dot{W}_{dsc}\tau_{dsc} + \dot{W}_{dsc,i}\,\tau_i \\ \eta'_{RT} = \dfrac{\dot{W}_{dsc}\tau_{dsc}\eta_{RT} + \dot{W}_{dsc,i}\,\tau_i\eta_{RT,i}}{\dot{W}_{dsc}\tau_{dsc} + \dot{W}_{dsc,i}\,\tau_i} \end{cases} \qquad 4.8$$

Ideal cases were assessed considering fixed plant roundtrip efficiency $\eta_{RT}$ at design value. For cases with and without regulation, on the contrary, round trip efficiency values obtained from the off-design model were used, depending on the specific mode. During reserve provision, $\eta_{RT,i}$ was fixed at its design value. Finally, the yearly revenue for each mode was quantified by adding all the relevant revenue streams of Mode 1, 2 and 3, respectively, and subtracting the cost associated with electricity purchase; this is explained in Table 15.

Table 15: Economic model equations used to compute the revenue of each operating mode.

| Description | Equation | Relevant to Mode |
|---|---|---|
| Arbitrage revenue | $\dot{W}_{dsc}\tau_{dsc}\pi_{sell}^{el}$ | 1, 2, 3 |
| STOR revenue | $\dot{W}_{dsc,STOR}\tau_{STOR}\pi_{STOR}^{util} + \tau_{STOR}^{ava}\pi_{STOR}^{ava}$ | 2 |
| FR revenue | $\tau_{FR}\left(\dot{W}_{dsc,FR}\pi_{FR}^{util} + \pi_{FR}^{pos}\right) + \tau_{FR}^{ava}\pi_{FR}^{ava}$ | 3 |
| Electricity purchase | $\dot{W}_{chr}\tau_{chr}\pi_{buy}^{el}$ | 1, 2, 3 |

## 4.4 Results

In this section, results from the simulations performed highlighting the links between LAES thermodynamic performance and the operating modes are presented and discussed. First, model outcomes for the whole LAES plant are detailed in Section 4.4.1; then, in Section 4.4.2, the focus is shifted to specific plant components.

### 4.4.1 System-level assessment of LAES operating modes

Under the three modes considered, LAES ideal operation, i.e. charging and discharging at design conditions, is only possible in Mode 1. When participating in STOR and FR services (Mode 2 and Mode 3), only a reduced power output can be allocated for arbitrage purposes. Hence, the PRU is restricted to part-load operation in these modes. The main performance parameters summarised in Table 16 for each operating mode reflect such limitations, especially for the PRU, where the specific work output reduces from 473 to 301 kJ/kg between Mode 1 and Mode 3, and the specific hot recycled also decreases by about one third. Part-load inefficiencies represent the key mechanism leading to poor plant performance, as described below and in section 4.4.2. In contrast, the liquefaction cycle experiences little or no variations, and liquefaction work is steadily in the range 270-290 kWh per ton of liquid air, consistent with state-of-the-art cryogenic cycles [18,105].

**Table 16: Major LAES performance parameters under the different operating modes (variations are expressed relative to Mode 1).**

| Parameter | Mode 1 Value | Mode 2 Value | Δ | Mode 3 Value | Δ |
|---|---|---|---|---|---|
| Specific work output [kJ/kg$_{liq}$] | 473.0 | 451.1 | **-5%** | 301.1 | **-36%** |
| Specific liquefaction work [kJ/kg$_{liq}$] | 985 | 1015 | **3%** | 972 | **-1%** |
| Specific cold recycle [kJ/kg$_{liq}$] | 359 | 355 | **-1%** | 353 | **-2%** |
| Specific hot recycle [kJ/kg$_{liq}$] | 527 | 505 | **-4%** | 354 | **-33%** |
| Cold recycle temperature (point 3C) [K] | 93.0 | 93.0 | **0%** | 92.8 | **0%** |
| Cold recycle flow rate (point 3C) [kg/s] | 135 | 127 | **-6%** | 141 | **4%** |
| Liquid yield [%] | 77% | 75% | **-3%** | 78% | **1%** |

The thermodynamic states for the charging and discharging processes of the LAES plant for Mode 1 (only arbitrage) and Mode 3 (arbitrage and FR), as presented in the T-s diagrams of Figure 36, confirm such behviour. From Figure 36 left it can be appreciated that no noticeable change occurs in the air liquefaction process as LAES charging runs steadily at rated power, without departing from nominal operating conditions. On the contrary, thermodynamic conditions change considerably when discharge is operated according to Mode 3 instead of Mode 1.

In Mode 3, partial load conditions occur since part of the LAES power output is committed to delivering FR upon request from the network operator, as captured by the duty cycle from Figure 34. During part-load operation, the rotational speed of the cryogenic pump is decreased, circulating less liquid air flow rate for reduced power output. In turn, this results in a lower pressure head (point 17 in the T-s diagram), following the affinity law for pumps. The reduced air flow rate also impacts the temperature levels along the discharging cycle. The inlet temperature of each turbine increases slightly (points 20, 22 and 24) due to a higher heat transfer rate in the reheaters (higher $NTU$). However, a major temperature increase is also registered at the outlet of the expansion stages, leading to overall worse use of the available heat from the hot recycle (heat of compression). The absolute value plummets from 112 to only 58 MW, when LAES discharge is operated according to Mode 3, corresponding to a 33% decrease per unit liquid air flowing through the discharging process. A major effect from the reduced-power operation is also observed in the expansion processes (segments 20-21, 22-23 and 24-25).
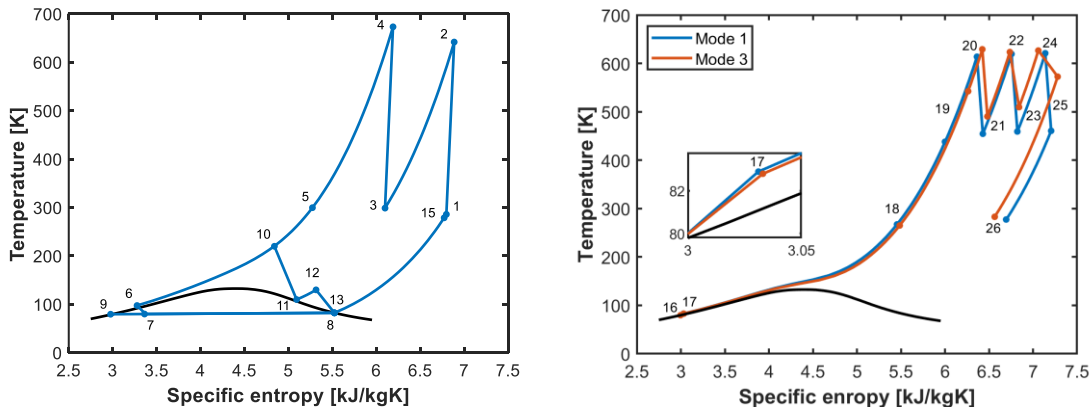


Figure 36: Temperature-entropy diagrams for LAES charging (left) and discharging (right) processes.

From a thermodynamic standpoint, the allocation of 10 MW to STOR has only a marginal effect on the plant, but when higher power commitments are required for reserve service provision, the impact is relevant. Lower working pressures in the PRU lead to slightly lower temperatures at the pump outlet, which could potentially be beneficial for cold recycle. However, deviations reported in Table 16 are small and make this effect negligible. Interestingly, this result suggests that, even if LAES charging and discharging are tightly interconnected [98], off-design operation independently affects the involved subprocess, with marginal mutual interaction.

## *Exergy analysis – system level*

To gain further insights into the impact of different irreversibility mechanisms on system performance, exergy pie charts were generated. Useful outputs are represented in yellow and defined as follows:

- *Charging process*: liquid air and hot thermal energy
- *Discharging process*: electrical power output and cold thermal energy

Shades of blue refer to exergy destruction through irreversibility (entropy generation) and losses from the system to the environment. All the quantities were expressed as a percentage of the net exergy input to charging and discharging subprocesses.

Liquefaction exergy efficiency is 84%, both when operating according to arbitrage alone and when adding reserve services. Only 14 MW of the input exergy is destroyed in the process, mostly due to heat exchange and compression. More interestingly, significant variations in the exergy distribution within the PRU are observed, under the different operating modes, as shown in Figure 37. Percentage comparison provides a piece of valuable information here, as absolute exergy values may be misleading given the different power outputs between the operating modes.
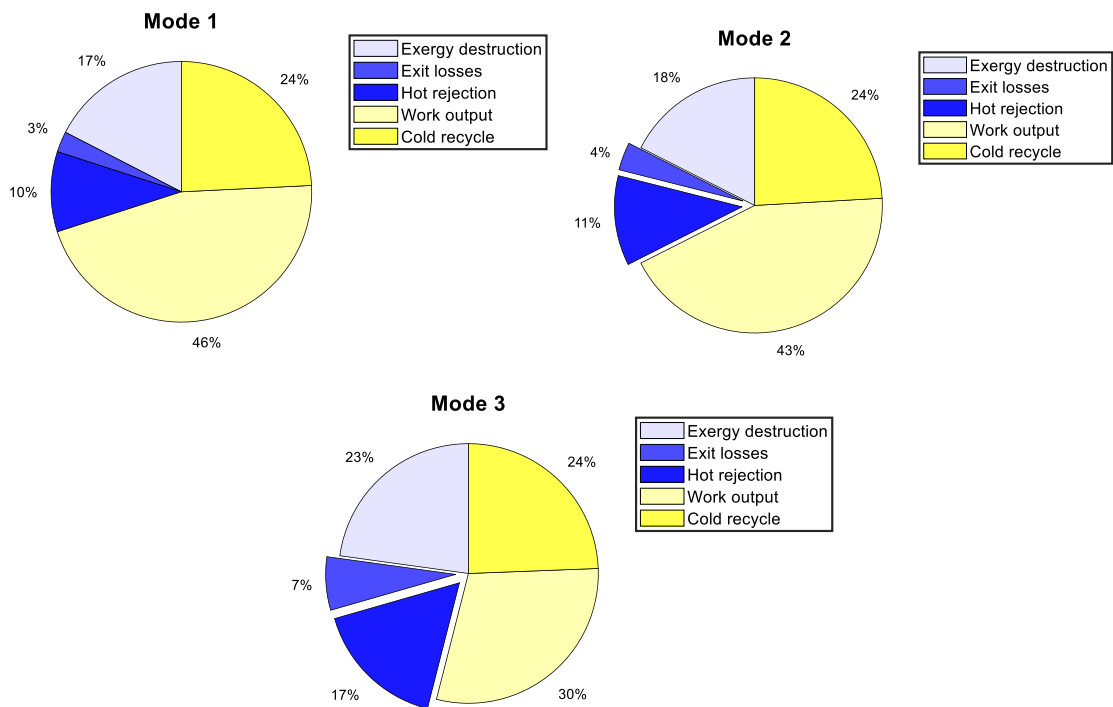
The exergy efficiency of the PRU is significantly affected when LAES participates in reserve services (Mode 2 and Mode 3): 3 percentage points are lost when considering STOR and 16 for FR. The variation is entirely due to the reduction in conversion efficiency to electrical power output, as the cold recycle was found not to be affected.

With LAES at part-load, exit losses (i.e. exergy losses from the pressure and temperature conditions of the outlet air stream being different from those of the ambient) and hot rejection in the hot recycle represent the key mechanisms leading to exergy loss, due to thermodynamic states drifting from design conditions. Air leaves the PRU at higher temperatures and pressures; increasing quantities of thermal energy are rejected towards the environment before point 9H. For operation under arbitrage and STOR, these are the only additional loss sources. However, when reserve services require higher power commitments (FR in this case), exergy destruction share also increases, meaning the thermodynamic process operates less efficiently.

### 4.4.2 Component-level assessment of LAES operating modes

Because the participation in reserve markets introduces performance deviations of LAES mainly in the discharging process, when looking at the impact of LAES part-load operation component by component, a particular focus is owed to the PRU. In particular, the performance of the cryogenic pump and heat exchangers is only partially affected by variations in the LAES power output. At part-load, pump efficiency drops from 75% to 71.5% in Mode 3. Less liquid air circulates through the power cycle, and the effectiveness of heat exchangers slightly increases with the increase in $NTU$. However, this variation is limited (within 1%) as the rated values of effectiveness are already large. Turbines, on the contrary, are significantly affected: their isentropic efficiency diminishes as well as the corresponding expansion ratios, as illustrated in Figure 38.
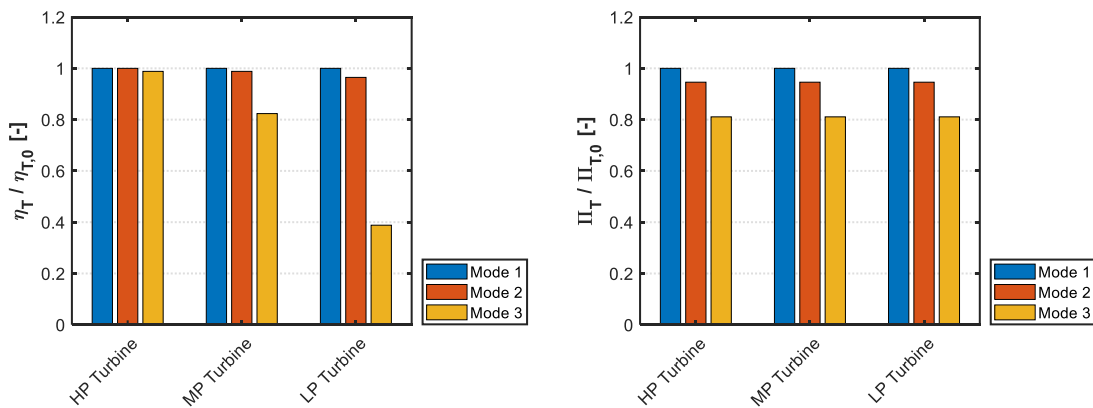


Figure 38: Turbine characteristic parameters for different operating modes.

The operating mode of the plant affects the thermodynamic states along LAES power recovery unit (see Figure 36). Therefore, all three expansion stages experience a deviation with respect to the rated inlet conditions in terms of mass flow rate, pressure and temperatures. This triggers off-design operation, with the associated reduction of turbine efficiency and achievable pressure ratio. However, Figure 38 shows that the impact of off-design conditions is different for each turbine stage and the low-pressure turbine experiences the largest variation in efficiency and pressure ratio. This is due to a

70

compounding effect of the off-design conditions occurring in the HP and MP turbine, which cause a significant change in the inlet conditions to the LP turbine, as illustrated by point 24 on the T-s diagram of Figure 36. As a result, the efficiency of LP turbine drops by 60% when the plant operates in Mode 3. Therefore, to reduce the impact of off-design operation it might be necessary to cap the maximum power allocated to reserve services. Expansion ratios also diminish for Mode 2 and 3. The effect is in this case comparable for each turbine stage. The inlet temperatures remain nearly constant for each stage, and thus expansion ratios are a function of mass flow rate only, whose change with respect to design values is identical for each stage when the plant operates in Mode 2 or 3.

Effects on efficiency and pressure ratio are the main drivers for the reduced specific work output observed in section 0. Indeed, a good estimation of the specific work output for LAES can be computed by neglecting the work required by the cryogenic pump (only 2-3% of the net energy production) and thus considering only the individual contribution from each expansion stage, according to Equation 4.9:

$$w_{dsc} \approx \sum_i \eta_{T,i} c_p T_{in,i} \left( \Pi_{T,i}^{\frac{\gamma-1}{\gamma}} - 1 \right)$$
4.9

Throughout the different operating modes, inlet temperatures $T_{in,i}$ remain basically constant for all the stages. On the contrary, expansion ratios $\Pi_{T,i}$ and isentropic efficiencies $\eta_{T,i}$ are reduced in value, compromising component efficiency when running at part-load. Along with the described effect on plant power output, lower expansion ratios also mean higher outlet temperatures from the turbines, as highlighted in section 0. Higher heat rejection in the hot recycle, observed for off-design conditions, is a direct consequence.

To conclude the discussion around turbines, Table 17 shows the inlet pressure in the turbine stages for the different operational modes. It is interesting to observe that inlet pressure for HP stage decreases in Mode 2 and 3 compared to Mode 1, while the opposite occurs for the MP and LP turbine. In Mode 2 and 3 the LAES power output is reduced compared with Mode 1, which results in a lower pressure in the air circuit of the discharge process, and thus a lower inlet pressure for the HP turbine. However, the expansion ratio for HP turbine stage decreases as well (see Figure 38), causing higher pressure downstream the HP turbine and thus for the MP and LP turbines (deviations up to almost 40%). A regulation strategy aiming to limit the inlet pressures to rated values for MP and LP stages was proposed; it is discussed in Section 4.5.1.

Table 17: Absolute and normalised inlet pressures to the turbine stages for different operating modes.

| Mode | HP Turbine | | MP Turbine | | LP Turbine | |
|---|---|---|---|---|---|---|
| | [bar] | [-] | [bar] | [-] | [bar] | [-] |
| Mode 1 | 72.9 | 1.00 | 19.6 | 1.00 | 5.2 | 1.00 |
| Mode 2 | 70.8 | 0.97 | 20.0 | 1.02 | 5.6 | 1.08 |
| Mode 3 | 67.4 | 0.92 | 21.4 | 1.09 | 7.1 | 1.37 |

## Exergy analysis – component level

A turbine performance deterioration is also apparent from an exergy standpoint and particularly severe for the low-pressure stage, as illustrated in Figure 39. Irreversibilities in the turbine stages add up to account for the majority of exergy destruction in the process. The total value attributed to turbines is 33% higher when participating to FR, as compared to arbitrage alone. Exergy destruction by expansion increases from 15 MW to almost 20 MW, causing a reduction in the turbine exergy efficiency, especially for the low-pressure stages. It is therefore crucial to guarantee high turbine efficiency to achieve good system performance. Thus, finding strategies for reducing the effect of off-design conditions in the expansion stages is important and may lead to large improvements in LAES operation.
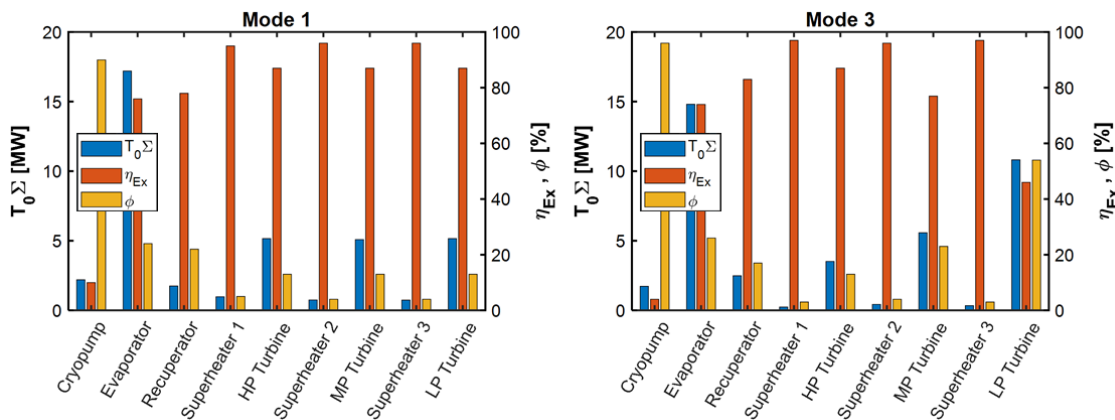


Figure 39: Exergy destruction and exergy indicators for the PRU components for different operating modes.

A significant share of exergy destruction takes place in the evaporator, in agreement with the findings from other studies [292]. However, off-design conditions do not alter significantly component operation: irreversibility in the evaporator is caused by variation of thermo-physical properties of air under supercritical conditions and the appearance of a pinch point inside the component. Exergy destruction is more evenly distributed between the evaporator and recuperator in Mode 3, due to higher $\Delta T$ in the latter. Evaporator exergy efficiency slightly diminishes from 76% to 74% due to poorer matching between temperature profiles of the hot and cold streams, as illustrated by the composite curves reported in Figure 40. Splitting the evaporation into multiple sections would allow adjusting the mass flow rate of the secondary streams independently [109], which could be particularly useful for optimising heat transfer under diverse operating conditions.
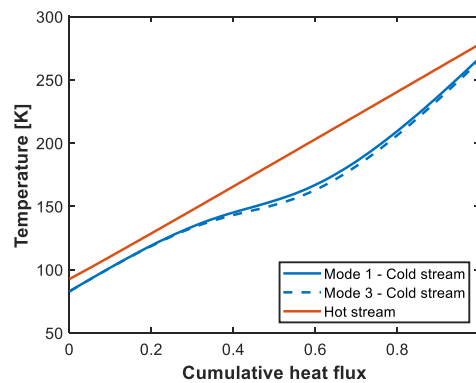


Figure 40: Composite curves in the evaporator of LAES.

72

## 4.5 Discussion

Further discussion on model results is provided hereafter. In particular, Section 4.5.1 presents and assesses a novel regulation strategy proposed thanks to the insights gained from previous results and aimed at reducing the impact of off-design operation on LAES performance. Finally, the technical impact of off-design conditions on LAES operation is generalised in Section 4.5.2 and Section 4.5.3 elaborates on the economic implications.

### 4.5.1 Proposed regulation strategy

Part-load operation of LAES induces a significant reduction in the performance of both components and the whole system. Temperatures and pressures along the cycle were found to deviate significantly in response to power reductions, impacting mostly on the low-pressure turbine stage. This led to uneven distribution of the power generated by each stage and additional inefficiencies in the use of the available compression heat within the process. A suitable regulation strategy for LAES, directed towards the mitigation of the off-design conditions and increased overall plant flexibility, consists of controlling air pressure upstream HP, MP and LP turbine stages. Indeed, as pressure ratios decrease for off-design (see Figure 38), higher turbine inlet pressures are achieved, which can be reduced to rated conditions by throttling with JT valves; this is represented in Figure 41.
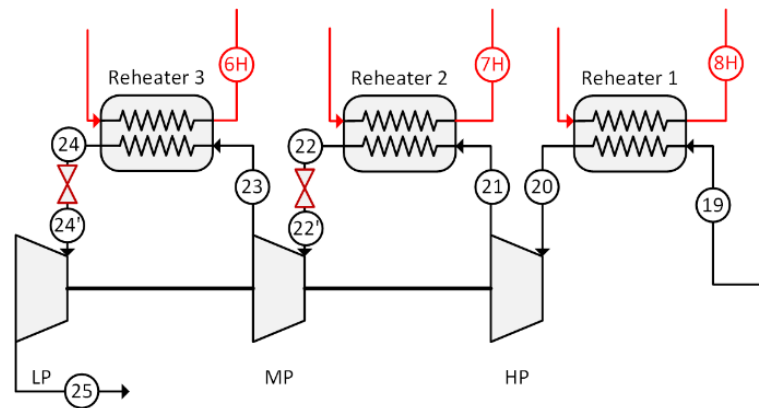


Figure 41: Detail of the proposed off-design LAES regulation strategy with JT valves upstream turbines.

Values of LAES off-design performance assessment under the proposed regulation strategy are presented in Table 18, referring to plant operation under Mode 3, i.e. the most demanding mode concerning off-design inefficiencies. Thermodynamic states are compared in Figure 42. At 50 MW power output, specific work is 12% higher when the regulation is applied. It can also be appreciated on the T-s diagram that thermodynamic conditions are closer to those for nominal conditions and that the slope of the expansion curves is similar for each turbine stage. This results in LP turbine efficiency of 72% instead of 33% (Mode 3 without regulation strategy). On the other hand, the cold recycled between discharging and charging slightly diminishes since lower mass flow rates are now required in the evaporator, and the evaporation temperature is higher for the higher cycle pressure. Liquid yield decreases as a consequence, but without significantly affecting plant performance. Overall, results illustrate the capability of this strategy to improve the LAES plant performance when operating at partial load.

**Table 18: LAES performance parameters with and without the regulation strategy.**

| Parameter | Mode 3 - without regulation Value | Mode 3 - with regulation Value | Δ |
|---|---|---|---|
| Specific work output [kJ/kg$_{liq}$] | 301.1 | 336 | **12%** |
| Specific liquefaction work [kJ/kg$_{liq}$] | 972 | 1019 | **5%** |
| Specific cold recycle [kJ/kg$_{liq}$] | 353 | 355 | **1%** |
| Specific hot recycle [kJ/kg$_{liq}$] | 354 | 386 | **9%** |
| Cold recycle temperature (point 3C) [K] | 92.8 | 93 | **0%** |
| Cold recycle flow rate (point 3C) [kg/s] | 141 | 126.5 | **-10%** |
| Liquid yield [%] | 78% | 74% | **-4%** |
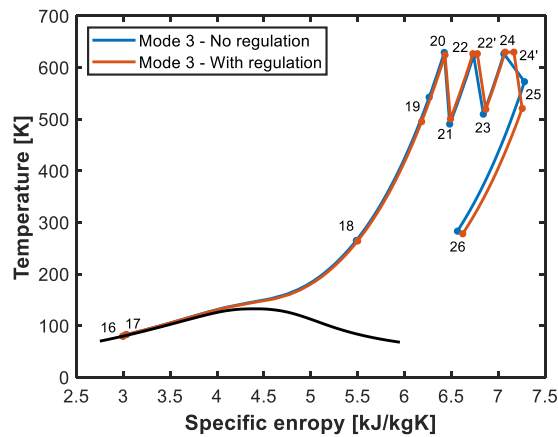


**Figure 42: Temperature-entropy diagram for LAES discharging process, with and without the regulation strategy.**

## Exergy analysis

Exergy analysis was used to further characterise the thermodynamic deviations introduced by implementing the proposed off-design regulation strategy. Figure 43 shows the component-wise breakdown of irreversibility, exergy efficiency and specific irreversibility. Results show throttling valves introduce additional losses. However, their effect on turbine off-design conditions brings an overall beneficial effect to the LAES process. Exergy destruction in the turbine stages is reduced by 22% in MP turbine and more than 50% in the LP turbine due to inlet pressures being closer to design. Less air mass flow rate is now needed to produce the same amount of power. With the introduction of throttling valves, pressure and temperature deviations from nominal conditions are now negligible. As a result, with the proposed regulation the main reason for off-design is the departure of the mass flow rate from its nominal value. Furthermore, power generation, as well as exergy destruction, is more evenly distributed across the components. Overall, total exergy destruction associated with the expansion process diminishes while the components work with higher thermodynamic efficiency.
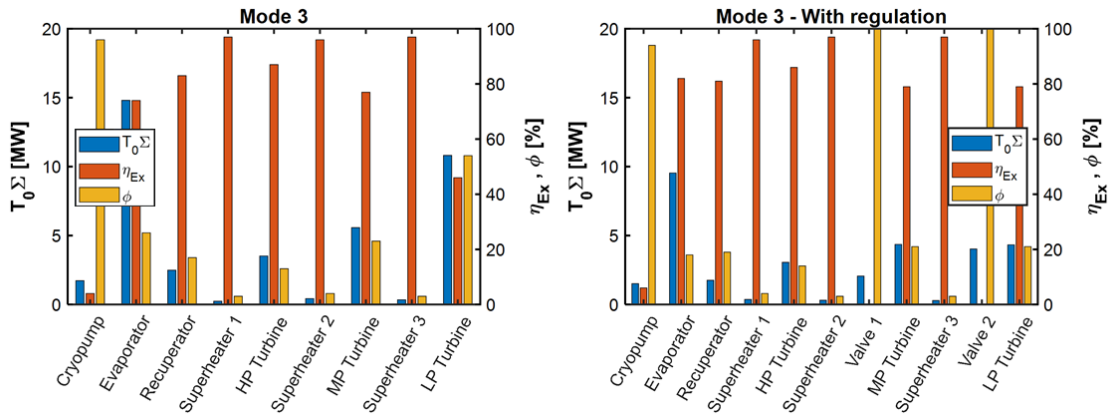
**Figure 43: Component-level exergy analysis during Mode 3, with and without the proposed regulation strategy.**

At system scale, the exergy performance is also improved by the proposed regulation strategy, as illustrated in Figure 44. Overall, exergy efficiency of discharging process increases from 54% to 60%, which means that additional throttling irreversibility due to the valves is offset by the improvement in performance induced in the other components. Exit losses are reduced by 4 MW since higher expansion ratios allow the air to approach ambient pressure when expanded through the turbines. The lower temperatures achieved after expansion also mean a larger amount of heat from the hot recycle can be used, limiting the heat wasted by the LAES system and ensuring better exploitation of the available energy streams within the process. In parallel, exergy destruction through heat exchange is decreased. This is due to two reasons: the superheating circuit working closely to design conditions and the better matching of the temperature profiles in the evaporator, where having higher pressure mitigates the change in variation of thermo-physical properties of air.
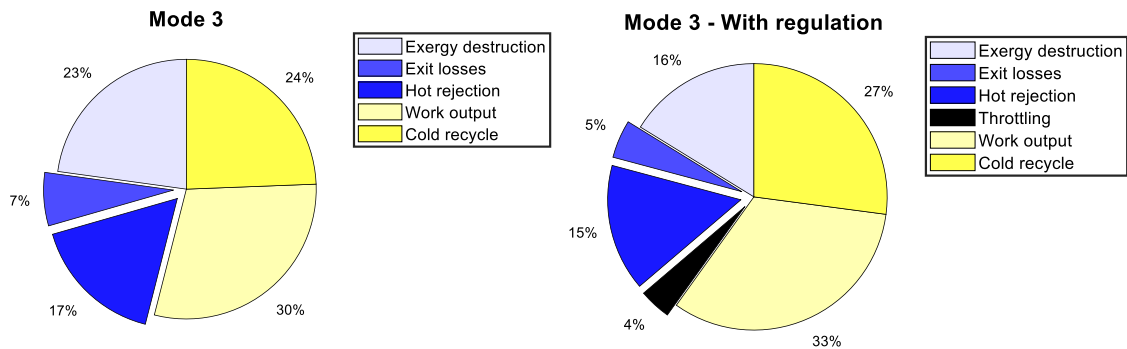


**Figure 44: Exergy analysis for LAES discharging process under Mode 3, with and without the proposed regulation strategy.**

## 4.5.2   Technical implications of LAES off-design operation

The presented results confirm that any time power is committed to reserve services, part-load conditions arise naturally during LAES operation, owing to the availability requirements imposed by market contracts. Therefore, it is crucial to account for the effect of off-design inefficiencies during realistic LAES operation, and generalise results over a broader range of reserve power commitment levels.

From Section 4.1, one could conclude $\eta_{RT}$ decreases from 48% to 44% in Mode 2 and 31% in Mode 3. However, this is only true *instantaneously*, i.e. at a specific instant of time during LAES operation. The portion of liquid air capacity devoted to STOR and FR and the associated power output is in a way *reserved*, as it would eventually be used upon a call from the grid operator. Hence, it should be accounted to evaluate $\eta_{RT}$. Figure 45 elaborates around this concept by looking at the *actual* liquid air usage for different percentages of committed power to reserve, for 1 h of sustained reserve (70-80% of STOR calls are within this value [163]). The effect of regulation from Section 4.5.1 is also evaluated.
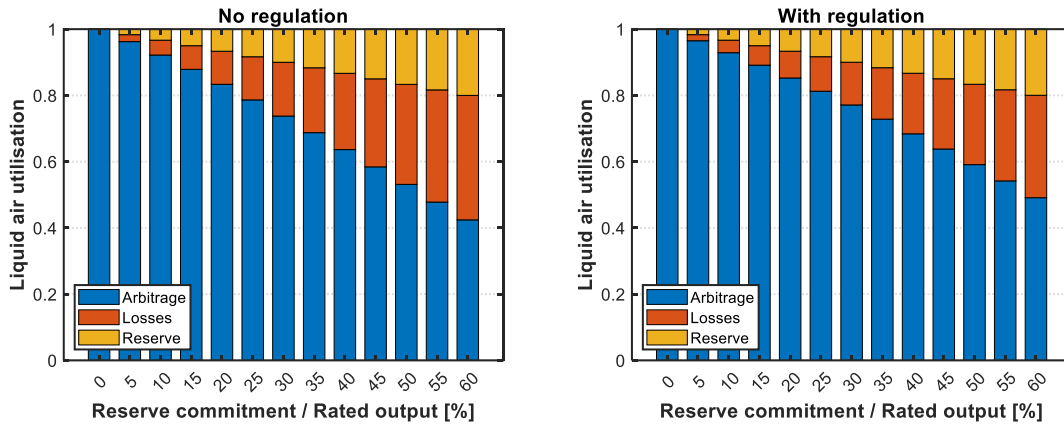


Figure 45: Liquid air utilisation for different levels of reserve service commitment, with and without the proposed regulation strategy.

In a multi-mode operation, the stored liquid air is partially used for arbitrage and partially for reserve. LAES consumes a higher amount of liquid air to generate a fixed power output at off-design conditions due to component-level inefficiencies. The extent of such loss is reported in Figure 45. On the other hand, when reserve is requested in real-time, the rated power output is established, and LAES power output is restored to the design value. In this context, a steady value for LAES roundtrip efficiency is clearly a first-level approximation. To account for real plant operation, an actual value of roundtrip efficiency should be defined and computed alongside the specification of the duty cycle of the LAES plant. This shows that a performance indicator like roundtrip efficiency is tightly linked to and depends on the actual plant operating profile, and it may differ from cycle to cycle. Based on the assumption of 1 h call to the reserve service, comparison between instantaneous and actual roundtrip efficiency is presented in Table 19. However, it is worth pointing out that the actual roundtrip efficiency would be ultimately defined once the real-time LAES dispatching profile is known.

Table 19: Comparison between LAES roundtrip efficiencies under 1-hour assumed reserve call duration.

| Operation | Instantaneous $\eta_{RT}$ | Actual $\eta_{RT}$ – without regulation | Actual $\eta_{RT}$ – with regulation |
|---|---|---|---|
| Mode 1 | 48% | 48% | 48% |
| Mode 2 | 44% | 44% | 45% |
| Mode 3 | 31% | 34% | 37% |

Even if the values are ultimately dependent on the call characteristics for reserve service, which may be different between STOR and FR, off-design conditions were shown to be impactful on LAES realistic operational modes. The effect of ignoring these conditions could be two-fold: on the one hand, it could lead to a misevaluation of LAES economic and technical value; on the other hand, scheduled commitment and dispatch profiles could result to be unfeasible a posteriori due to variations in the discharging hours effectively sustained [234]. This restricts the applicability of traditional steady

analyses commonly presented in the literature to the vicinity of design conditions or for comparison purposes between different concepts. However, the more LAES operation embraces a portfolio of balancing services, the more the study and the methodology presented in this work allow accurate predictions.

*LAES characteristic maps*

To characterise LAES off-design performance under a wide spectrum of operating conditions, characteristic maps were also derived from the numerical model for a variety of LAES power output and reheating temperatures. This latter parameter becomes particularly relevant in cases of LAES integration with co-located heat sources or external heat streams, where the reheating temperature can vary significantly from its rated value. Figure 46 shows the result for LAES specific work output, where values were normalised with respect to rated conditions in order to be widely applicable.
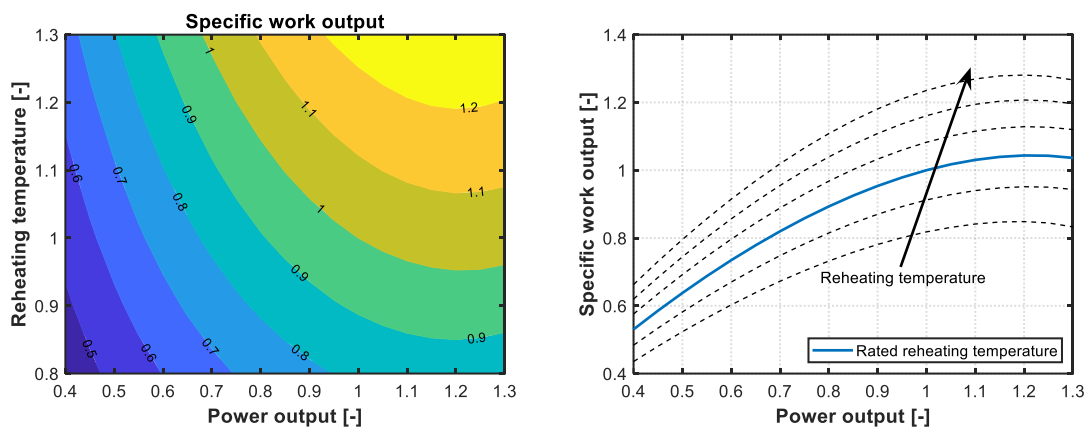


Figure 46: LAES characteristic operating maps. Contours and 1-D slices for selected values of reheating T.

The presented LAES characteristic maps offer an extremely valuable and compact tool which describes system operation over a variety of working conditions. By considering off-design conditions on LAES operation, a maximum for specific work (and thus plant efficiency) arises, which is almost insensitive to the reheating temperature. The position of the maximum work output in Figure 46 is determined by the trade-off between higher turbine expansion ratios and decreased efficiency, for higher plant power output. Some up-regulation above the rated power output appears to be possible, with the benefit of higher storage flexibility and efficiency. This may partially counterbalance the performance detriment observed for down-regulation, but feasibility is potentially limited by component technological constraints and lifetime. Finally, deviations in reheating temperature are more pronounced than power output variations on LAES performance. Particularly in cases of LAES integration with external heat sources, it is possible to compensate for the lower efficiencies for off-design conditions by acting on the reheating temperature.

### 4.5.3 Economic implications of LAES off-design operation

To conclude, the economic evaluation of LAES yearly operation according to the proposed operating modes was performed. This allowed gauging the impact of off-design performance variation also from a financial point of view, thus complementing the technical results discussed in the previous sections and leading to a comprehensive, far-reaching assessment.

Results shown in Figure 47 and Figure 48 demonstrate significant variations in the economic outcomes caused by the rigorous estimation of LAES performance. In essence, the higher the power committed to reserve services, the larger the deviation from ideal (i.e. design-point) behaviour due to off-design operation. Estimated economic variations are significant (around 20% in Mode 2 and 30-35% in Mode 3), which, on the one hand, highlight the relevance of the investigated mechanisms and, on the other hand, leave room for economic gains if off-design performance is improved. The proposed regulation strategy is efficient in this regard, boosting overall revenues by 3% and 9% in Mode 2 and Mode 3, respectively. Inefficiencies affect plant performance under arbitrage and the instantaneous $\eta_{RT}$ becomes 44% in Mode 2 (44.5% with regulation) and it plummets to 31% (34% with regulation) for Mode 3; hence, arbitrage revenues decrease. On the contrary, the financial value of reserve services is less affected by storage efficiency as part of the remuneration comes from availability alone. In such a context, being capable of correctly predicting LAES performance becomes paramount for achieving the best compromise between competing revenue streams and defining the optimal capacity to be allocated to different services.
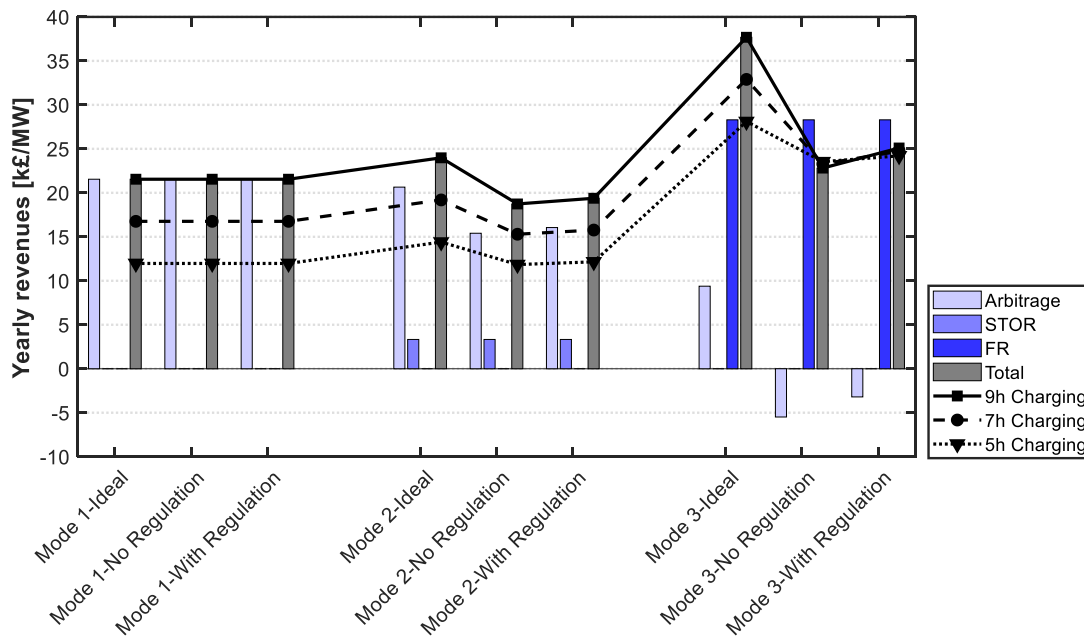


Figure 47: Results of the economic assessment of LAES operation and sensitivity analysis on the charging time.

It is worth pointing out that, although the above analysis is limited to the considerations of selected duty cycles, off-design operation takes place any time LAES generates power during a reserve availability window. Given such windows are designed to ensure backup generation mostly in periods of high power demand, it is likely they will coincide with high electricity prices – when it is advisable to operate LAES. Hence, it can be inferred results are also well representative of a number of situations other than the specific duty cycles adopted here. Anyhow, price variability overtime and physical restrictions on LAES tank capacity are additional constraints which could make some of the predicted revenues from arbitrage not accessible. We explored these situations by performing two sensitivity analyses. Firstly, we decreased the number of charging hours (equivalent here to a reduced amount of arbitrage cycles) and secondly, we observed the impact of variations in energy sell prices. Results for total revenues are superimposed to the bars of Figure 47 and Figure 48.
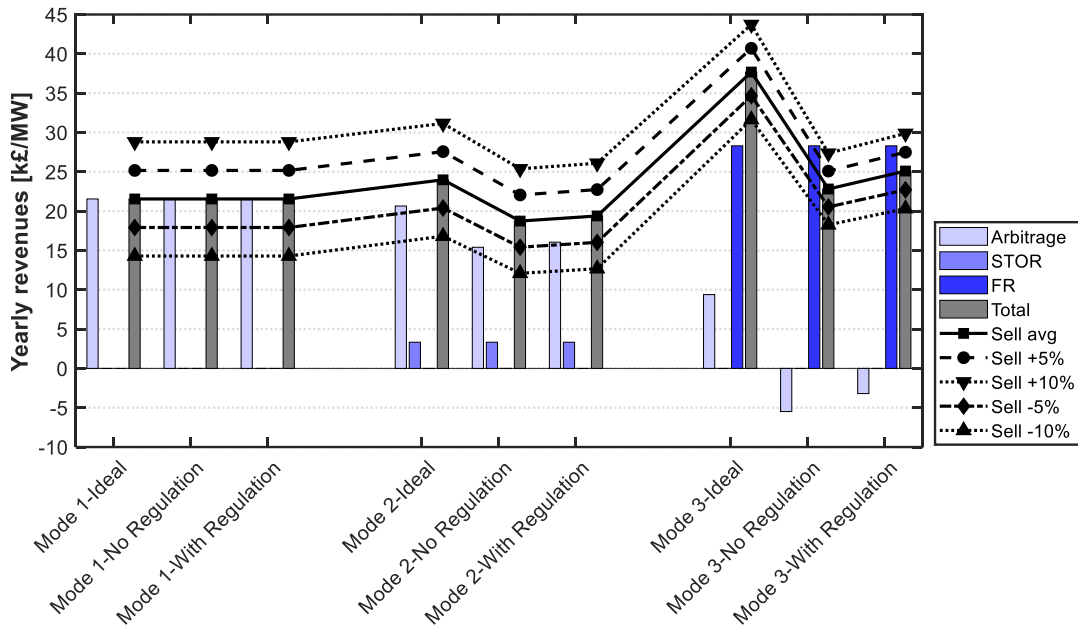
**Figure 48: Results of the economic assessment of LAES operation and sensitivity analysis on electricity price.**

As expected, arbitrage revenues decrease with a reduced number of cycles. However, the overall impact is influenced by two factors: share of arbitrage on the overall profit and roundtrip efficiency $\eta_{RT}$. Indeed, higher sensitivity to variations in the number of cycles is observed for the cases with a higher share of arbitrage over the total profit; secondly, smaller variations in revenues are associated with modes exhibiting lower values of $\eta_{RT}$ during arbitrage (since each charge-discharge cycle is less profitable in the first place). The described effects of a higher share of arbitrage and plant roundtrip efficiency concur in leading to percentage variations in revenues which are 22% for Mode 1, 9% for Mode 2 and only 1% for Mode 3, when the charging time is reduced to 7 h. Similarly, for variations in the electricity selling price, changes in yearly revenues are bigger, the higher the electricity purchase price. This makes Mode 1 the most sensitive to price oscillations, while Mode 2 and Mode 3, where revenues from the reserve markets are not subject to variations, are progressively more stable. Multi-service operation can indeed be regarded as a robust option for reducing the dependence on the number of cycles and price volatility, by diversifying over a portfolio of revenue streams.

Results also corroborate the economic viability of operating storage over multiple energy and reserve services [140,162]. However, the relative financial value of different modes changes and performance during off-design conditions makes the trade-off between competing revenue streams less straightforward. For example, Mode 2 is more profitable than Mode 1 in the ideal (i.e. design-point) case, whereas this happens if only 5 hours of charging are accessible in the real case. Thus, being able to capture these dependencies is key in avoiding misevaluations of LAES economic values with subsequent lack of revenues.

## 4.6    Conclusion and outlook

Results presented in this chapter address the thermodynamic and economic performance of LAES operating under realistic conditions in the electricity market. Representative duty cycles reflecting the operational constraints imposed by reserve service specifications and a numerical model to predict variable component and plant performance over a wide range of operating conditions are combined. This generates new understanding of the link between the operation of LAES in the electricity market and plant performance. Key takeaways from the case study of the UK market can be generalised, leading to wide-ranging conclusions on the techno-economic effects of operating LAES under a portfolio of energy and reserve services.

At component scale**,** *the effect of off-design conditions is unevenly distributed across LAES components*, with turbines – especially LP stages – affected the most (isentropic efficiencies more than halve for LAES participation to FR). On the contrary, performance and exergy losses in cryogenic pumps and heat exchangers are almost unaltered by LAES operating mode, with supercritical air conditions in the evaporator causing heat transfer limitations regardless of the specific operating mode. *The impact of off-design conditions can be mitigated with a suitable regulation strategy* which controls the inlet pressure to LP and MP turbine stages.

At plant scale, *exergy losses increase from 30% to 46% when reserve services are considered alongside arbitrage*. Higher thermodynamic losses occur primarily within the power recovery unit due to the appearance of off-design conditions and consume up to 40% of the stored liquid air, while air liquefaction is barely affected. The amount of cold thermal energy recovered from LAES discharge process and made available during discharge is marginally affected by LAES operating mode, with variations within 6% of the nominal conditions. *Throttling losses caused by the proposed regulation strategy are justified* by the ultimate benefit brought to overall plant performance, both from an energy and exergy standpoint.

Crucially, results show the roundtrip efficiency of LAES depends on the actual duty cycle performed by the plant. A constant plant roundtrip efficiency – common in the literature [140,204] – may serve comparative purposes. Still, it does not reflect the link between operation and performance for LAES and, potentially, not even for other TMES technologies relying on turbomachinery. Considering off-design behaviour of the power recovery unit is crucial for accurate economic assessments, too. Not only LAES profits are affected, but also the relative financial value of the different operating modes is revised. In essence, the higher the power committed to reserve services, the larger the deviation from design-point behaviour due to off-design operation. The significant economic variations registered (around 20% in Mode 2 and 30-35% in Mode 3), on the one hand, highlight the relevance of the investigated mechanisms and, on the other hand, leave room for economic gains if off-design performance is improved.

### 4.6.1    Chapter relevance within this thesis

The results from this chapter address the research objective O1 by enriching the understanding of LAES performance and limitations under multi-service operation and over a wide range of power outputs.

Both aspects are highly relevant in a context where LAES is expected to provide a diversified operation with reserve and energy-balancing services. Contributions to the existing body of the literature are:

- Off-design modelling of a liquid air energy storage plant
- Description of the link between the service provided and the technical plant performance
- Proposal and assessment of a regulation strategy aimed at limiting the extent of off-design conditions along LAES process
- Economic assessment of the impact of off-design operation on plant profitability in the UK electricity market.

The following result chapters further build on the highlighted relevance of accurate thermodynamic modelling of LAES and TMES. In particular, Chapter 5 proposes a framework to include LAES off-design response in the evaluation of LAES optimal scheduling and plant design for multi-service operation within the power system. Given off-design effects can change the relative financial value of the different operating modes (see Section 4.5.3), strategies to allocate power to reserve service are also discussed. Similar to the present chapter, a bottom-up analysis including performance and technical limitations of the major plant components is presented in Chapter 6 to study multi-energy provision from LAES. On the other hand, steady-state assessment of TMES plant performance at rated conditions is appropriate for comparative purposes and is adopted in Chapter 7.

# CHAPTER 5

# Multi-service operation of liquid air energy storage in the power system

*The analysis presented in this results chapter builds on the findings from Chapter 4 and uses LAES real-life performance predictions to explore pathways for LAES value maximisation in the power system. LAES simultaneous participation in energy balancing and reserve services can be profitable but introduces additional operational constraints affecting storage performance. Therefore, an MILP tool is developed in this chapter, which suitably includes LAES thermodynamic characteristics and balancing service constraints to optimise plant scheduling. It is used to simulate 1-year LAES operation for energy and reserve service provision and estimate its value over different service portfolios and storage designs. Results demonstrate that: i) the inclusion of LAES thermodynamic characteristics ensures feasible plant dispatch and avoids loss of revenues, especially for multi-service operation; ii) the independent sizing of LAES charge and discharge power is key for tailoring the plant to the specific operating mode; and iii) storage capacities above 2-3 h do not significantly increase LAES profitability under the market conditions considered. As multi-service LAES provision is financially advantageous but deteriorates storage roundtrip efficiency, a techno-economic trade-off should be sought. Results in this chapter can inform such decisions in terms of plant design, dispatch profile and portfolio of services to provide, thus addressing the thesis objective to identify pathways for LAES value maximisation as part of the power system. The presented modelling framework is suitable for extension to other TMES technologies to establish strategies supporting their future deployment.*

## 5.1 Introduction

As emerged from the literature review in Chapter 2, a limited number of operational studies is available where LAES provides a portfolio of energy balancing and reserve services. In addition, these few works treat the energy storage according to the battery-like model (see Section 2.5.2), assuming a constant roundtrip efficiency, which refers to the operation at rated conditions. However, results from Chapter 4 have shown that LAES performance and operational setpoint may shift significantly, especially when a diversified operation strategy over energy and reserve services is chosen. Therefore, to overcome the current limitations and better understand the value and contribution of LAES to grid stability, storage thermodynamic characteristics should be included in the analysis of LAES integration in the power system through a suitable model.

This results chapter addresses the lack of a coherent modelling framework simultaneously including LAES thermodynamics, provision of a portfolio of services and optimal plant dispatch. The interaction of all these drivers is also captured in the MILP optimisation tool developed, which relies on the model reduction techniques presented in Chapter 3 to include LAES thermodynamic characteristics in the analysis. The case study analysed considers energy and reserve services supply in the UK electricity market. The discussion covers: i) the interaction between service requirements (e.g. minimum committed capacity) and thermodynamic performance of LAES; ii) the inclusion and prioritization of multiple services; and iii) the selection of LAES plant size when providing a portfolio of services.

In this chapter, the relevant background and assumptions are laid out in Section 5.2. Section 5.3 presents the essential aspects and formulation for the MILP model developed. Section 5.4 and Section 5.5 outline and discuss the results, focussing on the relevance of including storage thermodynamic characteristics in the analysis, the guidelines for LAES sizing and the power allocation to a portfolio of energy balancing and reserve services. Section 5.6 concludes the chapter with the main takeaways.

## 5.2 Background and assumptions

### 5.2.1 Overview of the proposed modelling framework

A unique modelling framework has been proposed for this piece of work, driven by the need to consider multiple aspects of LAES operation as part of the grid (multi-service specifications, plant performance variability, sizing etc.) in a coherent manner. As a consequence, LAES thermodynamics, reserve services specifications and optimal storage dispatching are the building blocks for the developed methodology; they are brought together into a LAES-centric optimal dispatch problem based on MILP.

The MILP problem formulation is central to the proposed approach, as shown in Figure 49, and used to optimise the yearly LAES dispatch. Specific constraints associated with provision of reserve services and the variability of the electricity prices were included. The dynamic thermodynamic performance of LAES and plant size specification were captured through performance maps and a suitable piecewise

formulation. Finally, the model was run according to specific case studies proposed to answer the research questions in Figure 49. More information on the model formulation is provided in Section 5.3.
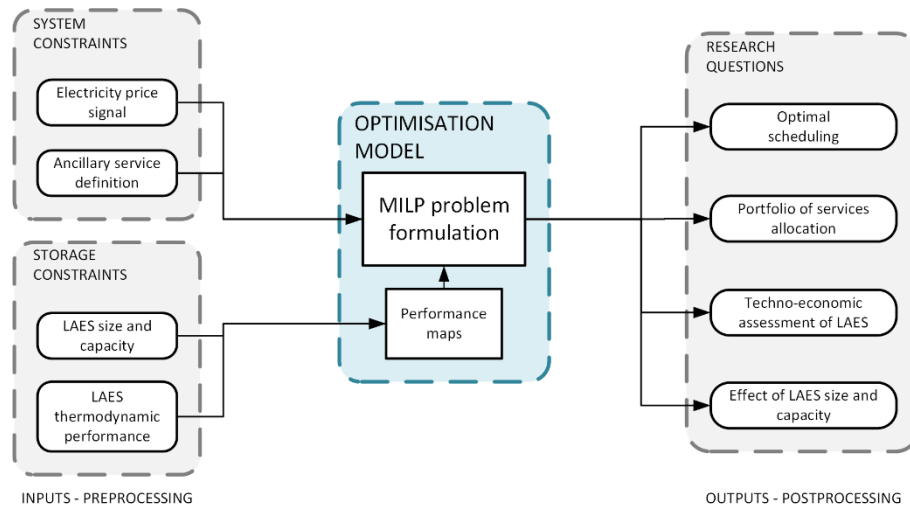


Figure 49: Mind map of the adopted modelling framework.

## 5.2.2 LAES thermodynamics

Detailed thermodynamic analysis of standalone LAES plant performance is discussed in Chapter 4. In particular, due to external constraints limiting the delivered power or the intrinsic dynamic behaviour of some components (e.g. packed bed cold storage), off-design conditions arise along the LAES process. Turbine isentropic efficiency and expansion ratios vary accordingly. So, if a generation level is defined as the delivered power output relative to its rated value, the specific LAES work output per unit liquid air and the liquid air consumption will vary according to the generation level, as Figure 50 shows.
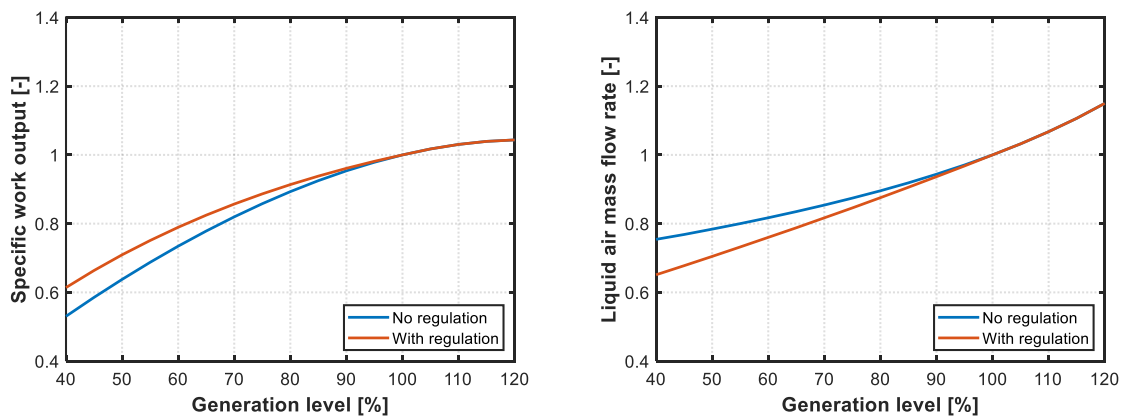


Figure 50: LAES thermodynamic characteristics in the power recovery unit, as a function of plant generation level.

In an ideal case, LAES should produce a constant specific work output, regardless of its operating setpoint, so that the mass flow rate of liquid air linearly changes with the generation level. On the contrary, the graphs show a performance detriment in the specific work output at part-load. Turbine efficiencies and expansion ratios both decay, leading to poor LAES performance. Therefore, the air mass flow rate consumption varies with the generation level in a nonlinear fashion. A suitable regulation strategy was proposed to limit inefficiencies for part-load operation (i.e. generation level

below 100%) in Section 4.5.1. From Figure 50, it is clear that, even with that regulation strategy, the impact of off-design conditions can be partially mitigated but not avoided. To account for this inherent link between LAES generation level and its technical performance, a higher liquid air expenditure when running at part-load must be considered as a major thermodynamic constraint to LAES operation.

### 5.2.3    Reserve services considered and revenue schemes

As explained in Section 2.4.1, different reserve services assist the energy system operator over different instances of grid balancing. The same service selection of Chapter 4 (STOR and FR provision, alongside arbitrage, in the UK market) was considered for consistency and in line with LAES size and ramp-up capability. Both STOR and FR require providers to be available to deliver the contracted capacity in the agreed availability windows. Representative values for the season 2016/2017 were used in the present analysis [163] for STOR, while for FR, tendered windows were 6:00 to 23:00 during weekdays and 7:00 to 23:00 at weekends [289]. Other technical requirements to be met by STOR and FR providers, as well as the respective availability, positional and utilisation fee remuneration is reported in Table 20.

It is worth stressing that, at the time of this analysis, the simultaneous provision of reserve services within the same tendered availability window is not allowed in the UK electricity market [165,166]. However, this option would not pose any issue from the technical point of view, provided the cumulative power level committed remains within the feasible generation level for the plant, and sufficient energy is stored to provide the services. Therefore, the concurrent provision of STOR and FR is also contemplated here to inform of the associated potential economic benefits.

Table 20: Technical specifications and revenue schemes for STOR and FR services in the UK market [163,289].

| | STOR | FR |
|---|---|---|
| Technical specifications | • Minimum commitment: 3 MW<br>• Response time*: < 240 min<br>• Sustained period: > 2 hours<br>• Delivery capability: > 3 times a week | • Minimum commitment: 25 MW<br>• Response time: < 2 min<br>• Sustained period: > 15 min<br>• Ramp-up rate: > 25 MW/min |
| Revenue scheme | • Availability fee [£/MW/h]: 3.30-6.10<br>• Positional fee [£/h]: n.a.<br>• Utilisation fee [£/MWh]: 147-155 | • Availability fee [£/h]: 175-380<br>• Positional fee [£/h]: 0-320<br>• Utilisation fee [£/MWh]: 100-115 |

* National Grid also adds that "response times within 20 minutes are preferable", and indeed technical requirements have been modified so STOR providers must now be able to respond to an instruction within a maximum of 20 min.

## 5.3    MILP model formulation

The MILP model optimises LAES dispatch profile over the selected energy balancing and reserve services, subject to technical constraints form LAES and dictated by the operation within the system. Optimisation decision variables are denoted in bold fonts in the following and are presented in Table 21. They track the time evolution of LAES state (charging, discharging, state of charge) and interaction with the grid (power input and output). In compliance with the common practice for gas liquefaction

processes discussed in Section 2.3.1, LAES was here assumed to always charge at rated power input. Therefore, the binary variable $x_t^{chr}$ was sufficient to fully characterise the power input to the plant.

Table 21: Optimisation variables of the MILP optimisation problem.

| Symbol | Definition | Type | Units |
|---|---|---|---|
| $\dot{W}_t^{dsc}$ | Discharge power output | Continuous | [MW] |
| $x_t^{dsc}$ | Discharge status | Binary | [-] |
| $x_t^{chr}$ | Charge status | Binary | [-] |
| $LAI_t$ | Liquid air inventory in the tank | Continuous | [ton] |
| $LAE_t$ | Liquid air expenditure | Continuous | [ton/h] |
| $x_{n,t}^{PW}$ | Piecewise interval identifier | Binary | [-] |
| $\omega_{n,t}$ | Auxiliary variable | Continuous | [-] |

Additional parameters were necessary to characterise grid constraints (e.g. electricity price signal, typical reserve call duration, probability, etc.) and storage constraints (e.g. rated conversion efficiencies or minimum level for the LAES power output). They are gathered in Table 22. Further parameters completing the formulation of the optimisation are discussed throughout the section.

Table 22: Input parameters to the MILP optimisation problem.

| Symbol | Definition | Value | Units | Reference |
|---|---|---|---|---|
| $\pi_t^{el}$ | Wholesale electricity price (year 2017) | Time-varying | [£/MWh] | [293] |
| $\pi_{STOR}^{ava}$ | STOR availability fee | 4.25 | [£/MW/h] | [163] |
| $\pi_{STOR}^{util}$ | STOR utilisation fee | 150 | [£/MWh] | [163] |
| $\pi_{STOR}^{pos}$ | STOR positional fee | 0 | [£/h] | [163] |
| $\kappa_{STOR}$ | STOR call probability | 2.9 | [%] | [163] |
| $\tau_{STOR}$ | Nominal STOR call duration | 1.5 | [h] | [163] |
| $\pi_{FR}^{ava}$ | FR availability fee | 210 | [£/h] | [289] |
| $\pi_{FR}^{util}$ | FR utilisation fee | 100 | [£/MWh] | [289] |
| $\pi_{FR}^{pos}$ | FR positional fee | 90 | [£/h] | [289] |
| $\kappa_{FR}$ | FR call probability | 5 | [%] | [289] |
| $\tau_{FR}$ | Nominal FR call duration | 0.5 | [h] | [289] |
| $w_0^{chr}$ | Rated liquefier conversion efficiency | 0.219* | [MWh/ton] | Model |
| $w_0^{dsc}$ | Rated PRU conversion efficiency | 0.131* | [MWh/ton] | Model |
| $\dot{W}_{min}^{dsc}$ | Minimum power output from PRU | $0.4\dot{W}_{MAX}^{dsc}$ | [MW] | Model |
| $\dot{W}_{MAX}^{dsc}$ | Maximum power output from PRU | Multiple | [MW] | See Section 0 |
| $\dot{W}_{MAX}^{chr}$ | Maximum power input to liquefaction | Multiple | [MW] | See Section 0 |
| $LAI_{MAX}$ | Maximum storage capacity | Multiple | [ton] | See Section 0 |

* These values are consistent with a rated roundtrip efficiency of 60% for LAES [140,179].


*Objective function*

The optimal LAES dispatch profile maximises the coordinated provision of energy balancing and reserve services described in Section 5.2.3. The objective function comprises four contributions: 1) revenue from arbitrage, driven by variations in price signal $\pi_t^{el}$ with hourly granularity; 2) availability

revenue from reserve $i$; 3) utilisation revenue from reserve $i$; and 4) positional revenue from reserve $i$.

$$Max \sum_{t=1}^{T} \left[ \underbrace{\left( \dot{W}_t^{dsc} - \dot{W}_{MAX}^{chr} x_t^{chr} \right) \pi_t^{el}}_{1} \right.$$
$$\left. + \sum_{i=1}^{I} \left( \underbrace{RC_{t,i} \pi_i^{ava}}_{2} + \underbrace{\kappa_i RC_{t,i} \pi_i^{util}}_{3} + \underbrace{\kappa_i x_{t,i}^{RC} \pi_i^{pos}}_{4} \right) \right] \qquad 5.1$$
$$\cdot \Delta t$$

Earnings from reserve market participation were evaluated using the parameters $RC_{t,i}$ and $x_{t,i}^{RC}$. $RC_{t,i}$ elements equal the committed power level to reserve service $i$ within its respective window, while are null elsewhere; analogous concept was used for the binary $x_{t,i}^{AC}$. The inherently stochastic nature of reserve services was accounted in Equation 5.1 by the term $\kappa_i$, which weights the revenue from a reserve call. $\kappa_i$ represents a call probability as the ratio between the average yearly period when reserve is delivered and the total duration of the availability window.

### *LAES thermodynamic characteristics*

Chapter 4 demonstrated that the conversion efficiency of the PRU, $w^{dsc}$, cannot be approximated by a fixed parameter, and should be treated as an optimisation variable (i.e. $w_t^{dsc} = f(\dot{W}_t^{dsc})$). This dependency was presented in Figure 50 and is nonlinear, thus requiring an *ad-hoc* mathematical treatment to maintain the linearity of the optimisation.

The value $\dot{W}_t^{dsc}/w_t^{dsc}$ represents the instantaneous liquid air expenditure in each specific timestep. This term was substituted by the variable $LAE_t = \dot{W}_t^{dsc}/w_t^{dsc}$, which captures in a unique variable the inherent connection between power output and conversion efficiency and allows linearisation. Characteristic curves extracted from the thermodynamic model were used to express this nonlinear dependence and, as illustrated in Figure 51, a piecewise linear approximation was used to retain linearity [284].
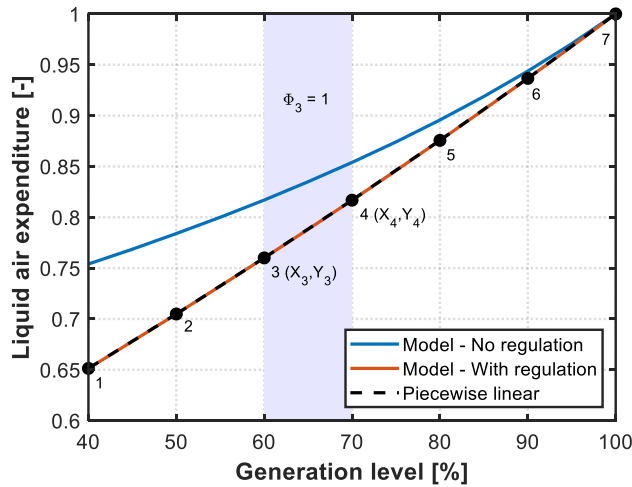


Figure 51: Characteristic liquid air expenditure for LAES, as a function on the generation level and its piecewise approximation. LAE figures have been normalised to the value referring to rated conditions.

The 1-D linearisation technique described in Section 3.4.3 was used. The feasible region of the generation level was subdivided into $N-1$ contiguous intervals and $N-1$ binary variables $\boldsymbol{\Phi_{n,t}}$ were defined accordingly, each one mapping to one of the six piecewise intervals used for the problem specification, as illustrated in Figure 51. During LAES discharge at any given time, the amount of liquid air expenditure is constrained within at most one single interval:

$$\sum_{n=1}^{N-1} x_{n,t}^{PW} \leq x_t^{dsc} \tag{5.2}$$

By knowing the values of liquid air expenditure $Y$ and generation level $X$ at the extremes of the relevant interval along the characteristic curve, a unique operating point for each timestep was finally determined as a linear combination of these values, through the definition of the auxiliary set of variables $\boldsymbol{\omega_{n,t}}$:

$$\begin{cases} \omega_{n,t} \leq x_{n-1,t}^{PW} + x_{n,t}^{PW} \\ \omega_{1,t} \leq x_{1,t}^{PW} \\ \omega_{N,t} \leq x_{N-1,t}^{PW} \end{cases} \tag{5.3}$$

$$\sum_{n=1}^{N} \omega_{n,t} = 1 \tag{5.4}$$

$$LAE_t \geq \sum_{n=1}^{N} \omega_{n,t} Y_n \tag{5.5}$$

$$\dot{W}_t^{dsc} \leq \sum_{n=1}^{N} \omega_{n,t} X_n \tag{5.6}$$

For $\boldsymbol{LAE_t}$ and $\boldsymbol{\dot{W}_t^{dsc}}$ to lie on the thermodynamic characteristic curve, equations 5.5 and 5.6 would need to satisfy their associated equality constraints. However, the objective function was formulated in such a way that the optimisation would drive these constraints to be binding and thus they were relaxed to inequalities to assist with the solution convergence.

### *LAES dispatch constraints*

Constraints considering the technical as well as the electrical side of LAES operation are listed in the equations below. Limitations associated with LAES power and capacity, mass (and thus energy) stored within the liquid air tank and storage cyclability over a periodic horizon of one week were specified as follows:

$$x_t^{dsc} \dot{W}_{min}^{dsc} \leq \dot{W}_t^{dsc} \leq x_t^{dsc} \dot{W}_{MAX}^{dsc} \tag{5.7}$$

$$LAI_t = LAI_{t-1} + \left[\frac{x_{t-1}^{chr}\dot{W}_{min}^{chr}}{w_0^{chr}} - LAE_{t-1}\right] \cdot \Delta t \qquad 5.8$$

$$0 \leq LAI_t \leq LAI_{MAX} \qquad 5.9$$

$$LAI_0 = LAI_{0+168a} = 0.5LAI_{MAX} \qquad 5.10$$

where $a$ is an integer number, denoting each individual week. The choice of a weekly margin allows to benefit from longer planning horizons (for example exploiting price differentials between weekdays and weekends) yet gives confidence in the accuracy of the hourly electricity price profile supplied to the model and thus on the estimated revenues. Above one week, point (i.e. hourly) price predictions ahead are typically substituted by price distributions over future periods [294].

Model consistency against a real-time reserve call was ensured following a robust optimisation approach [217]. Thus, additional constraints were used to enforce the restrictions introduced by participation in the different reserve services. First, a cap on the LAES power output was imposed when inside the availability window (Equation 5.11) to enable a power turn-up in case of a reserve call. Second, a minimum level in the liquid air tank was enforced (see Equation 5.12), which is needed to fulfil service provision, should this be requested by the grid operator. These two constraints ensured the predicted dispatch profile for LAES could accommodate a real-time reserve call at any time.

$$\dot{W}_t^{dsc} + \sum_{i=1}^{I} RC_{t,i} \leq \dot{W}_{MAX}^{dsc} \qquad 5.11$$

$$0 \leq LAI_t - LAE_t - \frac{\sum_{i=1}^{I} RC_{t,i}\,\tau_i}{w_0^{dsc}}\Delta t \leq LAI_{MAX} \qquad 5.12$$

Since cryogenic air liquefaction should be operated at its rated conditions [180], LAES charging was restricted to be operated outside of the reserve windows, excluding the possibility of a reserve call which would enforce a power modulation while charging:

$$x_t^{chr} + x_t^{RC} \leq 1 \qquad 5.13$$

Here, $x_t^{AC}$ is a binary parameter which assumes the unit value when at least one of the $RC_{t,i}$ is non-zero, indicating a reserve availability window.

### 5.3.2 Performance indicators

To quantify the technical performance of LAES, plant roundtrip efficiency $\eta_{RT}$ was computed according to the definition given in Section 2.2, considering the entire operating horizon of LAES. Given the optimal dispatch timeseries:

$$\eta_{RT} = \frac{\sum_t \dot{W}_t^{dsc} \Delta t}{\sum_t \dot{W}_{MAX}^{chr} x_t^{chr} \Delta t}$$
5.14

Additionally, a part-load coefficient, $\xi$ was computed every time LAES power output is nonzero (i.e. LAES is discharging) and used to characterise the link between plant scheduling and its roundtrip efficiency. $\xi$ is defined as the ratio between the instantaneous power output of the LAES and its maximum discharge capability:

$$\xi = \frac{\dot{W}_t^{dsc}}{\dot{W}_{MAX}^{dsc}} \qquad \forall\, t : x_t^{dsc} \neq 0$$
5.15

Finally, a static payback time (PBT) was chosen as the economic metric in this study. It is defined as the ratio between plant investment cost ($CAPEX$) and the yearly revenues from storage operation ($Rev$):

$$PBT = \frac{CAPEX}{Rev}$$
5.16

In Equation 5.16, $CAPEX$ represents the capital expenditure for LAES plant construction, and $Rev$ is the yearly revenue from LAES participation in energy and reserve markets, i.e. the value of the MILP objective function. The cost contribution of each of the three LAES sub-systems: power recovery unit $K^{dsc}$, liquefaction $K^{chr}$ and storage tanks $K^{cap}$ were independently considered in the estimation of $CAPEX$:

$$CAPEX = K^{dsc} + K^{chr} + K^{cap}$$
5.17

Individual cost functions are gathered in Table 23; they are based on the supply chain quotes indicated by Highview Power Ltd for a 10 MW plant [295] and scaled up with a 0.6 exponent and a learning rate assuming 17.5% cost reduction for a double number of units [97]. Cost units are 2012 k\$. The conversion to 2017 k£ was performed by adopting a proportionality factor of 1.47, which accounts for the average \$-£ exchange rate in 2012 [296] and UK inflation between 2012 and 2017, from the Office of National Statistics [297]. The accuracy of the costing approach was tested by comparing its predictions with results available in the literature for a variety of LAES plants [139,140,179], showing a satisfactory agreement within $\pm6\%$.

Table 23: Selected cost function for independent LAES subsystems. Values are based on quotations by manufacturers.

| LAES subsystem | Cost function | Description of variable $x$ |
|---|---|---|
| Power recovery unit | $K^{dsc} = 5653 \left(\dfrac{x}{10}\right)^{0.6}$ | LADS rated power output, MW |
| Air liquefaction | $K^{chr} = 11406 \left(\dfrac{x}{4}\right)^{0.6}$ | LAES rated power input, MW |
| Storage | $K^{cap} = 1778 \left(\dfrac{x}{86}\right)^{0.6}$ | LAES energy storage capacity, MWh |

### 5.3.3 Case studies and model runs

The model described in Section 5.3 was compiled in MATLAB and solved by Gurobi 8.1.1 [267], with a 0.5% relative gap as stop criterion for the iterations. Different model runs were conceived to address specific studies with the inclusion of thermodynamic constraints within the MILP optimisation, and in particular:

- *Optimal LAES scheduling*: how the technical performance of LAES – and consequently its optimal dispatch profile – varies when considering plant thermodynamic limitations
- *Optimal LAES sizing*: how plant sizing may affect LAES performance and economic value and what design guidelines can be followed depending on the services to be supplied
- *LAES multi-mode operation*: how providing a portfolio of balancing services to the grid impacts LAES technical performance and the final economic value for the plant

Figure 52 summarizes the set of model runs performed in this work, and presents the specific aspects considered and the strategy adopted for each run. Each run will consider a number of case studies, referring individually to a given set of storage services, from Case 0 – only arbitrage – to Case 3 – complete portfolio of services. The cases are detailed in Table 24, where values are expressed as a percentage of the rated power $\dot{W}_{MAX}^{dsc}$ to allow generalisation throughout model runs where LAES size is one of the aspects to be investigated. The design parameters for each of the runs are summarised below.
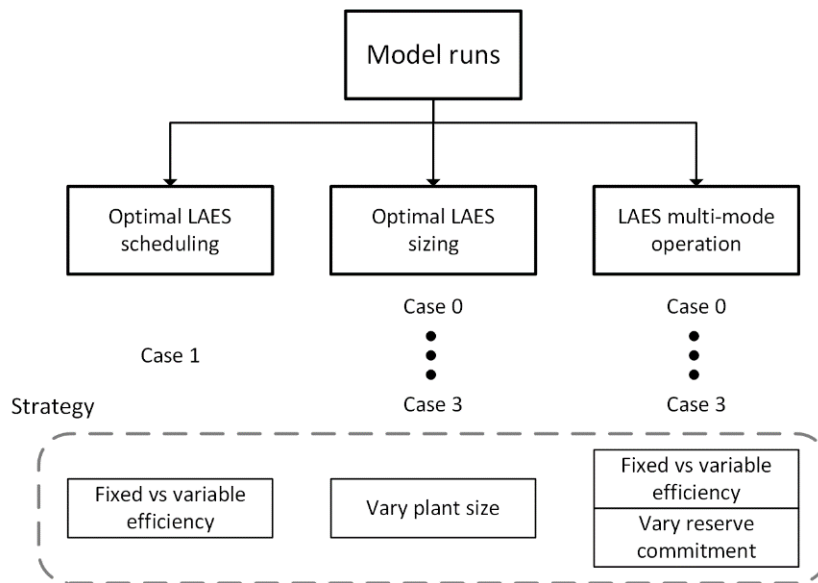


**Figure 52: Overview of the model runs performed, with associated case studies and strategy.**

**Table 24: Summary of the considered case studies. Values of committed power are expressed as percentages of the rated power output.**

| Case Study | | Arbitrage | | STOR | | Fast Reserve |
|---|---|---|---|---|---|---|
| Case 0 | ✓ | 100% | | | | |
| Case 1 | ✓ | 90% | ✓ | 10% | | |
| Case 2 | ✓ | 75% | | | ✓ | 25% |
| Case 3 | ✓ | 65% | ✓ | 10% | ✓ | 25% |

### *Optimal LAES scheduling*

A reference plant of 200 MW power output, 100 MW input and 3 h of rated discharge capacity (600 MWh) was considered for these runs. Outcomes from the full MILP model integrating the LAES thermodynamic characteristics (real approach) were compared with those obtained if a fixed conversion efficiency was considered (ideal approach). Results from one-week operation according to arbitrage and STOR (Case 1) are discussed in Section 5.4.1.

### *Optimal LAES sizing*

For this analysis, a range of LAES sizing options was explored for each of the four cases of Table 24. The design parameters were identified as plant power output $\dot{W}_{MAX}^{dsc}$, power input $\dot{W}_{MAX}^{chr}$ and capacity $K^{MAX}$. The effect from each of them was then assessed by independently varying one parameter at a time within the design space defined in Table 25, and running the model for 1-year operation; results are presented in Section 5.4.2.

**Table 25: Selected design space for the LAES plant.**

| Design parameter | Symbol | Range | Increment step |
|---|---|---|---|
| PRU power output | $\dot{W}_{MAX}^{dsc}$ | 100 MW - 300 MW | 50 MW |
| Liquefaction power input | $\dot{W}_{MAX}^{chr}$ | $0.1\dot{W}_{MAX}^{dsc}$ - $\dot{W}_{MAX}^{dsc}$ | $0.1\dot{W}_{MAX}^{dsc}$ |
| Storage tank capacity | $LAI_{MAX}$ | 2 h - 10 h | 1 h |

### LAES multi-mode operation

Based on the outcomes from the sizing study, a LAES plant of 200 MW output, 40 MW input (20% $\dot{W}_{MAX}^{dsc}$) and 3 hours discharge capacity was chosen as a versatile solution to serve the four cases of Table 24. In Section 5.4.3, techno-economic results from the model are assessed for such a plant over a one-year operation.

## 5.4    Results

In discussing the results of the present chapter, it is worth defining the nomenclature adopted. In particular, ideal, corrected and real cases identify the following set of results:

- **Ideal**: it refers to results obtained using a constant LAES roundtrip efficiency for optimal dispatch scheduling, which is the first-order assumption widely adopted in the literature [179,181,191]
- **Corrected:** it refers to results obtained accounting for the variations of LAES conversion efficiency (by including plant thermodynamic characteristics), but using the ideal dispatch schedule
- **Real**: it refers to results obtained accounting for the variations of LAES conversion efficiency (by including plant thermodynamic characteristics) for optimal dispatch scheduling.

### 5.4.1 Optimal LAES scheduling

The optimal weekly dispatch for LAES, when operating according to Case 1 (arbitrage + STOR) is presented here to highlight the key variations originating from the inclusion of thermodynamic constraints within the optimisation framework. Figure 53 refers to the ideal case, while results in Figure 55 account for the thermodynamic characteristics (real case). The shaded area represents the weekly reserve availability windows.
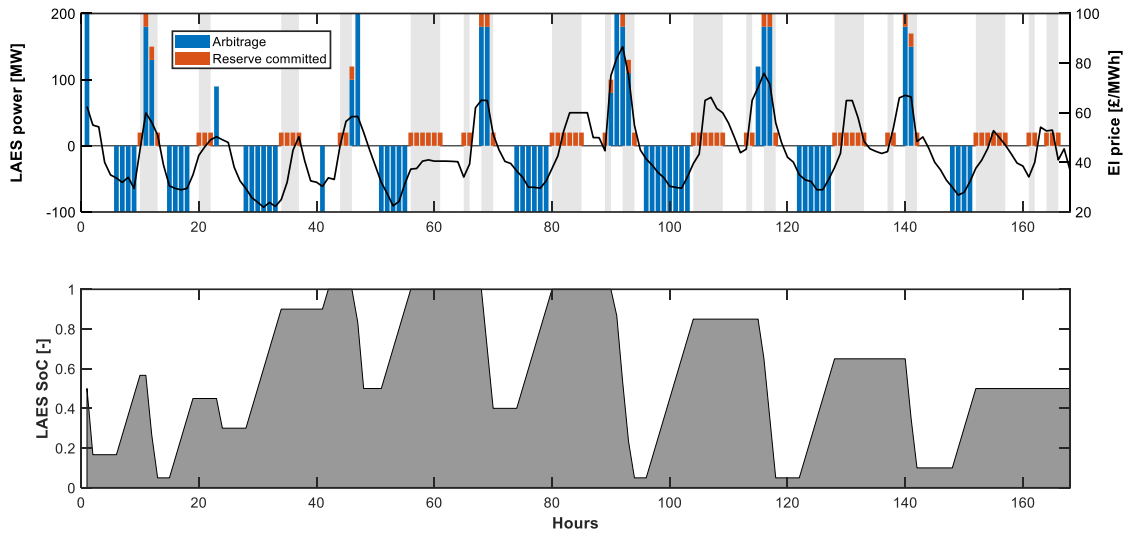


**Figure 53: One-week LAES dispatch when providing arbitrage and STOR. Constant conversion efficiency case.**

In both cases, LAES is charged preferentially during periods of low electricity price, while discharged at peak times. When discharging, 100% power output is preferred, but within the reserve windows, only a portion of LAES power output can be devoted to arbitrage. In the likely event of availability windows coinciding with the highest electricity prices, part-load discharging is imposed on the LAES due to the constraints associated with reserve provision. Additionally, a minimum LAES state of charge (SoC) must be guaranteed within the reserve windows to ensure service deliverability, further limiting the possibility of rated discharge.

As the scheduling in Figure 53 is ideal, reduced performance at off-design conditions is not accounted for, which could lead to an optimistic and unfeasible dispatch profile. To verify this, a corrected solution was computed, and results are presented as a dashed line in the bottom plot of Figure 54 (Corrected – Unfeasible). Clearly, the ideal scheduling is not feasible, as the LAES SoC would drop below 0 multiple times. This is because, during part-load operation, off-design conditions reduce the specific work output from the PRU (see the top plot of Figure 54); therefore, more air than expected is necessary for sustaining the given power output, leading to a sharper decrease in LAES SoC.
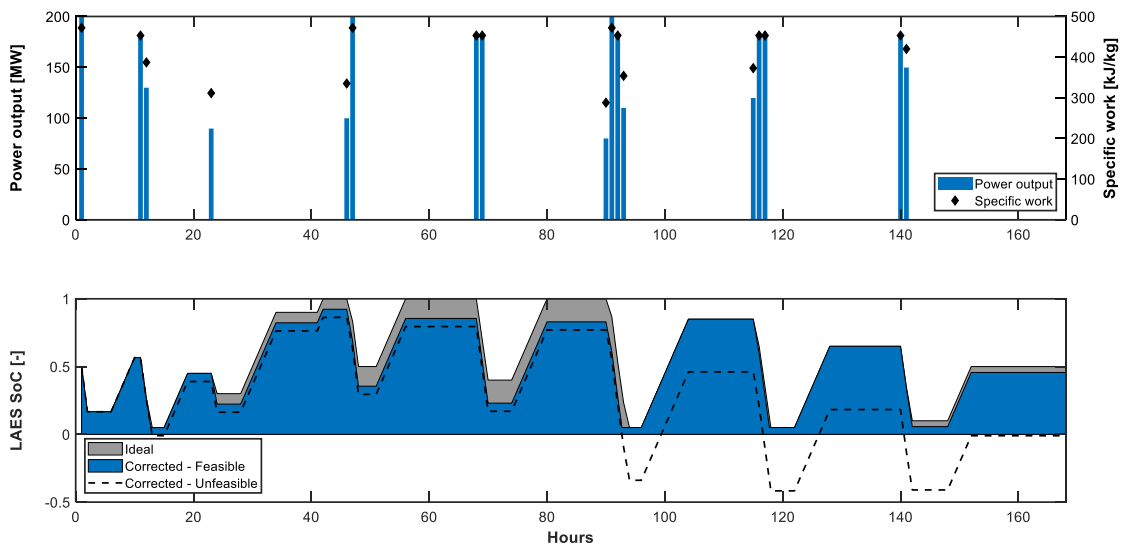
Figure 54: Corrected LAES dispatch by a posteriori accounting for thermodynamic characteristics.

The major consequence of not accounting for thermodynamic characteristics within the optimisation is a dispatch profile which is not feasible, a posteriori. By sustaining LAES power output for a shorter period, the model constraints can still be satisfied, and the scheduling fulfilled by LAES (resulting in the Corrected – Feasible area in Figure 54, for LAES SoC). However, this means 3 out of the total 17 power generation instances cannot be fully sustained for the entire 1-h timestep. This causes loss of revenues, potentially incurring penalty payments and, more importantly, reduced contribution of LAES to grid stability. Also, LAES roundtrip efficiency would be 54.7% in this case: a 10% reduction from the nominal value 60%.
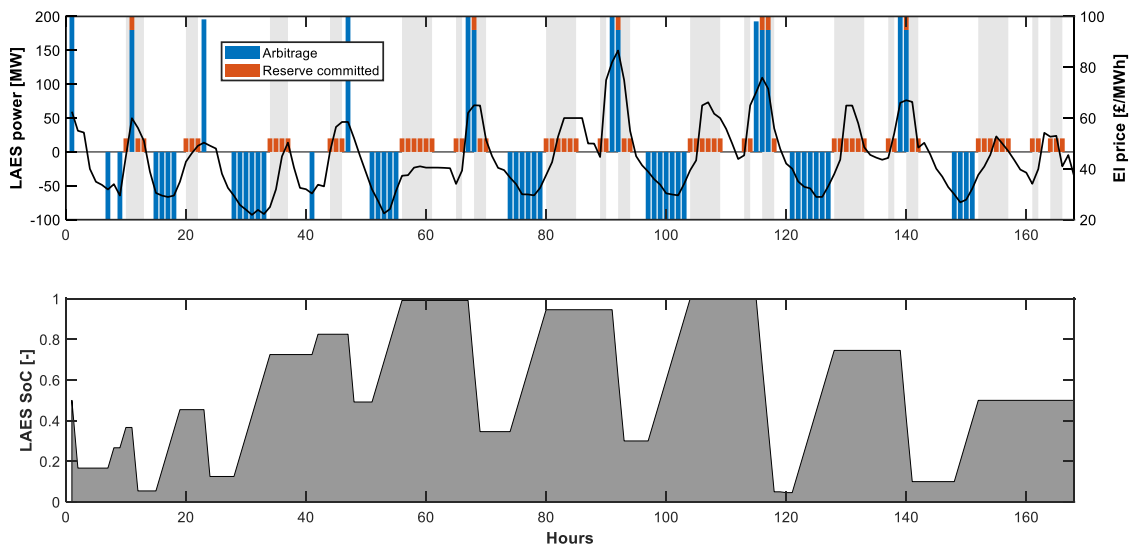


Figure 55: One-week LAES dispatch profile when providing arbitrage and STOR. Variable conversion efficiency case.

When thermodynamic characteristics are accounted in the MILP framework (Figure 55), the optimal scheduling would require shorter LAES discharge periods but higher power output. The optimisation seeks to discharge preferentially at nominal condition, as can be inferred by the comparison of the

average $\dot{W}_t^{dsc}$ values presented in Table 26. Discharging hours decrease from 17 to 13, but this allows the LAES to run at full power output during the highest electricity price peaks. The variations of LAES SoC suggest that the plant is providing inter-day arbitrage, capitalising on the largest energy price differentials. This highlights the importance of modelling large-scale storage over extended periods [181], in contrast with the typical patterns for technologies such as batteries [183]. The computed roundtrip efficiency for the real case is 58.64%, which is higher than the value referring to the feasible corrected dispatch. This demonstrates truly optimal scheduling can be achieved only by including the thermodynamic characteristics of LAES *within* the optimisation, as opposed to the re-elaboration of an ideal, unfeasible scheduling profile. Detailed discussion is provided section 5.5.1.

Table 26: Scheduling and performance metrics for the ideal and real weekly dispatch optimisation.

| Metrics | Model run | |
| --- | --- | --- |
| | Ideal | Real |
| Discharging hours [h] | 17 | 13 |
| Average sell price [£/MWh] | 67.36 | 67.5 |
| Average power output [MW] | 155.2 | 189.9 |
| Energy output [MWh] | 2639 | 2468 |
| Charging hours [h] | 44 | 42 |
| Average buy price [£/MWh] | 30.39 | 30.2 |
| Energy input [MWh] | 4400 | 4200 |
| LAES roundtrip efficiency, $\eta_{RT}$ [%] | 60 | 58.6 |
| Number of equivalent cycles [-] | 4.4 | 4.11 |

## 5.4.2 Optimal LAES sizing

In the following, we refer to optimal sizing as the process of choosing storage design based on the outcomes from the sensitivity-type analysis carried out on the rating of each LAES sub-system: liquefaction, PRU and tank capacity. This approach is meant to shed light on the complex relationship between system design, portfolio of services to be provided and techno-economic performance, as opposed to identifying a unique, optimised LAES size as the outcome of a formal optimisation.

Figure 56 captures the effect of each independent design parameter on LAES payback time, as a function of the considered operating strategy. On the left-hand axes, PBT values are plotted; they have been normalised to the PBT of the reference 200 MW, 100 MW input and 600 MWh LAES, which lies sufficiently in the middle of the design space. On the right-hand axes, the sensitivity of PBT to the relevant design parameter is reported as $\partial PBT / \partial X$, where $X$ is the design parameter. Each row in Figure 56 captures the individual effect of one of the design parameters. From the top row downwards: PRU power output, liquefaction power input and storage capacity.
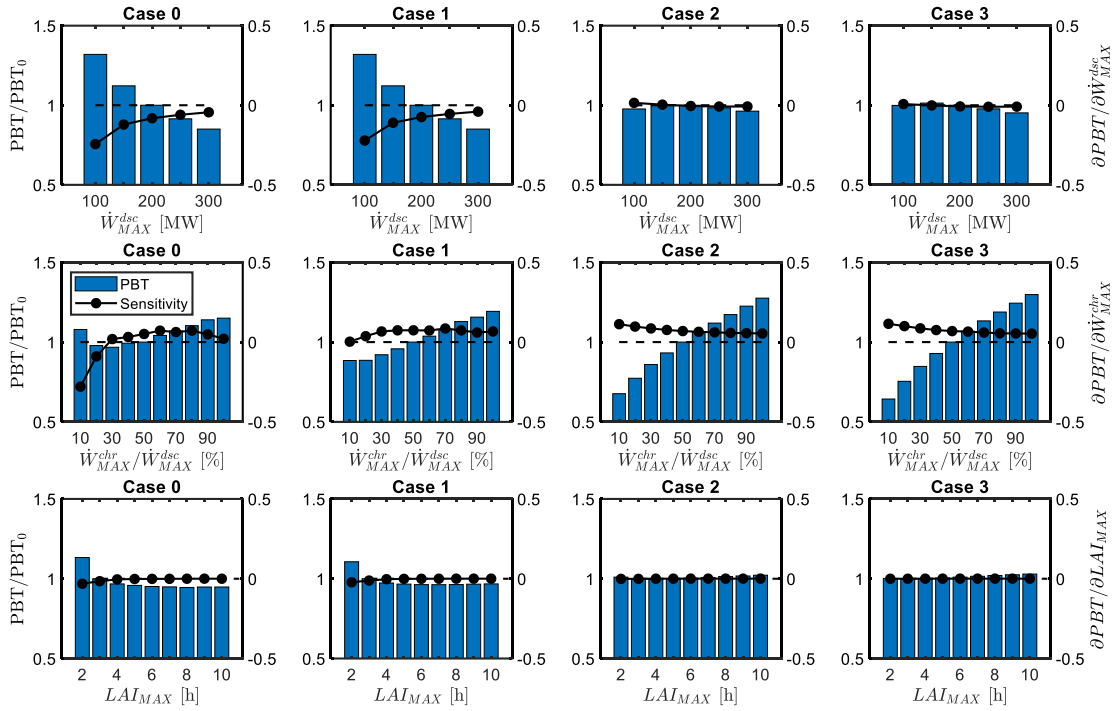
**Figure 56: Independent impact of LAES design parameters on its profitability for different operating modes. Row 1: PRU power output; row 2: liquefaction power input; row 3: storage tank capacity.**

Minimum PBT is determined by the ratio between the CAPEX associated with the selected design and the cash inflows from LAES operation. This latter value is determined by the specific dispatch profile for the plant – which clearly depends on the operating mode – as well as the revenue scheme.

When dealing with power sizing, larger PRU generally leads to better economic results (see row 1 of Figure 56). This is expected for cases heavily relying on arbitrage (Case 0 and Case 1), since costs increase with exponent 0.6, while arbitrage revenues are proportional to the PRU size, $\dot{W}_{MAX}^{dsc}$ (doubling $\dot{W}_{MAX}^{dsc}$ yields a double revenue). The behaviour is different when the share of reserve revenues is high (Case 2 and Case 3). At small PRU values (below 150 MW), the constant availability fee represents the main source of income, in such a way that the increase in revenues for larger PRU is not enough to offset the increase in CAPEX. For PRU above 150 MW, the increase in revenue is mainly driven by the utilisation fee, outpacing the CAPEX increase.

Considering liquefaction size (second row in Figure 56), an optimum value minimising PBT is found for Case 0 when the liquefier rating is 30% of the PRU. Because of the high share of CAPEX associated with the liquefier (in the range of 60-70%) this is the most important parameter to minimise. However, this optimum value is relevant for arbitrage alone. When reserve is added, it provides additional revenues, which are little influenced by the liquefier rating, $\dot{W}_{MAX}^{chr}$. Therefore, the optimum is displaced progressively towards smaller values of $\dot{W}_{MAX}^{chr}$, and eventually below the lower limit considered for the current analysis.

Looking at capacity sizing (i.e. choosing the optimal energy storage capacity for given values of charging and discharging rated power), Figure 56 demonstrates how the storage tank size, $LAI_{MAX}$, is in general the least sensitive factor. This is no surprise since the share associated with the tank is marginal with respect to plant costs, at less than 10% of the total CAPEX. Apart from relatively small storage capacities (2 h of rated discharge or less), the predicted PBT displays only minor improvements for each additional hour of storage, with negligible influence of the operating mode.

In general, outcomes show that the optimal decision on LAES sizing for minimising the investment payback time should ultimately be tailored to the specific operating mode, especially concerning the choice of the rated power input and output. However, for the assessment of LAES multi-mode operation, a single plant design is desirable. A 200 MW LAES featuring 40 MW liquefaction (20% $\dot{W}_{MAX}^{dsc}$) and 3 hours of storage capacity was thus identified as a versatile solution yielding close-to-optimal PBT value for all the case studies. Further elaboration around sizing aspects is part of the Discussion section, where LAES size is also related to scheduling and thermodynamic performance metrics.

### 5.4.3 LAES multi-mode operation

The techno-economic results obtained from the MILP model for the individuated 200 MW LAES plant are presented here. Figure 57 shows the existing correlation between LAES operating mode and its technical performance, as captured by roundtrip efficiency $\eta_{RT}$ and the power indicator $\xi$.
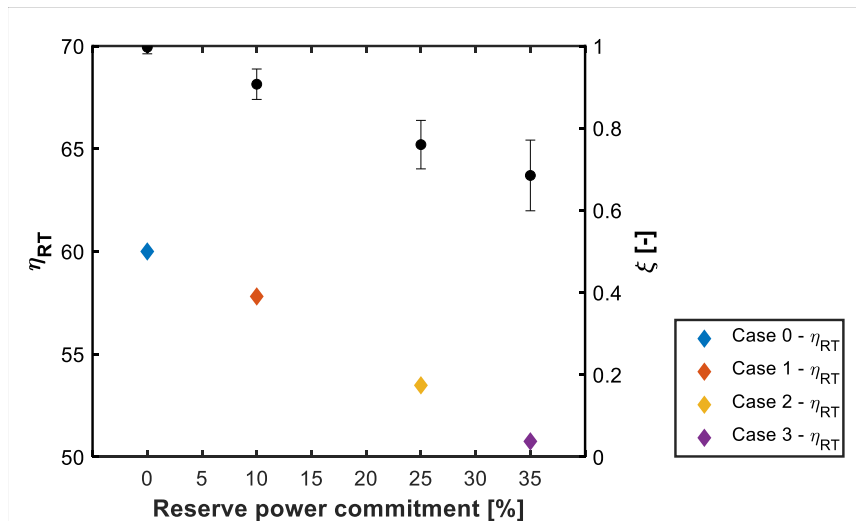


Figure 57: Link between operating mode and LAES plant technical performance.

It demonstrates that the value of roundtrip efficiency over the whole year can change significantly (variation of up to 17% of nominal efficiency – from 60% to about 50% $\eta_{RT}$) when committing generation capacity to reserve services. While for Case 0 (arbitrage alone), LAES is mostly run around the rated generation level ($\xi \approx 1$), the larger the commitment to reserve, the larger the deviation from the rated power output, with associated off-design losses. Also, the values of the power indicator $\xi$ become more distributed, meaning higher variability of LAES generation levels.

The more services LAES provides, the more likely it is to operate at off-design conditions. This results in lower conversion efficiency and reduced power exchange between LAES and the grid. However,

LAES can benefit from more favourable differentials between average buy and sell prices and, on top of this, additional revenue from reserve services. The financial viability of multi-mode operation is confirmed in Figure 58, which shows a breakdown of the yearly revenues for the reference plant as a function of the operating mode and of the modelling approach. It demonstrates that committing power to reserve is economically justified by higher earnings, despite poorer plant efficiency. Multi-mode cases are found to be significantly more profitable than arbitrage alone, in agreement with what was highlighted in [298].
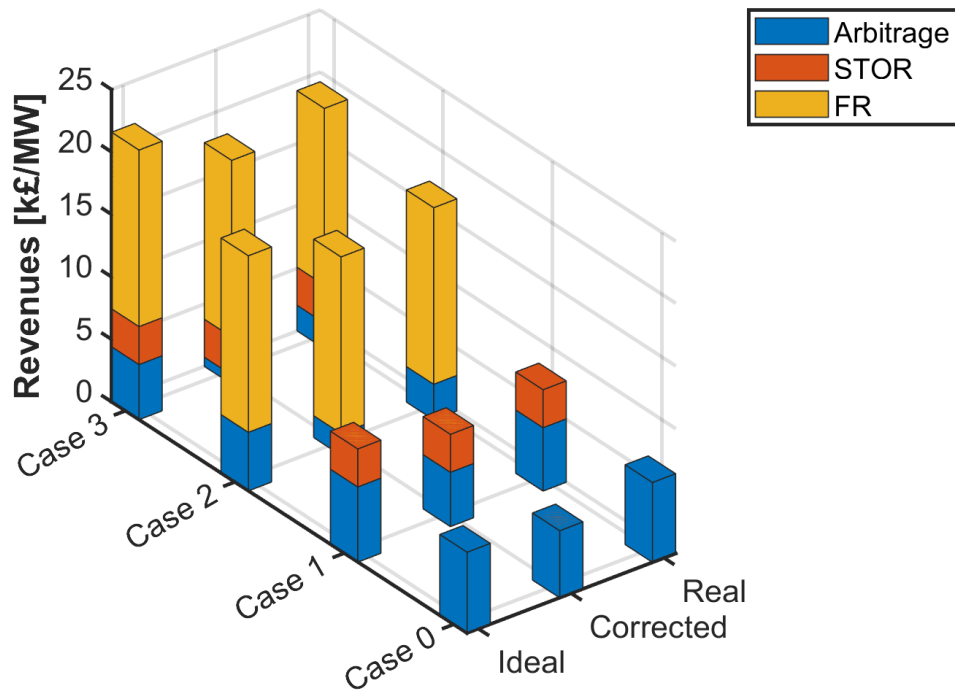


**Figure 58: Yearly revenues for LAES as a function of the modelling approach for the four selected operating modes.**

When multi-mode operation is based on arbitrage and STOR (Case 1), the former accounts for the majority of revenue; this agrees with the findings in [140]. In Case 2 and 3, on the contrary, earnings from FR provide the most significant source of income. The share of revenue provided by arbitrage decreases progressively: from 62% in Case 1 to 17% in Case 2 and down to only 11% in Case 3. This is due to the availability of additional revenue streams as well as to the lower conversion efficiency of LAES when committing power to reserve, as shown previously in Figure 57.

## 5.5    Discussion

Results presented so far confirm the unique capability of the developed model to provide an optimal dispatch profile, leading to more accurate estimations of LAES techno-economic value than traditional models based on constant efficiency. In this section, further discussion is given on the interdependence between LAES scheduling, size and operation, captured thanks to the proposed modelling framework.

### 5.5.1 The financial impact of accurate thermodynamic modelling

Based on the values in Figure 58, Table 27 compares the revenue from the ideal, constant efficiency model with revenues from both the a posteriori correction and the realistic MILP model. One can see that the correction of the ideal scheduling profile yields a significant reduction in revenues. This is due to an infeasible profile which forces the storage to discharge for shorter timespans in order to comply with the constraints. Being able to capture LAES behaviour within the optimisation ensures the computation of a truly optimal and feasible scheduling profile. This is crucial and improves the average LAES profitability over one-year operation. However, it is also interesting to observe how the inclusion of LAES thermodynamic characteristics may also result in lower profitability, *instantaneously*. Indeed, as the LAES dispatch is optimised over the selected optimisation horizon, situations arise where it is best not to operate LAES (i.e. incurring a revenue loss) to enable operation at a higher thermodynamic performance at a different time and, on average, across the whole year. This behaviour can be observed by comparing Figure 53 (ideal) and Figure 55 (real) between hours 40 and 50 and its discussion is of clear interest to LAES operators.

Table 27: Predicted variation of LAES economic value with respect to the constant conversion efficiency case.

|  | Lost revenue - Corrected | | Lost revenue - Real | |
|---|---|---|---|---|
|  | [k£/MWh] | [%] | [k£/MWh] | [%] |
| Case 0 | 1.12 | 17% | 0.11 | 2% |
| Case 1 | 1.67 | 18% | 0.95 | 10% |
| Case 2 | 2.94 | 16% | 1.84 | 10% |
| Case 3 | 3.67 | 17% | 2.36 | 11% |

Revenues from the realistic model display an average 2% reduction over one year from the ideal case for arbitrage alone (Case 0); this value increases up to 11% for Case 3 (complete portfolio of services). This suggests accurate modelling of LAES is necessary for multi-mode operation, in agreement with the conclusions drawn for a compressed air energy storage plant in [234]. The more services LAES provides, the more revenue is lost for the corrected case due to frequent off-design discharge (see Section 5.4.3). Misevaluation of storage performance in these conditions would lead to a major impact on LAES financial viability.

### 5.5.2 Design guidelines for LAES

A key technological benefit of LAES is the possibility to design a plant in such a way that rated power for charge and discharge processes can be selected independently [100,140,179]. This feature of LAES is especially relevant for enabling a tailored design for specific operating strategies, as described in Section 5.4.2.

LAES economic performance, as measured by the payback time, is most sensitive to LAES power sizing (in terms of both liquefaction input and PRU output) when operating for arbitrage alone, which shows the need for case-dependent design choices driven by the local fluctuation of electricity prices. When increasing the participation in reserve services, the dependency of PBT on power sizing progressively reduces. A larger portion of the revenues can be accessed via service commitment rather than energy dispatch, with the latter being primarily affected by LAES size. The final choice of $\dot{W}_{MAX}^{dsc}$ and $\dot{W}_{MAX}^{chr}$ in

these cases is likely to be driven by the technical limitations associated with the integration of LAES with the grid and its infrastructure (e.g. network constraints), rather than storage-centric considerations.

When considering storage capacity $LAI_{MAX}$, limited PBT improvement is predicted for LAES capacities above 2-3 h of rated discharge. This contradicts the typical guidelines for TMES, deriving from a purely economic assessment of the low costs per unit kWh of this storage class [20,97]. However, different conclusions arise when technical considerations and storage dispatch are considered. Reserve services involve power delivery for relatively short periods and are unaffected by capacity specifications. Hence, every extra hour of added capacity yields progressively lower improvement of plant profitability if LAES power rating is not increased accordingly. As an example, Figure 59 shows how around 15% of tank capacity is not used for Case 1, when tank size is 6 h, as opposed to Figure 55, where tank size is 3 h and is fully utilised. LAES capacity reduction has also the added benefit of containing the land area required by the installation, which is greatly dependent on dimensions for liquid air and cold storage tanks [127].
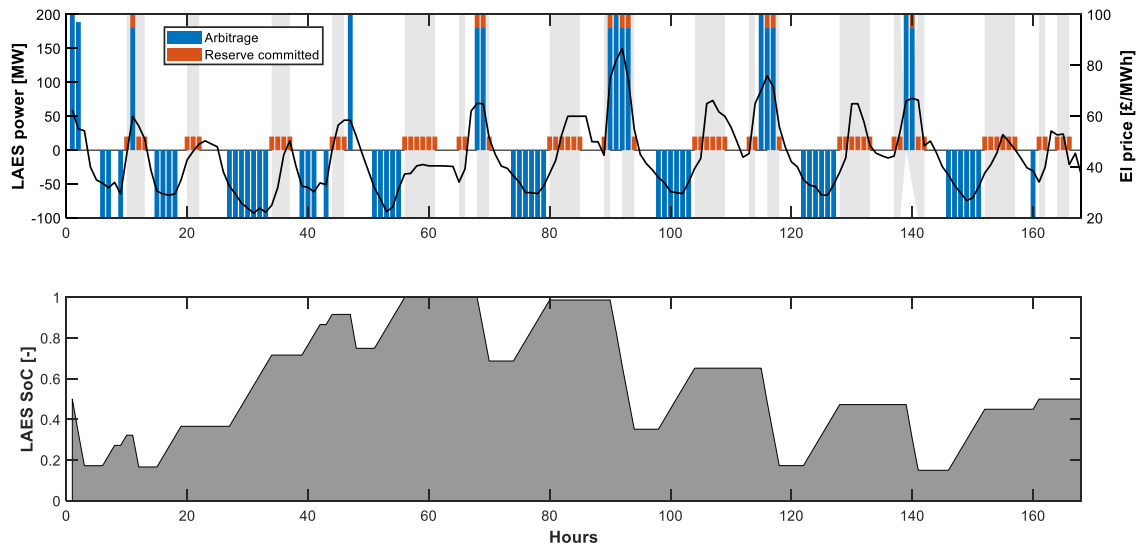


Figure 59: One-week LAES dispatch when providing arbitrage and STOR. 6 hours tank capacity.

Tank capacity affects LAES thermodynamic performance by constraining its power output setpoint: Table 28 shows how larger tanks correspond to better roundtrip efficiency. Due to the increased LAES capacity, it becomes less likely that the constraints involving a minimum SoC are binding. This in turn reduces the likelihood of LAES part-load discharging due to capacity constraints, and it is reflected by the average values of the power indicator $\xi$ being closer to the ideal value 1. Together with higher LAES thermodynamic efficiency, the total number of charging and discharging instances over the year increases, creating a compounding effect that leads to higher total revenues. However, once a critical amount of storage is established, additional capacity has very little effect economically, except to match the associated increase in CAPEX. The critical amount to be ensured is 4-5 h if operating arbitrage alone, while only 2-3 h is sufficient for simultaneous reserve provision.

Table 28: Scheduling and performance metrics for LAES, as a function of the storage capacity.

| Case | $LAI_{MAX}$ [h] | Discharging hours [h] | Off-design hours [h] | Power indicator, $\bar{\bar{\xi}}$ [-] | Charging hours [h] | LAES roundtrip efficiency, $\eta_{RT}$ [%] |
|------|-----------------|------------------------|----------------------|-----------------------------------------|--------------------|-------------------------------------------|
| 0 | 2 | 532 | 150 | 0.99 | 1774 | 59.4 |
| | 6 | 676 | 76 | 1.00 | 2238 | 60.0 |
| | 10 | 686 | 60 | 1.00 | 2258 | 60.0 |
| 1 | 2 | 448 | 404 | 0.89 | 1396 | 57.1 |
| | 6 | 592 | 536 | 0.91 | 1848 | 58.2 |
| | 10 | 620 | 556 | 0.91 | 1924 | 58.6 |
| 2 | 2 | 334 | 324 | 0.76 | 952 | 53.1 |
| | 6 | 380 | 366 | 0.76 | 1068 | 54.0 |
| | 10 | 382 | 366 | 0.76 | 1062 | 54.7 |
| 3 | 2 | 266 | 258 | 0.68 | 716 | 50.8 |
| | 6 | 306 | 296 | 0.68 | 814 | 51.3 |
| | 10 | 308 | 292 | 0.68 | 808 | 52.1 |

### 5.5.3 Effect of reserve market participation

Focus is now given to the role reserve commitment plays in defining the financial viability of LAES. Figure 60 shows plant roundtrip efficiency as a function of the committed power to STOR and FR. The same amount of capacity annexed for FR has a higher impact on performance than STOR. This is explained through the larger availability window associated with FR, which limits the LAES to part-load discharge over longer periods. The power indicator $\xi$ varies from 0.78 to 0.71 if 30% is devoted to STOR or FR, respectively.
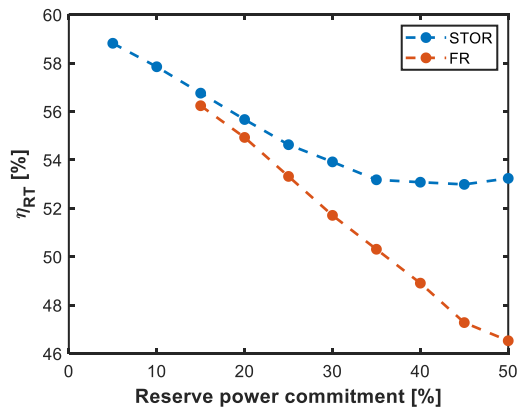


Figure 60: LAES roundtrip efficiency for different levels of power commitment to STOR and FR.

Additionally, the larger the power commitment, the greater the difference between the two considered reserve services. This is because more power is needed to ensure reserve deliverability and LAES is restricted to discharge at lower output for longer periods. Services requiring larger availability windows are further penalised (e.g. FR more than STOR), because price peaks are now more likely to coincide with availability windows. A reduced roundtrip efficiency limits the accessible profit from

arbitrage, and a techno-economic trade-off must be achieved to maximise revenues. Figure 61 illustrates the economic impact of different choices in reserve power commitment.
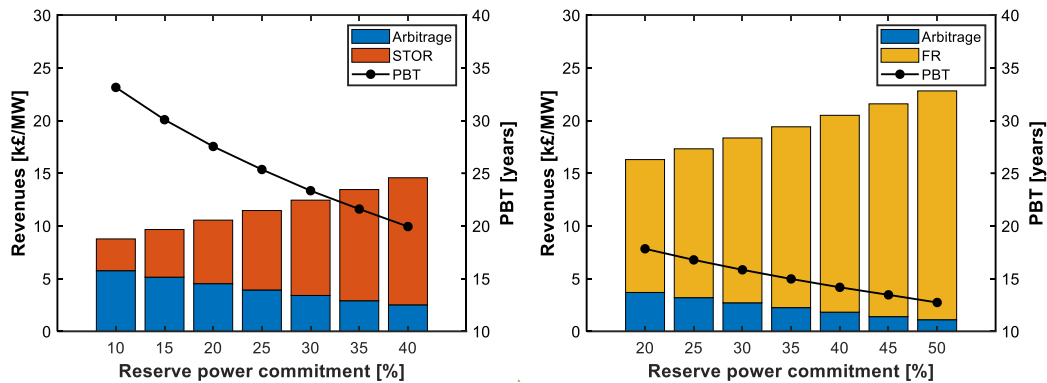


Figure 61: Yearly revenues for different levels of power commitment to reserve: STOR (left) and FR (right).

Higher revenues from increased reserve market participation are obtained, despite worse technical performance for LAES. Therefore, the most profitable approach could be to allocate more power to reserve services and possibility solely provide reserve services. PBT drops from 33 to 23 years when 30% of the rated output is committed to STOR, rather than 10%. For FR, figures change from 18 to 14 years when committing 40% instead of 20%. However, LAES scheduling would now be mostly subject to real-time calls from the grid operator, making it challenging to achieve meaningful predictions for the dispatch profile.

The possibility of supplying reserve alongside arbitrage drastically changes the dispatch pattern of LAES. Additional constraints to storage operation are introduced, resulting in times of competition between energy and reserve services. This is more significant for higher power commitment but enables the storage operator to benefit from higher profits. At lower commitment levels, revenues from FR are significantly higher than those from STOR, while the difference decreases as the commitment levels increase. In this case, bidding in different reserve markets could be particularly suitable. Ultimately, diversifying over a portfolio of revenue streams is necessary to decrease the risks associated with the variable profitability of reserve services over the markets and the seasons. Therefore, a balanced power commitment should be sought.

## 5.6    Conclusion and outlook

Following the description of LAES performance variations during plant operation in Chapter 4, results from this chapter explore the flexible use of LAES over a portfolio of energy balancing and reserve services. In so doing, a novel methodology to include LAES thermodynamic characteristics from Chapter 4 into an MILP optimisation is presented along with the associated merit compared to battery-like storage models with constant roundtrip efficiency. Study outcomes produce new understanding resulting from the accurate prediction of LAES dispatch profile, whilst shedding light on two critical aspects for LAES financial viability: plant sizing and power allocation to different reserve services. Key takeaways can be summarised as follows.

Results demonstrate how *considering storage thermodynamic characteristics is necessary for feasible scheduling*: failing to do so results in missed storage participation in grid balancing and lower revenues. Indeed, thermodynamic limitations alter LAES optimal dispatch schedule, with the plant being run over fewer cycles at higher power output, thus closer to rated conditions, regardless of the operating mode. On the contrary, *guidelines for optimal plant sizing depend on the operating mode and the revenues that can be accrued*, hence on the electricity price profile and reserve service remuneration schemes. For arbitrage only, liquefier sized at 30% of the PRU rating seem to provide the best solution. For multi-mode operation, the ideal plant features a large PRU, a small liquefier (10% of the PRU, or less), and capacity equivalent to 2-3 h of rated discharge duration.

*Multi-service operation negatively impacts LAES thermodynamic performance*, with roundtrip efficiency variations up to 10 points for the cases explored; reserve services involving longer availability windows cause larger performance detriment. However, *LAES thermodynamic performance is economically more than offset by larger revenues in multi-service cases* with simultaneous arbitrage, STOR and/or FR provision, resulting in below 20 years payback time. This points clearly towards the future provision of a portfolio of reserve and energy balancing services from LAES, rather than traditional arbitrage-only operation. Hence, LAES flexibility and performance improvement under off-design conditions are essential future avenues to boost plant profitability. In addition, the higher the power committed to reserve services, the more capturing the variations of storage conversion efficiency helps avoid unfeasible scheduling and missed revenues (up to about 2 k£/MW per year). Compared to traditional storage models with constant roundtrip efficiency, the proposed LAES model reduction through piecewise linear characteristic curves limits such lost revenues by between 37 and 90%.

## 5.6.1 Chapter relevance within this thesis

The results from this chapter address the research objective O2 by also informing on how to tailor plant design to different operational scenarios and should be used for proper LAES dispatch planning in power systems. Such rigorous assessment is essential to best operate LAES and TMES in the energy market, thus maximising the techno-economic benefits. The following contributions are added to the existing literature:

- Multi-market modelling framework which captures the link between operating setpoint and plant performance through LAES thermodynamic characteristics
- Demonstration of how variations in LAES thermodynamic performance affect the provision of energy balancing and reserve services
- Quantification of lost revenues from traditional LAES modelling approaches
- Description of how the provision of multiple balancing services impacts the techno-economic viability and optimal design of LAES.

After characterisation of the technically feasible operation and value of standalone LAES in the power system, Chapter 6 explores a potential LAES integration in the broader energy system with multi-energy provision under an analogous workflow, including technical limitations in the dispatch

algorithm. Then, Chapter 7 addresses LDS applications of TMES, complementing the analysis of reserve services with energy balancing services over longer timescales.

# CHAPTER 6

## Multi-energy provision from liquid air energy storage

*Following the assessment of LAES real-life operation and value within the power system in Chapter 4 and Chapter 5, this third results chapter proposes a new perspective for LAES operation by exploring its potential as a multi-energy asset. In this context, compression heat and evaporation cold generated by LAES process are used to supply heat and cold, alongside electricity, externally to a neighbouring district, rather than for internal hot and cold recycle. The techno-economic value and limitations of this novel operating paradigm are compared to traditional electricity storage application. A reduced thermodynamic model of LAES is presented, validated and used to: i) quantify the thermodynamic efficiency of a multi-energy LAES, generalising its output capability over the three energy vectors considered; ii) link different plant integration conditions with the associated multi-energy LAES performance; and iii) describe multi-energy LAES operation as part of two district sizes, for provision of peaks and baseload. Results show that by leveraging vector-coupling capability, LAES energy efficiency rises from 47% to 72.8%, with an associated reduction up to 8–12% in district operating costs for the considered case studies. By demonstrating the technical feasibility of multi-energy LAES operation with the associated trade-offs, the thesis objective to techno-economically assess the opportunities and limitations for multi-energy provision from LAES is addressed. Outcomes suggest TMES solutions with embedded TES can play a greater role in decarbonisation than what speculations considering purely electrical applications so far predicted.*

## 6.1 Introduction

As largely discussed, LAES system comprises two (one hot and one cold) or more TES, which store the hot and cold thermal streams produced during plant operation. Chapter 2 shows most works have either looked at the internal use of such thermal streams or the hybridisation with external processes (ORC, Kalina cycles) to boost electricity output and roundtrip efficiency. However, the stored heat and cold could in principle be delivered externally, alongside electricity, and, crucially, with no additional components. Such a strategy represents a paradigm shift from the traditional operation of LAES in the power system, which Chapter 4 and Chapter 5 assessed. Districts characterised by simultaneous electricity, heating and cooling needs represent a relevant integration setting, in this case, to shed light on the opportunities and limitations of multi-energy provision from LAES.

This results chapter characterises the operation of LAES as a multi-energy provider and explores the expected benefits from district integration compared to the use as electrical storage only. In line with the central role of accurate technical modelling emerged in Chapter 4, thermodynamic constraints are included to study component and process interaction over variable power output setpoints and different temperatures for the heat and cold energy to be delivered. Such a model highlights the potential and limitations of multi-energy provision from LAES. The integration with districts of different sizes is then evaluated through a dispatch algorithm that considers the time profile of users' load and LAES operation for peak shaving or load following.

The chapter is organised as follows: study background and assumptions are presented in Section 6.2. The numerical model of multi-energy LAES developed is described and validated in Section 6.3, alongside the approach used for the district integration studies. Then, model results are presented in Section 6.4, with discussion on the multi-energy capability of LAES and the techno-economic benefits from district integration reported in Section 6.5. Conclusions and outlook are reported in Section 6.6.

## 6.2 Background and assumptions

### 6.2.1 Overview of multi-energy liquid air energy storage

The concept proposed in the present result chapter is denoted as multi-energy LAES (M-LAES), and represents a unique solution that can independently supply electricity, heating and cooling output. The plant layout is no different from the conventional standalone LAES (such as that investigated in Chapter 4). However, M-LAES uses the flexibility provided by the hot and cold TES to decouple in time the generation and external use of the individual energy vectors (electricity, heat and cold). So, it effectively embodies a novel operation paradigm for LAES, which, contrary to the multi-vector plants investigated in [137] or [138], does not require any plant components to be added. For this reason, the key aspect to examine besides the thermodynamics of M-LAES operation is plant integration with a model district energy system. For this, district scales ranging from 10s to 100s MW peak power demand were considered, which represent a well-established target for LAES in the literature [22].

Figure 62 illustrates the district integration layout considered for M-LAES, as inspired by the proposed integrations of LAES and other TMES with local industrial parks [299] and energy communities [199]. LAES is charged from the grid at night – when surplus baseload generation is likely available due to a lower overnight electricity demand [300] – and, similarly to [191], directly supplies electricity to the district. On the thermal side, a district heating network (DHN) and a district cooling network (DCN) were considered in this case to couple M-LAES generation with the aggregated thermal load from the users. However, as distribution networks were not explicitly modelled, this layout is equally suitable to represent cases where single localised thermal users (e.g. industrial or commercial facilities [301]), instead on full networks, are supplied by M-LAES. Clearly, local generation or other means of procurement are necessary besides LAES, to fully cover district load. However, these assets were not included, as the present analysis focuses on M-LAES operation and comparison with the traditional LAES use as electricity storage only (and not with alternative storage and multi-energy solutions).
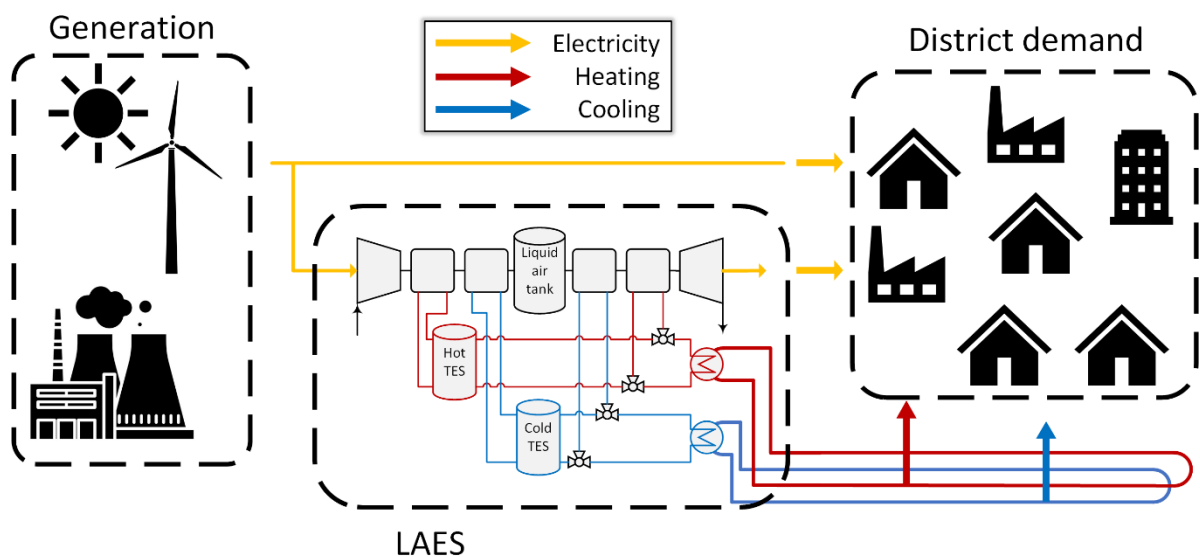


**Figure 62: Multi-energy LAES (M-LAES) operated in a district energy system setting.**

## 6.2.2 Liquid air energy storage multi-energy operation strategy

Given the focus is LAES multi-energy operation, no reserve services were considered in this chapter. Rather, two energy balancing services were explored, namely peak shaving and load shifting, which are relevant to both electricity and thermal supply. As we shall see in Section 6.4.1, interlinks and technical limitations associated with multi-energy provision from LAES mean the power and thermal output depend on one another in a nonlinear fashion. So, to understand the link between LAES operation and its techno-economic value across different scenarios in the energy system integration study, a heuristic dispatch algorithm was preferred here to nonlinear optimisation.

*Scheduling* and *prioritisation* are two central concepts such heuristic algorithm uses to determine the multi-energy plant dispatch based on the aggregated district load signals.

- **Scheduling**: identifies the process of selecting the times in the day when M-LAES is charging or discharging, whereby discharge scheduling is driven by the operation chosen:

- o *Peaker*: to cover high-demand periods, LAES provides a constant output anytime district load (electrical or thermal) is more than 20% above its mean value
- o *Load-following:* to shift loads over time, LAES provides a variable output proportional to the difference between the instantaneous load and its mean anytime district load (electrical or thermal) is above its mean value.

- **Prioritisation**: identifies the process of selecting M-LAES scheduling and output setpoint to privilege either electric or heating output, according to:
  - o *Electrical prioritisation:* LAES output scheduling is based on the electric signal. Should heating be needed at the same time, this is also provided; LAES setpoint maximises electricity delivery
  - o *Thermal prioritisation:* LAES output scheduling is based on the thermal signal. Should electricity be needed at the same time, this is also provided; LAES setpoint maximises heating delivery
  - o *No prioritisation:* LAES output scheduling delivers electricity and heating every time these are required, even if not at the same time. LAES setpoint maximises joint energy dispatch*.

The joint effect of scheduling and prioritisation ultimately defines M-LAES operation strategy and dispatch, as visualised in Figure 63. More details on M-LAES dispatch profile and the operation strategy considered in the district integration assessment are given in Section 6.3.3
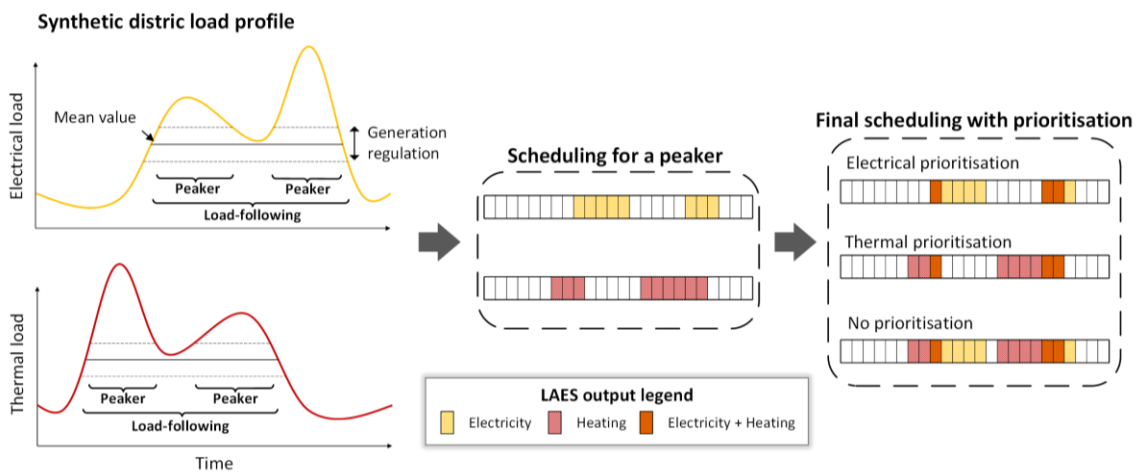


Figure 63: Definition of multi-energy LAES dispatch based on the selected operating strategy (scheduling and prioritisation).

# 6.3 Numerical modelling of M-LAES and district integration

## 6.3.1 Technical modelling of M-LAES

A numerical model was built to simulate plant operation by detailed modelling of the central process units for M-LAES, i.e. units where the conversion between electricity and heat takes place. These are the multistage compression and expansion processes and the transcritical heat exchangers, which have all been highlighted by dashed boxes in Figure 64. As far as the remaining components are

concerned, 0-dimensional energy, mass and momentum conservation equations were specified and complemented by component characteristic equations, making use of isentropic efficiency for turbomachinery and effectiveness for the heat exchangers (see Section 3.2.1). The following subsections detail the modelling of key process units.
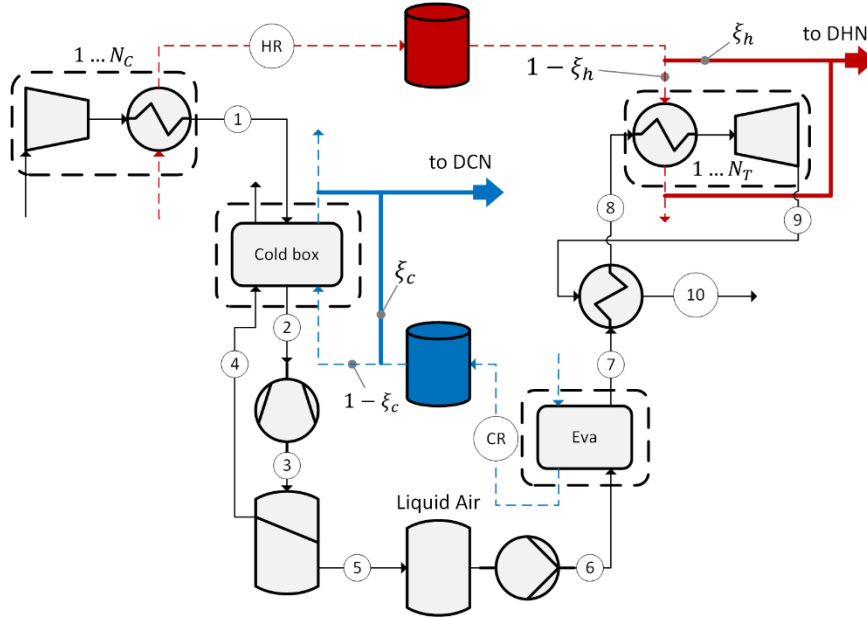


**Figure 64: Process flow representation of LAES used for mathematical model set up.**

## Multistage intercooled compression

Each intercooled compression stage was modelled according to the representation in Figure 65, where the same compression ratio $\Pi_C$ was considered for all the $N_C$ stages. The $\Pi_C$ value was computed from the inlet and outlet pressure values for the whole train, $p_{C,in}$ and $p_{C,out}$, with pressure losses in the intercoolers estimated as a given percentage $\beta$ of the inlet pressure, as in [88]:

$$\Pi_C = \frac{1}{(1-\beta)}\left(\frac{p_{C,out}}{p_{C,in}}\right)^{1/N_C} \qquad 6.1$$

**(a) Multistage compression**          **(b) Multistage expansion**
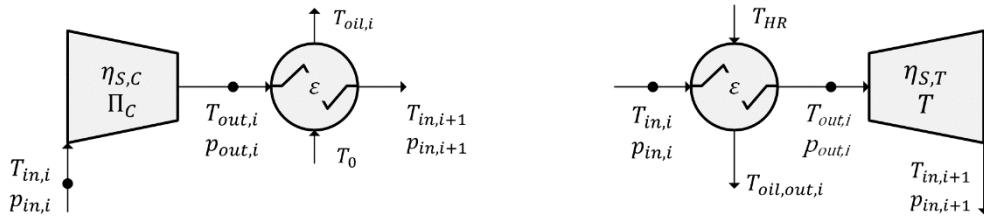


**Figure 65: Sketch of a generic stage of the intercooled compression train (a) and reheated expansion train (b).**

The power input to each stage was computed from the isentropic efficiency of the compressor, $\eta_{S,C}$, and the given heat exchange effectiveness value $\varepsilon$ of the intercooler was used to evaluate the exit temperature of air and the oil in the hot recycle loop, under the assumption of balanced flows:

$$\dot{W}_{C,i} = \eta_{S,C}\dot{m}(h_{S,out,i} - h_{in,i}) \qquad 6.2$$

$$\varepsilon = \frac{(T_{out,i} - T_{in,i+1})}{(T_{out,i} - T_0)} = \frac{(T_{oil,i} - T_{Amb})}{(T_{out,i} - T_0)} \qquad 6.3$$

The term $h_{S,out,i}$ in Equation 6.2 represents air enthalpy at the outlet of the compression stage for an isentropic transformation, whose value was estimated from the equation of state developed by the NIST and implemented in EES [302]. Finally, the total oil heat capacity rate, $\dot{C}_{oil} = \sum_{i=1}^{N_C} \dot{C}_{oil,i}$, and the hot recycle recovered from the compression train, $\dot{Q}_{HR}$, were evaluated from the energy balance over each intercooler. The hot recycle temperature was estimated as a weighted average:

$$T_{HR} = \frac{\sum_{i=1}^{N_C} \dot{C}_{oil,i} T_{oil,i}}{\sum_{i=1}^{N_C} \dot{C}_{oil,i}} \qquad 6.4$$

### Multistage expansion with reheating

The approach used for the multistage expansion with reheating is also illustrated in Figure 65. Similarly to what has been described for the compression train, the expansion ratio for each stage was computed first, correcting for the pressure losses:

$$\Pi_T = (1 - \beta) \left( \frac{p_{T,in}}{p_{T,out}} \right)^{1/N_T} \qquad 6.5$$

It was assumed the thermal oil in the hot recycle was split into $N_T$ equivalent streams – one for each reheater – and temperature and enthalpy variations for the two streams across the reheaters were computed based on the heat exchanger effectiveness and steady-state energy balance:

$$\varepsilon = \frac{\dot{C}_{oil,i}(T_{HR} - T_{oil,out,i})}{\dot{C}_{min}(T_{HR} - T_{in,i})} \qquad 6.6$$

$$h_{out,i} = h_{in,i} + \frac{\dot{Q}_i}{\dot{m}} = h_{in,i} + \frac{\dot{C}_{oil,i}(T_{HR} - T_{oil,out,i})}{\dot{m}} \qquad 6.7$$

$\dot{C}_{min}$ in Equation 6.6 denotes the lowest flow heat capacity value between hot and cold streams. Finally, turbine isentropic efficiency allowed to quantify the power output from each stage based on the ideal outlet enthalpy for an isentropic expansion, $h_{S,in,i+1}$:

$$\dot{W}_{T,i} = \eta_{S,T} \dot{m}(h_{out,i} - h_{S,in,i+1}) \qquad 6.8$$

The return oil temperature was computed as the mean value for the $N_T$ oil streams at $T_{oil,out,i}$.

### Transcritical heat exchangers

Although resulting in efficient heat transfer and better LAES performance [109], significant thermal property variations in the supercritical range necessitate a specific treatment of the transcritical heat

exchangers in the system, namely the cold box and the evaporator. A partitioned approach was adopted for these two components, as exemplified in Figure 66, by subdividing the heat exchanger into subsequent sections with locally constant fluid properties. As explained in [106], one aggregated hot and one cold stream were considered in each section, including the contributions from all the fluids in the specific temperature range. Finally, the solution of an energy balance over each partition enabled the computation of the heat transferred and the local temperature evolution of each stream, thus ensuring the specified value of temperature difference at the pinch point.
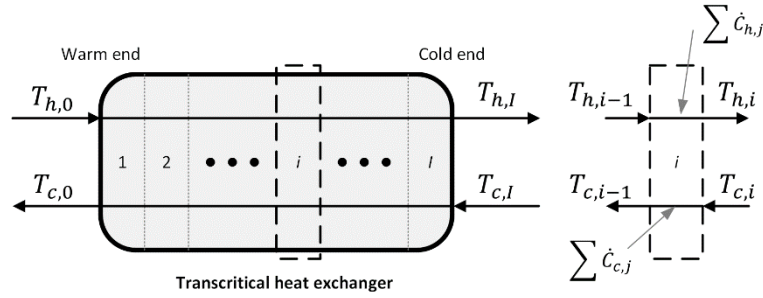


Figure 66: Sketch of the partitioned modelling approach for the transcritical heat exchangers.

### Heating and cooling provision

External LAES provision of heating and cooling to DHN and DCN reduces the amount of heat and cold recycled within the LAES process itself. Vice versa, complete recycling of heat and cold with the LAES process diminishes the heating and cooling that can externally be provided to the DHN and DCN. So, the split parameters $\xi_h$ and $\xi_c$ were defined to accurately track the amount of heat and cold energy recycled within the LAES process and that provided to the DHN and DCN.

Considering DHN provision, and knowing the compression heat produced during LAES liquefaction, the split parameter $\xi_h$ was defined as the portion of such heat directly supplied to the DHN and therefore not available internally for reheating process to the LAES system:

$$\xi_h = \frac{\dot{m}_{oil,DHN}}{\dot{m}_{oil,chr}}$$   6.9

As illustrated in Figure 64, the thermal power delivered to DHN was then quantified by the summation of two contributions: (1) that from the recycled oil which directly supplied the DHN; and (2) that from the outlet oil exiting the reheating circuit, should its temperature be higher than the return temperature for the district heating network, $T_{DHN,ret}$.

$$\dot{Q}_{DHN} = \underbrace{\xi_h \dot{m}_{oil,chr} c_{p,oil} (T_{oil} - T_{DHN})}_{1}$$
$$+ \underbrace{(1 - \xi_h) \dot{m}_{oil,chr} c_{p,oil} (T_{oil,out} - T_{DHN})}_{2}$$   6.10

Variations of the parameter $\xi_h$ allow modifying the power and thermal output of the LAES plant, providing operational flexibility. Similar considerations apply to the parameter $\xi_c$, i.e. the portion of recycled evaporation cold directly supplied to the DCN.

## 6.3.2 Model validation

One key feature of the proposed model is its capability to evaluate different plant layouts and operating conditions: by adjusting parameters such as charge and discharge pressure or the number of compression/expansion stages, a variety of LAES system configurations can be explored. Thus, model performance was validated against the four works presented in Table 29, which exhibit different plant design and operating conditions.

Table 29: Key input parameters for model validation.

| Parameter | Peng et al. [101] | Guizzi et al. [98] | Sciacovelli et al. [106] | She et al. [303] |
|---|---|---|---|---|
| Turbine isentropic efficiency [-] | 0.9 | 0.85 | 0.85 | 0.9 |
| Compressor isentropic efficiency [-] | 0.9 | 0.85 | 0.85 | 0.9 |
| Cryopump efficiency [-] | 0.75 | 0.7 | 0.75 | 0.7 |
| Cryoturbine efficiency [-] | 0.75 | 0.7 | 0.7 | 0.8 |
| Pinch point temperature difference [K] | 3 | 5 | 5 | 2 |
| Pressure loss coefficient [-] | 0.01 | 0.01 | 0.01 | 0 |
| Expansion train inlet pressure [bar] | 78 | 63 | 73 | 120 |
| Compression train outlet pressure [bar] | 135 | 180 | 183 | 90 |
| Liquid air storage pressure [bar] | 1.1 | 1.02 | 1.1 | 1 |
| Plant roundtrip efficiency [%] | 57.7 | 54.5 | 48.3 | 50.3 |

Figure 67 compares model and literature results for LAES roundtrip efficiency. Three out of four validation points fall below 13% deviation from the reference, and all remain within the 20% range. In absolute terms, roundtrip efficiency values in the range between 40% and 45% - as predicted by the present model - are not uncommon in the literature for LAES, and may be associated with the simplifying assumptions adopted here for the liquefaction cycle [119]. Furthermore, the model presented in this chapter has the unique capability to evaluate different LAES plant layouts. Thus, its ability to achieve close accuracy to that of models specialised for a single LAES layout is remarkable.
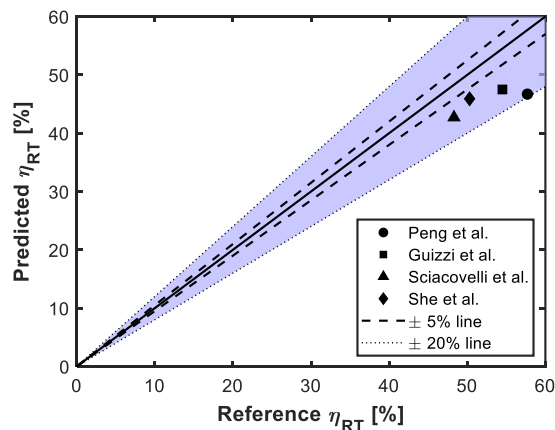


Figure 67: Reference versus predicted values of LAES roundtrip efficiency; used for model validation.

To further inspect the model prediction capability, specific work output and liquefaction work are validated in Figure 68. The former is always accurate to a 5% threshold, which is notable; liquefaction performance estimations are instead underestimated. Such behaviour can be explained by realising

114

that the selected references consider either spillage and expansion from the cold box or a two-fluids cold recycle layout: all solutions that have been proven to increase liquefaction performance. Conversely, none of these was considered in the present model to retain generality and allow exploring a range of designs and operational choices. Therefore, the developed model can capture the links between electrical and thermal provision and, although slightly underestimating LAES electrical performance, it is suitable for the current analysis and comparative assessments.
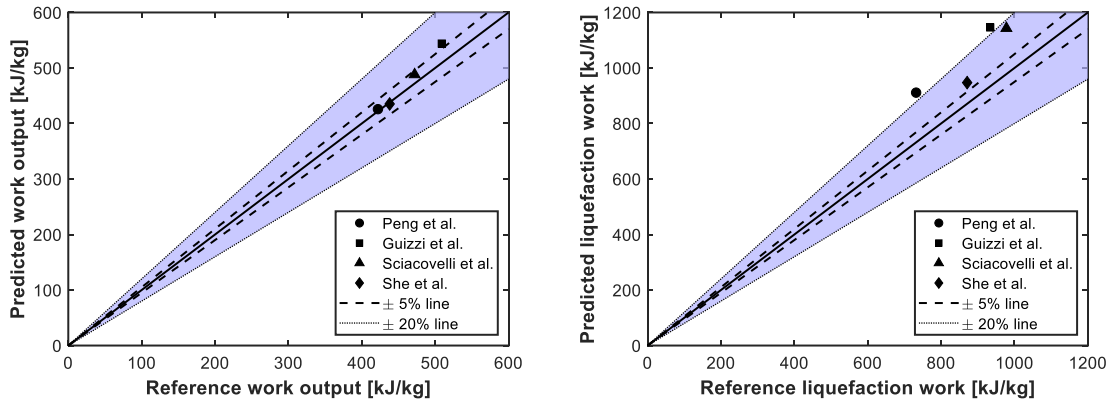


Figure 68: Reference versus predicted values of LAES liquefaction work and specific work output; used for model validation.

### 6.3.3 Multi-energy districts and scenarios considered for M-LAES integration

Two settings were investigated for the integration of LAES, namely a large and a small-scale district, both located in a temperate climate zone. As reported in Table 30, the proposed districts are characterised by different shares of residential and commercial buildings and different DHN temperature levels: 120-80°C for the large and 80-60°C for the small district [304]. Synthetic load profiles were generated by superimposing hourly demand values for a reference 200 m$^2$ residential dwelling [226] and a 3-stories, 5000 m$^2$ office model developed in EnergyPlus [305]. Year-round energy demand was then constructed based on the hourly load pattern for three representative days [306] for winter (150 days), summer (125) and midseasons (90), respectively.

Table 30: Characteristics of large and small district energy systems considered for LAES integration.

| District | $T_{DHN}$ [°C] | Residential dwellings [-] | Offices /Commercial [-] | Peak power [MW] | Mean power [MW] | Peak heating [MW] | Peak cooling [MW] |
|---|---|---|---|---|---|---|---|
| Large | 120 – 80 | 4000 | 1500 | 390 | 230 | 550 | 60 |
| Small | 80 – 60 | 7000 | 100 | 28 | 17.8 | 122 | 9 |

Subsequently, a total of 12 scenarios for M-LAES integration studies were defined, as summarised in Table 31: they represent the possible combinations of district size and LAES operating strategy. Different LAES plant power and capacity ratings were also identified for each scenario, to reflect different district sizes. More specifically, the plant capacity was determined to supply 25% of the surplus electricity when district load is above its mean value (this corresponds to approximately 10% of the daily electrical needs). Given plant roundtrip efficiency and the assumed 8 h of overnight charge at rated conditions [142], LAES power input was finally computed. Surplus electricity is ~1200 MWh for the large district, meaning 300 MWh of storage capacity and 80 MW power input, whereas sizing

for the small district resulted in 20 MWh capacity and 5 MW input. Hot and cold TES of the LAES were sized to store, respectively, the compression heat and evaporation cold generated during one full charge/discharge cycle. The input parameters for the LAES model, which characterise the investigated plant, are listed in Table 32; they resulted in 47% roundtrip efficiency.

Table 31: Summary of the explored scenarios for district integration of M-LAES.

| Scenario | District size | LAES input | LAES capacity | Scheduling | Prioritisation |
|---|---|---|---|---|---|
| 1 | Large | 80 MW | 300 MWh | Peaker | Electrical |
| 2 | Large | 80 MW | 300 MWh | Peaker | Thermal |
| 3 | Large | 80 MW | 300 MWh | Peaker | No |
| 4 | Large | 80 MW | 300 MWh | Load-following | Electrical |
| 5 | Large | 80 MW | 300 MWh | Load-following | Thermal |
| 6 | Large | 80 MW | 300 MWh | Load-following | No |
| 7 | Small | 5 MW | 20 MWh | Peaker | Electrical |
| 8 | Small | 5 MW | 20 MWh | Peaker | Thermal |
| 9 | Small | 5 MW | 20 MWh | Peaker | No |
| 10 | Small | 5 MW | 20 MWh | Load-following | Electrical |
| 11 | Small | 5 MW | 20 MWh | Load-following | Thermal |
| 12 | Small | 5 MW | 20 MWh | Load-following | No |

Table 32: Input parameters characterising the investigated LAES plant for the integration studies.

| Symbol | Parameter | Value |
|---|---|---|
| $T_0$ | Ambient temperature | 288.15 K |
| $p_0$ | Ambient pressure | 1.01 bar |
| $\eta_{S,T}$ | Turbine isentropic efficiency | 0.90 |
| $\eta_{S,C}$ | Compressor isentropic efficiency | 0.90 |
| $\eta_P$ | Cryopump efficiency | 0.75 |
| $\eta_T$ | Cryoturbine efficiency | 0.75 |
| $\varepsilon$ | Heat exchanger efficiency | 0.95 |
| $\Delta T$ | Pinch point temperature difference | 5 K |
| $\beta$ | Pressure loss coefficient | 0.01 |
| $p_{T,in}$ | Expansion train inlet pressure | 70 bar |
| $p_{C,out}$ | Compression train outlet pressure | 170 bar |
| $N_C$ | Number of compression stages | 4 |
| $N_T$ | Number of expansion stages | 4 |

## 6.3.4 Heuristic dispatch algorithm and performance indicators

Outcomes from the M-LAES numerical model presented in Section 6.3.1, together with the synthetic district loads and M-LAES operation scenario described above, were supplied as input to a heuristic dispatch algorithm, which ultimately enabled the assessment of M-LAES district integration. The algorithm is illustrated in Figure 69: for each day, hourly power, heating and cooling load profiles for the district were passed as input. Then, during charging, the LAES model was used to compute the

produced amount of liquid air, hot recycle and available cold recycle to liquefaction, based on the power input and the cooling level to be supplied. The hot and cold TES state of charge and the liquid air tank level were finally updated with a mass balance to the new conditions after 8 hours of charge. LAES discharge was evaluated based on district demand and plant operating strategy, which define LAES scheduling and setpoint (see Section 6.2.2). Given the number of discharging hours, the plant output level was constrained by the amount of liquid air and compression heat stored during the charging process. Then, liquid air and hot recycle consumption, together with cold recycle production were evaluated from the LAES model. Again, the hot and cold TES state of charge and the liquid air level in the vessel were updated with a mass balance.
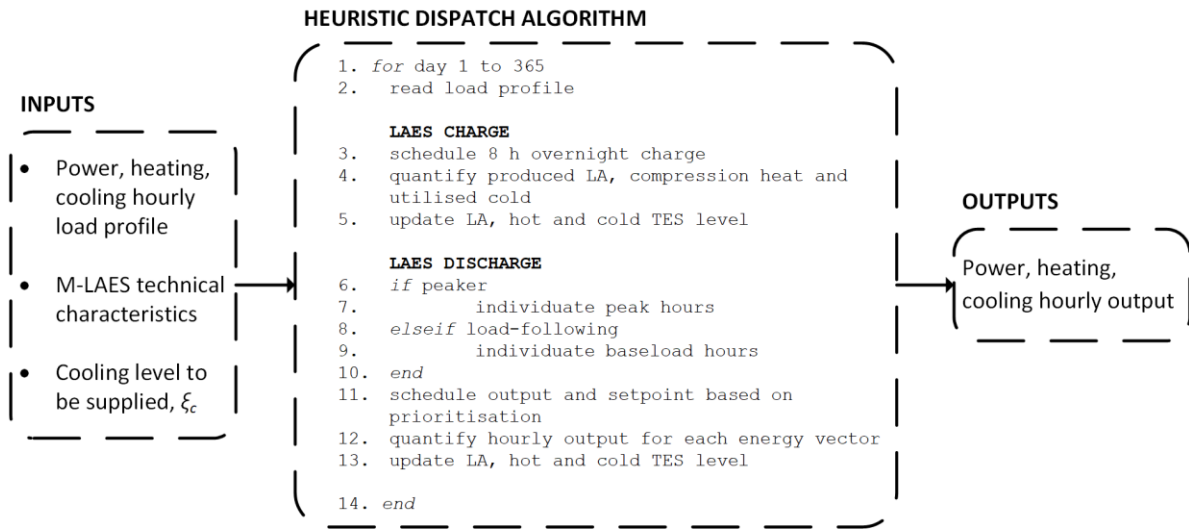


Figure 69: Structure of the heuristic dispatch algorithm used to assess LAES integration with multi-vector districts.

### Performance indicators

Three technical performance indicators were defined in the current study to gauge M-LAES integration by addressing each output vector individually technically. These are, respectively, electrical, heating and cooling conversion efficiency:

$$\eta_{el} = \frac{W_{el}}{W_{chr}} \cdot 100 \qquad\qquad 6.11$$

$$\eta_{h} = \frac{Q_{DHN}}{W_{chr}} \cdot 100 \qquad\qquad 6.12$$

$$\eta_{c} = \frac{Q_{DCN}}{W_{chr}} \cdot 100 \qquad\qquad 6.13$$

In the above formulae, $W_{el}$ represents plant electric output, while $Q_{DHN}$ and $Q_{DCN}$ the thermal energy delivered to DHN and DCN, respectively; the denominator is the net electricity drawn from the grid during charge. From the above values, a first law efficiency was also computed as the ratio between the total energy delivered and the energy input:

$$\eta_I = \frac{W_{el} + Q_{DHN} + Q_{DCN}}{W_{chr}} \cdot 100 = \eta_{el} + \eta_h + \eta_c \qquad 6.14$$

For economic assessment, two different cost-saving ($CS$) metrics were defined and used as indicators: they evaluate the yearly operational savings of supplying the district through M-LAES, compared to two benchmark cases where LAES provides only electricity output. In the first, ($CS_{purch}$), the district operator pays a fixed price for heating and cooling to the owner of the thermal generation assets, while in the second, ($CS_{gen}$), the generation infrastructure is owned by the district operator, who locally generates heating and cooling. In both cases, operational costs for M-LAES, $K_{M-LAES}$, include the electricity purchase solely from the grid to charge LAES. For the benchmark cases, extra costs are associated with the purchase, or local generation, of the heating and cooling amounts otherwise provided by M-LAES throughout the year. Cost-saving metrics, $CS_{purch}$ and $CS_{gen}$, were computed for each scenario, according to the definitions reported below:

$$CS_{purch} = \frac{K_{LAES+purch} - K_{M-LAES}}{K_{LAES+purch}}$$
$$= 1 - \frac{\pi_{buy}^{el} W_{chr}}{\pi_{buy}^{el} \dfrac{W_{dsc}}{\eta_{el,LAES}} + \pi_h Q_{DHN} + \pi_c Q_{DCN}} \qquad 6.15$$

$$CS_{gen} = \frac{K_{LAES+gen} - K_{M-LAES}}{K_{LAES+gen}}$$
$$= 1 - \frac{\pi_{buy}^{el} W_{chr}}{\pi_{buy}^{el} \left(\dfrac{W_{dsc}}{\eta_{el,LAES}} + \dfrac{Q_{DCN}}{EER}\right) + \pi_f \dfrac{Q_{DHN}}{\eta_B}} \qquad 6.16$$

$W_{chr}$ and $W_{dsc}$ represent the yearly electricity input and output, while $Q_{DHN}$ and $Q_{DCN}$ are the overall heating and cooling delivered from M-LAES to the district: all outputs from the dispatch algorithm. $\eta_{el,LAES}$ is the nominal electric efficiency for the plant operated as electricity storage only (i.e. LAES roundtrip efficiency).

In equation 6.15, $\pi_{buy}^{el}$, $\pi_h$ and $\pi_c$ stand for off-peak electricity price, heating and cooling price, respectively; their values were all retrieved from [307] and are gathered in Table 33, together with other input values used to compute $CS_{purch}$ and $CS_{gen}$. For the case of local production of hot and cold, cooling generation through an electric chiller with conversion efficiency $EER$ and heat provision by a gas boiler with efficiency $\eta_B$ at a fuel cost $\pi_F$ of 35 $/MWh, as indicated in [308], were assumed. No other cost contributions were considered at this stage (investment, balance of plant, additional components, etc.) as the analysis looks at operational savings only. Indeed, investment and maintenance costs are expected to be comparable for multi-energy use of LAES and the benchmark cases, if not higher for the latter.

| Symbol | Parameter | Value | Reference |
|---|---|---|---|
| $\eta_{el,LAES}$ | LAES roundtrip efficiency | 47% | Numerical model |
| $EER$ | Chiller conversion efficiency | 4 | [306] |
| $\eta_B$ | Gas boiler conversion efficiency | 90% | [309] |
| $\pi_{buy}^{el}$ | Off-peak electricity price | 40 $/MWh | [307] |
| $\pi_h$ | Heating price | 38 $/MWh | [307] |
| $\pi_c$ | Cooling price | 27 $/MWh | [307] |
| $\pi_f$ | Fuel price | 35 $/MWh | [308] |

# 6.4 Results

## 6.4.1 Independent and combined heating or cooling provision from liquid air energy storage

Results referring to the *independent* provision of heating or cooling from LAES, alongside electricity, are presented in Figure 70. These plots show the effect of the technical variations on the LAES process, introduced by the multi-energy output on specific work and thermal output. Different levels of external heating (subplot (a)) and cooling (subplot (b)) are measured by the split parameter $\xi$.

As expected, the thermal output of LAES varies with the split parameter $\xi$, i.e. the portion of available hot or cold recycle being sent directly from the TES to DHN or DCN, which then affects the charging and discharging process of the LAES plant. However, the effect is remarkably different for heating and cooling. Heating provision affects charge operation only. In Figure 70 (a), a higher thermal supply to the DHN progressively reduces the amount of heat recycled through the reheating stages, ultimately lowering turbine inlet temperatures. In turn, this causes a decrease in specific work output from LAES ($w_{dsc}$), while the specific amount of cold recycled in the liquefaction process ($q_{CR}$) remains constant. Conversely, cooling impacts both charge and discharge. In Figure 70 (b), both the specific liquefaction work ($w_{chr}$) and the heat recycled ($q_{HR}$) increase linearly for higher cooling output, as more air must now be compressed to ensure a given liquid production (liquid yield decreases).
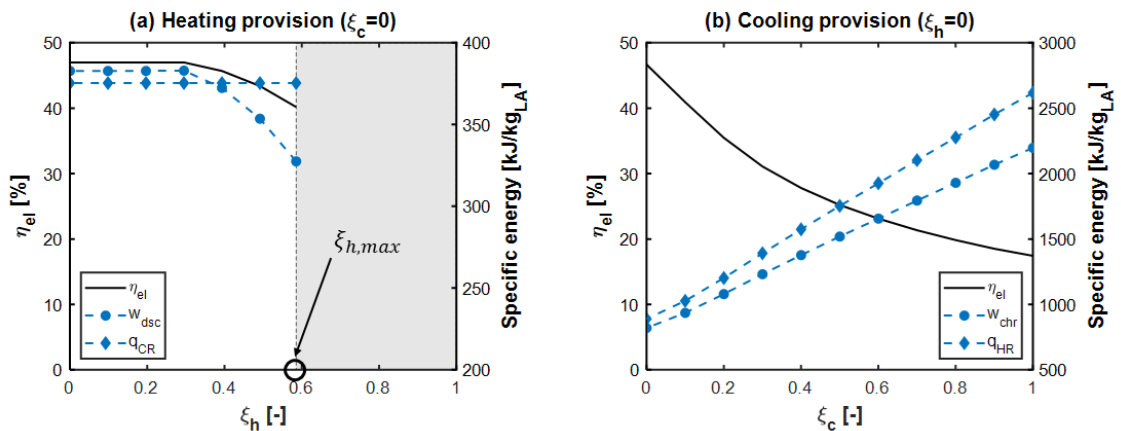


Figure 70: Individual effect of heating (a) and cooling (b) provision on LAES performance

Another key difference between heating and cooling provision relates to the associated variation of LAES electrical efficiency. LAES electrical efficiency is most sensitive to the level of cooling provision (a 0.1 increase in the $\xi$ parameter leads up to a 14% reduction of $\eta_{el}$), confirming the tight link between cold recycle and LAES efficiency also described in other works [101]. When heating is provided, no variation in electrical efficiency is registered initially. This is because two mechanisms result in some excess compression heat being stored during air liquefaction: i) process irreversibilities, in the form of thermal energy and ii) liquid yield, whereby larger amounts of air need to be compressed per unit air liquefied, thus generating more compression heat [126]. Only once such excess heat is fully consumed to supply the DHN, reheating temperatures begin to drop, and so does $\eta_{el}$. However, compared to cooling, a 0.1 increase in the $\xi_h$ parameter leads at most to a 7% reduction of $\eta_{el}$.

Finally, in the operation of LAES for delivery of heat and electricity, a maximum level of external heat provision, corresponding to the value $\xi_{h,max}$, may be imposed to keep outlet temperatures from the turbine train above ambient conditions, thus avoiding freezing at LAES outlet. This results in a technical limitation on the maximum external heat provision level, which is represented by the shaded area in Figure 70. On the contrary, no such technical bound exists for $\xi_c$ and up to 375 kJ/kg$_{LA}$ could be devoted to external cooling if required. In practice, restrictions may be imposed to ensure a target liquefaction performance (and thus electrical efficiency) is met. At $\xi_c = 1$ (i.e. full cold recycle delivery to DCN), the specific liquefaction work would be approximately 600 kWh per ton of liquid air: a figure consistent with "microgrid scale" plants [93], but nearly twice the value for large LAES systems or state-of-the-art liquefiers [18,310].

The same underlying effects illustrated in Section 6.4.1 drive the general case of *combined* provision of heating, cooling and electricity, as illustrated in Figure 71, for six different levels of multi-energy output. Changes in the level of heating provision affect electricity output and electrical efficiency, due to competition between the use of hot recycle for external DHN supply or internal air reheating. Instead, variations in the cooling provision affect both the electricity and heating output by modifying liquefaction performance and the compression heat available for LAES discharge. These results show that M-LAES can ensure cross-coupling between energy vectors by simply managing the energy produced during the process with no extra equipment (e.g. boilers and/or chillers). As an example, with 100 MWh of input electricity, LAES can supply 21.6 to 47 MWh of electricity, 8.8 to 50 MWh of heating and 8 to 12 MWh of cooling. However, $\eta_{el}$ decreases the more plant output is diversified over the vectors and the thermal efficiency (heating and cooling) increases. Therefore, economic benefits might make up for the reduced electrical efficiency, as discussed in Section 6.5.2.
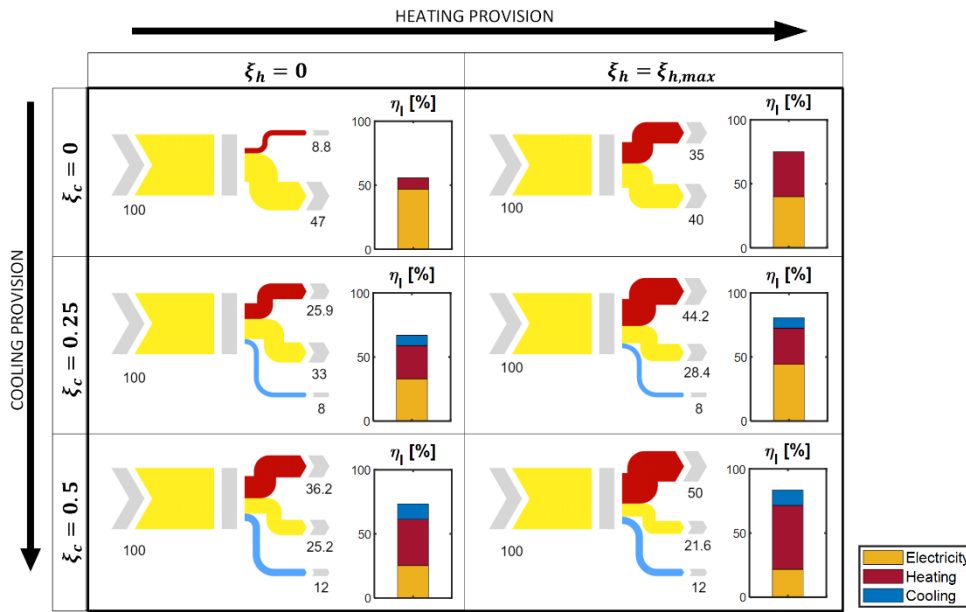
**Figure 71: Energy Sankey diagrams of a multi-energy LAES, for different levels of combined heating and cooling provision.**

## 6.4.2 M-LAES performance for district integration

Alongside technical considerations introduced by multi-energy LAES operation, additional operational constraints also need to be met when integrating LAES with district heating and cooling networks. These are, for example, the extent and variation in time of the demand for individual energy vectors and the supply temperatures of the DHN and DCN. The prediction of LAES technical performance under such an ensemble of constraints is the focus of this section.

To this end, Figure 72 illustrates the total energy output of LAES over a one-year operation, as well as the relative share of electricity, heating and cooling delivered to the district for the scenarios presented in Section 6.3.3, in the case $\xi_c = 0.25$. By comparing the first law efficiency values across Figure 71 and Figure 72, it can be appreciated how additional integration constraints result in significantly lower performance than predicted considering the technical feasibility alone. However, focussing exclusively on efficiency comparison does not allow to fully appreciate the system value of LAES during multi-energy operation. For example, in scenarios with heat prioritisation, LAES electrical efficiency $\eta_{el}$ drops below 10%, suggesting that for efficient plant operation heating should be considered a by-product of LAES operation instead of the main driver. Nonetheless, strategies that aim at maximising both electrical and heating output yield consistently the highest LAES efficiency. In scenario 3, for instance, $\eta_{el}$=33%, $\eta_h$=25% and $\eta_c$=4.7%. LAES first law efficiency in these cases is therefore well above 60% for the large district and 70% for the small district, indicating that M-LAES operation can outperform that of conventional LAES exclusively focused on electricity provision. M-LAES can ensure higher energy delivery and enhanced district support.
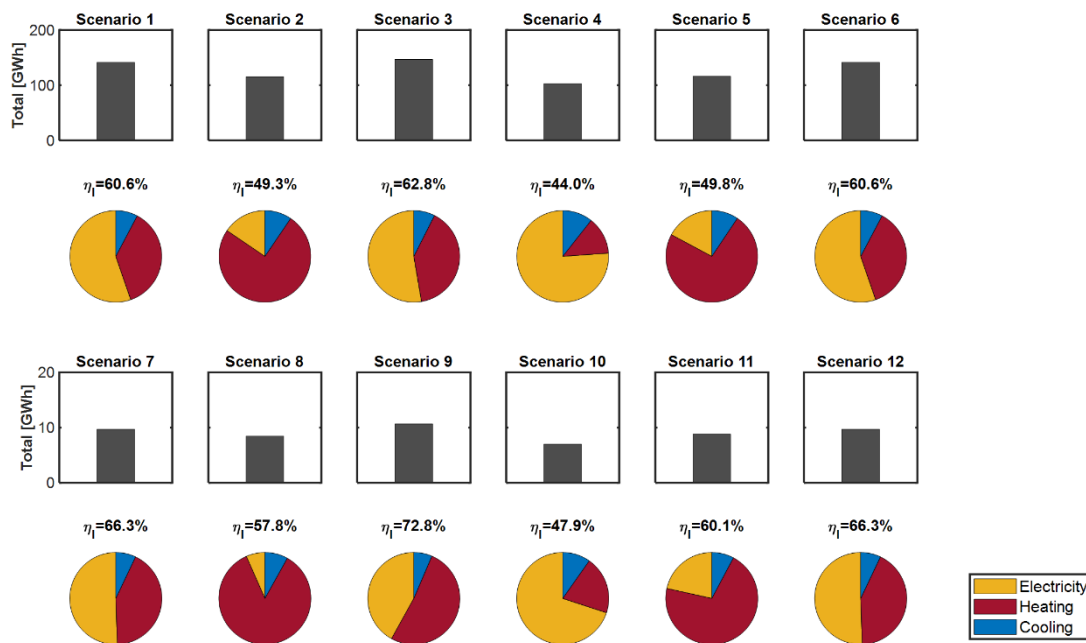
Figure 72: Total energy delivery and output energy share for LAES. Large district (top) and small district (bottom) integration.

The effect of district size on LAES performance can be observed by comparing efficiency values in Figure 72 by column. In our analysis, small residential districts are characterised by lower DHN return temperatures and higher demands for heating over electricity. In these cases, higher values of first law efficiency are achieved consistently across all scenarios, showing potential for M-LAES integration within new-generation, low-temperature DHN. Such a setting favours thermal efficiency and the diversification of plant output compared to electricity-only operation. Since lower network temperatures allow for a higher heating supply from LAES, first law efficiency increment is higher for scenarios prioritising heating or joint electricity and heating delivery.

## 6.5 Discussion

The results so far presented highlight the capability of LAES to supply a multi-energy output, with no requirement of additional components and by redirecting the hot and cold streams generated through the process. However, this comes with some associated technical constraints and additional limitations due to the integration setting considered. In this section, further generalisation of the above conclusions and the techno-economic value for a multi-energy LAES is sought.

### 6.5.1 Liquid air energy storage vector-coupling capability

Multi-energy capability maps were obtained from the developed model for LAES, as a visual representation of the space containing all the technically feasible combinations of cooling, heating and electricity output that can be sustained [239]. These are shown in Figure 73, normalised to the rated power output of the LAES plant considered. For a fixed level of cooling delivery $\xi_c$, LAES operating point must lie on the shaded area of the electricity-heating plane. Then plant output regulation can be achieved by: i) acting on the $\xi_h$ parameter to tune the relative share between heating and electricity; and ii) changing the air mass flow rate circulated through the system to adjust LAES absolute output,

at a constant share of energy vectors. Analogous regulation through $\xi_c$ and the air flow rate applies to cooling provision.

Figure 73, shows that changes in cooling provision have the effect of reshaping the capability maps. For increased cooling level, the range of feasible LAES operation narrows in terms of power delivery (less liquid air is produced for a given energy input), while it is enhanced for heating output as more compression heat is made available, for internal recycle or DHN provision. Consequently, the inflexion point B where turbine inlet temperature starts to drop occurs now at higher shares of heating supply. Capability maps for additional levels of $\gamma_C$ would be intermediate to those shown here.
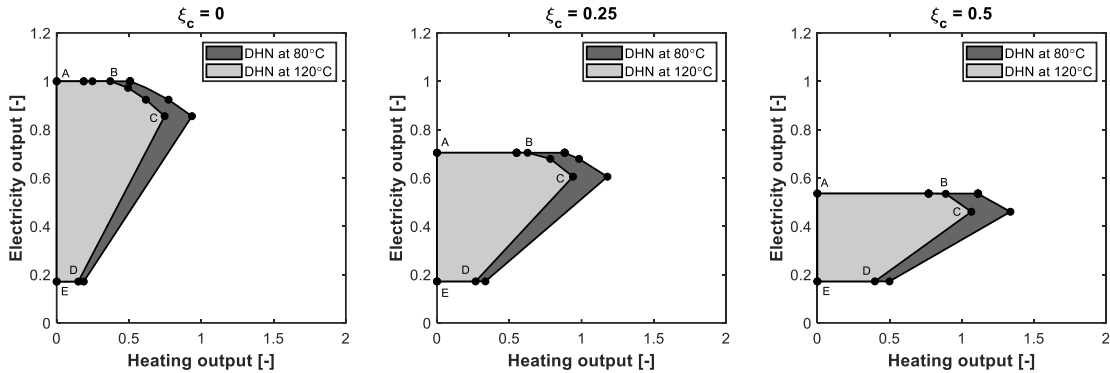


Figure 73: Capability maps for a multi-energy LAES plant, describing the technically feasible operating region.

The capability maps derived also capture the effect of DHN supply temperatures, which bound the minimum temperature at which heat from LAES can be used. DHN temperature variation is found not to affect LAES electricity output by any means. Conversely, as more heat can be externally supplied for lower DHN temperatures, the capability region enlarges, accounting for added operational flexibility and an increased energy efficiency of LAES.

*Generalised liquid air energy storage multi-energy operation*

Findings from Section 6.5.1 have shown the operating point for a given multi-energy LAES plant is univocally determined by three parameters: two ($\xi_h$ and $\xi_c$) characterising the thermal delivery and hence the hot and cold recycle, plus the liquid air mass flow rate ($\dot{m}_{LA}$). Therefore, if the analysis is carried out in specific terms (per unit flow of liquid air), two recycle variables, naturally associated with charge and discharge, become sufficient to uniquely describe LAES operation. This generalised way to synthesise the technical operation of M-LAES is presented in Figure 74, where the selected recycle variables are $c_{oil,dsc} = \left(\frac{\dot{C}_{oil}}{\dot{m}_{LA}}\right)_{dsc}$ and $c_{CR,chrg} = \left(\frac{\dot{C}_{CR}}{\dot{m}_{LA}}\right)_{chr}$. Through data fitting, analytical functions can be obtained, which generalise the multi-energy operating point for the considered LAES plant.

From Figure 74, LAES operating point, i.e. the power input and output, heating and cooling delivery, can be identified. On the bottom plots, the $c_{CR,chr}$ value on the x-axis can be fixed (considering the difference between the energy available in the cold TES minus the desired external cooling delivery), which allows reading the produced mass flow rate of liquid air produced and compression heat in the hot recycle, from subfigure (d) and (e), respectively, given external power input. Similarly, when discharging, the compression heat recycled in the reheating process can be computed based on hot TES availability and external supply to DHN. The $c_{oil,dsc}$ value is thus fixed on the top plots; LAES power

output and the cold recycle production per unit mass flow rate of liquid air are given by subfigure (a) and (b), respectively. Finally, given the supply temperatures for DHN and DCN, the specific thermal output can be evaluated from the two contributions of Equation 6.10:

$$q_{DHN} = \underbrace{\xi_h \dot{c}_{oil,chr}(T_{oil} - T_{DHN})}_{1} + \underbrace{(1 - \xi_h)\dot{c}_{oil,chr}(T_{oil,out} - T_{DHN})}_{2} \quad 6.17$$

$$q_{DCN} = \underbrace{\xi_c \dot{c}_{CR,dsc}(T_{DCN} - T_{CR})}_{1} + \underbrace{(1 - \xi_c)\dot{c}_{CR,dsc}(T_{DCN} - T_{CR,out})}_{2} \quad 6.18$$

The first contributions involve known values, while the second contributions – downstream reheating or the cold box – are to be obtained by subfigure (c) and (f), respectively, depending on the specific temperature of operation of the DHN and DCN.
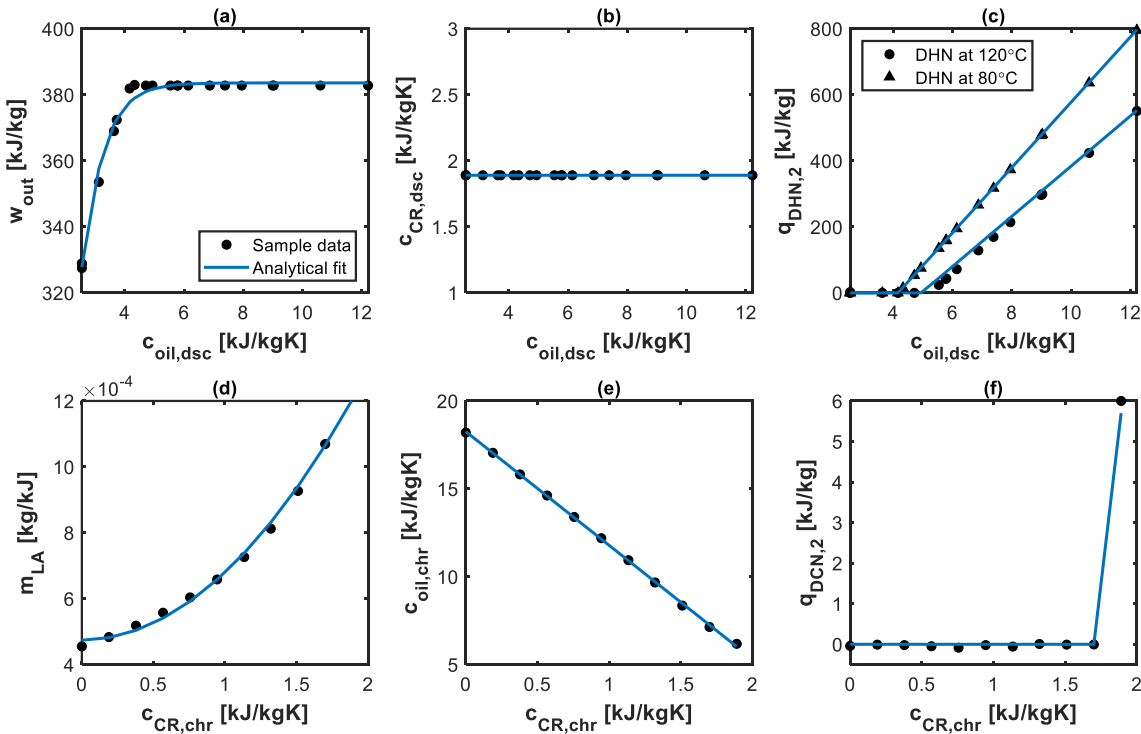


Figure 74: Synthetic representation of a trigenerative LAES plant operation through conversion functions.

Note the specific set of relations in Figure 74 applies to a given LAES design, but enables a compact description of plant operation; a similar generalisation approach for design purposes can be found in Tafone et al. [311]. Variable dependency is, in this case, nonlinear and energy output calculation requires knowledge of the liquid air mass flow rate, which is typically an outcome of operational studies/optimisations [236]. Nonetheless, this approach is directly applicable to heuristic dispatch algorithms such as the one presented in Section 6.3.4 and was used in the district integration assessment.

### 6.5.2   Benefits from multi-energy liquid air energy storage integration with districts

To visualise LAES impact on district system operation, Figure 75 shows the *residual* district load profile obtained for the midseason case and $\xi_c = 0.25$ by subtracting the results of LAES dispatch algorithm from the original district load. When the multi-energy capability is leveraged, the net demand profile over each vector is reshaped, and its final shape ultimately depends on the specific operating strategy and vector prioritisation chosen for LAES.

The top row of Figure 14 addresses LAES operation as a peaker; in these cases, heating, cooling and electricity peaks are effectively shaved. Notably, the morning peak in electricity demand reduced from 392 to 284 MW for electricity, while the peak in heating demand diminished from 274 to 193 MW. During peak times, LAES can supply 29% of district's electricity needs and, on top of this, up to 37% of the heating and 31% of the cooling requirements. This implies lower operating costs for the district. A reduced electricity demand must be imported from the grid and at lower associated ratings. Similarly, in the district heating and cooling, thermal peaks can now be provided at lower ratings, with less generation turnup or need for backup units. In existing networks, this may also allow decreasing the supply temperature.

For load-following operation (bottom row of Figure 75), LAES output is proportional to district demand to smooth load profiles. The change in residual load is less evident in this case, as longer supplied periods entail lower LAES output: for example, in scenario 4, LAES power level varies from 33 to 14 MW. However, this still results in a steadier electricity load and similar considerations apply to the heating and cooling loads. Less output flexibility is thus required for the generating assets, which would operate closer to design conditions for longer periods, boosting system efficiency.
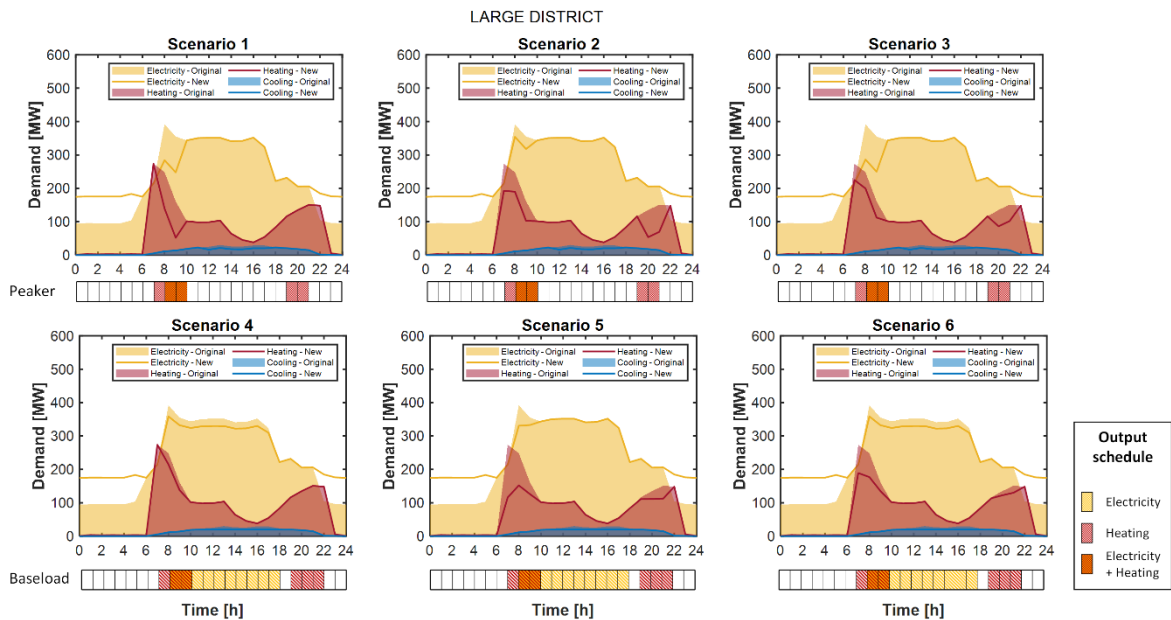


Figure 75: Daily residual load profiles and operating schedule for M-LAES in the large district - Midseason results. Top row: peaker operation; bottom row: load-following operation.

During plant operation, the parameter $\xi_h$ and the liquid air flow rate can be adjusted to prioritise LAES contribution to district electricity or heating demand fulfilment, or alternatively to maximise the joint

LAES energy delivery for both heating and electricity. This is for example the case of scenario 3, where up to 210 MWh of peak electricity and 243 MWh of peak heating are provided (and overall daily plant output increases to 504 MWh, as compared to 483 MWh in scenario 1 and 485 MWh in scenario 2).

## Economic benefits

Economic results comparing multi-energy output to the electricity storage-only operation of LAES are presented in Figure 76 and Figure 77, where red bars highlight positive values of the cost-saving metric. As detailed in Section 6.3.3, two benchmark cases were considered for this assessment; Figure 76 addresses the case of external purchase of heating and cooling at a fixed price, while Figure 77 the local generation of heating and cooling.
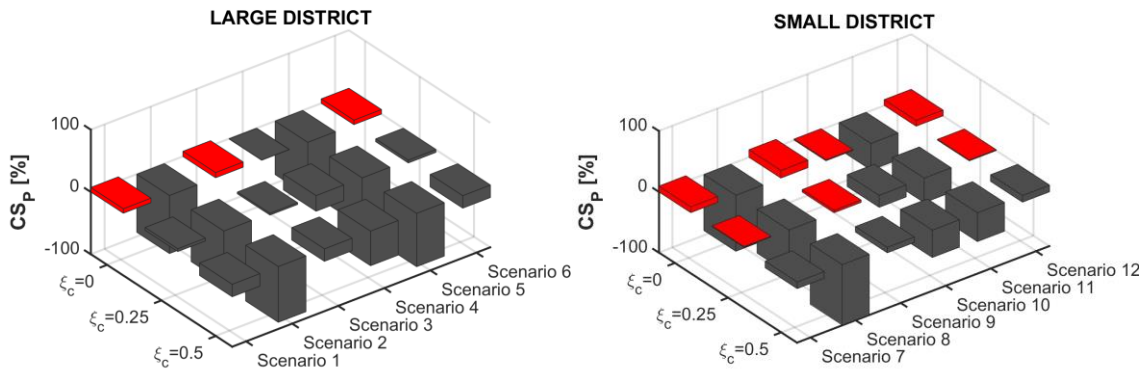


Figure 76: Cost-saving metric for the selected integration scenarios in the case of fixed-price heating and cooling purchase.

Overall, results demonstrate that multi-energy LAES operation can be economically viable in some of the scenarios considered. In these cases, the economic value from additional heating and cooling output offsets the reduction in electrical efficiency observed in Section 6.4. Should the extra thermal energy be externally purchased at a fixed price, up to 8.3% savings can be expected for the large district and up to 12.4% for the small one. For local heating and cooling production, cost-saving figures are up to 8.5% and 12.6%, respectively, still outlining M-LAES profitability.

Outcomes from the economic assessment also inform on the best M-LAES operating strategy. Across all the scenarios, the highest savings are obtained when maximising the joint plant output over heat and electricity, both for load-following and peak provision. This allows retaining high values of electrical efficiency ($\eta_{el} = 45\%$) and fully exploit the available compression heat for supplying the DHN. On the contrary, heating prioritisation is not economically viable since it excessively reduces LAES power output to favour an energy vector which presently has a lower associated economic value.

Economic results do not support high levels of cooling provision from LAES either, since a fast detriment in LAES electrical efficiency is observed (see Section 6.4.1). Only in the case of small districts, Figure 76 still shows positive cost-saving $CS$ for the condition $\xi_c = 0.25$, thanks to the enhanced heat delivery that higher cooling output and low DHN temperatures allow. In all the other cases, a constant cooling delivery throughout the year would generate losses for district operator, but cooling provision could still be profitable for limited periods when both cooling and heating are required and external delivery of the additional compression heat could make up for the low electric efficiency. The present

analysis suggests that, with only 4% increment in the cooling price, from 27 to 28.5 $/MWh, the fully trigenerative output becomes the most profitable operating strategy for times when heating, electricity and cooling are required.
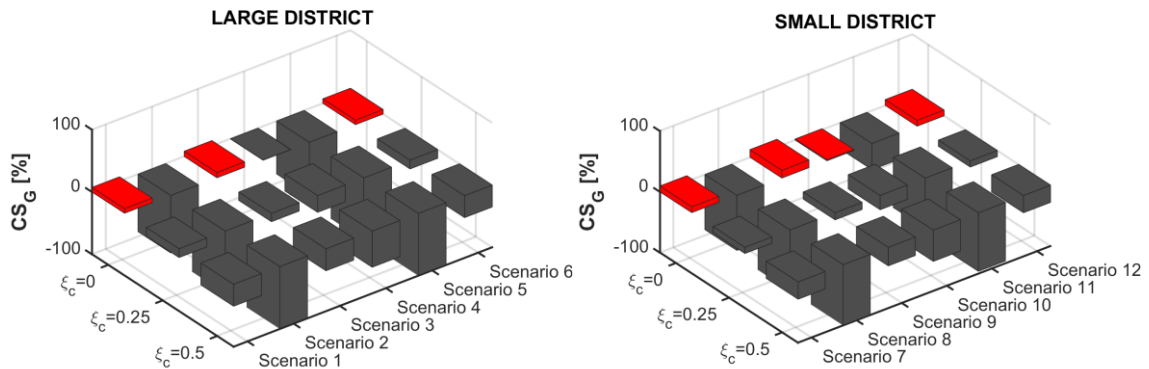


**Figure 77: Cost-saving metric for the selected integration scenarios, in the case of local generation of heating and cooling.**

Sensitivity analysis on the energy prices showed off-peak electricity tariff is the most influential parameter, with a 10% reduction yielding an increase from 12.4% to 14.6% in the $CS_P$ parameter and from 12.6% to 14.8% for $CS_G$. In this case, since M-LAES "trades" electricity output with multi-vector capability, the lower the cost of electricity, the higher the advantage of multi-energy operation. As the penetration of RES has the effect of lowering off-peak electricity prices [160], future cases for M-LAES can be envisioned. Also the gas price has a significant effect on the profitability of M-LAES operation: a 10% increase in gas price results in a higher $CS_G$ up to 14.6%, while the $CS_P$ indicator is not directly affected by variations in the gas price, under the considered assumption. Even disregarding exceptionally high gas prices due to current market distress [312], it is likely a carbon tax or other policy mechanism will drive upwards fossil fuel prices in the future. This analysis points to the value of multi-energy operation of LAES, as compared to electricity-storage-only, in those circumstances, particularly in locations with concurrent low electricity prices, e.g. coupled with large RES generation fields or inflexible baseload power plants. On the contrary, M-LAES viability is hardly affected by variations in the heating or cooling price: a 10% heating price reduction results in a $CS_P$ drop from 12.4% to 10.4% and the drop is from 3.8% to 3.5%, for $\gamma_C = 0.25$, when cooling price is varied.

Overall, Figure 76 and Figure 77 support the use of LAES as a multi-energy asset, compared to the electricity storage operation so far investigated. On top of the operational cost savings evaluated here, the combined production of electricity, heating and cooling from M-LAES requires very limited connection costs to DHN and DCN, no additional devices and reduces the need for extra generation onsite and associated investments. These considerations provide further rationale in support of multi-energy LAES adoption.

## 6.6 Conclusion and outlook

Following Chapter 4 and Chapter 5 focus on LAES potential within the power system, results from this chapter address an alternative and complementary strategy for LAES deployment. This involves looking at LAES as a multi-energy asset for the delivery of heating and cooling, alongside electricity and smart

district-scale energy management. A model that can capture LAES technical constraints from component to system level is presented and used to outline opportunities and limitations of the novel multi-energy operation strategy. The techno-economic value is quantified through a district integration study considering different synthetic load profiles and dispatch strategies for the plant operator. Crucially, the findings provide new understanding of the possibility of extending LAES value beyond the contribution to grid balancing capability, advancing the traditional electrical storage-only approach.

LAES can offer multi-energy flexibility with no requirement for additional components, but a set of *technical and operational constraints limit the extent to which combined power and thermal energy can be supplied*. Heat provision reduces electrical efficiency while cooling provision decreases electrical efficiency but increases heating output. As a consequence of such power and thermal output coupling, a feasible region of operation exists for multi-energy LAES, whose extent depends on the level of cooling to be provided.

Multi-energy LAES supports district operation by reducing peaks or supplying baseload demand over different energy vectors. In the cases explored, coverage of 5% and 10% of district electricity and thermal demand results in up to 12.6% operational cost savings. *Financial benefits mainly result from the joint output of electricity and heating*, while it is appropriate to consider cooling provision only for limited periods of simultaneous heating and cooling demand (e.g. midseason) or for high cooling prices. These results uncover a value in the additional flexibility arising from multi-energy LAES, which is proven to be important for the management of future energy districts; they demonstrate the combined electricity-heating provision as an alternative deployment pathway for LAES.

### 6.6.1  Chapter relevance within this thesis

Results in this chapter address the research objective O3, by studying the multi-energy operation of LAES. They shed light on the possibility of extending LAES value beyond the contribution to grid balancing, to supply heating, cooling and electric district loads for the orchestration of future multi-energy systems, thus extending its contribution to energy decarbonisation. The study complements the available analyses of purely electrical LAES operation and brings the following contributions to the existing body of literature:

- Technical assessment of a novel working paradigm for LAES with external delivery of compression heat and evaporation cold alongside electricity
- Multi-energy capability maps for LAES describing its feasible region of operation
- District integration assessment of M-LAES, considering different sizes, operating strategies and district hourly load profiles
- Techno-economic comparison to the traditional operation of LAES

The essential discussion of storage thermodynamic characteristics from Chapter 4 and Chapter 5 is extended in the present chapter to the multi-energy operation of LAES. Chapter 7 concludes this

research work by investigating the LDS application of LAES and other relevant TMES concepts, which is of great future relevance for highly decarbonised energy systems with large RES penetration.

# CHAPTER 7

## Thermo-mechanical energy storge concepts for long-duration storage applications

*After focussing on LAES and characterising its operation in the power and energy system in Chapter 4, Chapter 5 and Chapter 6, this final results chapter considers several TMES solutions and investigates their future potential for LDS applications. TMES performance is compared with the techno-economic requirements for LDS and the assessment of TMES is extended from the typical 10 h duration range, to 200 h duration. Technologies considered include traditional TMES (ACAES, LAES and PTES) and novel TMES concepts which store energy through, respectively, reversible oxidation, carbonation and hydration reactions. Thermodynamic storage models are presented and used to: i) quantify storage techno-economic performance at rated conditions; ii) observe the effect of component efficiency variation on system performance; and iii) study the evolution of techno-economic performance indicators with storage duration. Results for the selected concepts are cross-compared and benchmarked against targets for LDS and incumbent storage technologies. Outcomes show that, whereas traditional TMES – mostly ACAES and LAES – should be preferred for MDS, novel TMES based on oxidation and hydration reactions deliver the best economic performance for LDS. ACAES and novel TMES already fit the LDS cost target of 20 USD/kWh and become cost-competitive with the use of $H_2$ (at ~15 USD/kWh) under future technological developments. Through such comparative assessment, results from this chapter fulfil the thesis objective to assess selected TMES concepts for LDS applications. They demonstrate that, besides MDS applications, TMES also has significant potential to complement $H_2$ in helping balance the long-duration supply-demand mismatch of future low-carbon energy systems.*

## 7.1  Introduction

As introduced in Chapter 2, energy storage with discharge duration above 10 h becomes especially valuable in balancing supply and demand for RES shares above 50% in the energy mix. Chapter 4, Chapter 5 and Chapter 6 consider the daily operation of LAES, i.e. MDS application. However, identified investment costs of 100s £/kWh and the independent power/capacity sizing discussed in Chapter 5 highlight LAES duration could be cost-effectively extended to address the future needs of LDS. Besides LAES, other TMES options may be suitable too. To verify that and to highlight which technologies to adopt or further develop, TMES techno-economic performance should be evaluated for LDS applications and put into perspective with incumbent LDS options.

This final results chapter complements the analysis reported so far by: i) assessing the potential of TMES for LDS application; and ii) presenting a techno-economic performance comparison of established and novel TMES concepts. ACAES, LAES and Brayton PTES are considered among established TMES, while novel concepts comprise oxides energy storage (OES), carbonates energy storage (CES) and hydroxides energy storage (HES). Bottom-up thermodynamic models are developed for each concept to predict the key performance indicators and their variation with component performance and storage duration. Model outcomes are benchmarked against the target design space for LDS, thus achieving a twofold advancement. First, established and novel TMES concepts are cross-compared for MDS and LDS applications. Second, each technology is assessed by its current and future capability to provide LDS services at the target cost and performance, which instructs on the potential and development needs for the individual TMES concepts considered in the analysis.

The structure for this chapter is the following: analysis background and assumptions are listed in Section 7.2, while Section 7.3 describes the numerical model setup for the various TMES concepts. Study results are presented in Section 7.4, divided into MDS and LDS applications. Then, Section 7.5 discusses the effect of technological developments and storage duration on its techno-economic performance; results are compared with the target LDS design space. Finally, Section 7.6 outlines the conclusion and outlook.

## 7.2  Background and assumptions

### 7.2.1  Storage duration and duty cycles for medium- and long-duration storage

Duration represents in this work the time over which storage discharge at rated power output can be sustained, starting from fully charged conditions [313]. Hence, the difference between MDS and LDS applications is reflected by different storage durations, with MDS up to 10 h [314] and LDS above 12 h duration, to address multi-day and seasonal supply variability [168]. Similar to the approach pursued in Chapter 4, duty cycles were used to mimic storage operation, this time considering one full charge and discharge at rated power, and two idle periods of equal length between charge and discharge. As summarised in Table 34, daily cycles were considered for MDS applications, weekly cycles for LDS up to 50 h duration, and monthly cycles above. Idle periods length was determined from storage rated

power – 100 MW for all technologies, consistently with TMES intended size [143] – duration and cycling pattern, under an equal charge and discharge time.

Table 34: Medium- and long-duration storage and duty cycle features considered for this analysis.

| Cycling pattern | Storage duration [h] | Idle periods [h] | $\tau_{chr}:\tau_{dsc}$ |
|---|---|---|---|
| Daily | 8-10 | 2-4 | 1:1 |
| Weekly | 12-50 | 34-72 | 1:1 |
| Monthly | 52-200 | 160-308 | 1:1 |
| **Example of duty cycles** | | | |
| MDS (8 h capacity) | Charge: 8 h; Idle: 4 h; Discharge: 8 h; Idle: 4 h | | |
| LDS (200 h capacity) | Charge: 200 h; Idle 160 h; Discharge: 200 h; Idle: 160 h | | |

## 7.2.2 Investigated storage concepts and respective layout

Figure 78 shows the process flow diagram of the six TMES storage concepts investigated in this chapter; these include three established solutions – largely discussed in Chapter 2 – and three novel concepts. Among established TMES, a conventional 2-stage compression and expansion ACAES with sensible TES and air storage in a salt cavern was considered [248]. LAES layout consists of a 3-stage compression and expansion process, Claude-based liquefaction, sensible TES for hot and cold recycle and a low-pressure liquid air tank [126]. PTES operates a closed Brayton cycle using argon, with sensible hot and cold reservoirs and indirect heat transfer. The latter design choice was shown to only marginally affect PTES performance, whilst avoiding the need for pressurised hot and cold TES vessels [38]. Pressure vessels investment was though to excessively weight on PTES cost, especially at long-durations/large capacities, hence driving the decision of the investigated PTES layout. Packed bed TES was considered for all concepts due to its low cost, reliability, and thermal stability of the storage medium (gravel) across the temperature range covered [116].

The novel TMES concepts considered here were inspired by the chemical looping energy storage presented in Section 2.2.3, but use different chemical species and associated system components among those proposed for high-temperature thermochemical TES [75]. These are oxidation/reduction in OES, carbonation/calcination in CES and hydration/dehydration in HES. As illustrated in Figure 78, OES, CES and HES all consist of an open Brayton cycle for both the storage and the power generation phase, with air as working fluid; differences lie in the technological solutions for TES. OES uses $O_2$ from the air as gaseous reactant and a packed bed as both the direct heat transfer reactor and TES facility [70]. On the contrary, both CES and HES necessitate a different reactive gas than air, so indirect heat transfer and a fluidised bed layout inspired by industrial carbonation equipment [15] were considered for the chemical reactors. To store gaseous reactants, a 75 bar pressurised vessel was considered for supercritical $CO_2$ in CES [315], while $H_2O$ in the HES system can be stored in liquid form. Thermochemical materials considered are $Mn_2O_3/MnO$ for OES [71], the largely investigated $CaCO_3/CaO$ for CES [316] and $Ca(OH)_2/CaO$ for HES, as the company SaltX seem to have solved the kinetic and stability problems that were affecting it [14].

This work adopts one representative layout for each of the six TMES considered, among the many considered in the literature. Although by no means unique, the choice was driven the absence of one

established commercial layout for most of the TMES concepts investigated and the need to confine the scope of the analysis. Selected layouts for each TMES concept are presented in Figure 79.
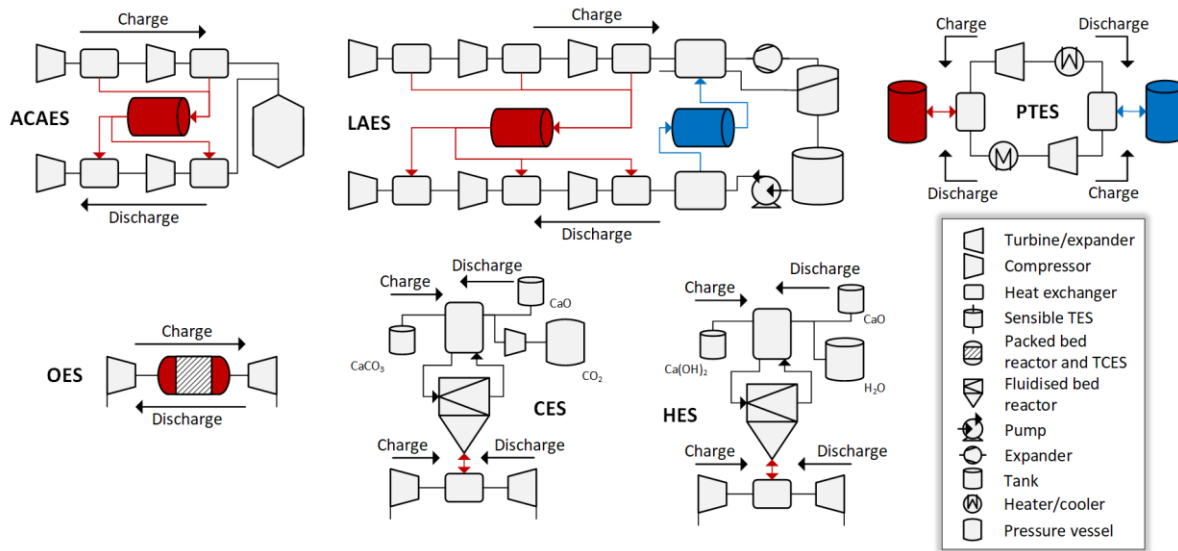


**Figure 78: Detailed system layout for the six TMES concepts considered and compared in this chapter. ACAES: adiabatic compressed air energy storage; LAES: liquid air energy storage; PTES: pumped thermal energy storage; OES: oxides energy storage; CES: carbonates energy storage; HES: Hydroxides energy storage.**

## 7.3 Numerical modelling of long-duration storage technologies and case studies

### 7.3.1 Modelling of the proposed storage technologies

Reduced thermodynamic models for each of the TMES concepts described in Section 7.2.2 were set up by explicitly modelling the devices involved in conversion processes between power and thermal energy and thermal energy storage. In such a bottom-up approach, model estimations are grounded on the key technical features of each system, which is suited for preliminary performance assessment and a quantitative cross-comparison in this analysis. A similar method was pursued elsewhere to compare different options for sorption energy storage [317]. Models were implemented in MATLAB, using the CoolProp library for fluid properties and the HSC chemistry database for chemical reactions.

*Conversion processes between power and thermal energy*

Three main components enable conversion between electricity and heat in the TMES concepts: compressors, expanders and heat exchangers. The model setup for each of the investigated TMES systems based on these components and thermal energy storage is exemplified in Figure 79. For compressors and expanders, the approach proposed in [272] was adopted, which can conveniently model both volumetric devices and turbomachinery, based on the definition of a thermal loss coefficient $\zeta_C$ for the compressors and gain $\zeta_T$ for turbines, together with device polytropic efficiency $\eta$. Hence, the specific work of the $i$-th compression stage, $w_{C,i}$, and the outlet temperature condition $T_{out,i}$ were computed as enthalpy difference, based on the stage inlet temperature $T_{in,i}$, the isentropic coefficient for the gas $\gamma$ and the compression ratio $\Pi_C$.

$$T_{out,i} = T_{in,i}\Pi_C^{\theta_C} \qquad\qquad 7.1$$

$$\theta_C = \frac{1}{\eta_C}\frac{\gamma-1}{\gamma}(1-\zeta_C) \qquad\qquad 7.2$$

$$w_{C,i} = \frac{h_{out,i}-h_{in,i}}{1-\zeta_C} \qquad\qquad 7.3$$

Similar analysis led to the evaluation of the specific work produced and the outlet temperature of the working fluid from each expansion stage:

$$T_{out,i} = T_{in,i}\Pi_T^{\theta_T} \qquad\qquad 7.4$$

$$\theta_T = -\eta_T\frac{\gamma-1}{\gamma}(1-\zeta_T) \qquad\qquad 7.5$$

$$w_{T,i} = \frac{h_{in,i}-h_{out,i}}{1-\zeta_T} \qquad\qquad 7.6$$

Heat exchangers and intercoolers/reheaters were all modelled based on device heat transfer effectiveness and the assumption of balanced flow between the hot and the cold fluid stream [318]. The thermal energy exchanged was computed as an enthalpy difference. Based on the system arrangement, $T_h$ or $T_c$ also represent the temperature of the streams exchanged with the TES.

$$\begin{pmatrix} T_{h,out} \\ T_{c,out} \end{pmatrix} = \begin{bmatrix} 1-\varepsilon & \varepsilon \\ \varepsilon & 1-\varepsilon \end{bmatrix}\begin{pmatrix} T_{h,in} \\ T_{c,in} \end{pmatrix} \qquad\qquad 7.7$$

$$q_{HX} = h_{h,in}-h_{h,out} = h_{c,out}-h_{c,in} \qquad\qquad 7.8$$

The suitable connection of compressors and heat exchanger or turbines and heat exchanger for each TMES system (see Figure 79) allows the forward and backward conversion between heat and electricity.
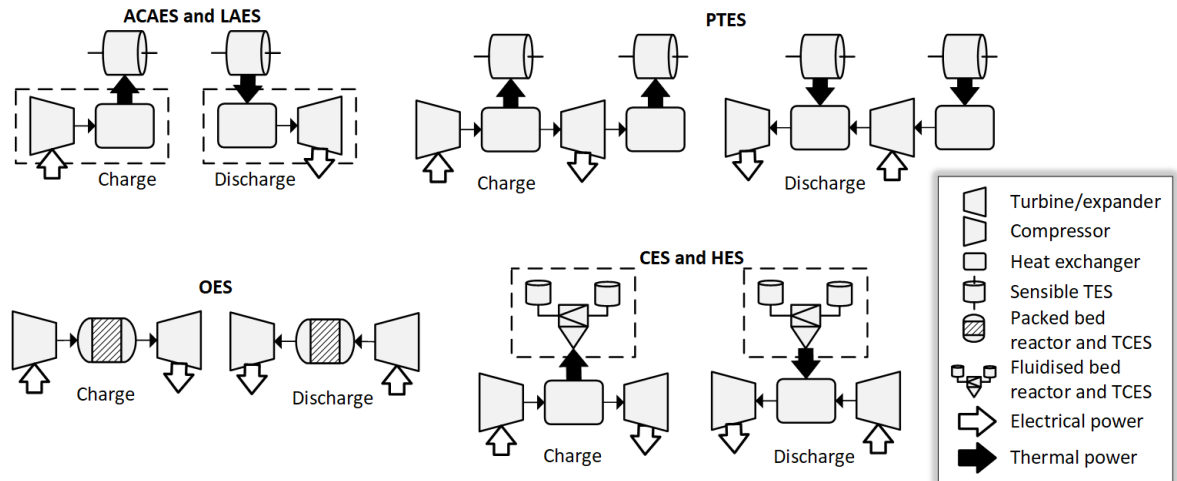


Figure 79: TMES model setup based on modelling conversion and thermal energy storage processes.

### 7.3.2 Thermal energy storage processes

Proper modelling of the thermal energy storage process was necessary for accurate estimation of plant performance, energy density and associated investment costs. In particular, the reversible chemical reactions involved in thermochemical energy storage are ruled by thermodynamic equilibrium so that, for any specified reactor pressure $p_r$, storage charging takes place if the working fluid temperature is bigger or equal to $T_{eq}$ and vice versa for discharging:

$$p_r = p_0 \exp\left(\frac{-\Delta H + T_{eq}\Delta S}{RT_{eq}}\right) \qquad 7.9$$

$\Delta H$ and $\Delta S$ represent the reaction enthalpy and entropy (per mole of reactant) associated with the specific reaction considered. Representative figures at high temperatures were computed following Hess law [319] and the tabulated values at standard conditions (as reported in Table 35), the stoichiometric coefficient $a_i$ for each compound (negative for reactants) and the $c_{p,i}$ of the chemical species involved, the latter being retrieved from the HSC database as polynomial regression:

$$\Delta H(T_r) = \Delta H_0 \pm \sum_i a_i \int_{T_0}^{T} c_{p,i}\, dT \qquad 7.10$$

$$\Delta S(T_r) = \Delta S_0 \pm \sum_i a_i \int_{T_0}^{T} c_{p,i}\, \frac{dT}{T} \qquad 7.11$$

Three different approaches were used to model the technological TES solutions considered (see Figure 79). These are sensible TES for ACAES, LAES and PTES, thermochemical TES with a packed bed open reactor for OES and thermochemical TES based on fluidised bed reactors for CES and HES, as described hereafter.

Table 35: Standard values of reaction enthalpy and entropy for the considered reactions for thermochemical energy storage.

| Chemical reaction | $\Delta H_0$ [kJ/kmol] | $\Delta S_0$ [kJ/kmolK] |
|---|---|---|
| $4MnO_2 \leftrightarrow 2Mn_2O_3 + O_2$ | 170347 | 213.691 |
| $CaCO_3 \leftrightarrow CaO + CO_2$ | 178000 | 160.16 |
| $Ca(OH)_2 \leftrightarrow CaO + H_2O$ | 109213 | 143.731 |

*Sensible thermal energy storage*

The TES volume was computed knowing the thermal energy to be stored ($\dot{Q}_{chr}\tau_{chr}$), the value and associated temperature of the thermal energy produced during the charging process, and the thermophysical properties of the storage medium, $\rho$ and $c_p$. An energy balance was defined and rearranged for the TES volume $V_{TES}$:

$$V_{TES} = \frac{\dot{Q}_{chr}\tau_{chr}}{\rho c_p (1 - \sigma)\Delta T_{TES}} \qquad 7.12$$

The outlet temperature of the working fluid could be computed according to Equation 7.7. In addition to the void fraction $\sigma$ in the packed bed, a heat loss coefficient $\Lambda$ was associated with the sensible TES, to represent the thermal losses as a percentage of the stored energy while in idle conditions [206], so that:

$$\frac{Q_{loss}}{\dot{Q}_{chr}\tau_{chr}} = 1 - exp(-\Lambda\tau_{idl}) \tag{7.13}$$

### *Thermochemical energy storage with packed bed reactor*

Despite eliminating the need for additional components such as heat exchangers and storage tanks, analysis of packed bed reactors with direct heat transfer reveals a dynamic behaviour whereby the thermal profile inside the reactor is pushed forward and backward by TES charging and discharging [320]. Under the sharp front assumption in [321], the outlet temperature will be first $T_{c,TES}$ and then $T_{eq,chr}$ during charging, $T_{h,TES}$ and then $T_{eq,chr}$ during discharging. The associated time of each outlet temperature condition was computed by an energy balance over the reactor. For instance, during storage charging:

$$\dot{m}_f c_{p,f}\left(T_{h,TES} - T_{c,TES}\right)\tau_1 \tag{7.14}$$
$$= V_{TES}(1 - \sigma)\left[\Delta H \frac{\rho}{MM} + \rho c_p\left(T_{eq,chr} - T_{c,TES}\right)\right]$$
$$\dot{m}_f c_{p,f}\left(T_{h,TES} - T_{eq,chr}\right)\tau_2 = V_{TES}(1 - \sigma)\left[\rho c_p\left(T_{h,TES} - T_{eq,chr}\right)\right] \tag{7.15}$$

The storage volume was estimated, in this case, including the chemical contribution to the storage capacity:

$$V_{TES} = \frac{\dot{Q}_{chr}\tau_{chr}}{\rho c_p(1 - \sigma)\left(T_{h,TES} - T_{c,TES}\right) + \Delta H \frac{\rho}{MM}(1 - \sigma)} \tag{7.16}$$

### *Thermochemical energy storage with fluidised bed reactor*

Fluidised bed reactors have been widely considered for carbonation/calcination [322] and hydration/dehydration [323] reactions of CaO. As heat recovery schemes have been proven beneficial for system overall performance [324], an ideal recuperation process between products leaving the reactor and incoming reactants was assumed here, meaning the equilibrium temperature can be maintained constant in the reactor. Hence, outlet temperature for the air stream was computed from Equation 7.7, while the total volume of TES, in this case, accounts only for the chemical contribution, plus the extra volume required to store the reactants (respectively, $CO_2$ at 75 bar, and water at ambient pressure):

$$V_{TES} = \frac{\dot{Q}_{chr}\tau_{chr}}{\Delta H \frac{\rho}{MM}(1 - \sigma)CF} + \frac{m_{CO_2/H_2O}}{\rho_{CO_2/H_2O}} \tag{7.17}$$

The mass of the reactant was computed from a mass balance, including the value of conversion factor ($CF$) (20% for Carbonation [325] and 80% for CaO Hydration [326]) and the excess gas ($EG$):

$$\dot{m}_{CO_2/H_2O} = (1 + EG)\frac{\dot{Q}_{chr}MM}{CF\Delta H}\left(\frac{MM_{CO_2/H_2O}}{MM}\right)\left(\frac{\nu_{CO_2/H_2O}}{\nu}\right) \qquad 7.18$$

The specific parameters for TMES model setup are gathered in Table 36.

Table 36: Characteristic parameters for the TMES technologies investigated.

| Characteristic parameter | Rated value |
|---|---|
| Heat exchanger efficiency | 0.92 |
| Machinery thermal losses/gains | 0.00 |
| Machinery polytropic efficiency | 0.85 |
| Specific cold recycle of LAES | 350 kJ/kg |
| Liquid yield of LAES | 0.8 |
| Void fraction in solid beds | 0.38 |
| Sensible TES loss coefficient | 0.00083 1/h |
| CaO conversion factor carbonation | 20% |
| CaO conversion factor hydration | 80% |
| Excess gas carbonation | 42.75% |
| Excess gas hydration | 10% |
| Pressure $CO_2$ storage | 75 bar |

### 7.3.3 Estimation of plant investment costs

Plant investment cost was evaluated from the cost functions for individual devices, namely compressors, heat exchangers, turbines, reactors, storage tanks, vessels and the air cavern, as well costs of the TES storage media. Functions from the literature and material price from sellers were used for this purpose, as reported in Table 37; they were chosen as already applied in the literature to the study of specific TMES systems, and particularly LAES. On top of these mentioned costs, an additional 33% on power-related costs was considered for LAES (based on [327]), covering mainly air liquefaction equipment, cryopumps and evaporator. For the other technologies, a 10% surplus was added for auxiliaries. Cost figures were finally adjusted from 2017 k€ values in Table 37 to 2020 £, using the CEPCI index and a currency conversion factor.

Table 37: Cost functions used to evaluate long-duration storage investment cost. All values are in 2017 k€.

| Component | Cost function | Variable $X$ | Notes | Ref |
|---|---|---|---|---|
| Compressors | $2035\left(\frac{X}{10}\right)^{0.6}$ | Power input, MW | Carbon steel | [327] |
| Turbines | $1002 \cdot 3\left(\frac{X}{10}\right)^{0.67}$ | Power output, MW | Carbon steel | [327] |
| Intercoolers and reheaters | $(1.3 + 1.88)65\frac{X}{1000}$ | Heat transfer area, m$^2$ | Carbon steel, $U$=500 W/m$^2$K | [327] |
| TCES fluidised bed reactors, charge | $193X^{0.65}$ | Thermal input, MW | Calciner | [316] |

| | | | | |
|---|---|---|---|---|
| TCES fluidised bed reactors, discharge | $3830 + 217X^{0.65}$ | Thermal output, MW | Carbonator | [316] |
| Air cavern | $\left(\dfrac{7.5}{1.15}\right)X$ | Capacity, MWh | Salt cavern | [328] |
| Liquid air tanks | $2760\left(\dfrac{X}{1200}\right)^{0.6}$ | Liquid mass, ton | Atmospheric pressure | [97] |
| Thermal storage tanks | $563 + 0.22X$ | Tank volume, m$^3$ | Large field tank | [327] |
| Pressure vessels | $\left(\dfrac{1.24}{1000}\right)$ $\cdot 10^{[3.49+0.44 Log(x)+0.11(Log(x))^2]}$ | Vessel volume, m$^3$ | Vertical | [329] |
| Gravel | $80\left(\dfrac{X}{1000}\right)$ | Mass, ton | Material cost | [330] |
| MnO$_2$ | $534\left(\dfrac{X}{1000}\right)$ | Mass, ton | Material cost | [331] |
| CaO | $27.5\left(\dfrac{X}{1000}\right)$ | Mass, ton | Material cost | [332] |

### 7.3.4 Considered studies and performance indicators

Two reference durations were used to represent MDS and LDS applications. These are 8 h for MDS [45] and 200 h for LDS, given 100+ h is used as a reference in [176]. Techno-economic comparison of the investigated TMES concepts for MDS and LDS is presented in Section 7.4. There, a sensitivity analysis of device characteristic parameters by varying machines' polytropic efficiency between 0.8 and 0.9 and heat exchanger effectiveness between 0.87 and 0.97 informs on the effect of future technological improvements.

Then, duration values spanning between 2 and 200 h and according to the duty cycles in Table 34 were considered to explore the impact of storage duration on TMES techno-economics; results are reported in Section 7.5.17.5. Finally, the LDS case study with 200 h duration was used to compare TMES economic figures with target values identified by system-scale analyses for prospective LDS technologies.

### *Performance indicators*

Selected performance indicators used in this study are summarised in Table 38. Besides conventional metrics such as electric roundtrip efficiency (the ratio between the electricity output and input, over a complete storage charge/discharge cycle) or specific work, the energy density, $ED$, informs on the TMES compactness. Both the thermal and the TES share, respectively $\chi_{th}$ and $\chi_{TES}$ provides useful technical insights into the proportion of TES volume required and the potential for external provision of heat. Finally, power and capacity-specific costs are useful to gauge plant economics and, crucially, are used as a benchmark against the indicated target for LDS applications.

Table 38: Description of selected performance indicators used to evaluate and cross-compare different storage concepts.

| Key performance indicator | Description | Expression |
|---|---|---|
| Roundtrip efficiency, $\eta_{RT}$ [%] | Ratio between electricity output and input, over a complete charge/discharge cycle | $\eta_{RT} = \dfrac{\dot{W}_{out}\tau_{dsc}}{\dot{W}_{in}\tau_{chr}}$ |

| Energy density, $ED$ [kWh/m³] | Ratio between electricity storage capacity and total storage volume | $ED = \dfrac{\dot{W}_{out}\tau_{dsc}}{V_{tot}}$ |
|---|---|---|
| Specific work input, $w_{in}$ [kJ/kg] | Electric output per unit working fluid | N. A. |
| Specific work output, $w_{out}$ [kJ/kg] | Electric input per unit working fluid | N. A. |
| Thermal share, $\chi_{th}$ [%] | Ratio between thermal energy stored and electricity storage capacity | $\chi_{th} = \dfrac{\dot{Q}_{tot}\tau_{chr}}{\dot{W}_{out}\tau_{dsc}}$ |
| TES share, $\chi_{TES}$ [%] | Ratio between TES and total storage volume | $\chi_{th} = \dfrac{V_{TES}}{V_{tot}}$ |
| Power-specific cost, $PC$ [£/kW] | CAPEX per unit storage power output | $PC = \dfrac{CAPEX}{\dot{W}_{out}}$ |
| Energy-specific cost, $EC$ [£/kWh] | CAPEX per unit storage capacity | $EC = \dfrac{CAPEX}{\dot{W}_{out}\tau_{dsc}}$ |

## 7.4    Results

### 7.4.1    Pressure optimisation for novel TMES options

The extensive literature on ACAES, LAES and PTES demonstrates consensus on the range and best values for the main operating parameters in traditional TMES (e.g. cycle pressures and temperatures) [333]. Contrarily, these aspects are only marginally explored for OES and to date fully unaddressed for the proposed CES and HES layout. Therefore, a preliminary optimisation of cycle charge and discharge pressure was carried out for the thermochemical TMES, to maximise roundtrip efficiency and illustrate the features of each concept. Pressure design maps are shown in Figure 80, visualising roundtrip efficiency variations with charge and discharge pressure; optimisation results are reported in Table 39.

Table 39: Optimal charge and discharge pressures for maximum roundtrip efficiency of selected TMES options.

| TMES concept | Pressure range | Optimal charge pressure | Optimal discharge pressure | Optimal roundtrip efficiency |
|---|---|---|---|---|
| OES | 5-200 bar | 200 bar | 10.2 bar | 21% |
| CES | 5-200 bar | 200 bar | 11.7 bar | 22% |
| HES | 5-200 bar | 57.4 bar | 5 bar | 12% |

Each concept displays a clear maximum in the roundtrip efficiency, meaning cycle pressures are relevant parameters to optimise for the effective operation of OES, CES and HES. For OES, higher charge pressure are shown to increase plant performance as result in higher temperatures in the TES and increased work output (a similar effect was observed by Saghafifar [70]). The optimum discharge pressure depends on the selected value during charging. However, this is not the case for CES (and, analogously, HES), since chemical equilibrium constrains the inlet temperature conditions before expansion so that the optimal discharge pressure only depends on the equilibrium temperature for the specific material and thermochemical reaction chosen for TES. The higher value 11.7 bar for CES reflects a higher equilibrium temperature of 900-1000 °C, as compared to 4 bar and 500-550 °C for HES. The optimal charge pressure for CES and HES also depends on the storage material selected, for the same reason.
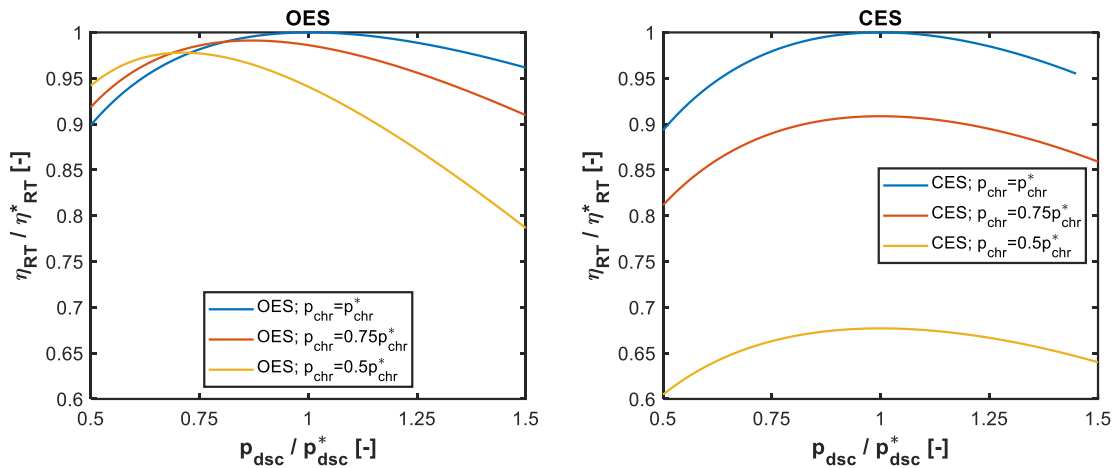
**Figure 80: Pressure design maps for OES and CES.**

A common constraint across novel TMES relates to the outlet temperature from the compressor, which must be above the equilibrium temperature to allow charging. However, the associated pressure limit is far from the optima in all cases, thus not limiting the design space. On the contrary, high optimal values computed for cycle pressures require multi-stage compression and expansion and call for advancements of compression technology to handle very high outlet temperatures in novel TMES [71].

### 7.4.2 Techno-economic concept comparison for medium-duration storage

With the optimised pressure values from Table 39, the technical performance of novel and traditional TMES is compared in Figure 81, while specific cost metrics are reported in Figure 82, for 8 h duration. In both figures, error bars include the performance variations observed through sensitivity analysis. ACAES and LAES roundtrip efficiency align with values from the literature, while the predicted 28% value for PTES is due to the rather low machine efficiency considered in the present study (0.85) as compared to most of the literature [45]. Also the design choice with indirect heat transfer in the hot and cold TES clearly penalises PTES technical performance. However, assuming 0.95 polytropic efficiency PTES roundtrip efficiency would increase to 54%, with such large variation reflected by the errorbars. For MDS applications, none of OES, CES or HES can reach roundtrip efficiency values above 50% of traditional TMES. Novel TMES only reach up to 29%, in the case of OES and CES and 21% with HES, under high device performance. This is due to the significant pressure difference between charge and discharge required for reactants to be, respectively, above and below the equilibrium temperature, which results in large process irreversibility as a consequence.

**Figure 81: Roundtrip efficiency and energy density values for the TMES technologies investigated at 8 h duration. Errorbars have been obtained by changing the machine polytropic efficiency and heat exchanger effectiveness between 0.8 and 0.9 and 0.87 and 0.97, respectively.**

On the contrary, novel TMES outperform traditional options in energy density by up to 2 orders of magnitude, thanks to compact thermochemical TES, notwithstanding the low roundtrip efficiency. OES and HES, respectively, reach 214 and 41 $kWh/m^3$, whereas LAES and PTES only achieve 24 and 19 $kWh/m^3$, and ACAES 6 $kWh/m^3$. In CES, compactness is hindered by the only 20% conversion efficiency of CaO in the carbonator [325] and the additional pressure vessel necessary to store gas reactants. The supercritical $CO_2$ tank accounts for 57% of the overall storage volume (~43500 $m^3$), resulting in only 18 $kWh/m^3$ for CES, which is comparable with traditional TMES. Note the inclusion of reactors in the volume requirement would further decrease the energy density of both CES and HES, whereas OES integrates reactor and storage in a single device and does not suffer from this drawback. Energy density variations with machine efficiency are smaller for sensible TES, since temperature levels in TES are lower for more efficient components.

Regarding economic results, the cost associated with power equipment (mainly turbines and compressors) represents by far the biggest contribution (between 50% and 83%) to the investment cost for MDS, in line with [139]. This penalises PTES and novel TMES relying on Brayton heat pump/power cycles, where the overall power input/output during charge/discharge results from the difference between compression and expansion work. Significantly bigger component sizes are therefore required, which escalates costs. As an example, for a 100 MW output, the PTES plant investigated requires a 262 MW compression train and 362 MW expansion train, whereas ACAES and LAES simply involve a 100 MW expansion train. In these regards, the proposed reversible operation of compression/expansion devices between charge and discharge [38] would reduce the number of components, with the potential to lower price from 1157 to 852 £/kW and from 145 to 106 £/kWh for the investigated PTES. However, satisfactory efficiency values still have to be demonstrated at these scales [334].
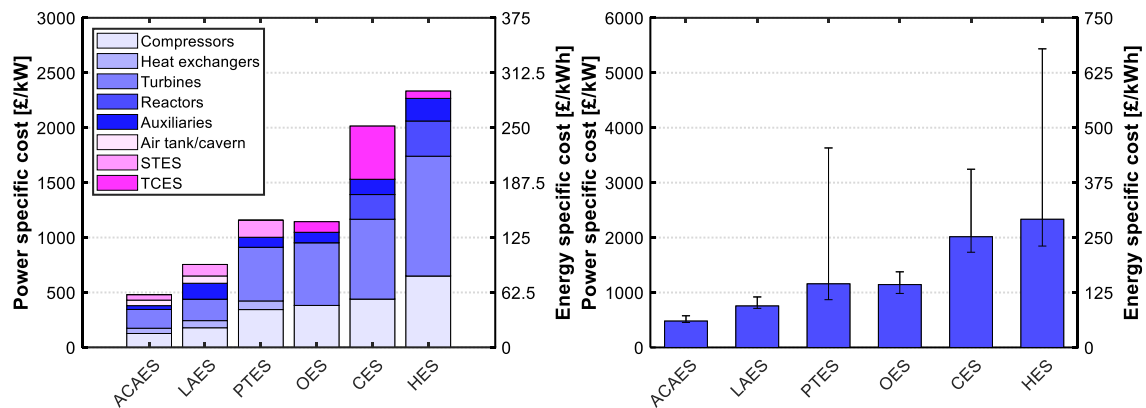
**Figure 82: Power and energy-specific cost values (left) and their variation with device characteristic parameters (right) for the TMES technologies investigated at 8 h duration.**

It is interesting to observe that, out of the thermochemical solutions, OES is competitive with PTES. Benefits come from the absence of heat exchangers and the use of a single, compact TES (of volume ~3700 m$^3$) rather than two packed beds (cumulatively ~42500 m$^3$). Higher specific costs per unit volume for the pressurised vessel are more than offset by its compactness. The conclusion would change for increased device performance. At 0.90 polytropic efficiency for the machines and 0.97 heat exchanger effectiveness, the higher roundtrip efficiency of PTES results in overall costs of 871 £/kW and 108.8 £/kWh, whereas OES is less sensitive to device performance and only reaches 983 £/kW and 123 £/kWh.

Cost estimated for CES and HES show these solutions are significantly more expensive than other TMES, for MDS. One reason is the presence of fluidised bed reactors accounting for 11% and 14% of the overall investment. Additionally, HES is operated at lower temperature levels (in the range 500-550 °C) and suffers from lower values of roundtrip efficiency, resulting in larger sizes for the power components. On the contrary, 25% of CES cost is associated with storage capacity. Absolute values are ~75 USD/kWh, i.e. above the ~54 $/kWh indicated by Ortiz for calcium-looping TES [316], and mainly due to the large pressure vessel required for supercritical $CO_2$. So, besides energy density, also costs are negatively impacted by storing gas reactants for carbonation. CES and HES, alongside PTES, are very sensitive to component performance improvements. However, even under machines and heat exchangers advancements, their power and capacity-specific costs would still be 1733 £/kW and 214 £/kWh for CES, and 1846 £/kW and 230 £/kWh for HES: about twice as much as other TMES.

### 7.4.3   Techno-economic concept comparison for long-duration storage

Results obtained for 200 h duration (LDS application) are discussed in this section, with values for the technical performance indicators visualised in Figure 83 and the economic metrics displayed in Figure 84. Due to standing losses in the TES, roundtrip efficiency predictions are lower than the MDS case for ACAES, LAES and PTES. Values drop to 68%, 33% and 24%, respectively. Hence, the performance gap with novel TMES solutions based on loss-free, thermochemical TES process, is reduced for at longer duration. Studies showed roundtrip efficiency is not of primary importance at the first stages of storage deployment, i.e. when large amounts of otherwise wasted energy are available [175]. However, it certainly affects the competition with alternative storage technologies and flexibility sources.

Therefore, this analysis proves it is vital to include representative values of standing losses in TMES assessment for LDS. Overall, only ACAES can operate for LDS with an efficiency above 60%, while other TMES sit in the range 25-35%. Energy density consequently decreases for traditional TMES to between 5 and 18 kWh/m³, while it does not change for OES, CES and HES.
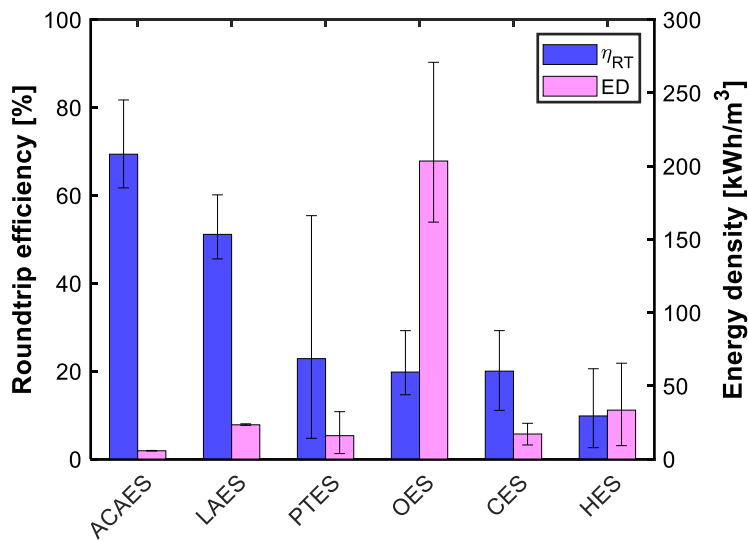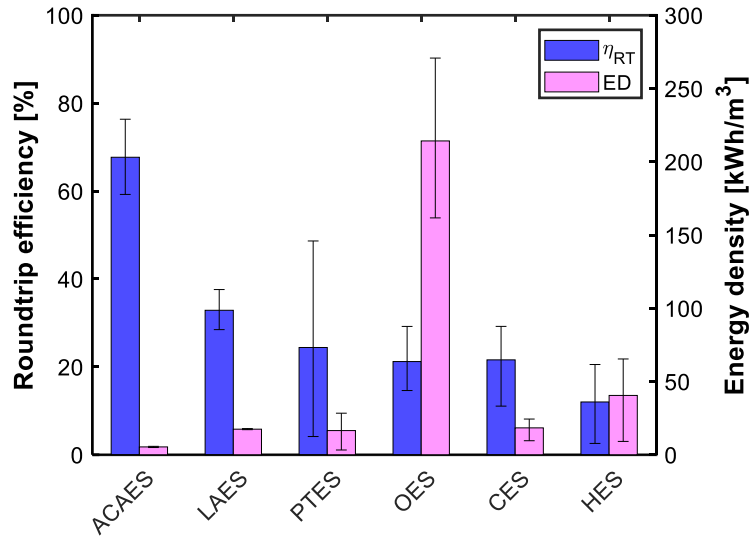


Figure 83: Roundtrip efficiency and energy density values for the TMES technologies investigated at 200 h duration. Errorbars have been obtained by changing the machine polytropic efficiency and heat exchanger effectiveness between 0.8 and 0.9 and 0.87 and 0.97, respectively.

Economic figures significantly change between LDS and MDS applications, with a major switch in the cost contribution of power and capacity equipment. Turbines and compressors now represent 8-17% of the total investment cost for most TMES, while 80-90% is associated with capacity equipment (i.e. vessels and TES) – the only exception is CES, where large volumes for the $CO_2$ pressure vessel result in prohibitively high specific costs. Such variations contribute to making PTES and other TMES concepts based on Brayton cycles more competitive at LDS.
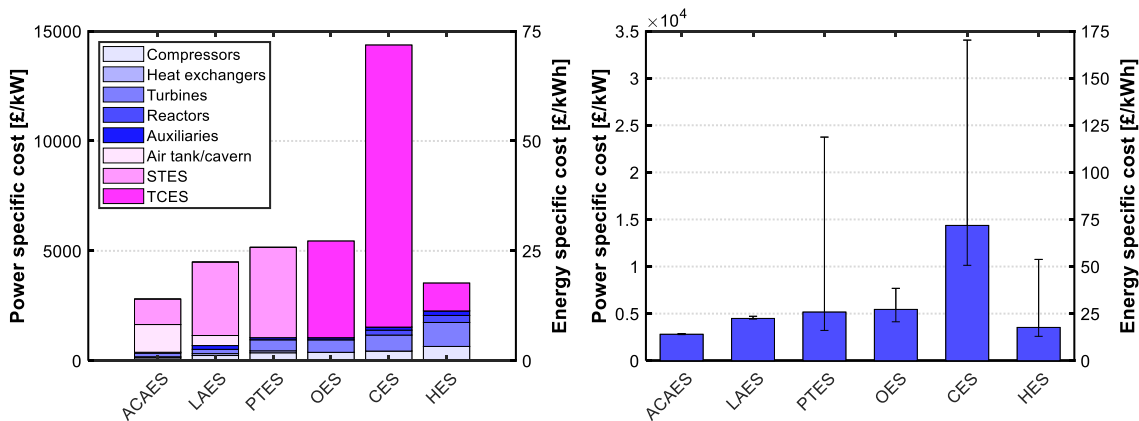


Figure 84: Power and energy-specific cost values (left) and their variation with device characteristic parameters (right) for the TMES technologies investigated at 200 h duration.

Among the novel TMES solutions based on thermochemical TES, the use of CaO hydration/dehydration seems very well suited for LDS. TES compactness, cheap storage medium and liquid $H_2O$ storage at ambient conditions concur in HES achieving the lowest investment with respect to OES and CES. Future device improvement would result in up to 20% roundtrip efficiency and further cut costs to 3235

USD/kW and 16 USD/kWh, which is less than the estimates for ACAES. The use of oxidation/reduction reactions in OES, although reaching higher values of roundtrip efficiency, appears more expensive than CES and, for LDS, also than PTES. However, this is associated with using a pressurised vessel for TES in the direct heat transfer reactor investigated. The very high storage density of OES results in a storage volume of only ~94000 $m^3$. For reference, HES requires an overall ~494000 $m^3$. A different system layout could be though for OES, with indirect heat transfer in the reactor to avoid pressurisation. The estimation of storage costs in this case (which neglects the marginal cost contribution from the additional heat exchanger at long durations and the lower effectiveness of indirect heat transfer) is 142.5 k£, i.e. only 32% of the required investment for a pressurised vessel. This more than halves the investment costs, to 2473 £/kW and 12 £/kWh for the indirect OES: the lowest values in this study.

## 7.5    Discussion

Techno-economic results agree with the literature in presenting ACAES and LAES as currently the most economically viable options for MDS, with PTES becoming competitive through advancement in component performance. Among the TCES options, only OES can reach power costs close to 1000 £/kW and capacity-specific cost ~150 £/kWh, with roundtrip efficiency not above 30% but very high energy density. Different is the picture at LDS, where HES becomes the second cheapest storage solution and significantly better than PTES and LAES, with ~13 £/kWh energy cost. These results demonstrate significant changes in the relative performance and cost ranking between alternative TMES concepts, depending on the target storage duration. The following sections explore the sources of those changes and give an outlook on TMES application at LDS.

### 7.5.1    Effect of capacity on storage techno-economic metrics

Technical performance indicators for 8, 50 and 200 h storage duration are visualised in Figure 85, while Figure 86 shows the power and capacity cost evolution with different durations up to 200 h. As noted in Section 7.4.3, the technical performance variations between MDS and LDS in Figure 85 should be attributed to standing losses during prolonged idle periods. ACAES efficiency drops from 71.3 to 67.7%, while values for PTES decrease more in relative terms, from 27.9 to 24.4%, because more heat is stored (and thus subject to losses) per unit power output, as measured by $\chi_{th}$. However, idle times mostly affect LAES operation, as liquid yield decreases due to less cold recycle available, from 79 to 45%, resulting in a roundtrip efficiency drop to 32.9%. LAES energy density decreases accordingly, from 23 to 17 kWh/$m^3$.
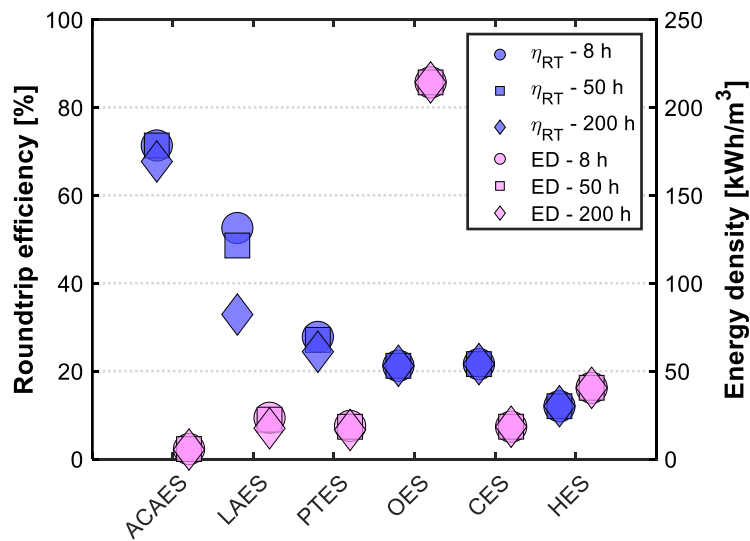
**Figure 85: Technical performance indicators for the TMES technologies and their evolution with different storage capacities.**

Whereas power cost in the left-hand plot of Figure 86 only increases at longer durations, capacity costs on the right-hand side decrease sharply initially and eventually reach an asymptote once the increase in investment costs varies linearly with storage capacity. Depending on the specific TMES technology and its cost structure, the extent to which $EC$ decreases and the duration to reach asymptotic behaviour are different in Figure 86. HES is the most expensive TMES option below 10 h duration, but it notably becomes the second cheapest solution above 100 h and approaches ACAES with the lowest energy costs at 200 h. The high (45%) share of power-related CAPEX at 200 h, means additional cost reduction can be achieved by further extending HES capacity above this threshold, as demonstrated by the slope in the figure detail. PTES becomes more economically viable than OES above 150 h.
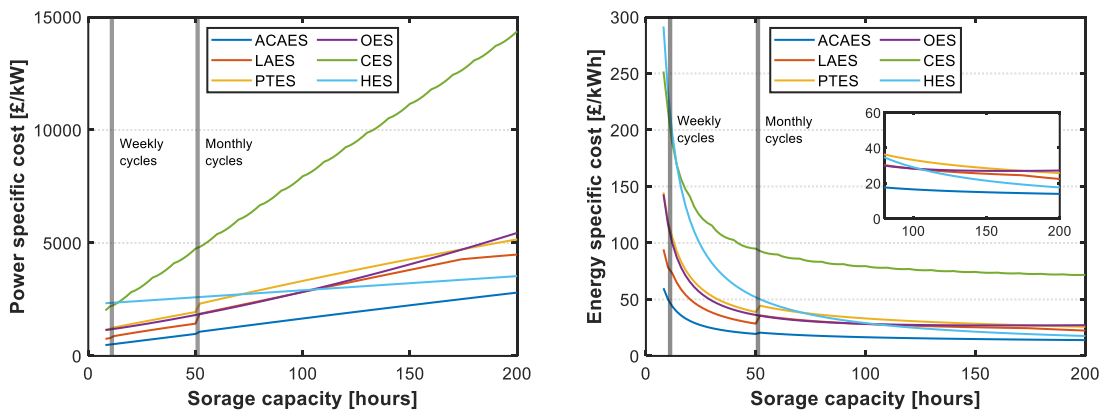


**Figure 86: Power (left) and energy (right) specific cost for the TMES technologies and their evolution with different storage capacities.**

Overall, technical and economic results display significant variations when transitioning from durations typically associated with MDS to the LDS domain, as reflected in the spider plots of Figure 87. The largest variations are associated with costs. Although the extent is ultimately technology-dependent, deviations are significant, e.g. cost metrics can reduce to one quarter or less between applications at 10 and 50 h. Especially for technologies such as TMES, normally investigated for daily cycling, the use of well-established performance and cost metrics may hinder their application for longer storage

146

scales. However, these results demonstrate different TMES technologies are best suited for the application in different subdomains of MDS and LDS duration regions.
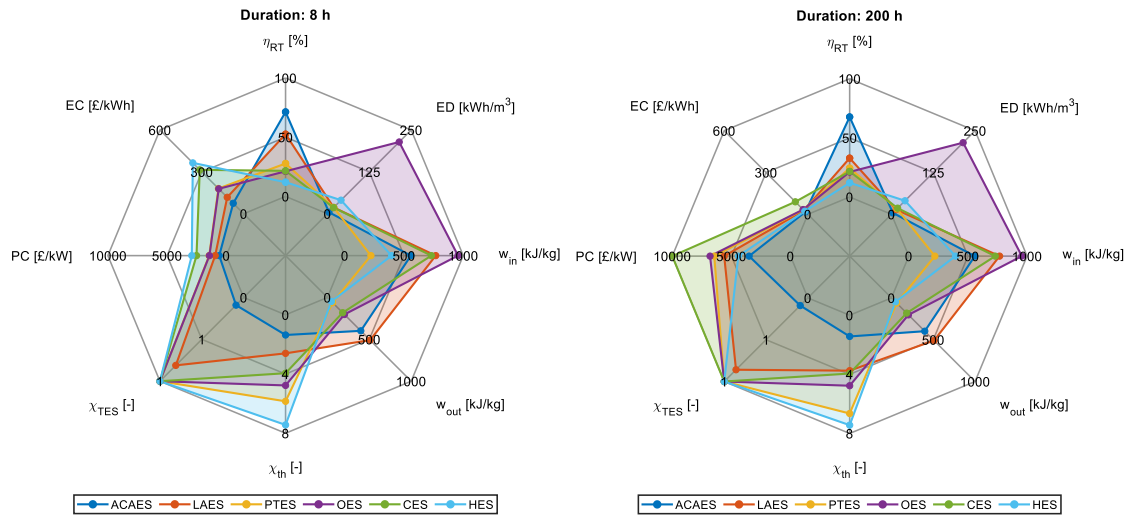


**Figure 87: Different techno-economic performance indicators for the investigated thermo-mechanical energy storage technologies at 8 h and 200 h storage duration.**

## 7.5.2  Benchmark with incumbent storage technologies and target design space

LCOS results computed for TMES are overlaid, in Figure 88, with those of incumbent technologies that are suited for daily and monthly cycles, namely Li-ion batteries and power-to-$H_2$-to-power [314]. For daily cycling, a crossover point exists above which LAES and CAES become more cost-effective than Li-ion batteries. In the present analysis, this happens around 2-4 h duration, for a 100 $MW_e$ power output. Although several Li-ion battery projects are in operation worldwide with a duration above 10 h [335], at sufficiently large scales and above 4 h duration TMES should be preferred instead. Novel TMES based on thermochemical TES are less attractive on LCOS basis, both for daily and monthly cycling, as penalised by the low roundtrip efficiency. Yet, this analysis indicates that under selected duration range TMES outperforms storage alternatives. 4-150 h can be recommended as the ideal scope where TMES offer the most cost-effective storage solution. Synthetic fuels should be preferred at longer storage duration and technologies with lower power costs – like batteries – below 4 h. Selecting the best storage solution ensures lower investment requirements for the energy transition.
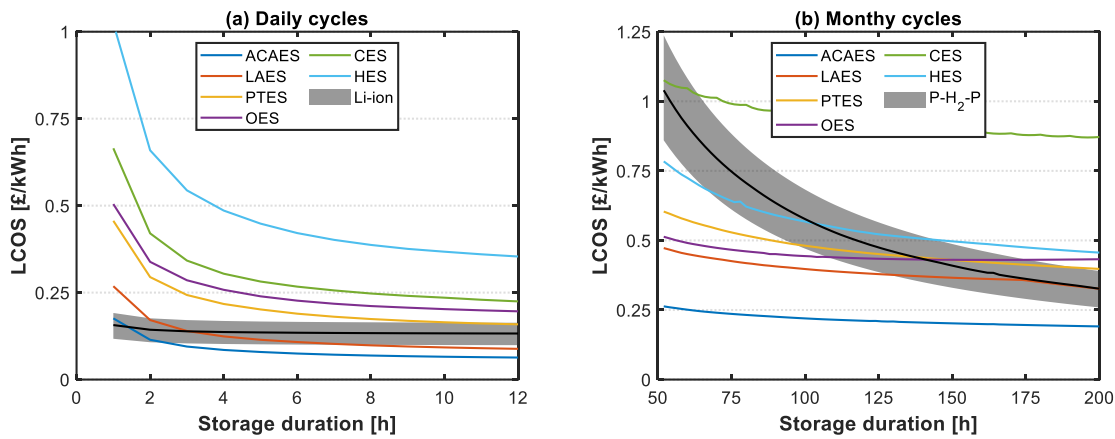
Figure 88: Levelised cost of storage (LCOS) for the TMES concepts investigated under daily and monthly cycles.

To conclude, Figure 89 benchmarks TMES solutions against the target design space for LDS applications for a baseline case (0.85 machine efficiency and 0.92 heat exchanger effectiveness) and a best case (0.95 and 0.97, respectively), at 200 h capacity. The cost range for incumbent LDS solutions from [314] is also reported, together with the cost targets from [176], i.e. 20 $/kWh, to result in 10% lower system adaptation cost (solid black line) and 10 $/kWh, to start displacing firm generators (dashed black line).
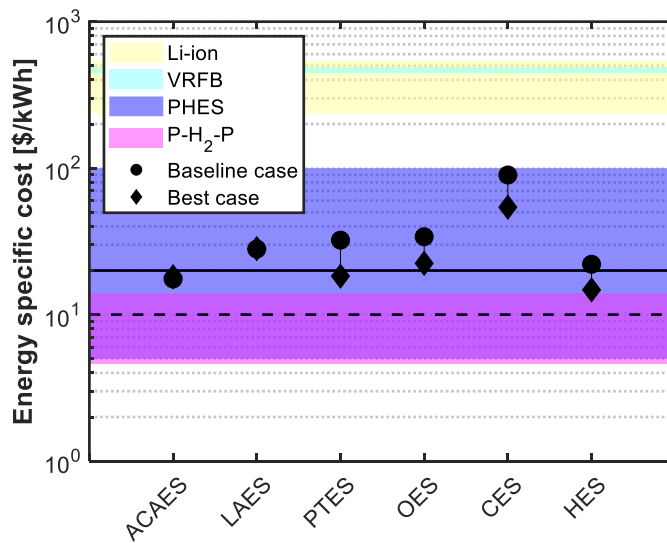


Figure 89: Target design space for long-duration storage: thermos-mechanical energy storage concepts and other storage options.

Cost estimations for TMES are consistent with the range for pumped hydro energy storage, but without geographical restriction to the deployment of most TMES solutions. Results show that, even under the baseline case assuming current device performance, ACAES can already provide the required LDS services at the target costs. However, under future technological development also PTES and HES are predicted to achieve costs below 20 $/kWh, with HES becoming the cheapest TMES solution for LDS and competitive with power to $H_2$ to power pathways at ~14 $/kWh. OES can reach the same or even better economic values than HES if the thermal energy storage can be indirectly coupled to the process via an intermediate heat transfer step, thus removing the need for a pressurised vessel.

148

## 7.6 Conclusion and outlook

Results in the literature and so far in this thesis have looked at LAES and TMES for day and intra-day balancing. In this chapter, LDS application is explored. Alongside ACAES, LAES, and Brayton PTES, three novel TMES concepts are evaluated, which exploit recent developments in thermochemical energy storage for the TMES field. Thermodynamic models are used to predict storage techno-economic performance, its evolution with storage duration, and future compliance with LDS design targets. The study explores a limited yet representative subset of the possible TMES system design, so, besides a cross-comparison of the traditional and novel TMES concepts considered, new evidence on the current and future pathways for TMES application as LDS is provided.

Results agree with the literature showing *ACAES and LAES as the most viable solutions for MDS*, due to high roundtrip efficiency (71% and 53%) and the lowest specific cost (480 £/kW, 755 £/kW). ACAES, in particular, remains techno-economically the best option for both MDS and LDS applications. However, since geographical constraints limit its deployment, novel TMES based on thermochemical energy storage provide comparable cost per unit capacity. Whether concepts using Brayton cycles are currently less financially attractive for MDS due to high power equipment costs, this chapter proves they could become competitive under component technical advancements, which are particularly sensitive to.

Additionally, the present study shows that *TMES already meets the cost targets for LDS*. *Novel TMES concepts based on reversible CaO hydration/dehydration or oxidation/reduction emerge as promising for LDS applications*, ensuring loss-free thermal storage at a very marginal capacity cost. Notably, under the proposed advancements at material, device and system scale, these two concepts are *expected to become cost-competitive with long-duration solutions such as power-to-$H_2$-to-power at below 15 $/kWh* and be valuable assets in bringing relief to the balancing needs of future low-carbon energy systems.

### 7.6.1 Chapter relevance within this thesis

This chapter addresses the research objective O4, by assessing both traditional and novel TMES concepts for LDS applications, which are deemed vital for the operation of highly decarbonised future energy systems. Two promising concepts, HES and OES, are individuated, along with the research strategies and associated development needs required to make them competitive. Additionally, the identification of TMES value in the LDS domain is necessary to guide future technology selection/cost assumptions in system modelling. The contributions to the existing body of literature are:

- Proposal and assessment of two novel TMES concepts based on CaO carbonation and hydration reactions
- Techno-economic assessment and cross-comparison of established and novel TMES concepts, both for medium- and long-duration storage applications
- Identification of promising research strategies for future improvement of TMES performance for LDS, with an estimation of the associated reduction in storage costs.

Adding to the results in Chapter 4, Chapter 5 and Chapter 6, targeting LAES, this final chapter focuses broadly on TMES concepts. Opportunities for TMES uptake and clear strategies for future technological development are pointed out, thus complementing and concluding the research work in this thesis. Key outcomes and recommendations for future research work are now reported in the Conclusion.

# CHAPTER 8

## Conclusion and future work

## 8.1    Thesis summary and contributions

Several energy storage technologies are currently available and capable of providing the flexibility necessary to accommodate large shares of renewables, increase efficiency and reduce losses in the energy system, thus supporting decarbonisation plans towards net-zero. Among them, this work targets the so-called thermo-mechanical energy storage, which is well suited for the medium-duration storage segment up to 12 h duration, exhibits efficiencies above 60%, energy density of 10s kWh/m$^3$, specific costs in the low 100s $/kWh and no geographical restrictions. The applications and strategies to integrate LAES and other TMES in future low-carbon power systems are investigated. Process- and system-scale considerations are merged into a comprehensive assessment of TMES that seeks an accurate representation of storage behaviour and, from there, a more representative description of storage potential and limitations. The presented results address each one of the research objectives formulated in the Introduction as summarised hereafter.

**O1 To characterise and techno-economically evaluate the operation of LAES under real-life conditions**

A sophisticated LAES model was developed to link device to system performance during plant operation, capturing the off-design behaviour of all the main plant components. It was run under three operating strategies suitable for LAES, which are representative of different combinations of energy balancing and reserve services. Although disregarding LAES power input variations and in the absence of field tests, results contribute to the existing body of literature by: i) clarifying the effect of different balancing services supply on LAES techno-economic performance on the basis of off-design component and system operation; ii) proposing a regulation strategy for LAES, aimed at limiting the observed roundtrip efficiency reduction of up to 17 percentage points; and iii) highlighting up to 30-35% reduction in LAES economic value, to be contained by future off-design performance improvements.

**O2 To identify pathways for LAES value maximisation as part of the power system**

A MILP optimisation tool was developed to optimise LAES dispatch over multiple energy and reserve services. Model formulation includes both the constraints imposed by the power system on service provision and storage restrictions in the form of thermodynamic characteristics. The model was used to explore the multi-service LAES operation, the guidelines for optimising its size under different portfolios of balancing services and the impact of accurate storage modelling on its resulting value. Results provide new understanding of: i) how disregarding LAES thermodynamic limitations leads to infeasible storage scheduling, especially for multi-service provision, and up to 11% lost revenue (2.36 £/kW each year); ii) how different charge/discharge size criteria decrease LAES payback time, depending on the portfolio of services provided; and iii) how power allocation to a portfolio of balancing services can enhance the value and lead to payback time below 20 years for a standalone LAES. Expansion of the proposed optimisation framework to include other energy generation assets and flexibility options for power system simulations would be advisable.

**O3 To techno-economically assess the opportunities and limitations for multi-energy provision from LAES**

A thermodynamic model for LAES was developed to understand the underlying phenomena affecting plant performance when different output levels, not only of electricity but also heating and cooling, are extracted from LAES. Such model was reduced and included in a system-integration assessment, where the economic benefit of multi-energy LAES operation compared to the traditional electrical storage only was evaluated for two district sizes and different operating strategies. Results complement the existing assessment of LAES as electrical storage by: i) showing the potential to increase plant energy efficiency above 75% with multi-energy output; and ii) deriving multi-energy capability maps that show the feasible region of power and thermal output for LAES. Although a techno-economic assessment of other storage/generation solutions at district scale is ultimately needed to determine the best solution, heat provision can lead to 12% cost savings compared to a purely electrical LAES; cold provision should be limited to periods of simultaneous heat demand or high cooling prices.

**O4 To assess selected TMES concepts for long-duration storage applications**

Individual models for six TMES technologies, including traditional as well as novel options based on thermochemical energy storage, were built to predict system performance and investment costs. Their results were used to cross-compare the performance of the investigated technologies for both medium- and long-duration storage and benchmark against the intended design space for LDS, evaluating the impact of future developments through sensitivity analysis. Despite the simplified analysis, clear directions to progress TMES research are highlighted by: i) showing TMES already fits the target cost for LDS of 20 $/kWh; ii) highlighting TMES based on thermochemical energy storage can achieve low losses and the best economic performance above 100 h capacity; and iii) demonstrating research is needed to advance TMES solutions based on reversible oxidation or hydration reactions, with the potential to achieve costs below 15 $/kWh, i.e. aligned with those for $H_2$.

## 8.2   Perspectives and recommendations for future work

The results presented in this thesis have addressed some research questions on TMES but opened others. More work is needed to advance the TMES field and support its future uptake. In particular, a broader understanding of TMES potential, challenges and limitations in relation to alternative flexibility options and case-dependent considerations is required. Based on the learnings from this thesis, the following research pathways seem particularly relevant:

- Dynamic modelling of TMES, focussing on predicting plant start-up/shut-down periods, ramp rates and load modulation, with validation against field tests, where available. Given the confirmed financial value of multi-service operation, such analysis will support market service definition with a rigorous assessment of the capability of different TMES options to cope with response times specifications of different services and access the associated revenue streams. It will also enable comparison with other storage/generating assets and inclusion of further technical details into system-scale assessments.

- LAES and other TMES assessment in generation expansion planning problems, including thermodynamic characteristics and in conjunction with different storage technologies. Given the suitability of TMES for medium-duration storage, a mix of storage technologies with diverse durations is likely to result in the most cost-effective transition. A rigorous evaluation of the optimal power and capacity of each technology will minimise energy system investment and operation costs to support the net-zero transition.

- Extension of the developed model reduction framework and derivation of multi-energy capability maps for other TMES. Particularly for PTES, the large amounts of thermal energy stored and the associated temperature range make external heating and cooling provision relevant. Exploiting such a promising pathway toward industrial decarbonisation requires studies accounting for plant operational limitations, in comparison with alternative technologies.

- Techno-economic assessment of hybrid TMES concepts aimed at increasing the number of services to be provided. As demonstrated for LAES, the presence of TES in the system opens up several avenues for efficient TMES plant hybridisation, where applications are not limited to the power system, but potentially extend to thermal energy management. The aggregation of different energy storage technologies or storage as a retrofit to generation solutions may lead to favourable business opportunities.

- Layout improvement and detailed system modelling of HES and OES concepts using, respectively, metal hydroxides and oxides for long-duration storage applications. Technical advancement should pursue the limitation of pressures along OES system, increase machine performance and thermochemical reaction conversion efficiency for both concepts. Alternative metal oxides should also be evaluated for thermochemical storage in HES and OES.

# Bibliography

[1]     Rosenzweig C, Karoly D, Vicarelli M, Neofotis P, Wu Q, Casassa G, et al. Attributing physical and biological impacts to anthropogenic climate change. Nat 2008 4537193 2008;453:353–7. doi:10.1038/nature06937.

[2]     United Nations. Paris Agreement - English 2015:25.

[3]     Ray, Douglas. Lazard's Levelized Cost of Energy Analysis—Version 13.0 2020.

[4]     IRENA. Global Energy Transformation: A roadmap to 2050. Abu Dhabi: 2018. doi:10.1057/9780230244092.

[5]     IEA. Net Zero by 2050 A Roadmap for the Global Energy Sector 2021:222.

[6]     Pfenninger S, Keirstead J. Renewables, nuclear, or fossil fuels? Scenarios for Great Britain's power system considering costs, emissions and energy security. Appl Energy 2015;152:83–93. doi:10.1016/j.apenergy.2015.04.102.

[7]     Chen H, Cong TN, Yang W, Tan C, Li Y, Ding Y. Progress in electrical energy storage system: A critical review. Prog Nat Sci 2009;19:291–312. doi:10.1016/j.pnsc.2008.07.014.

[8]     Blanco H, Faaij A. A review at the role of storage in energy systems with a focus on Power to Gas and long-term storage. Renew Sustain Energy Rev 2018;81:1049–86. doi:10.1016/j.rser.2017.07.062.

[9]     National Grid. Future Energy Scenarios in five minutes 2021.

[10]    Gür TM. Review of electrical energy storage technologies, materials and systems: challenges and prospects for large-scale grid storage. Energy Environ Sci 2018;11:2696–767. doi:10.1039/C8EE01419A.

[11]    Bolund B, Bernhoff H, Leijon M. Flywheel energy and power storage systems. Renew Sustain Energy Rev 2007;11:235–58. doi:10.1016/J.RSER.2005.01.004.

[12]    Ali S, Stewart RA, Sahin O. Drivers and barriers to the deployment of pumped hydro energy storage applications: Systematic literature review. Clean Eng Technol 2021;5:100281. doi:10.1016/J.CLET.2021.100281.

[13]    Luo X, Wang J, Dooner M, Clarke J. Overview of current development in electrical energy storage technologies and the application potential in power system operation. Appl Energy 2015;137:511–36. doi:10.1016/j.apenergy.2014.09.081.

[14]    Vulusala G VS, Madichetty S. Application of superconducting magnetic energy storage in electrical power and energy systems: a review. Int J Energy Res 2018;42:358–68. doi:10.1002/ER.3773.

[15]    Rehman S, Al-Hadhrami LM, Alam MM. Pumped hydro energy storage system: A technological review. Renew Sustain Energy Rev 2015;44:586–98. doi:10.1016/J.RSER.2014.12.040.

[16]    Akhurst M, Atkins A, Uk R, Bruges R, Cooper S, Consulting S, et al. Liquid Air in the energy and transport systems. 2013.

[17]    Wang S, Xue X, Zhang X, Guo J, Zhou Y, Wang J. The Application of Cryogens in Liquid Fluid Energy Storage Systems. Phys Procedia 2015;67:732. doi:10.1016/j.phpro.2015.06.123.

[18]    Castle WF. Air separation and liquefaction: recent developments and prospects for the beginning of the new millennium. Int J Refrig 2002;25:158–72. doi:10.1016/S0140-7007(01)00003-2.

[19]    Lyseng B, Niet T, English J, Keller V, Palmer-Wilson K, Robertson B, et al. System-level power-to-gas energy storage for high penetrations of variable renewables. Int J Hydrogen Energy 2018;43:1966–79. doi:10.1016/j.ijhydene.2017.11.162.

[20]    Steinmann W-D. Thermo-mechanical concepts for bulk energy storage. Renew Sustain Energy

Rev 2017;75:205–19. doi:10.1016/j.rser.2016.10.065.

[21] Das T, Krishnan V, Mccalley JD. Assessing the benefits and economics of bulk energy storage technologies in the power grid. Appl Energy 2015;139:104–18. doi:10.1016/j.apenergy.2014.11.017.

[22] Damak C, Leducq D, Hoang HM, Negro D, Delahaye A. Liquid Air Energy Storage (LAES) as a large-scale storage technology for renewable energy integration-A review of investigation studies and near perspectives of LAES. Int J Refrig 2020;110:208–18. doi:10.1016/j.ijrefrig.2019.11.009.

[23] Vecchi A, Li Y, Ding Y, Mancarella P, Sciacovelli A. Liquid air energy storage (LAES): A review on technology state-of-the-art, integration pathways and future perspectives. Adv Appl Energy 2021;3:100047. doi:10.1016/j.adapen.2021.100047.

[24] Farres-Antunez P, Xue H, White AJ. Thermodynamic analysis and optimisation of a combined liquid air and pumped thermal energy storage cycle. J Energy Storage 2018;18:90–102. doi:10.1016/j.est.2018.04.016.

[25] Kantharaj B, Garvey S, Pimm A. Thermodynamic analysis of a hybrid energy storage system based on compressed air and liquid air. Sustain Energy Technol Assessments 2015;11:159–64. doi:10.1016/j.seta.2014.11.002.

[26] Abarr M, Geels B, Hertzberg J, Montoya LD. Pumped thermal energy storage and bottoming system part A: Concept and model. Energy 2017;120:320–31. doi:10.1016/J.ENERGY.2016.11.089.

[27] Cetin TH, Kanoglu M, Yanikomer N. Cryogenic energy storage powered by geothermal energy. Geothermics 2019;77:34–40. doi:10.1016/j.geothermics.2018.08.005.

[28] Trieb F, Thess A. Storage plants – a solution to the residual load challenge of the power sector? J Energy Storage 2020;31. doi:10.1016/j.est.2020.101626.

[29] Venkataramani G, Ramalingam V, Viswanathan K. Harnessing Free Energy From Nature For Efficient Operation of Compressed Air Energy Storage System and Unlocking the Potential of Renewable Power Generation. Sci Reports 2018 81 2018;8:1–11. doi:10.1038/s41598-018-28025-5.

[30] Crotogino F, Mohmeyer K-U, Scharf R. Huntorf CAES : More than 20 Years of Successful Operation. Solut Min Res Inst Conf 2001:1–7.

[31] Luo X, Wang J, Dooner M, Clarke J, Krupke C. Overview of Current Development in Compressed Air Energy Storage Technology. Energy Procedia 2014;62:603–11. doi:10.1016/J.EGYPRO.2014.12.423.

[32] Budt M, Wolf D, Span R, Yan J. A review on compressed air energy storage: Basic principles, past milestones and recent developments. Appl Energy 2016;170:250–68. doi:10.1016/J.APENERGY.2016.02.108.

[33] Wang JJ, Lu K, Ma L, Wang JJ, Dooner M, Miao S, et al. Overview of Compressed Air Energy Storage and Technology Development. Energies 2017;10:991. doi:10.3390/en10070991.

[34] Cárdenas B, Hoskin A, Rouse J, Garvey SD. Wire-wound pressure vessels for small scale CAES. J Energy Storage 2019;26:100909. doi:10.1016/J.EST.2019.100909.

[35] Wang Z, Xiong W, Ting DSK, Carriveau R, Wang Z. Comparison of underwater and underground CAES systems for integrating floating offshore wind farms. J Energy Storage 2017;14:276–82. doi:10.1016/J.EST.2017.11.001.

[36] Benato A, Stoppato A. Pumped Thermal Electricity Storage: A technology overview. Therm Sci Eng Prog 2018;6:301–15. doi:10.1016/j.tsep.2018.01.017.

[37] Thess A. Thermodynamic Efficiency of Pumped Heat Electricity Storage 2013. doi:10.1103/PhysRevLett.111.110602.

[38] Zhang H, Wang L, Lin X, Chen H. Technical and economic analysis of Brayton-cycle-based pumped thermal electricity storage systems with direct and indirect thermal energy storage. Energy 2021:121966. doi:10.1016/J.ENERGY.2021.121966.

[39]     McTigue JD, White AJ, Markides CN. Parametric studies and optimisation of pumped thermal electricity storage. Appl Energy 2015;137:800–11. doi:10.1016/j.apenergy.2014.08.039.

[40]     Dumont O, Frate GF, Pillai A, Lecompte S, De paepe M, Lemort V. Carnot battery technology: A state-of-the-art review. J Energy Storage 2020;32:101756. doi:10.1016/j.est.2020.101756.

[41]     Benato A. Performance and cost evaluation of an innovative Pumped Thermal Electricity Storage power system. Energy 2017;138:419–36. doi:10.1016/j.energy.2017.07.066.

[42]     Mctigue J, Farres-Antunez P, Ellingwood K, Neises T, White A. Pumped Thermal Electricity Storage with Supercritical CO 2 Cycles and Solar Heat Input Preprint. 2019.

[43]     Garvey SD, Pimm AJ, Buck JA, Woolhead S, Liew KW, Kantharaj B, et al. Analysis of a Wind Turbine Power Transmission System with Intrinsic Energy Storage Capability n.d.

[44]     Wang L, Lin X, Chai L, Peng L, Yu D, Liu J, et al. Unbalanced mass flow rate of packed bed thermal energy storage and its influence on the Joule-Brayton based Pumped Thermal Electricity Storage. Energy Convers Manag 2019;185:593–602. doi:10.1016/j.enconman.2019.02.022.

[45]     White A, Parks G, Markides CN. Thermodynamic analysis of pumped thermal electricity storage. Appl Therm Eng 2013;53:291–8. doi:10.1016/j.applthermaleng.2012.03.030.

[46]     Wang L, Lin X, Chai L, Peng L, Yu D, Chen H. Cyclic transient behavior of the Joule–Brayton based pumped heat electricity storage: Modeling and analysis. Renew Sustain Energy Rev 2019;111:523–34. doi:10.1016/J.RSER.2019.03.056.

[47]     Desrues T, Ruer J, Marty P, Fourmigué JF. A thermal energy storage process for large scale electric applications. Appl Therm Eng 2009;30:425–32. doi:10.1016/j.applthermaleng.2009.10.002.

[48]     McTigue JD, White AJ, Markides CN. Parametric studies and optimisation of pumped thermal electricity storage. Appl Energy 2015;137:800–11. doi:10.1016/j.apenergy.2014.08.039.

[49]     Wang L, Lin X, Chai L, Peng L, Yu D, Chen H. Cyclic transient behavior of the Joule–Brayton based pumped heat electricity storage: Modeling and analysis. Renew Sustain Energy Rev n.d.;111:523–34. doi:10.1016/j.rser.2019.03.056.

[50]     Dumont O, Parthoens A, Dickes R, Lemort V. Experimental investigation and optimal performance assessment of four volumetric expanders (scroll, screw, piston and roots) tested in a small-scale organic Rankine cycle system. Energy 2018;165:1119–27. doi:10.1016/j.energy.2018.06.182.

[51]     Davenne TR, Peters BM. An Analysis of Pumped Thermal Energy Storage With De-coupled Thermal Stores. Front Energy Res 2020;8. doi:10.3389/fenrg.2020.00160.

[52]     Zhang H, Wang L, Lin X, Chen H. Combined cooling, heating, and power generation performance of pumped thermal electricity storage system based on Brayton cycle 2020. doi:10.1016/j.apenergy.2020.115607.

[53]     Simpson MC, Olympios A, Mersch M, Sapin P, Olympios A V, Markides CN. Cost-benefit analysis of reversible reciprocating-piston engines with adjustable volume ratio in pumped thermal electricity storage. n.d.

[54]     Davenne TRG, Garvey SD, Cardenas B, Rouse JP. Stability of packed bed thermoclines. J Energy Storage 2018;19:192–200. doi:10.1016/j.est.2018.07.015.

[55]     Benato A, Stoppato A. Heat transfer fluid and material selection for an innovative Pumped Thermal Electricity Storage system. Energy n.d.;147:155–68. doi:10.1016/j.energy.2018.01.045.

[56]     Steger D, Regensburger C, Eppinger B, Will S, Karl J, Schlücker E. Design aspects of a reversible heat pump - Organic rankine cycle pilot plant for energy storage. Energy 2020;208. doi:10.1016/j.energy.2020.118216.

[57]     Frate GF, Ferrari L, Desideri U. Multi-criteria investigation of a pumped thermal electricity storage (PTES) system with thermal integration and sensible heat storage 2020. doi:10.1016/j.enconman.2020.112530.

[58]     Vinnemeier P, Wirsum M, Malpiece D, Bove R. Integration of Pumped-Heat-Electricity-Storage

into Water / Steam Cycles of Thermal Power Plants. 5th Int Supercrit CO2 Power Cycles Symp 2016;49.

[59]     Jockenhöfer H, Steinmann W, Bauer D. Detailed numerical investigation of a pumped thermal energy storage with low temperature heat integration 2018;145:665–76. doi:10.1016/j.energy.2017.12.087.

[60]     Abarr M, Geels B, Hertzberg J, Montoya LD. Pumped thermal energy storage and bottoming system part A: Concept and model. Energy n.d.;120:320–31. doi:10.1016/j.energy.2016.11.089.

[61]     Steinmann WD. The CHEST (Compressed Heat Energy STorage) concept for facility scale thermo mechanical energy storage. Energy n.d.;69:543–52. doi:10.1016/j.energy.2014.03.049.

[62]     Morandin M, Maréchal F, Mercangöz M, Buchter F. Conceptual design of a thermo-electrical energy storage system based on heat integration of thermodynamic cycles - Part B: Alternative system configurations. Energy 2012;45:386–96. doi:10.1016/j.energy.2012.03.033.

[63]     Mercangöz M, Hemrle J, Kaufmann L, Z'Graggen A, Ohler C. Electrothermal energy storage with transcritical CO2 cycles. Energy 2012;45:407–15. doi:10.1016/j.energy.2012.03.013.

[64]     Abarr M, Hertzberg J, Montoya LD. Pumped Thermal Energy Storage and Bottoming System Part B: Sensitivity analysis and baseline performance. Energy 2017;119:601–11. doi:10.1016/j.energy.2016.11.028.

[65]     Wang G-B, Zhang X-R. Thermodynamic analysis of a novel pumped thermal energy storage system utilizing ambient thermal energy and LNG cold energy. Energy Convers Manag n.d.;148:1248–64. doi:10.1016/j.enconman.2017.06.044.

[66]     Joshua McTigue  Kevin Ellingwood, Ty Neises, and Alexander White PF-A. Pumped Thermal Electricity Storage with Supercritical CO2 Cycles and Solar Heat Input. 2019 Sol Power Chem Energy Syst Conf 2019.

[67]     Kim Y-M, Shin D-G, Lee S-Y, Favrat D. Isothermal transcritical CO2 cycles with TES (thermal energy storage) for electricity storage. Energy n.d.;49:484–501. doi:10.1016/j.energy.2012.09.057.

[68]     Frate GF, Ferrari L, Desideri U. Rankine Carnot Batteries with the Integration of Thermal Energy Sources: A Review. Energies n.d.;13. doi:10.3390/en13184766.

[69]     Gil A, Medrano M, Martorell I, Lázaro A, Dolado P, Zalba B, et al. State of the art on high temperature thermal energy storage for power generation. Part 1—Concepts, materials and modellization. Renew Sustain Energy Rev 2010;14:31–55. doi:10.1016/J.RSER.2009.07.035.

[70]     Saghafifar M, Schnellmann MA, Scott SA. Chemical looping electricity storage. Appl Energy 2020;279. doi:10.1016/j.apenergy.2020.115553.

[71]     Saghafifar M, Scott SA. The use of high decomposition temperature materials for chemical looping electricity storage. Chem Eng J 2021;423:128789. doi:10.1016/j.cej.2021.128789.

[72]     Lutz M, Schmidt M, Bürger I, Linder M. Electricity storage based on coupled thermochemical reactions: The Thermochemical Battery. J Energy Storage 2021;33:102104. doi:10.1016/J.EST.2020.102104.

[73]     Jahnke A, Strenge L, Fleßner C, Wolf N, Jungnickel T, Ziegler F. First cycle simulations of the Honigmann process with LiBr/H 2 O and NaOH/H 2 O as working fluid pairs as a thermochemical energy storage n.d. doi:10.1093/ijlct/ctt022.

[74]     Thiele E, Jahnke A, Ziegler F. Efficiency of the Lamm–Honigmann thermochemical energy storage. Therm Sci Eng Prog 2020;19. doi:10.1016/j.tsep.2020.100606.

[75]     Pardo P, Deydier A, Anxionnaz-Minvielle Z, Rougé S, Cabassud M, Cognet P. A review on high temperature thermochemical heat energy storage. Renew Sustain Energy Rev 2014;32:591–610. doi:10.1016/J.RSER.2013.12.014.

[76]     Wu S, Zhou C, Doroodchi E, Nellore R, Moghtaderi B. A review on high-temperature thermochemical energy storage based on metal oxides redox cycle. Energy Convers Manag 2018;168:421–53. doi:10.1016/J.ENCONMAN.2018.05.017.

[77]     Criado YA, Alonso MM, Abanades JC. Kinetics of the CaO/Ca(OH) 2 Hydration/Dehydration

Reaction for Thermochemical Energy Storage Applications 2014. doi:10.1021/ie404246p.

[78]    Bailera M, Lisbona P, Romeo LM, Díez LI. Calcium looping as chemical energy storage in concentrated solar power plants: Carbonator modelling and configuration assessment. Appl Therm Eng 2020;172:115186. doi:10.1016/J.APPLTHERMALENG.2020.115186.

[79]    Fujii I, Ishino M, Akiyama S, Murthy MS, Rajanandam KS. Behavior of Ca(OH)2/CaO pellet under dehydration and hydration. Sol Energy 1994;53:329–41. doi:10.1016/0038-092X(94)90036-1.

[80]    Strö Hle S, Haselbacher A, Jovanovic ZR, Steinfeld A. The effect of the gas-solid contacting pattern in a high-temperature thermochemical energy storage on the performance of a concentrated solar power plant †. Energy Environ Sci 2016;9:1375. doi:10.1039/c5ee03204k.

[81]    Zhao Y, Zhao CY, Markides CN, Wang H, Li W. Medium- and high-temperature latent and thermochemical heat storage using metals and metallic compounds as heat storage media: A technical review. Appl Energy 2020;280:115950. doi:10.1016/J.APENERGY.2020.115950.

[82]    Smith EM. Storage of electrical energy using supercritical liquid air. Proc Inst Mech Eng 1977;191:289–98.

[83]    Kishimoto K, Hasegawa K, Asano T. Development of generator of liquid air storage energy system. Mitsubishi Heavy Ind Ltd Tech Rev 1998:117–120.

[84]    Araki H, Nakabaru M, Chino K. Simulation of heat transfer in the cool storage unit of a liquid-air energy storage system. Heat Transf - Asian Res 2002;31:284–96. doi:10.1002/htj.10035.

[85]    Chino K, Araki H. Evaluation of Energy Storage Method Using Liquid Air. Chem Pharm Bull 2000;29:347–57.

[86]    Chen H, Ding Y, Peters T, Berger F. A method of storing energy and a cryogenic energy storage system. WO 2007/096656, 2007.

[87]    Morgan RE. Liquid air energy storage – from theory to demonstration. Int J Environ Stud 2016:460–80. doi:10.1080/00207233.2016.1189741.

[88]    Peng X, She X, Li C, Luo Y, Zhang T, Li Y, et al. Liquid air energy storage flexibly coupled with LNG regasification for improving air liquefaction. Appl Energy 2019;250:1190–201. doi:10.1016/j.apenergy.2019.05.040.

[89]    Highview Enterprises Ltd. Highview power storage. http:// www.highview-power.com/ n.d.

[90]    Timmerhaus KD. Cryogenic Process Engineering. 2004. doi:10.1016/b0-12-227410-5/00156-3.

[91]    Popov D, Fikiin K, Stankov B, Alvarez G, Youbi-idrissi M, Damas A, et al. Cryogenic heat exchangers for process cooling and renewable energy storage: A review. Appl Therm Eng 2019;153:275–90. doi:10.1016/j.applthermaleng.2019.02.106.

[92]    Hamdy S, Morosuk T, Tsatsaronis G. Exergetic and economic assessment of integrated cryogenic energy storage systems. Cryogenics (Guildf) 2019;99:39–50. doi:10.1016/j.cryogenics.2019.02.009.

[93]    Borri E, Tafone A, Romagnoli A, Comodi G. A preliminary study on the optimal configuration and operating range of a "microgrid scale" air liquefaction plant for Liquid Air Energy Storage. Energy Convers Manag 2017;143:275–85. doi:10.1016/j.enconman.2017.03.079.

[94]    Guo H, Xu Y, Chen H, Zhou X. Thermodynamic characteristics of a novel supercritical compressed air energy storage system. Energy Convers Manag 2016;115:167–77. doi:10.1016/j.enconman.2016.01.051.

[95]    Lee I, Park J, Moon I. Conceptual design and exergy analysis of combined cryogenic energy storage and LNG regasification processes: Cold and power integration. Energy 2017;140:106–15. doi:10.1016/j.energy.2017.08.054.

[96]    Lee I, Park J, You F, Moon I. A novel cryogenic energy storage system with LNG direct expansion regasification: Design, energy optimization, and exergy analysis. Energy 2019;173:691–705. doi:10.1016/j.energy.2019.02.047.

[97]    Morgan R, Gibson E, Brett G. An analysis of a large-scale liquid air energy storage system. Proc Inst Civ Eng - Energy 2015;168:135–44. doi:10.1680/ener.14.00038.

[98]    Guizzi GL, Manno M, Tolomei LM, Vitali RM, Leo Guizzi G, Manno M, et al. Thermodynamic

analysis of a liquid air energy storage system. Energy 2015;93:1639–47. doi:10.1016/j.energy.2015.10.030.

[99] Guo L, Gao Z, Ji W, Xu H, Chen L, Wang J. Thermodynamics and Economics of Different Asymmetric Cold Energy Transfer in a Liquid Air Energy Storage System. Energy Technol 2020;1901487:1–11. doi:10.1002/ente.201901487.

[100] Legrand M, Rodríguez-Antón LM, Martinez-Arevalo C, Gutiérrez-Martín F. Integration of liquid air energy storage into the spanish power grid. Energy 2019;187:115965. doi:10.1016/j.energy.2019.115965.

[101] Peng X, She X, Cong L, Zhang T, Li C, Li Y, et al. Thermodynamic study on the effect of cold and heat recovery on performance of liquid air energy storage. Appl Energy 2018;221:86–99. doi:10.1016/j.apenergy.2018.03.151.

[102] Li Y, Chen H, Ding Y. Fundamentals and applications of cryogen as a thermal energy carrier: A critical assessment 2010. doi:10.1016/j.ijthermalsci.2009.12.012.

[103] Xie Y, Xue X, Xie Y, Xue X. Thermodynamic Analysis on an Integrated Liquefied Air Energy Storage and Electricity Generation System. Energies 2018;11:2540. doi:10.3390/en11102540.

[104] Incer-Valverde J, Hamdy S, Morosuk T, Tsatsaronis G, Incer J, Hamdy S, et al. Improvement perspectives of cryogenics-based energy storage. Renew Energy 2021. doi:10.1016/j.renene.2021.01.032.

[105] Dutta R, Ghosh P, Chowdhury K. Process configuration of Liquid-nitrogen Energy Storage System (LESS) for maximum turnaround efficiency 2017. doi:10.1016/j.cryogenics.2017.10.003.

[106] Sciacovelli A, Vecchi A, Ding Y. Liquid air energy storage (LAES) with packed bed cold thermal storage – From component to system level performance through dynamic modelling. Appl Energy 2017;190:84–98. doi:10.1016/j.apenergy.2016.12.118.

[107] Krawczyk P, Szabłowski Ł, Badyda K, Karellas S, Kakaras E. Impact of selected parameters on the performance of adiabatic liquid air energy storage with steam module. J Power Technol 2016;4:238–44.

[108] Tafone A, Borri E, Comodi G, van den Broek M, Romagnoli A. Liquid Air Energy Storage performance enhancement by means of Organic Rankine Cycle and Absorption Chiller. Appl Energy 2018;228:1810–21. doi:10.1016/j.apenergy.2018.06.133.

[109] Yu Q, Song W, Al-Duri B, Zhang Y, Xie D, Ding Y, et al. Theoretical analysis for heat exchange performance of transcritical nitrogen evaporator used for liquid air energy storage 2018. doi:10.1016/j.applthermaleng.2018.06.028.

[110] Ameel B, T'joen C, De Kerpel K, De Jaeger P, Huisseune H, Belleghem V, et al. Thermodynamic analysis of energy storage with a liquid air Rankine cycle. Appl Therm Eng 2013;52:130–40. doi:10.1016/j.applthermaleng.2012.11.037.

[111] Borri E, Tafone A, Comodi G, Romagnoli A. Improving liquefaction process of microgrid scale Liquid Air Energy Storage (LAES) through waste heat recovery (WHR) and absorption chiller. Energy Procedia 2017;143:699–704. doi:10.1016/j.egypro.2017.12.749.

[112] Sciacovelli A, Smith D, Navarro MEE, Vecchi A, Peng X, Li Y, et al. Performance Analysis and Detailed Experimental Results of the First Liquid Air Energy Storage Plant in the World. J Energy Resour Technol Trans ASME 2018;140. doi:10.1115/1.4038378.

[113] Chai L, Liu J, Wang L, Yue L, Yang L, Sheng Y, et al. Cryogenic energy storage characteristics of a packed bed at different pressures. Appl Therm Eng 2014;63:439–46. doi:10.1016/j.applthermaleng.2013.11.030.

[114] Hüttermann L, Span R, Maas P, Scherer V. Investigation of a liquid air energy storage (LAES) system with different cryogenic heat storage devices. Energy Procedia 2019;158:4410–5. doi:10.1016/j.egypro.2019.01.776.

[115] Dutta R, Sandilya P. Experimental Investigations on Cold Recovery Efficiency of Packed-bed in Cryogenic Energy Storage System n.d. doi:10.1088/1757-899X/755/1/012103.

[116] White AJ. Loss analysis of thermal reservoirs for electrical energy storage schemes. Appl Energy

2011;88:4150–9. doi:10.1016/j.apenergy.2011.04.030.

[117] She X, Li Y, Peng X, Ding Y. Theoretical analysis on performance enhancement of stand-alone liquid air energy storage from perspective of energy storage and heat transfer. Energy Procedia 2017;142:3498–504. doi:10.1016/j.egypro.2017.12.236.

[118] McTigue JD, White AJ. A comparison of radial-flow and axial-flow packed beds for thermal energy storage. Appl Energy 2018;227:533–41. doi:10.1016/J.APENERGY.2017.08.179.

[119] Hamdy S, Morosuk T, Tsatsaronis G. Cryogenics-based energy storage: Evaluation of cold exergy recovery cycles. Energy 2017;138:1069–80. doi:10.1016/j.energy.2017.07.118.

[120] An B, Chen J, Deng Z, Zhang T, Wang J, Yang L, et al. Design and testing of a high performance liquid phase cold storage system for liquid air energy storage. Energy Convers Manag 2020;226. doi:10.1016/j.enconman.2020.113520.

[121] Peng H, Shan X, Yang Y, Ling X. A study on performance of a liquid air energy storage system with packed bed units. Appl Energy 2018;211:126–35. doi:10.1016/J.APENERGY.2017.11.045.

[122] Bernagozzi M, Panesar AS, Morgan R. Molten salt selection methodology for medium temperature liquid air energy storage application. Appl Energy 2019;248:500–11. doi:10.1016/j.apenergy.2019.04.136.

[123] Zhang T, Zhang X, Xue X, Wang G, Mei S, Zhang T, et al. Thermodynamic Analysis of a Hybrid Power System Combining Kalina Cycle with Liquid Air Energy Storage. Entropy 2019;21:220. doi:10.3390/e21030220.

[124] Ryu J-Y, Alford A, Lewis G, Ding Y, Li Y, Ahmad A, et al. A novel liquid air energy storage system using a combination of sensible and latent heat storage. Appl Therm Eng 2021:117890. doi:10.1016/J.APPLTHERMALENG.2021.117890.

[125] Tafone A, Borri E, Cabeza LF, Romagnoli A. Innovative cryogenic Phase Change Material (PCM) based cold thermal energy storage for Liquid Air Energy Storage (LAES) − Numerical dynamic modelling and experimental study of a packed bed unit. Appl Energy 2021;301:117417. doi:10.1016/J.APENERGY.2021.117417.

[126] She X, Peng X, Nie B, Leng G, Zhang X, Weng L, et al. Enhancement of round trip efficiency of liquid air energy storage through effective utilization of heat of compression. Appl Energy 2017;206:1632–42. doi:10.1016/j.apenergy.2017.09.102.

[127] Krawczyk P, Szabłowski Ł, Karellas S, Kakaras E, Badyda K. Comparative thermodynamic analysis of compressed air and liquid air energy storage systems 2018. doi:10.1016/j.energy.2017.07.078.

[128] Antonelli M, Barsali S, Desideri U, Giglioli R, Paganucci F, Pasini G. Liquid air energy storage: Potential and challenges of hybrid power plants. Appl Energy 2017;194:522–9. doi:10.1016/j.apenergy.2016.11.091.

[129] Li Y, Cao H, Wang S, Jin Y, Li D, Wang X, et al. Load shifting of nuclear power plants using cryogenic energy storage technology. Appl Energy 2014;113:1710–6. doi:10.1016/j.apenergy.2013.08.077.

[130] Lee I, You F. Systems design and analysis of liquid air energy storage from liquefied natural gas cold energy. Appl Energy 2019;242:168–80. doi:10.1016/j.apenergy.2019.03.087.

[131] Wang C, Akkurt N, Zhang X, Luo Y, She X. Techno-economic analyses of multi-functional liquid air energy storage for power generation, oxygen production and heating 2020. doi:10.1016/j.apenergy.2020.115392.

[132] Al-Zareer M, Dincer I, Rosen MA. Analysis and assessment of novel liquid air energy storage system with district heating and cooling capabilities. Energy 2017;141:792–802. doi:10.1016/j.energy.2017.09.094.

[133] Kim J, Chang D. Pressurized cryogenic air energy storage for efficiency improvement of liquid air energy storage. Energy Procedia 2019;158:5086–91. doi:10.1016/j.egypro.2019.01.638.

[134] Zhang J, Meerman H, Benders R, Faaij A. Comprehensive review of current natural gas liquefaction processes on technical and economic performance 2019.

doi:10.1016/j.applthermaleng.2019.114736.

[135]    Yu Q, Zhang T, Peng X, Cong L, Tong L, Wang L, et al. Cryogenic Energy Storage and Its Integration With Nuclear Power Generation for Load Shift 2019. doi:10.1016/B978-0-12-813975-2.00008-9.

[136]    Zhang T, Zhang XL, He YL, Xue XD, Mei SW. Thermodynamic analysis of hybrid liquid air energy storage systems based on cascaded storage and effective utilization of compression heat. Appl Therm Eng 2020;164. doi:10.1016/j.applthermaleng.2019.114526.

[137]    Gao Z, Guo L, Ji W, Xu H, An B, Wang J. Thermodynamic and economic analysis of a trigeneration system based on liquid air energy storage under different operating modes 2020. doi:10.1016/j.enconman.2020.113184.

[138]    She X, Zhang T, Peng X, Wang L, Tong L, Luo Y. Liquid Air Energy Storage for Decentralized Micro Energy Networks with Combined Cooling , Heating , Hot Water and Power Supply 2021;30:1–17.

[139]    Georgiou S, Shah N, Markides CN. A thermo-economic analysis and comparison of pumped-thermal and liquid-air electricity storage systems. Appl Energy 2018;226:1119–33. doi:10.1016/j.apenergy.2018.04.128.

[140]    Xie C, Hong Y, Ding Y, Li Y, Radcliffe J. An economic feasibility assessment of decoupled energy storage in the UK: With liquid air energy storage as a case study 2018. doi:10.1016/j.apenergy.2018.04.074.

[141]    Kim J, Noh Y, Chang D. Storage system for distributed-energy generation using liquid air combined with liquefied natural gas. Appl Energy 2018;212:1417–32. doi:10.1016/j.apenergy.2017.12.092.

[142]    Hamdy S, Morosuk T, Tsatsaronis G. Exergoeconomic optimization of an adiabatic cryogenics-based energy storage system. Energy 2019;183:812–24. doi:10.1016/j.energy.2019.06.176.

[143]    Olympios A, McTigue J, Farres Antunez P, Tafone A, Romagnoli A, Li Y, et al. Progress and prospects of thermo-mechanical energy storage – A critical review. Prog Energy 2021. doi:10.1088/2516-1083/abdbba.

[144]    Park J, You F, Cho H, Lee I, Moon I. Novel massive thermal energy storage system for liquefied natural gas cold energy recovery 2020. doi:10.1016/j.energy.2020.117022.

[145]    Li Y, Wang X, Ding Y. A cryogen-based peak-shaving technology: systematic approach and techno-economic analysis. Int J Energy Res 2013;37:547–57. doi:10.1002/er.1942.

[146]    Pimm AJ, Garvey SD, Kantharaj B. Economic analysis of a hybrid energy storage system based on liquid air and compressed air. J Energy Storage 2015;4:24–35. doi:10.1016/j.est.2015.09.002.

[147]    Qi M, Park J, Kim J, Lee I, Moon I. Advanced integration of LNG regasification power plant with liquid air energy storage: Enhancements in flexibility, safety, and power generation. Appl Energy 2020;269:115049. doi:10.1016/j.apenergy.2020.115049.

[148]    Park J, Lee I, You F, Moon I, Frederick R. Economic Process Selection of Liquefied Natural Gas Regasification: Power Generation and Energy Storage Applications 2019. doi:10.1021/acs.iecr.9b00179.

[149]    Novotny V, Basta V, Smola P, Spale J. Review of Carnot Battery Technology Commercial Development. Energies 2022, Vol 15, Page 647 2022;15:647. doi:10.3390/EN15020647.

[150]    Castillo A, Gayme DF. Grid-scale energy storage applications in renewable energy integration: A survey. Energy Convers Manag 2014;87:885–94. doi:10.1016/j.enconman.2014.07.063.

[151]    Balasubramanian S, Balachandra P. Effectiveness of demand response in achieving supply-demand matching in a renewables dominated electricity system: A modelling approach. Renew Sustain Energy Rev 2021;147:111245. doi:10.1016/J.RSER.2021.111245.

[152]    Voss D, Underwood J, Kerth J, Bellman DK, Pykkonen K, Bryden KM. Path to commercialization. Therm Mech Hybrid Chem Energy Storage Syst 2021:513–68. doi:10.1016/B978-0-12-819892-6.00009-5.

[153] Dodds PE, Garvey SD. The Role of Energy Storage in Low-Carbon Energy Systems. Storing Energy With Spec Ref to Renew Energy Sources 2016:3–22. doi:10.1016/B978-0-12-803440-8.00001-4.

[154] Wang H, Riaz S, Mancarella P. Integrated techno-economic modeling, flexibility analysis, and business case assessment of an urban virtual power plant with multi-market co-optimization. Appl Energy 2019;259. doi:10.1016/j.apenergy.2019.114142.

[155] Leighty B, Holbrook J. Transmission and Firming of GW-Scale Wind Energy via Hydrogen and Ammonia. vol. 32. 2008.

[156] Zakeri B, Syri S, Wagner F. Economics of energy storage in the German electricity and reserve markets. Int Conf Eur Energy Mark EEM 2017:1–6. doi:10.1109/EEM.2017.7981914.

[157] Paraschiv F, Erni D, Pietsch R. The impact of renewable energies on EEX day-ahead electricity prices. Energy Policy 2014;73:196–210. doi:10.1016/J.ENPOL.2014.05.004.

[158] Kintner-Meyer M, Balducci P, Colella W, Elizondo M, Jin C, Nguyen T, et al. National Assessment of Energy Storage for Grid Balancing and Arbitrage: Phase I, WECC. Pacific Northwest Natl Lab 2012:204.

[159] Wesselmann M, Wilkening L, Kern TA. Techno-Economic evaluation of single and multi-purpose grid-scale battery systems. J Energy Storage 2020;32. doi:10.1016/j.est.2020.101790.

[160] Antonelli M, Desideri U, Franco A. Effects of large scale penetration of renewables: The Italian case in the years 2008–2015. Renew Sustain Energy Rev 2018;81:3090–100. doi:10.1016/j.rser.2017.08.081.

[161] Newbery D, Pollitt MG, Ritz RA, Strielkowski W. Market design for a high-renewables European electricity system. Renew Sustain Energy Rev 2018;91:695–707. doi:10.1016/J.RSER.2018.04.025.

[162] Locatelli G, Palerma E, Mancini M. Assessing the economics of large Energy Storage Plants with an optimisation methodology. Energy 2015;83:15–28. doi:10.1016/j.energy.2015.01.050.

[163] ESO N. Short Term Operating Reserve - Annual Report 2016/17. 2017.

[164] Electricity balancing services | National Grid ESO n.d. https://www.nationalgrideso.com/balancing-services (accessed January 8, 2020).

[165] Short term operating reserve (STOR) | National Grid ESO n.d. https://www.nationalgrideso.com/balancing-services/reserve-services/short-term-operating-reserve-stor (accessed August 9, 2019).

[166] Fast reserve | National Grid ESO n.d. https://www.nationalgrideso.com/balancing-services/reserve-services/fast-reserve (accessed August 9, 2019).

[167] Frunt J, Kling WL, Van Den Bosch PPJ. Classification and quantification of reserve requirements for balancing. Electr Power Syst Res 2010;80:1528–34. doi:10.1016/j.epsr.2010.06.018.

[168] Zhang J, Guerra OJ, Eichman J, Pellow MA. Benefit Analysis of Long-Duration Energy Storage in Power Systems with High Renewable Energy Shares. Front Energy Res 2020;8. doi:10.3389/fenrg.2020.527910.

[169] Bussar C, Moos M, Alvarez R, Wolf P, Thien T, Chen H, et al. Optimal allocation and capacity of energy storage systems in a future European power system with 100% renewable energy generation. Energy Procedia 2014;46:40–7. doi:10.1016/j.egypro.2014.01.156.

[170] Allen P, Blake L, Harper P, Hooker-Stroud A, James P, Kellner T. Zero Carbon Britain: Rethinking the Future. 2010. doi:10.1007/s10531-004-9513-9.

[171] Solomon AA, Kammen DM, Callaway D. The role of large-scale energy storage design and dispatch in the power grid: A study of very high grid penetration of variable renewable resources 2014. doi:10.1016/j.apenergy.2014.07.095.

[172] Budischak C, Sewell D, Thomson H, MacH L, Veron DE, Kempton W. Cost-minimized combinations of wind power, solar power and electrochemical storage, powering the grid up to 99.9% of the time. J Power Sources 2013;225:60–74. doi:10.1016/j.jpowsour.2012.09.054.

[173] Petkov I, Gabrielli P. Power-to-hydrogen as seasonal energy storage: an uncertainty analysis for

optimal design of low-carbon multi-energy systems Seasonal energy storage Multi-energy systems Renewable energy Optimization with uncertainty Global sensitivity analysis 2020. doi:10.1016/j.apenergy.2020.115197.

[174] Bussar C, Stöcker P, Cai Z, Moraes L, Magnor D, Wiernes P, et al. Large-scale integration of renewable energies and impact on storage demand in a European renewable power system of 2050-Sensitivity study. J Energy Storage 2016;6:1–10. doi:10.1016/j.est.2016.02.004.

[175] Strbac G, Aunedi M, Pudjianto D, Djapic P, Teng F, Sturt A, et al. Strategic Assessment of the Role and Value of Energy Storage Systems in the UK Low Carbon Energy Future Report for. 2012.

[176] Sepulveda NA, Jenkins JD, Edington A, Mallapragada DS, Lester RK. The design space for long-duration energy storage in decarbonized power systems. Nat Energy 2021. doi:10.1038/s41560-021-00796-8.

[177] Ziegler MS, Mueller JM, Pereira GD, Song J, Ferrara M, Chiang YM, et al. Storage Requirements and Costs of Shaping Renewable Energy Toward Grid Decarbonization. Joule 2019;3:2134–53. doi:10.1016/j.joule.2019.06.012.

[178] Albertus P, Manser JS, Litzelman S. Long-Duration Electricity Storage Applications, Economics, and Technologies n.d. doi:10.1016/j.joule.2019.11.009.

[179] Lin B, Wu W, Bai M, Xie C, Radcliffe J. Liquid air energy storage: Price arbitrage operations and sizing optimization in the GB real-time electricity market. Energy Econ 2019;78:647–55. doi:10.1016/J.ENECO.2018.11.035.

[180] Khani H, Zadeh MRD, Seethapathy R. Optimal weekly usage of Cryogenic Energy Storage in an open retail electricity market. IEEE Power Energy Soc Gen Meet 2013. doi:10.1109/PESMG.2013.6672626.

[181] Khani H, Dadash Zadeh MR. Real-time optimal dispatch and economic viability of cryogenic energy storage exploiting arbitrage opportunities in an electricity market. IEEE Trans Smart Grid 2015;6:391–401. doi:10.1109/TSG.2014.2357253.

[182] Frate GF, Ferrari L, Desideri U. Critical review and economic feasibility analysis of electric energy storage technologies suited for grid scale applications n.d. doi:10.1051/e3sconf/201913701037.

[183] Fares RL, Webber ME. What are the tradeoffs between battery energy storage cycle life and calendar life in the energy arbitrage application? J Energy Storage 2018;16:37–45. doi:10.1016/j.est.2018.01.002.

[184] Hou Q, Zhang N, Du E, Miao M, Peng F, Kang C. Probabilistic duck curve in high PV penetration power system: Concept, modeling, and empirical analysis in China. Appl Energy 2019;242:205–15. doi:10.1016/j.apenergy.2019.03.067.

[185] Morgan R, Nelmes S, Gibson E, Brett G. Liquid air energy storage - Analysis and first results from a pilot scale demonstration plant 2015. doi:10.1016/j.apenergy.2014.07.109.

[186] Siemens. Gas Turbine Portfolio Brochure 2019. https://assets.new.siemens.com/siemens/assets/public.1551272853.5001be9f0e51e56dbb66dcf0c0130538bf5722cd.gas-turbines-siemens-int.pdf (accessed January 8, 2020).

[187] GE. GE Product Catalog 2019 n.d. https://www.ge.com/content/dam/gepower-pgdp/global/en_US/documents/product/gas-power-systems-product-catalog-2019.pdf (accessed January 8, 2020).

[188] Zhang, Qi; Grossmann, Ignatio E.; Heuberger, Clara F.; Sundaramoorthy, Arul; Pinto JM. Air Separation with Cryogenic Energy Storage: Optimal Scheduling Considering Electric Energy and Reserve Market. Alche 2015;61:1547–58. doi:10.1002/aic.14730.

[189] Park J, Lee I, Moon I. A Novel Design of Liquefied Natural Gas (LNG) Regasification Power Plant Integrated with Cryogenic Energy Storage System 2017. doi:10.1021/acs.iecr.6b04157.

[190] Zamani-Gargari M, Kalavani F, Abapour M, Mohammadi-Ivatloo B. Reliability assessment of generating systems containing wind power and air separation unit with cryogenic energy storage. J Energy Storage 2018;16:116–24. doi:10.1016/j.est.2017.12.013.

[191] Kalavani F, Mohammadi-Ivatloo B, Zare K. Optimal stochastic scheduling of cryogenic energy storage with wind power in the presence of a demand response program. Renew Energy 2019;130:268–80. doi:10.1016/j.renene.2018.06.070.

[192] Mazzoni S, Ooi S, Tafone A, Borri E, Comodi G, Romagnoli A. Liquid Air Energy Storage as a polygeneration system to solve the unit commitment and economic dispatch problems in micro-grids applications. Energy Procedia 2019;158:5026–33. doi:10.1016/j.egypro.2019.01.660.

[193] Comodi G, Carducci F, Sze JY, Balamurugan N, Romagnoli A. Storing energy for cooling demand management in tropical climates: A techno-economic comparison between different energy storage technologies. Energy 2017;121:676–94. doi:10.1016/J.ENERGY.2017.01.038.

[194] CryoHub - Cryogenic Energy Storage for Renewable Refrigeration and Power Supply n.d. https://cryohub.eu/en-gb/ (accessed September 14, 2020).

[195] Murrant D, Radcliffe J. Analysis of when and where the integration of LAES with refrigerated warehouses could provide the greatest value to Europe. Energy Procedia 2018;151:144–9. doi:10.1016/j.egypro.2018.09.039.

[196] Bai J, Chen L, Liu F, Mei S. Interdependence of electricity and heat distribution systems coupled by an AA-CAES-based energy hub. IET Renew Power Gener 2020;14:399–407. doi:10.1049/iet-rpg.2019.0660.

[197] Yan Y, Zhang C, Li K, Wang Z. An integrated design for hybrid combined cooling, heating and power system with compressed air energy storage. Appl Energy 2018;210:1151–66. doi:10.1016/j.apenergy.2017.07.005.

[198] Li Y, Wang X, Li D, Ding Y. A trigeneration system based on compressed air and thermal energy storage. Appl Energy 2012;99:316–23. doi:10.1016/j.apenergy.2012.04.048.

[199] Steinmann WD, Bauer D, Jockenhöfer H, Johnson M, Steinmann WD, Bauer D, et al. Pumped thermal energy storage ( PTES ) as smart sector-coupling technology for heat and electricity. Energy 2019;183:185–90. doi:10.1016/j.energy.2019.06.058.

[200] Ahmad A, Al-Dadah R, Mahmoud S. Liquid nitrogen energy storage for air conditioning and power generation in domestic applications 2016. doi:10.1016/j.enconman.2016.09.063.

[201] Tafone A, Romagnoli A, Li Y, Borri E, Comodi G. Techno-economic Analysis of a Liquid Air Energy Storage (LAES) for Cooling Application in Hot Climates. Energy Procedia 2017;105:4450–7. doi:10.1016/j.egypro.2017.03.944.

[202] Wang P, Wang W, Wang C, Varga L. Optimal scheduling of multi-carrier energy networks considering liquid air energy storage. 2018 2nd IEEE Conf Energy Internet Energy Syst Integr 2018:1–4.

[203] Kalavani F, Mohammadi-Ivatloo B, Karimi A, Kalavani F. Stochastic optimal sizing of integrated cryogenic energy storage and air liquefaction unit in microgrid. Renew Energy 2019;136:15–22. doi:10.1016/J.RENENE.2018.12.101.

[204] Georgiou S, Aunedi M, Strbac G, Markides CN. On the value of liquid-air and pumped-thermal electricity storage systems in low-carbon electricity systems. Energy 2020;193. doi:10.1016/j.energy.2019.116680.

[205] Ma X, Zhang C, Li K, Li F, Wang H, Chen J. Optimal dispatching strategy of regional micro energy system with compressed air energy storage. Energy 2020;212. doi:10.1016/j.energy.2020.118557.

[206] Gabrielli P, Gazzani M, Martelli E, Mazzotti M. Optimal design of multi-energy systems with seasonal storage. Appl Energy 2018;219:408–24. doi:10.1016/j.apenergy.2017.07.142.

[207] Mavromatidis G, Petkov I. MANGO: A novel optimization model for the long-term, multi-stage planning of decentralized multi-energy systems. Appl Energy 2021;288:116585. doi:10.1016/j.apenergy.2021.116585.

[208] Van Beuzekom I, Gibescu M, Slootweg JG. A review of multi-energy system planning and optimization tools for sustainable urban development. 2015 IEEE Eindhoven PowerTech,

PowerTech 2015 2015:1–7. doi:10.1109/PTC.2015.7232360.

[209] Comodi G, Bartolini A, Carducci F, Nagaranjan B, Romagnoli A. Achieving low carbon local energy communities in hot climates by exploiting networks synergies in multi energy systems. Appl Energy 2019;256. doi:10.1016/j.apenergy.2019.113901.

[210] Ameri M, Besharati Z. Optimal design and operation of district heating and cooling networks with CCHP systems in a residential complex. Energy Build 2016;110:135–48. doi:10.1016/j.enbuild.2015.10.050.

[211] Thiem S, Danov V, Metzger M, Sch J, Afer €, Hamacher T. Project-level multi-modal energy system design-Novel approach for considering detailed component models and example case study for airports 2017. doi:10.1016/j.energy.2017.05.159.

[212] Rivarolo M, Greco A, Massardo AF. Thermo-economic optimization of the impact of renewable generators on poly-generation smart-grids including hot thermal storage. Energy Convers Manag 2013;65:75–83. doi:10.1016/j.enconman.2012.09.005.

[213] Zhang L. Combined Heat and Power Scheduling : Utilizing Building-Level Thermal Inertia for Short-Term Thermal Energy Storage in District Heat System 2018:804–14. doi:10.1002/tee.22633.

[214] Ahmed A, Mancarella P. Strategic techno-economic assessment of heat network options for distributed energy systems in the UK 2014. doi:10.1016/j.energy.2014.07.011.

[215] Liu X, Mancarella P. Modelling, assessment and Sankey diagrams of integrated electricity-heat-gas networks in multi-vector district energy systems. Appl Energy 2015. doi:10.1016/j.apenergy.2015.08.089.

[216] Mohammadi M, Noorollahi Y, Mohammadi-Ivatloo B B, Hosseinzadeh M, Yousefi H, Khorasani T. Optimal management of energy hubs and smart energy hubs-A review Keywords: Energy hub Multi-energy systems Distributed energy resources Demand side management Smart energy hubs Social network Sustainable energy systems 2018. doi:10.1016/j.rser.2018.02.035.

[217] Good N, Mancarella P. Flexibility in Multi-Energy Communities with Electrical and Thermal Storage: A Stochastic, Robust Approach for Multi-Service Demand Response. IEEE Trans Smart Grid 2019;10:503–13. doi:10.1109/TSG.2017.2745559.

[218] Bischi A, Taccari L, Martelli E, Amaldi E, Manzolini G, Silva P, et al. A detailed MILP optimization model for combined cooling, heat and power system operation planning 2014. doi:10.1016/j.energy.2014.02.042.

[219] Li Z, Wu W, Shahidehpour M, Wang J, Zhang B. Combined heat and power dispatch considering pipeline energy storage of district heating network. IEEE Trans Sustain Energy 2016;7:12–22. doi:10.1109/TSTE.2015.2467383.

[220] Naughton J, Cantoni M. A Modelling Framework for a Virtual Power Plant with Multiple Energy Vectors Providing Multiple Services n.d.

[221] Reynolds J, Ahmad MW, Rezgui Y, Hippolyte J. Operational supply and demand optimisation of a multi-vector district energy system using artificial neural networks and a genetic algorithm. Appl Energy 2019;235:699–713. doi:10.1016/j.apenergy.2018.11.001.

[222] Morvaj B, Evins R, Carmeliet J. Optimising urban energy systems: Simultaneous system sizing, operation and district heating network layout 2016. doi:10.1016/j.energy.2016.09.139.

[223] Rigo-Mariani R, Chea Wae SO, Mazzoni S, Romagnoli A. Comparison of optimization frameworks for the design of a multi-energy microgrid. Appl Energy 2020;257. doi:10.1016/j.apenergy.2019.113982.

[224] Fazlollahi S, Becker G, Ois Maréchal F. Multi-objectives, multi-period optimization of district energy systems: II-Daily thermal storage. Comput Chem Eng 2014;71:648–62. doi:10.1016/j.compchemeng.2013.10.016.

[225] Ortiga J, Bruno JC, Coronas A. Selection of typical days for the characterisation of energy demand in cogeneration and trigeneration optimisation models for buildings n.d. doi:10.1016/j.enconman.2010.11.022.

[226] Baldi F, Wang L, Pérez-Fortes M, Maréchal F. A cogeneration system based on solid oxide and proton exchange membrane fuel cells with hybrid storage for off-grid applications. Front Energy Res 2019;6. doi:10.3389/fenrg.2018.00139.

[227] Pan G, Gu W, Wu Z, Lu Y, Lu S. Optimal design and operation of multi-energy system with load aggregator considering nodal energy prices 2019. doi:10.1016/j.apenergy.2019.01.217.

[228] Casisi M, Buoro D, Pinamonti P, Reini M. A Comparison of Different District Integration for a Distributed Generation System for Heating and Cooling in an Urban Area. Appl Sci 2019;9:3521. doi:10.3390/app9173521.

[229] Fazlollahi S, Laurent Bungener S, Becker G, Maréchal F. Multi-Objectives, Multi-Period Optimization of district heat-ing networks Using Evolutionary Algorithms and Mixed Inte-ger Linear Programming (MILP). 2012.

[230] Gabrielli P, Fürer F, Mavromatidis G, Mazzotti M. Robust and optimal design of multi-energy systems with seasonal storage through uncertainty analysis. Appl Energy 2019;238:1192–210. doi:10.1016/j.apenergy.2019.01.064.

[231] Naughton J, Wang H, Riaz S, Cantoni M, Mancarella P. Optimization of multi-energy virtual power plants for providing multiple market and local network services. Electr Power Syst Res 2020;189:106775. doi:10.1016/j.epsr.2020.106775.

[232] Li Y, Miao S, Yin B, Yang W, Zhang S, Luo X, et al. A real-time dispatch model of CAES with considering the part-load characteristics and the power regulation uncertainty. Electr Power Energy Syst 2018;105:179–90. doi:10.1016/j.ijepes.2018.08.024.

[233] Ibrahim AA, Kazemtabrizi B, Bordin C, Dent CJ, McTigue JD, White AJ, et al. Pumped thermal electricity storage for active distribution network applications. 2017 IEEE Manchester PowerTech, Powertech 2017 2017:1–6. doi:10.1109/PTC.2017.7980837.

[234] Shafiee S, Zareipour H, Knight AM. Considering Thermodynamic Characteristics of a CAES Facility in Self-Scheduling in Energy and Reserve Markets. IEEE Trans Smart Grid 2018;9:3476–85. doi:10.1109/TSG.2016.2633280.

[235] Li Y, Miao S, Yin B, Yang W, Zhang S, Luo X, et al. A real-time dispatch model of CAES with considering the part-load characteristics and the power regulation uncertainty. Int J Electr Power Energy Syst 2019;105:179–90. doi:10.1016/J.IJEPES.2018.08.024.

[236] Bai J, Wei W, Chen L, Mei S. Modeling and dispatch of advanced adiabatic compressed air energy storage under wide operating range in distribution systems with renewable generation 2020. doi:10.1016/j.energy.2020.118051.

[237] Liu B, Lin Q, Zheng T, Chen L, Mei S. Low carbon economic dispatch for multi-energy distribution network with compressed air energy storage system as energy hub. Chinese Control Conf CCC 2017;1:3083–8. doi:10.23919/ChiCC.2017.8027831.

[238] Li R, Chen L, Yuan T, Li C. Optimal dispatch of zero-carbon-emission micro Energy Internet integrated with non-supplementary fired compressed air energy storage system. J Mod Power Syst Clean Energy 2016;4:566–80. doi:10.1007/s40565-016-0241-4.

[239] Chicco G, Riaz S, Mazza A, Mancarella P. Flexibility From Distributed Multienergy Systems 2020:1–22.

[240] Lahdelma R, Hakonen H. An efficient linear programming algorithm for combined heat and power production. Eur J Oper Res 2003;148:141–51. doi:10.1016/S0377-2217(02)00460-5.

[241] Colella F, Rein G, Verda V, Borchiellini R. Multiscale modeling of transient flows from fire and ventilation in long tunnels. Comput Fluids 2011;51:16–29. doi:10.1016/J.COMPFLUID.2011.06.021.

[242] Bejan A. Advanced engineering thermodynamics. John Wiley & Sons; 2006.

[243] Li Y. Cryogen Based Energy Storage : Process Modelling and Optimisation. PhD Thesis Univ Leeds 2011.

[244] Courtois N, Najafiyazdi M, Lotfalian R, Boudreault R, Picard M. Analytical expression for the evaluation of multi-stage adiabatic-compressed air energy storage (A-CAES) systems cycle

efficiency. Appl Energy 2021;288:116592. doi:10.1016/J.APENERGY.2021.116592.

[245] Wang C, Zhang X, You Z, Zhang M, Huang S, She X. The effect of air purification on liquid air energy storage – An analysis from molecular to systematic modelling. Appl Energy 2021;300:117349. doi:10.1016/J.APENERGY.2021.117349.

[246] Peng H, Li R, Ling X, Dong H. Modeling on heat storage performance of compressed air in a packed bed system. Appl Energy 2015;160:1–9. doi:10.1016/j.apenergy.2015.09.029.

[247] Guo H, Xu Y, Zhang X, Liang Q, Wang S, Chen H. Dynamic characteristics and control of supercritical compressed air energy storage systems 2020. doi:10.1016/j.apenergy.2020.116294.

[248] Sciacovelli A, Li Y, Chen H, Wu Y, Wang J, Garvey S, et al. Dynamic simulation of Adiabatic Compressed Air Energy Storage (A-CAES) plant with integrated thermal storage – Link between components performance and plant performance. Appl Energy 2017;185:16–28. doi:10.1016/j.apenergy.2016.10.058.

[249] Guo H, Xu Y, Zhang Y, Liang Q, Tang H, Zhang X, et al. O ff -design performance and an optimal operation strategy for the multistage compression process in adiabatic compressed air energy storage systems. Appl Therm Eng 2019;149:262–74. doi:10.1016/j.applthermaleng.2018.12.035.

[250] Zhao P, Gao L, Wang J, Dai Y. Energy efficiency analysis and off-design analysis of two different discharge modes for compressed air energy storage system using axial turbines. Renew Energy 2016;85:1164–77. doi:10.1016/j.renene.2015.07.095.

[251] Sciacovelli A, Verda V. Sensitivity analysis applied to the multi-objective optimization of a MCFC hybrid plant. Energy Convers Manag 2012;60:180–7. doi:10.1016/j.enconman.2012.02.011.

[252] Manente G, Toffolo A, Lazzaretto A, Paci M. An Organic Rankine Cycle off-design model for the search of the optimal control strategy. Energy 2013;58:97–106. doi:10.1016/j.energy.2012.12.035.

[253] Nellis GF, Klein S a. Heat Transfer. 2009.

[254] Ciani M, Consoli D, Manente G, Lazzaretto A. Design and off-design models of a hybrid geothermal-solar power plant enhanced by a thermal storage. Renew Energy 2018;128:460–72. doi:10.1016/j.renene.2017.05.078.

[255] Mahmoudimehr J, Sebghati P. A novel multi-objective Dynamic Programming optimization method : Performance management of a solar thermal power plant as a case study. Energy 2019;168:796–814. doi:10.1016/j.energy.2018.11.079.

[256] Riahi S, Jovet Y, Saman WY, Belusko M, Bruno F. Sensible and latent heat energy storage systems for concentrated solar power plants , exergy efficiency comparison. Sol Energy 2019;180:104–15. doi:10.1016/j.solener.2018.12.072.

[257] Berkenkamp F, Gwerder M. Hybrid model predictive control of stratified thermal storages in buildings. Energy Build 2014;84:233–40. doi:10.1016/j.enbuild.2014.07.052.

[258] Waser R, Ghani F, Maranda S, O'Donovan TS, Schuetz P, Zaglio M, et al. Fast and experimentally validated model of a latent thermal energy storage device for system level simulations. Appl Energy 2018;231:116–26. doi:10.1016/j.apenergy.2018.09.061.

[259] Coutiert JP, Farber EA. TWO APPLICATIONS OF A NUMERICAL APPROACH OF HEAT TRANSFER PROCESS WITHIN ROCK BEDS. vol. 29. 1982.

[260] Pizzolato A, Donato F, Verda V, Santarelli M, Sciacovelli A. CSP plants with thermocline thermal energy storage and integrated steam generator – Techno-economic modeling and design optimization. Energy 2017;139:231–46. doi:10.1016/j.energy.2017.07.160.

[261] Theo WL, Lim JS, Ho WS, Hashim H, Lee CT. Review of distributed generation (DG) system planning and optimisation techniques: Comparison of numerical and mathematical modelling methods. Renew Sustain Energy Rev 2017;67:531–73. doi:10.1016/J.RSER.2016.09.063.

[262] Ghazouani S, Zoughaib A, Bourdiec S Le. An MILP model for simultaneous mass allocation and heat exchange networks design. Chem Eng Sci 2017;158:411–28.

doi:10.1016/J.CES.2016.10.041.

[263] Atabay D. An open-source model for optimal design and operation of industrial energy systems. Energy 2017;121:803–21. doi:10.1016/j.energy.2017.01.030.

[264] Firouzmakan P, Homayie SB, Hooshmand RA. Optimal power management of electrical energy storage system, CHP, conventional and heat-only units considering both electrical and thermal loads for assessment of all-electric ship's system. IET Electr Syst Transp 2020;10:213–23. doi:10.1049/iet-est.2018.5070.

[265] De Chalendar JA, Glynn PW, Benson SM. City-scale decarbonization experiments with integrated energy systems. Energy Environ Sci 2019;12:2020. doi:10.1039/c8ee03706j.

[266] IBM. IBM ILOG CPLEX Optimization Studio CPLEX User's Manual n.d.

[267] LLC G optimization. Gurobi optimizer reference manual - Version 8.1. 2018.

[268] Winston WL. Operations research: Applications and algorithms. 2004.

[269] Sierksma G. Linear and integer programming - theory and practice. 1996.

[270] Pfenninger S. Dealing with multiple decades of hourly wind and PV time series in energy models: A comparison of methods to reduce time resolution and the planning implications of inter-annual variability. Appl Energy 2017;197:1–13. doi:10.1016/j.apenergy.2017.03.051.

[271] Zhang M, Wu Q, Wen J, Lin Z, Chen Q. Optimal operation of integrated electricity and heat system: A review of modeling and solution methods 2020. doi:10.1016/j.rser.2020.110098.

[272] White AJ. Thermodynamic analysis of the reverse Joule-Brayton cycle heat pump for domestic heating. Appl Energy 2009;86:2443–50. doi:10.1016/j.apenergy.2009.02.012.

[273] Incropera FP, DeWitt DP, Bergman TL, Lavine AS. Introduction to heat transfer. 2006.

[274] Negoescu CC, Li Y, Al-Duri B, Ding Y. Heat transfer behaviour of supercritical nitrogen in the large specific heat region flowing in a vertical tube 2017. doi:10.1016/j.energy.2017.04.047.

[275] Scheidt F vom, Medinová H, Ludwig N, Richter B, Staudt P, Weinhardt C. Data analytics in the electricity sector – A quantitative and qualitative literature review. Energy AI 2020;1:100009. doi:10.1016/j.egyai.2020.100009.

[276] Severson KA, Attia PM, Jin N, Perkins N, Jiang B, Yang Z, et al. Data-driven prediction of battery cycle life before capacity degradation. Nat Energy 2019 45 2019;4:383–91. doi:10.1038/s41560-019-0356-8.

[277] Fisher R, Ding Y, Sciacovelli A. Hydration kinetics of K2CO3, MgCl2 and vermiculite-based composites in view of low-temperature thermochemical energy storage. J Energy Storage 2021;38:102561. doi:10.1016/J.EST.2021.102561.

[278] Bayón R, Rojas E. Analytical function describing the behaviour of a thermocline storage tank: A requirement for annual simulations of solar thermal power plants. Int J Heat Mass Transf 2014;68:641–8. doi:10.1016/j.ijheatmasstransfer.2013.09.070.

[279] Pizzolato A, Donato F, Verda V, Santarelli M. CFD-based reduced model for the simulation of thermocline thermal energy storage systems. Appl Therm Eng 2015;76:391–9. doi:10.1016/j.applthermaleng.2014.11.029.

[280] Quarteroni A, Saleri F, Gervasio P. Scientific Computing with MATLAB and Octave. 4th Ed. Springer; 2010.

[281] Garrett DE. Chemical Engineering Economics. vol. 5. Springer; 2012. doi:10.1080/00137916008965102.

[282] Jensen JK, Ommen T, Reinholdt L, Markussen WB, Elmegaard B. Heat pump COP, part 2: Generalized COP estimation of heat pump processes. Refrig Sci Technol 2018;2018-June:1255–64. doi:10.18462/iir.gl.2018.1386.

[283] Huang W, Zhang N, Wang Y, Capuder T, Kuzle I, Kang C. Matrix modeling of energy hub with variable energy efficiencies. Int J Electr Power Energy Syst 2020;119. doi:10.1016/j.ijepes.2020.105876.

[284] D'Ambrosio C, Lodi A, Martello S. Piecewise linear approximation of functions of two variables in MILP models. Oper Res Lett 2010;38:39–46. doi:10.1016/j.orl.2009.09.005.

[285] Huchette J, Vielma JP. Nonconvex piecewise linear functions: Advanced formulations and simple modeling tools. ArXiv 2017:1–40.

[286] Gabrielli P, Acquilino A, Siri S, Bracco S, Sansavini G, Mazzotti M. Optimization of low-carbon multi-energy systems with seasonal geothermal energy storage: The Anergy Grid of ETH Zurich. Energy Convers Manag X 2020:100052. doi:10.1016/j.ecmx.2020.100052.

[287] Petrou K, Liu MZ, Procopiou AT, Ochoa LF, Theunissen J, Harding J. Operating envelopes for prosumers in LV networks: A weighted proportional fairness approach. IEEE PES Innov Smart Grid Technol Conf Eur 2020;2020-October:579–83. doi:10.1109/ISGT-EUROPE47291.2020.9248975.

[288] Scapino L, De Servi C, Zondag HA, Diriken J, Rindt CCM, Sciacovelli A. Techno-economic optimization of an energy system with sorption thermal energy storage in different energy markets. Appl Energy 2019:114063. doi:10.1016/j.apenergy.2019.114063.

[289] ESO N. Fast Reserve Market Information Delivery from December-18. n.d.

[290] Du Y, Yang Y, Hu D, Hao M, Wang J, Dai Y. Off-design performance comparative analysis between basic and parallel dual-pressure organic Rankine cycles using radial inflow turbines. Appl Therm Eng 2018;138:18–34. doi:10.1016/j.applthermaleng.2018.04.036.

[291] Smallbone A, Jülch V, Wardle R, Roskilly AP. Levelised Cost of Storage for Pumped Heat Energy Storage in comparison with other energy storage technologies. Energy Convers Manag 2017;152:221–8. doi:10.1016/j.enconman.2017.09.047.

[292] Guo J, Cai L, Chen J, Zhou Y. Performance optimization and comparison of pumped thermal and pumped cryogenic electricity storage systems. Energy 2016;106:260–9. doi:10.1016/J.ENERGY.2016.03.053.

[293] Nord Pool. Historical Market Data n.d.

[294] Weron R. Electricity price forecasting: A review of the state-of-the-art with a look into the future. Int J Forecast 2014;30:1030–81. doi:10.1016/j.ijforecast.2014.08.008.

[295] Brett G, Barnett M. The application of liquid air energy storage for large scale long duration solutions to grid balancing. EPJ Web Conf 2014;79:3002. doi:10.1051/epjconf/20137903002.

[296] HMRC yearly average and spot rates - GOV.UK n.d. https://www.gov.uk/government/publications/exchange-rates-for-customs-and-vat-yearly (accessed October 9, 2019).

[297] CPIH INDEX 00: ALL ITEMS 2015=100 - Office for National Statistics n.d. https://www.ons.gov.uk/economy/inflationandpriceindices/timeseries/l522/mm23 (accessed October 14, 2019).

[298] Moreira R, Moreno R, Strbac G. Synergies and conflicts among energy storage services. 2016 IEEE Int Energy Conf ENERGYCON 2016 2016:1–6. doi:10.1109/ENERGYCON.2016.7513945.

[299] Energy Innovation Zone - Tyseley Energy Park n.d. https://www.tyseleyenergy.co.uk/energy-innovation-zone/ (accessed June 20, 2020).

[300] Soler MS, Sabaté CC, Santiago VB, Jabbari F. Optimizing performance of a bank of chillers with thermal energy storage 2016;172:275–85. doi:10.1016/j.apenergy.2016.03.099.

[301] Centre for Low Carbon Futures and Liquid Air Energy Network. Liquid Air Technologies – a guide to the potential 2013:28.

[302] Lemmon EW, Jacobsen RT, Penoncello SG, Friend DG. Thermodynamic properties of air and mixtures of nitrogen, argon, and oxygen from 60 to 2000 K at pressures to 2000 MPa. MPa J Phys Chem Ref Data 2000;29:1509. doi:10.1063/1.1285884.

[303] She X, Peng X, Zhang T, Ding Y. Configuration optimization of stand-alone Liquid Air Energy Storage for efficiency improvement n.d. doi:10.1088/1757-899X/502/1/012015.

[304] Abdur R, Mazhar S, Liu ∗, Shukla A. A state of art review on the district heating systems 2018. doi:10.1016/j.rser.2018.08.005.

[305] OpenEI project. Energy Information and Data | OpenEI.org n.d.

https://openei.org/wiki/Main_Page (accessed March 5, 2020).

[306] Chicco G, Mancarella P. Trigeneration primary energy saving evaluation for energy planning and policy development. Energy Policy 2007;35:6132–44. doi:10.1016/j.enpol.2007.07.016.

[307] Yao E, Wang H, Wang L, Xi G, Maréchal F. Thermo-economic optimization of a combined cooling, heating and power system based on small-scale compressed air energy storage. Energy Convers Manag 2016;118:377–86. doi:10.1016/j.enconman.2016.03.087.

[308] Li K, Wei X, Yan Y, Zhang C. Bi-level optimization design strategy for compressed air energy storage of a combined cooling, heating, and power system 2020. doi:10.1016/j.est.2020.101642.

[309] Martínez-Lera S, Ballester J, Martínez-Lera J. Analysis and sizing of thermal energy storage in combined heating, cooling and power plants for buildings. Appl Energy 2013;106:127–42. doi:10.1016/j.apenergy.2013.01.074.

[310] Hamdy S, Moser F, Morosuk T, Tsatsaronis G. Exergy-based and economic evaluation of liquefaction processes for cryogenics energy storage. Energies 2019;12. doi:10.3390/en12030493.

[311] Tafone A, Borri E, Comodi G, Romagnoli A. Parametric performance maps for design and selection of Liquid Air Energy Storage system for mini to micro-grid scale applications. Energy Procedia 2019;158:5053–60. doi:10.1016/j.egypro.2019.01.649.

[312] Uribe JM, Mosquera-López S, Arenas OJ. Assessing the relationship between electricity and natural gas prices in European markets in times of distress. Energy Policy 2022;166. doi:10.1016/J.ENPOL.2022.113018.

[313] Cárdenas B, Swinfen-Styles L, Rouse J, Hoskin A, Xu W, Garvey SD. Energy storage capacity vs. renewable penetration: A study for the UK. Renew Energy 2021;171:849–67. doi:10.1016/j.renene.2021.02.149.

[314] Dowling JA, Rinaldi KZ, Ruggles TH, Davis SJ, Yuan M, Tong F, et al. Role of Long-Duration Energy Storage in Variable Renewable Electricity Systems. Joule 2020;4:1907–28. doi:10.1016/j.joule.2020.07.007.

[315] Bravo R, Ortiz C, Chacartegui R, Friedrich D. Hybrid solar power plant with thermochemical energy storage: A multi-objective operational optimisation. Energy Convers Manag 2020;205:112421. doi:10.1016/J.ENCONMAN.2019.112421.

[316] Ortiz C, Valverde JM, Chacartegui R, Perez-Maqueda LA, Giménez P. The Calcium-Looping (CaCO3/CaO) process for thermochemical energy storage in Concentrating Solar Power plants. Renew Sustain Energy Rev 2019;113:109252. doi:10.1016/J.RSER.2019.109252.

[317] Scapino L, Zondag HA, Van Bael J, Diriken J, Rindt CCM. Energy density and storage capacity cost comparison of conceptual solid and liquid sorption seasonal heat storage systems for low-temperature space heating. Renew Sustain Energy Rev 2017;76:1314–31. doi:10.1016/J.RSER.2017.03.101.

[318] Xue H, White A. A comparative study of liquid, solid and hybrid adiabatic compressed air energy storage systems. J Energy Storage 2018;18:349–59.

[319] Grosu Y, Anagnostopoulos A, Navarro ME, Ding Y, Faik A. Inhibiting hot corrosion of molten Li2CO3-Na2CO3-K2CO3 salt through graphitization of construction materials for concentrated solar power. Sol Energy Mater Sol Cells 2020;215:110650. doi:10.1016/J.SOLMAT.2020.110650.

[320] Iranshahi D, Pourazadi E, Paymooni K, Bahmanpour AM, Rahimpour MR, Shariati A. Modeling of an axial flow, spherical packed-bed reactor for naphtha reforming process in the presence of the catalyst deactivation. Int J Hydrogen Energy 2010;35:12784–99. doi:10.1016/J.IJHYDENE.2010.08.124.

[321] Noorman S, Van Sint Annaland M, Kuipers H. Packed Bed Reactor Technology for Chemical-Looping Combustion 2007. doi:10.1021/ie061178i.

[322] Padula S, Tregambi C, Solimene R, Chirone R, Troiano M, Salatino P. A novel fluidized bed "thermochemical battery" for energy storage in concentrated solar thermal technologies.

Energy Convers Manag 2021;236:113994. doi:10.1016/J.ENCONMAN.2021.113994.

[323] Uchino T, Fushimi C. Fluidized bed reactor for thermochemical heat storage using Ca(OH)2/CaO to absorb the fluctuations of electric power supplied by variable renewable energy sources: A dynamic model. Chem Eng J 2021;419:129571. doi:10.1016/J.CEJ.2021.129571.

[324] Tesio U, Guelpa E, Verda V. Integration of thermochemical energy storage in concentrated solar power. Part 1: Energy and economic analysis/optimization. Energy Convers Manag X 2020;6:100039. doi:10.1016/J.ECMX.2020.100039.

[325] Alovisio A, Chacartegui R, Ortiz C, Valverde JM, Verda V. Optimizing the CSP-Calcium Looping integration for Thermochemical Energy Storage. Energy Convers Manag 2017;136:85–98. doi:10.1016/j.enconman.2016.12.093.

[326] Schmidt M, Linder M. Power generation based on the Ca(OH)2/ CaO thermochemical storage system − Experimental investigation of discharge operation modes in lab scale and corresponding conceptual process design. Appl Energy 2017;203:594–607. doi:10.1016/J.APENERGY.2017.06.063.

[327] Legrand M, Labajo-Hurtado R, Rodríguez-Antón LM, Doce Y. Price arbitrage optimization of a photovoltaic power plant with liquid air energy storage. Implementation to the Spanish case. Energy 2022;239:121957. doi:10.1016/J.ENERGY.2021.121957.

[328] Kapila S, Oni AO, Kumar A. The development of techno-economic models for large-scale energy storage systems. Energy 2017;140:656–72. doi:10.1016/J.ENERGY.2017.08.117.

[329] Turton R, Shaeiwitz JA, Bhattacharyya D, Whiting WB. Analysis, Synthesis, and Design of Chemical Processes. 5th ed. Prentice Hall; 2018.

[330] Lancashire River Gravel 20mm Bulk Bag - Decorative River Gravel n.d. https://www.greenvaleproductsltd.com/lancashire-river-gravel-20mm-bulk-bag-121-p.asp (accessed November 14, 2022).

[331] Manganese dioxide price, 2022 manganese dioxide price Manufacturers & Suppliers | Made-in-China.com n.d. https://www.made-in-china.com/products-search/hot-china-products/manganese_dioxide_price.html (accessed November 14, 2022).

[332] Lime - How much does it cost and when should it be applied? - thatsfarming.com n.d. https://thatsfarming.com/farming-news/lime-how-much-does-it-cost-and-when-should-it-be-applied/ (accessed November 14, 2022).

[333] Olympios A V, McTigue JD, Farres-Antunez P, Tafone A, Romagnoli A, Li Y, et al. Progress and prospects of thermo-mechanical energy storage—a critical review. Prog Energy 2021;3:022001. doi:10.1088/2516-1083/ABDBBA.

[334] Howes J. Concept and development of a pumped heat electricity storage device. Proc IEEE 2012;100:493–503. doi:10.1109/JPROC.2011.2174529.

[335] Choi D, Shamim N, Crawford A, Huang Q, Vartanian CK, Viswanathan V V., et al. Li-ion battery technology for grid application. J Power Sources 2021;511:230419. doi:10.1016/J.JPOWSOUR.2021.230419.

[336] Xue XD, Wang SX, Zhang XL, Cui C, Chen LB, Zhou Y, et al. Thermodynamic analysis of a novel liquid air energy storage system. Phys Procedia 2015;67:733–8. doi:10.1016/j.phpro.2015.06.124.

[337] Lin X, Wang L, Xie N, Li G, Chen H. Thermodynamic analysis of the cascaded packed bed cryogenic storage based supercritical air energy storage system. Energy Procedia 2019;158:5079–85. doi:10.1016/j.egypro.2019.01.639.

[338] Li Y, Jin Y, Chen H, Tan C, Ding Y. An integrated system for thermal power generation, electrical energy storage and CO2 capture. Int J Energy Res 2011;35:1158–67. doi:10.1002/er.1753.

[339] Li Y, Wang X, Jin Y, Ding Y. An integrated solar-cryogen hybrid power system. Renew Energy 2012;37:76–81. doi:10.1016/j.renene.2011.05.038.

[340] Kantharaj B, Garvey S, Pimm A. Compressed air energy storage with liquid air capacity extension. Appl Energy 2015;157:152–64. doi:10.1016/j.apenergy.2015.07.076.

[341] Luyao L, Sixian W, Zhang D, Luwei Y, Zhou Y, Wang J. Performance analysis of liquid air energy storage utilizing LNG cold energy. IOP Conf Ser Mater Sci Eng 2017;171. doi:10.1088/1757-899X/171/1/012032.

[342] Ji W, Zhou Y, Sun Y, Zhang W, Pan CZ, Wang JJ. Thermodynamic characteristics of a novel wind-solar-liquid air energy storage system n.d. doi:10.1088/1757-899X/278/1/012070.

[343] Zhang T, Chen L, Zhang X, Mei S, Xue X, Zhou Y. Thermodynamic analysis of a novel hybrid liquid air energy storage system based on the utilization of LNG cold energy. Energy 2018;155:641–50. doi:10.1016/j.energy.2018.05.041.

[344] She X, Zhang T, Cong L, Peng X, Li C, Luo Y, et al. Flexible integration of liquid air energy storage with liquefied natural gas regasification for power generation enhancement ☆ 2019. doi:10.1016/j.apenergy.2019.113355.

[345] Wu S, Zhou C, Doroodchi E, Moghtaderi B. Techno-economic analysis of an integrated liquid air and thermochemical energy storage system 2020. doi:10.1016/j.enconman.2019.112341.

[346] Cetin TH, Kanoglu M, Bedir F. Integration of cryogenic energy storage and cryogenic organic cycle to geothermal power plants 2020. doi:10.1016/j.geothermics.2020.101830.

[347] He T, Lv H, Shao Z, Zhang J, Xing X, Ma H. Cascade utilization of LNG cold energy by integrating cryogenic energy storage, organic Rankine cycle and direct cooling. Appl Energy 2020;277:115570. doi:10.1016/j.apenergy.2020.115570.

[348] Nabat MH, Zeynalian M, Razmi AR, Arabkoohsar A, Soltani M. Energy, exergy, and economic analyses of an innovative energy storage system; liquid air energy storage (LAES) combined with high-temperature thermal energy storage (HTES). Energy Convers Manag 2020;226:113486. doi:10.1016/j.enconman.2020.113486.

# Appendices

## Appendix A: relevant studies on standalone and hybrid LAES

In the following, Table A 1 and Table A 2 summarise the most relevant studies on, respectively, standalone and hybrid LAES to date.

**Table A 1: Summary of the most relevant studies on standalone LAES.**

| Reference | Standalone LAES plant description | | | | Metho dology | p levels [bar] | | Specific work [kJ/kg] | | $\eta_{RT}$*** [%] | ECO value | Findings | Notes |
|---|---|---|---|---|---|---|---|---|---|---|---|---|---|
| | AL | PRU | Hot/cold recycle | Cap [MWh] | | AL | PRU | AL | PRU | | | | |
| Guizzi et al. 2015 [98] | Linde | Rankine | H: thermal oil - 2 tanks C: propane and methanol - 2 tanks | N.A. | TD | 181 | 65 | 787* | 428.2 | 54.4 | N.A. | Link parameters-performance Optimal charging pressure | Specific analysis |
| Morgan et al. 2015 [185] | Claude | Rankine | C: air - packed bed | 2.5 | EXP | 12 | 56 | 1560* | 125* | 8 | N.A. | Fully integrated LAES proven 32% higher efficiency with cold recycle | Experimental 51% cold recycled |
| Morgan et al. 2015 [97] | Kapitza 14.2* MW | Rankine 20 MW | H: N.A. C: air - packed bed | 80 | TD ECO | 56.2 | 190 | 708.5* | 333* | 47.0 | 995-1774 £/kW 150-100 £/MWh | Liquefier optimisation necessary | Cold store design |
| Xue et al. 2015 [336] | Linde | Rankine | H: N.A. C: air - regenerator | N.A. | TD | 140 | 70 | N.A. | N.A. | 49.0 | N.A. | Benefit from improved component efficiency | Simultaneous charge/discharge |
| Guo et al. 2016 [94] | Linde | Rankine 10 MW | H: thermal oil - 2 tanks C: air - regenerator | 10 | TD | 120 | 95 | 584.6* | 394* | 67.4 | N.A. | Liquid expander brings 7 points $\eta_{RT}$ increase Energy density 18 times CAES | High-pressure vessel |
| Hamdy et al. 2017 [119] | Heylandt 12.5* MW | Rankine 10 MW | H: water C: R218 and methanol - 2 tanks | 40 | TD | 180 | 150 | 1062* | 429 | 40.4 | N.A. | Indirect ORC for PRU increases output but 16.4% efficiency | Hybrid LAES concept |
| Sciacovelli et al. 2017 [106] | Kapitza 70 MW | Rankine 100 MW | H: thermal oil - 2 tanks C: air - packed bed | 300 | TD | 185 | 75 | 978 | 472 | 48.3 | N.A. | Cyclic LAES operation needed | Dynamic packed bed model |
| She et al. 2017 [126] | Linde 95 MW | Rankine 48 MW | H: thermal oil - 2 tanks C: propane and methanol - 2 tanks | N.A. | TD | 90 | 120 | 872* | 440* | 50.0 | N.A. | Up to 40% compression heat is wasted | No losses from cold TES |
| Xie et al. 2018 [103] | Linde | Rankine | H: N.A. - 2 tanks C: N.A. - regenerator | N.A. | TD | 80 | 70 | 996* | 458* | 46.0 | N.A. | Pressure effect on charge and discharge performance | Extensive sensitivity analysis |
| Sciacovelli et al. [112] | Claude | Rankine | C: air - packed bed | 2.5 | EXP | 12.2 | 46 | N.A. | N.A. | N.A. | N.A. | Stable output over 3 setpoints Process variables evolution | Experimental LAES discharge |
| Peng et al. 2018 [121] | Linde | Rankine | H: air - packed bed C: air - packed bed | 5.6 | TD | 121 | 50 | 818* | 462* | 56.3 | N.A. | Lower efficiency than CAES but 10 times higher energy density Scale above 100 MW | Comparison with A-CAES Dynamic hot TES |

| Reference | AL | PRU | TES | Cap | Type | | | | | | Cost | Notes | |
|---|---|---|---|---|---|---|---|---|---|---|---|---|---|
| Peng et al. 2018 [101] | Linde | Rankine | H: thermal oil - 2 tanks<br>C: propane and methanol - 2 tanks | N.A. | TD | 140 | 80 | 731.9 | 434.7 | 59.4 | N.A. | Lost cold recycle 7 times more impact than lost hot | No losses from cold TES |
| Tafone et al. 2018 [108] | Kapitza | Rankine 10 MW | H: Therminol 66 - 2 tanks<br>C: air | N.A. | TD | 110 | 180 | 874.8 | 421.8 | 48.2 | N.A. | System improvement by layout and waste heat recovery | 8 bar pressurised vessel<br>55% waste heat recovery |
| Georgiou et al. 2018 [139] | Claude | Rankine 12 MW | H: N.A.<br>Cd: N.A. | 50 | TD ECO | 170 | N.A. | N.A. | N.A. | 31.5 | 1.4-2.8 k$/kW | Better economy than PTES (at large power especially) | 3 costing approaches |
| Kim et al. 2019 [133] | Linde 51.5 MW | Rankine 100 MW | H: N.A. - 2 tanks<br>C: N.A. - 2 tanks | 200 | TD | 120 | N.A. | N.A. | N.A. | 64.7 | N.A. | Pressurised LAES with 9 points efficiency increase | Pressurised vessel, 45 bar |
| Lin et al. 2019 [337] | Kapitza 16.7 MW | Rankine 9.9 MW | H: thermal oil - 2 tanks<br>C: air - 2 T level packed bed | N.A. | TD | 120 | 87.7 | 604* | 359* | 59.4 | N.A. | Efficiency increases to 65% if storage at 9 bar | Sensitivity on vessel pressure |
| Hamdy et al. 2019 [142] | Heylandt 107* MW | Rankine 100 MW | H: pressurised water - 2 tanks<br>C: R218 and methanol - 2 tanks | 400 | TD ECO | 120 | 160 | 994* | 465* | 46.8 | 2087 €/kW | 60% investment cost maintaining efficiency above 40% | Trade-off efficiency vs investment cost |
| Legrand et al. 2019 [100] | Kapitza 72.5 MW | Rankine 100 MW | H: thermal oil - 2 tanks<br>C: air - packed bed | 300 | TD | 180 | 75 | 1068* | 552 | 51.2 | N.A. | 52% efficiency with detailed modelling, 235 Wh/L | Dynamic cold regenerator |
| Guo et al. 2020 [99] | Multiple 19.5* MW | Rankine 9.8* MW | H: N.A. - 2 tanks<br>C: air - 2 T level packed bed | 79 | TD ECO | 70 | 57.4 | 703* | 433* | 61.6 | Depends on site | 107 kWh/m³<br>Claude less sensitive to TES efficiency | Extensive sensitivity analysis |

Abbreviations: AL: air liquefaction, PRU: power recovery unit, Cap: capacity, H: hot, C: cold, TD: thermodynamic, ECO: economic, EXP: experimental

* Computed by the authors based on available data

** Value indicated in the referenced publication - Results from the unifying methodology proposed in this review are reported separately

Table A 2: Summary of the most relevant studies dealing with hybrid LAES.

| Reference | Hybrid LAES layout | Methodology | Advantages | $\eta_{RT}$* [%] | ECO value | Findings | Notes |
|---|---|---|---|---|---|---|---|
| Li *et al.* 2011 [338] | Open LA power cycle + closed CH$_4$ Brayton | TD | Peak shaving opportunity Cryogenic CO$_2$ capture | 54.0 | N.A. | Peaker size could be halved | Peaker operation Conversion coefficient for ASU |
| Li *et al.* 2012 [339] | Open LA power cycle + closed solar Brayton | TD, SQP opt | Peak shaving opportunity No combustion | N.A. | N.A. | Above 30% higher power than separate sub-systems | Peaker operation Conversion coefficient for ASU |
| Li *et al.* 2013 [145] | Open LA power cycle + closed oxyfuel Brayton | TD, ECO, GA opt | Peak shaving opportunity Cryogenic CO$_2$ capture | N.A. | 0.08-0.17 $/kWh peak generation | Competitive cost with CCGT Liquid gas from ASU can be sold | ASU constantly run Conversion coefficient for ASU |
| Li *et al.* 2014 [129] | LAES + nuclear power plant | TD | Nuclear power plant flexibility | 70.0 | N.A. | Peak power delivered increases by a factor 3 | Storage capabilities Thermal input at 560 K |
| Kantharaj *et al.* 2015 [340] | Co-designed LAES-CAES | TD | No geographical constraints Large capacity | N.A. | N.A. | Conversion compressed-liquid air: 62% forward, 67% backwards | Not economic unless charging above 36h |
| Lee *et al.* 2017 [95] | Co-designed LAES-LNG | TD | Fully integrated system No air recirculation in AL | 172.0 | N.A. | High exergy efficiency | Vessel pressure 200 bar |
| Al-Zareer *et al.* 2017 [132] | LAES + absorption chiller + CH$_4$ combustion | TD | Full use of compression heat Multi-vector output | 72.0 | N.A. | Technically feasible Efficiency depends on cooling temperature | Detailed modelling of absorption cycle |
| Luyao *et al.* 2017 [341] | LAES + LNG + ORC | TD | Low power input and extra power output | 60.0 | N.A. | Higher system performance from integration | Results dependence on LNG provision |
| Borri *et al.* 2017 [111] | LAES + absorption chiller | TD | Chiller supports AL Direct use of compression heat | N.A. | N.A. | 10% lower liquefaction work Higher exergy efficiency | Study of Kapitza liquefaction process alone |
| She *et al.* 2017 [126] | LAES + ORC | TD, ECO | Better use of compression heat | 55.5 | PBT below 3 years | ORC bottoming cycle gives 9-12% $\eta_{RT}$ improvement and short PBT | Economic study on ORC addition only |
| Ji *et al.* 2017 [342] | LAES + solar | TD | Higher reheating temperature with no combustion | 45.0 | N.A. | Feasible system Reasonable efficiency | Compression heat not recycled TES for solar needed |
| Kim *et al.* 2018 [141] | LAES + LNG + CH$_4$ combustion | TD, ECO | Simultaneous power generation from LNG and air | 72.0 | 1300 $/kW | High efficiency Similar economic value to CAES | Regenerator to recover LNG cold |
| Peng *et al.* 2018 [101] | LAES + ORC + absorption chiller | TD | Full use of compression heat | 61.3 | N.A. | High heat usage ORC alone has higher efficiency | System complexity |
| Zhang *et al.* 2018 [343] | LAES + LNG + multistage ORC | TD | LNG assists liquefaction Evaporation cold partially used for power production | 45.4 | N.A. | High efficiency and energy density Pressures are key parameters | System complexity |
| Farres-Antunez *et al.* 2018 [24] | Co-designed LAES-PTES | TD | Cold TES in LAES and PTES not necessary Simultaneous charge/discharge | 70.0 | N.A. | High energy density Layout optimisation opportunities | Full liquefaction in the cryoturbine |
| Krawczyk *et al.* 2018 [127] | LAES + CH$_4$ combustion | TD | Higher specific work output Large plant: 271.5 MW | 55.2 | N.A. | Specific work output 905 kJ/kg | Comparison with CAES Compression heat not recycled |
| Tafone *et al.* 2018 [108] | LAES + ORC | TD | Full use of compression heat | 54.4 | N.A. | Improvement in $\eta_{RT}$ and waste heat utilisation | 85% use of compression heat |
| Tafone *et al.* 2018 [108] | LAES + ORC + absorption chiller | TD | Full use of compression heat Multi-vector output | 54.4 | N.A. | Unchanged $\eta_{RT}$ | 90% use of compression heat |

178

| Reference | System | Analysis | Objective/Features | Value | Economics | Results | Notes |
|---|---|---|---|---|---|---|---|
| Cetin et al. 2019 [27] | Co-designed LAES-geothermal | TD | Reduced geothermal losses<br>Fully dispatchable plant | 46.0 | N.A. | 30% higher energy output if trigenerative<br>Full system efficiency 24%<br>Flash pressure to be optimised | Compression heat not recycled |
| Zhang et al. 2019 [123] | LAES + Kalina cycle | TD | Better temperature match in the ORC evaporator | 57.0 | N.A. | $\eta_{RT}$ from 52% to 57%<br>55%-75% heat utilisation | 80 bar charge pressure 40 bar discharge<br>Multi-level hot TES |
| Lee et al. 2019 [96] | Co-designed LAES-LNG | TD, SRQPD opt | Fully integrated system<br>No air recirculation in AL | 130.0 | N.A. | Feasible system<br>Air can be fully liquefied | Reduced pressures from initial layout |
| Peng et al. 2019 [88] | LAES + LNG | TD | Independent operation of LAES and LNG through cold storage | 78.0 | N.A. | High liquid yield and $\eta_{RT}$ between 78% and 89%<br>Effect of ambient temperature | Year-round performance estimates |
| She et al. 2019 [344] | LAES + LNG + $N_2$ power cycle | TD | LAES and LNG operate simultaneously<br>LNG as sink for $N_2$ cycle | 72.0 | N.A. | Roundtrip comparable with large storage solutions | Effect of Brayton outlet pressure studied |
| Lee et al. 2019 [130] | Co-designed LAES-LNG + ORC | TD, ECO | Full use of LNG evaporation cold through ORC | N.A. | NPV 8-32 M$ | High exergy and energy efficiency<br>Low cost | 70% exergy efficiency |
| Zhang et al. 2020 [136] | LAES + ORC and LAES + Kalina cycle | TD | Cascaded hot recycle | 57.0 | N.A. | ORC and Kalina cycle perform similarly but ORC is less complex | Alternative bottoming cycles compared |
| Wu et al. 2020 [345] | LAES + TCES | TD, ECO | High temperatures<br>High energy density | 47.4 | 2130 $/kW | 36.8 kWh/m³<br>Higher $\eta_{RT}$ than TCES<br>Similar techno-economics to LAES | Compression heat not recycled<br>Discharge at 850 °C |
| Park et al. 2020 [144] | Co-designed LAES-LNG | TD, ECO | Independent operation of LAES and LNG through cold storage | 85.1 | 2680 $/kW | 0.37 kW/kg LNG, high capacity<br>8.7-11.7% peak power contribution in the case study | Efficiency depends on assumptions on LNG use |
| Qi et al. 2020 [147] | Co-designed LAES-LNG + ORC | TD, ECO | Flexible operation with target efficiency or power output | 129.2 | N.A. | 85.7-94.8 kJ/kg LNG<br>Adjustable power output to support grid | Compression heat not recycled |
| Wang et al. 2020 [131] | LAES + $O_2$ production + heating | TD, ECO | Multifunctional LAES<br>Adaptability to operating scenario | 39.0 | 3000 $/MW | Economic value 114-153% higher despite lower efficiency<br>45.7% hot recycle for heating | 1-D, transient absorber bed model for ASU |
| Gao et al. 2020 [137] | Trigenerative LAES | TD, ECO | Multi-vector output<br>Support to external thermal load | 45.7 | PBT about 5 years | Techno and financial feasibility<br>Case-dependent results based on the integration | Seasonal operating modes<br>Cooling from turbine outlet |
| Cetin et al. 2020 [346] | Co-designed LAES-geothermal + ORC | TD | Reduced geothermal losses<br>Fully dispatchable plant<br>Use of evaporation cold | 28.4 | N.A. | Higher geothermal temperature decreases efficiency | Compression heat not recycled<br>No cold recycle |
| He et al. 2020 [347] | LAES + LNG regassification + ORC + cooling | TD | Cascade cold recycle<br>Cooling capability | 142.0 | N.A. | 217 kW of cooling alongside 103.3 kW power output | ORC fluid composition is optimised for maximum power output |
| Nabat et al. 2020 [348] | LAES + ORC + thermoelectric device + DHW | TD, ECO | Diversified output<br>Limited losses | 61.1 | 3.91 years PBT, 18.6 M$ life revenues | Higher efficiency by 19 points<br>Besides 96 MW electricity, 2.5 kg/s DHW produced<br>104 MJ/m3 density | Charge pressure is critical, optimal value at 146 MPa |

| She *et al.* 2020 [138] | LAES + absorption chiller + heating + DHW | TD | Full use of compression heat<br>Multi-vector output | 55.0 | N.A. | Low charge pressure increases available heat<br>Energy efficiency up to 76% | Small scale system: 1 MW and 8h |

Abbreviations: LA: liquid air, AL: air liquefaction, TCES: Thermochemical energy storage, DHW: domestic hot water, TD: thermodynamic, ECO: economic, SQP: sequential quadratic programming, GA: genetic algorithm, SRQPD: successive reduced quadratic programming, opt: optimisation